

**INVESTIGATION OF POLYCYCLIC AROMATIC HYDROCARBONS (PAHs)  
ON DRY FLUE GAS DESULFURIZATION (FGD) BY-PRODUCTS**

DISSERTATION

Presented in Partial Fulfillment of the Requirements for  
the Degree Doctor of Philosophy in the Graduate  
School of The Ohio State University

By

Ping Sun, M.S.

\*\*\*\*\*

The Ohio State University  
2004

Dissertation Committee:

Professor Linda Weavers, Adviser

Professor Harold Walker

Professor Patrick Hatcher

Professor Yu-Ping Chin

Approved by

---

Adviser

Civil Engineering Graduate Program



## ABSTRACT

The primary goal of this research was to examine polycyclic aromatic hydrocarbons (PAHs) on dry FGD by-products to determine environmentally safe reuse options of this material. Due to the lack of information on the analytical procedures for measuring PAHs on FGD by-products, our initial work focused on analytical method development. Comparison of the traditional Soxhlet extraction, automatic Soxhlet extraction, and ultrasonic extraction was conducted to optimize the extraction of PAHs from lime spray dryer (LSD) ash (a common dry FGD by-product). Due to the short extraction time, ultrasonic extraction was further optimized by testing different organic solvents. Ultrasonic extraction with toluene as the solvent turned out to be a fast and efficient method to extract PAHs from LSD ash.

The possible reactions of PAHs under standard ultrasonic extraction conditions were then studied to address concern over the possible degradation of PAHs by ultrasound. By sonicating model PAHs including naphthalene, phenanthrene and pyrene in organic solutions, extraction parameters including solvent type, solute concentration, and sonication time on reactions of PAHs were examined. A hexane: acetone (1:1 V/V)

mixture resulted in less PAH degradation than a dichloromethane (DCM): acetone (1:1 V/V) mixture. The identified degradation by-products including methylphenanthrene and methyl-naphthalene after sonication of phenanthrene suggested that phenanthrene reacts by both direct pyrolysis and reaction with methyl radicals formed from pyrolysis of the alkane solvent.

After analytical method development, speciation and concentrations of PAHs on LSD ash were investigated. Low molecular weight compounds such as naphthalene, phenanthrene and pyrene were the primary PAHs identified. Although PAH speciation on LSD ash varied in the different samples, concentrations of PAHs identified were consistently low at the  $\mu\text{g kg}^{-1}$  level. The low concentrations indicate that the PAHs will not affect the environment during utilization or disposal of the LSD ash.

Changes in characteristics of the FGD by-products discourage its reuse. Therefore, daily, weekly, monthly, and yearly variability of PAHs on the LSD ash was also examined. Results showed a low variability of PAHs from 2001~2004. During monitoring the variability of PAHs on the LSD ash, results also suggested that total measured PAH concentrations were correlated with the organic carbon content of the LSD ash. It was then hypothesized that PAHs may be primarily associated with unburned carbon in the LSD ash. The LSD ash samples were fractionated and unburned carbon was further separated for PAH measurements to test this hypothesis. The PAH concentrations on the unburned carbon were the highest among all the fractions indicating an association between PAHs and unburned carbon. However, PAHs detected on the lime-enriched fraction suggested capture of PAHs by injected slaked lime in the LSD process.

Finally, solid by-products collected from the Ohio State carbonation and ash reactivation (OSCAR) process were examined for PAHs. Compared to the LSD ash, PAHs identified on the OSCAR solid by-products were primarily small molecular weight compounds. Due to the sorbent activation process in OSCAR, PAHs on the solid by-products may be different from the conventional dry FGD by-products (e.g. LSD ash). However, the compositions and concentrations of PAHs were found to be affected by the sorbent type for both sorbents studied. Samples collected from the baghouse had higher concentrations than the samples collected from the cyclone possibly due to the longer residence time of the particles and the lower temperature in the baghouse. Moreover, operational parameters such as sorbent injection rate, flue gas flow rate also were determined to affect the PAH concentrations on the solid by-products.

**Dedicated to my parents**

## ACKNOWLEDGMENTS

I wish to thank my adviser, Dr. Linda Weavers, for her guidance and availability. Her encouragement and advice make it possible for me to navigate around the common pitfalls and frustrations and finally finish my PhD studies.

I also want to thank my dissertation committee members: Dr. Harold Walker, Dr. Patrick Hatcher and Dr. Yu-ping Chin for their help during my research and course work.

I owe too many thanks to Johnny Brown, who taught me how to use the mass spectrometer. Johnny was always there to help me out when I had problems with the mass spectrometer in 2000 and 2001. Also, I would like to thank Gary Regier and Diana Baker, technical support representatives in Thermo Company. Their patience and fast responses to my phone calls and emails sped up my learning process of the GC/MS.

I am extremely thankful for my fellow students in the lab. Without them, my research work might have needed another 4 years to finish. Eric Onderak helped me to solve the problems of the auto-sampler. C. M. Cheng worked with me on the EPRI project and also helped me to conduct surface area and X-ray measurements. I will remember the hot breakfast at 8 AM at McDonald's after we finished making concrete. Mikko Lamminen not only helped me to fix my equipment such as cooling bath, but also

volunteered to be my English conversation partner. Without his corrections, I would have had a much harder time during my candidacy exam and my oral defense.

Most especially, I would like to thank Panuwat Taerakul for the friendship, the willingness to work together in the hot power plant during summer, the discussions about flue gas desulfurization by-products, and driving to Philadelphia.

I would also like to thank other former and current lab-mates: Yifang Lu, Aaron Frim, Mustafa Bob, Yaning Yang, June Ju Lee, Yusik Hwang, Limei Yang, Maggie Pee, Ziqi He, and the lab manager: Dr. Dan Golightly.

Some other friends made my life in Columbus happy and enjoyable. Particularly, I'd like to thank Bing Du, Dehua Liu and their wives for their friendship.

I can still remember my Mom's tears when I left Beijing airport. Life is very hard when you have to live far away from family. However, their love, support, and encouragement are always with me.

Finally, my love and appreciation goes to my dear husband: Jianyong Zhu for all his love and support. We made it!

## VITA

December 2, 1974 ..... Born-Wudi, China

1996 ..... B.S., Chemical Engineering, Qingdao  
Institute of Chemical Engineering, China

1999 ..... M.S., Environmental Engineering, Dalian  
University of Technology, China

1999-2000 ..... Research Scientist, DIC Qingdao Ltd.,  
China

2000-present ..... Graduate Research Associate, The Ohio  
State University

## FIELDS OF STUDY

Major Field: Civil Engineering

## TABLE OF CONTENTS

	Page
<b>Dedication</b> .....	v
<b>Acknowledgments</b> .....	vi
<b>Vita</b> .....	viii
<b>List of Figures</b> .....	xiii
<b>List of Tables</b> .....	xx
<b>Chapters</b>	
<b>1. Introduction and Background</b> .....	1
1.1. Flue Gas Desulfurization (FGD) System and By-products.....	1
1.2. Polycyclic Aromatic Hydrocarbons (PAHs) .....	4
1.3. PAH Formation Mechanism .....	5
1.4. Sorption of PAHs on solid particles.....	9
1.5. Analytical Procedure of PAHs on Solid Matrices .....	12
1.6. Ultrasound and Cavitation in Ultrasonic Extraction .....	15
1.7. Dissertation Overview.....	18
1.7.1. Characterization of PAHs on Dry FGD By-products: Effects of Extraction Method .....	20

1.7.2. Sonolytic Reactions of PAHs in Organic Extraction Solutions...	21
1.7.3. Distribution of PAHs in Lime Spray Dryer Ash .....	22
1.7.4. PAHs on By-products in the Ohio State Carbonization and Ash Reactivation (OSCAR) Process .....	22
References .....	24
<b>2. Effects of Extraction Method on Characterization of Polycyclic Aromatic Hydrocarbons (PAHs) on Lime Spray Dryer (LSD) Ash .....</b>	<b>36</b>
2.1. Abstract.....	36
2.2. Introduction.....	37
2.3. Materials and Methods.....	40
2.4. Results and Discussion.....	44
2.5. Conclusions.....	52
References.....	53
Tables and Figures.....	58
<b>3. Sonolytic Reactions of Polycyclic Aromatic Hydrocarbons (PAHs) in Organic Extraction Solutions.....</b>	<b>64</b>
3.1. Abstract.....	64
3.2. Introduction.....	65
3.3. Materials and Methods.....	67
3.4. Results and Discussion.....	70
References.....	83
Tables and Figures.....	86

<b>4. Distribution of Polycyclic Aromatic Hydrocarbons (PAHs) in Lime Spray Dryer (LSD) Ash .....</b>	<b>92</b>
4.1. Abstract.....	92
4.2. Introduction.....	93
4.3. Materials and Methods.....	95
4.4. Results and Discussion.....	99
4.5. Conclusions.....	108
References.....	109
Tables and Figures.....	112
<b>5. Characterization of Polycyclic Aromatic Hydrocarbons (PAHs) on Solid By-products Generated in The Ohio State Coal Ash Regeneration (OSCAR) Process.....</b>	<b>123</b>
5.1. Abstract.....	123
5.2. Introduction.....	124
5.3. Materials and Methods.....	126
5.4. Results and Discussion.....	128
5.5. Conclusions.....	137
References.....	139
Tables and Figures.....	142
<b>6. Conclusions and Future Work .....</b>	<b>153</b>
6.1. Conclusions .....	153
6.2. Future work.....	155

<b>APPENDIX A. Variability of Inorganic and Organic Constituents in Lime</b>	
<b>Spray Dryer Ash.....</b>	<b>158</b>
A.1. Abstract.....	159
A.2. Introduction.....	159
A.3. Experimental .....	161
A.4. Results and Discussion.....	165
A.5. Conclusions.....	176
References.....	178
Tables and Figures.....	181
<b>APPENDIX B. Gaseous Mercury from Dry-curing Concretes that Contain</b>	
<b>Fly Ash: Laboratory Measurements .....</b>	<b>193</b>
B.1. Abstract.....	194
B.2. Introduction.....	195
B.3. Experimental.....	196
B.4. Results.....	204
B.5. Discussion .....	207
References.....	213
Tables and Figures.....	216
<b>Bibliography .....</b>	<b>223</b>

## LIST OF FIGURES

Figure		Page
1.1	Reaction scheme for the formation of aromatic hydrocarbons .....	8
2.1	Major elemental composition of LSD ash.....	60
2.2	Spike recovery of 16 PAHs measured using traditional Soxhlet extraction, automatic Soxhlet extraction, and ultrasonic extraction with DCM as the solvent. Spike level was $10 \mu\text{g kg}^{-1}$ . Extraction time was 16 h in traditional Soxhlet extraction, 6 hr in automatic Soxhlet extraction. Ultrasonic extraction was repeated three times, 3 min each time with a pulse time of 5 sec.....	61
2.3	Solvent effect on spike recoveries of 16 PAHs measured using ultrasonic extraction. Spike level was $10 \mu\text{g kg}^{-1}$ . Each ultrasonic extraction includes 3 sonication exposures, 3 min each time with a pulse time of 5 sec.....	62

2.4	Recoveries of PAHs using ultrasonic extraction. Each ultrasonic extraction includes 3 sonication exposure, 3 min each time with a pulse time of 5 sec.....	63
3.1	Effects of solvents on ultrasonic extraction recovery of phenanthrene at initial concentrations of 1, 2, 5, 10, 50, 100, and 200 $\mu\text{g L}^{-1}$ in either hexane: acetone or DCM: acetone 1:1 V/V. Total ultrasonic irradiation time was 1.5 min; pulse time was 5 sec. Inset: enlargement of figure at the concentration ranging from 1 to 10 $\mu\text{g L}^{-1}$ .....	86
3.2	Recovery of phenanthrene at 100 $\mu\text{g L}^{-1}$ concentration in hexane: acetone 1:1 V/V under pulse sonication. Pulse time is 0.1, 0.5, 1, 3, and 5 sec respectively, pulse time equal to pulse off time, total ultrasonic irradiation time was 1.5 min.....	87
3.3	Recovery of PAHs in the presence of another PAH in either hexane: acetone or DCM: acetone 1:1 V/V solution. Total ultrasonic irradiation time is 1.5 min with pulse time of 5 sec). (a) Recovery of 0.284 $\mu\text{mol L}^{-1}$ naphthalene (Naph) in the presence of a 0.284 $\mu\text{mol L}^{-1}$ phenanthrene (Ph) addition or a pyrene (Py) addition and recovery rate of 0.568 $\mu\text{mol L}^{-1}$ Naph (single Naph); (b) Recovery of 0.284 $\mu\text{mol L}^{-1}$ of Ph in the presence of 0.284 $\mu\text{mol L}^{-1}$ Naph addition or Py addition and recovery rate of 0.568 $\mu\text{mol L}^{-1}$ Ph (single Ph); (c) Recovery of 0.284 $\mu\text{mol L}^{-1}$ of Py in the presence of 0.284 $\mu\text{mol L}^{-1}$ Naph	

	addition or Ph addition and recovery rate of 0.568 $\mu\text{mol L}^{-1}$ Py (single Py).....	88
3.4	Sonication of ternary mixture of naphthalene, phenanthrene and pyrene in either hexane: acetone or DCM: acetone 1:1 V/V. The concentration of each compound was 0.284 $\mu\text{mol L}^{-1}$ , total ultrasonic irradiation time was 1.5 min, pulse time was 5 sec.....	89
3.5	Recovery of 100 $\mu\text{g L}^{-1}$ and 200 $\mu\text{g L}^{-1}$ phenanthrene in hexane: acetone 1:1 V/V under different ultrasonic irradiation times of 1.5, 6, 10, 20, 30, 40 min. Pulse time is 5 sec. ....	90
3.6	Peak area change of degradation by-products formed from sonication of 200 $\mu\text{g L}^{-1}$ phenanthrene in hexane: acetone 1:1 V/V with different sonication time of 1.5, 6, 10, 20, 30, 40 min and pulse time = 5 sec. (●): 2-methylnaphthalene (2-methylNap); (○): 1-methylnaphthalene (1-methylNap); (▼): 2,6-dimethylnaphthalene (2,6-dimethylNap); (▽): 2,3,5-trimethylnaphthalene (2,3,5-trimethylNap); (■): Fluorene. ....	91
4.1	SEM images of whole LSD ash sample and components of fractionations. a: 4-LSD ash; b: 4-L (lime-enriched fraction of 4-LSD ash); c: 4-C (carbon-enriched fraction of 4-LSD); d: 4-UC (unburned carbon Separated from 4-LSD ash) .....	116

4.2	XRD pattern of 4 LSD ash samples, 4-L (separated lime-enriched fraction), 4-C (carbon-enriched fraction of 4-LSD), and 4-UC (unburned carbon separated from 4-LSD ash).....	117
4.3	Organic carbon content and measured total PAH concentrations on the 4 LSD ash samples. Inset: correlation between organic carbon content (%) and measured total PAH concentration ( $\mu\text{g}/\text{kg}$ ).....	118
4.4	Total PAH concentration ( $\mu\text{g}/\text{kg}$ ) in four LSD ash and correspondingly carbon-enriched, lime-enriched, and unburned carbon fractions.....	119
4.5	Total PAH concentration ( $\mu\text{g}/\text{kg}$ ) measured in lime-enriched fractions and concentrations calculated assuming PAHs were only associated with unburned carbon.....	120
4.6	Mass percentage of unburned carbon and PAH percentage on unburned carbon from 4 LSD ash samples.....	121
4.7	Comparison of measured and calculated PAH concentrations on LSD ash based on mass balance. 7a: 1-LSD ash; 7b: 2-LSD ash; 7c: 3-LSD ash; 7d: 4-LSD ash.....	122

5.1	X-Ray diffraction pattern of cyclone and baghouse samples collected in the OSCAR process with regenerated OSCAR sorbent injection.....	148
5.2	Major elemental composition in cyclone and baghouse samples collected in the OSCAR process. baghouse-1: baghouse samples with regenerated OSCAR sorbent injection; baghouse-2: baghouse samples with supersorbent injection; cyclone-1: cyclone samples with regenerated OSCAR sorbent injection; cyclone-2: cyclone samples with supersorbent injection.....	149
5.3	Speciation and concentrations of PAHs detected on the solid by-products with supersorbent injection. Fig. 3a: cyclone samples. Fig. 3b: baghouse samples.....	150
5.4	Correlation between Ca content and the total PAH concentration in the cyclone samples.....	151
5.5	Correlation between Hg and total PAH concentrations in the baghouse samples with supersorbent injection.....	152
A.1	X-Ray Diffraction Patterns of LSD Material from McCracken Power Plant....	186
A.2	SEM Images of LSD Material from McCracken Power Plant.....	187

A.3	Relative standard deviations of elements in LSD ash collected at different time periods .....	188
A.4	Profiles of Hg, As and Se concentrations in LSD material collected from McCracken Power Plant .....	189
A.5	Relative standard deviations of elements in leachates from LSD ash at different time periods .....	190
A.6	Profiles of As and Se concentrations in leachate solution from TCLP test of LSD material collected from McCracken Power Plant.....	191
A.7	Correlation between organic carbon content (%) and total PAH concentration measured on the LSD ash collected from McCracken Power Plant.....	192
B.1	Air Sampling Apparatus.....	220
B.2	Trends in mercury release rates from curing concretes. OPC: ordinary portland cement; FA33: concrete for which fly ash replaced 33% of the portland cement; FA55: concrete for which fly ash replaced 55% of the portland cement; HgPAC: concrete with 33% fly ash plus 0.5% mercury-loaded PAC. ....	221

B.3 Percent mercury released from different concretes after 2 days, 26 days and additional 28 days. OPC: ordinary portland cement; FA33: concrete for which fly ash replaced 33% of the portland cement; FA55: concrete for which fly ash replaced 55% of the portland cement; HgPAC: concrete with 33% fly ash plus 0.5% mercury-loaded PAC. .... 222

## LIST OF TABLES

Table		Page
1.1	Sixteen PAHs in the U.S. EPA priority pollutant list .....	6
2.1	PAHs detected using ultrasonic extraction with toluene, DCM: acetone (1:1), automatic Soxhlet extraction with DCM, and traditional Soxhlet Extraction with DCM.....	54
4.1	Major inorganic elemental composition (%) in LSD ash samples.....	106
4.2	Detected PAHs concentrations ( $\mu\text{g}/\text{kg}$ ) on different samples.....	107
4.3	Major inorganic elemental composition (%) and specific surface area of separated lime-enriched, carbon-enriched and unburned fractions.....	108
5.1	Specific surface area, organic C content and the concentration ( $\mu\text{g}/\text{kg}$ ) of PAHs detected on the lime, suporsorbent, LSD ash, and regenerated OSCAR sorbent.....	134

5.2	PAHs on samples collected from cyclone and baghouse using regenerated OSCAR sorbent. 3A-7, 4A-7, 5A-7 and 8A-7 are cyclone samples. 1B-8 is a baghouse sample.....	135
5.3	Measured PAH concentration on cyclone samples with supersorbent injection. #7 are cyclone sample, #8 are baghouse sample. Nap: naphthalane; Ace: acenaphthene; Phe: phenanthrene; Ant: anthracene; Py: pyrene; Flu: Fluoranthrene; Chy: chrysene; Ben(a): Benzo(a)anthracene; Ben(b): benzo(b)fluoranthene; Ben(k): benzo(k)fluoranthene.....	136
5.4	Specific surface area, organic C content and the concentration ( $\mu\text{g}/\text{kg}$ ) of PAHs on samples collected from cyclone and baghouse using regenerated OSCAR sorbent. 3A-7, 4A-7, 5A-7 and 8A-7 are cyclone samples. 1B-8 is a baghouse sample.....	137
5.5	Operational conditions in OSCAR process. ROS: regenerated OSCAR sorbent; SS: supersorbent.....	138
A.1	Elemental Composition of Lime Spray Dryer Ash, Quick Lime, and Coal Collected from McCracken Power Plant UDL – Under detection limit, N/A - No data available .....	171

A.2	Results of TCLP test of LSD ash from McCracken Power Plant	
	N/A – No data available.....	172
A.3	Results of ALI, CCE and TNP of LSD ash from McCracken Power Plant	
	N/A – No data available.....	173
A.4	Daily PAHs Concentration ( $\mu\text{g}/\text{kg}$ ) of Lime Spray Dryer Ash Collected from McCracken Power Plant Hopper F UDL – Under detection limit....	174
A.5	PAHs Concentration ( $\mu\text{g}/\text{kg}$ ) of Lime Spray Dryer Ash Collected from McCracken Power Plant from 05/2001 to 08/2003. UDL – Under detection limit.....	175
B.1	Mercury concentrations in concrete components. (1) Data is from reference 26; (2) data is from reference 27; (3) data is from reference 16...	205
B.2	Mercury contribution from each concrete component.....	206
B.3	Average mass release rates of mercury from curing concretes.....	207

## CHAPTER 1

### INTRODUCTION AND BACKGROUND

#### 1.1 Flue Gas Desulfurization (FGD) System and By-products

Coal has provided the bulk of electricity generation for many decades. Currently, more than a third of electricity generated worldwide comes from coal. In the United States, the contribution of coal to electricity generation is more than half (1). However, the use of coal produces air pollutants such as sulfur dioxide (SO<sub>2</sub>) and nitrogen oxides (NO<sub>x</sub>), which are the primary causes of acid rain. About two-thirds of all SO<sub>2</sub> and one fourth of all NO<sub>x</sub> emitted in the United States come from electric power generation that relies on burning fossil fuels like coal (2).

Control of SO<sub>2</sub> has been achieved by using flue gas desulfurization (FGD) technology. During this process, an alkaline sorbent (e.g. lime or lime stone) reacts with SO<sub>2</sub> in the flue gas resulting in the formation of calcium sulfate or calcium sulfite (3).

The typical reactions that occur during FGD processes that use lime can be simplified as:



FGD processes are broadly classified into wet or dry processes depending on whether wet or dry products (also called FGD by-products) are formed (4). In the wet FGD system, the limestone-water slurry comes into contact with flue gas containing  $\text{SO}_2$ ; the  $\text{SO}_2$  is absorbed into the slurry and reacts with the limestone to form an insoluble sludge (5). Wet lime or limestone FGD systems are the major wet FGD systems being installed for the following two reasons: they are mature technologies and they are cost effective (3). However, operational problems such as pipe corrosion, scale buildup in the scrubber and plugging occur (5). Handling and disposal of large amounts of wet sludge is another drawback of using wet FGD processes.

Dry FGD techniques using fine lime or limestone particles as sorbent for  $\text{SO}_2$  removal have drawn increasing interest. As an example, in one of the most common dry FGD techniques, the lime spray dryer (LSD) system, a slaked-lime slurry is atomized in a nozzle and sprayed into the spray dryer to mix and react with  $\text{SO}_2$  in the flue gas (3). The heat of the flue gas removes moisture in the reacted lime. The resulting dry calcium sulfite/sulfate mixture, along with fly ash, is collected as dry FGD by-product by an electrostatic precipitator or a baghouse (6, 7). Compared to the conventional wet FGD system, the initial capital cost of the dry FGD system is higher. However, the dry FGD system is expected to have lower operating costs. Also, the solid waste product generated during the dry FGD process is a dry powder, which offers potential advantages for handling and disposal (3).

The composition of FGD by-products vary widely ranging from products composed primarily of gypsum to material containing a high percentage of fly ash.

Factors that influence the final composition of the material include the source of the parent coal and the type of FGD system used (8).

It is estimated that approximately 31 million metric tons of FGD by-products including wet and dry forms are produced in the United States every year (9). The large amount of FGD by-products generated creates a challenge for handling and disposal. Currently, more than 18 million metric tons (72% of total production) of FGD by-products are landfilled as solid waste (9). Disposal of the enormous volume of FGD by-products has become increasingly difficult due to increased landfill costs and decreased landfill space (10). In addition, large amounts of by-products also represent a large unused resource. Therefore, many studies have been conducted to look for potential opportunities to reuse FGD by-products in a variety of applications including construction, agriculture and mine reclamation (11-15).

During the utilization of FGD by-products, there are concerns still remaining on the environmental impact. Previous studies have focused on the presence of inorganic trace elements such as mercury, arsenic, and boron (16, 17). Release of boron from FGD by-products and absorbed by plants (18-20) were observed, but no serious phytotoxicity has been reported. Compared to inorganic components, organic components are expected to be present in lower amounts and consequently are often neglected (21). However, some toxic organic compounds such as polycyclic aromatic hydrocarbons (PAHs) and dioxins may be present in the FGD by-products and thus may affect the environment during their disposal or utilization.

## 1.2. Polycyclic Aromatic Hydrocarbons (PAHs)

Polycyclic aromatic hydrocarbons (PAHs) are a class of organic compounds with varying numbers of carbon and hydrogen atoms connected in a fused ring structure (22). Due to their stable structure, PAHs are persistent in the environment for months to years (23). PAHs are ubiquitous and have been found in water, air, sediments, food, tobacco smoke, fossil fuels such as coal and oil, and even in pristine areas such as the Poles (24).

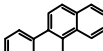
Generally, PAHs have low water solubilities, low volatilities and high hydrophobicities. Physical and chemical properties of PAHs vary with the number and position of aromatic rings and the substituents on the basic ring system (25). For example, with increasing molecular weight, the solubility and volatility decrease while the hydrophobicity increases (26). The carcinogenic activity of a particular PAH compound is also dependent on structural features of the PAH molecule such as shape, size, and steric factor. Thus, carcinogenicity of PAHs has mainly been observed for tri-, tetra-, penta-, and hexacyclic compounds (27). Some PAHs have been documented as carcinogenic or mutagenic in experimental animals. For example, benzo[a]pyrene caused breast cancer in rats when high doses were fed to rats and mice over a long period of time. It is believed that PAH molecules have a strong electrophilic character and interact with biological nucleophiles in metabolic processes resulting in the malfunction of organisms and thus cause cancer (28). Due to their toxicity, PAHs present a risk for the environment, especially if they enter the food chain through contact, inhalation or ingestion. For example, many PAHs present in aerosols have been found to be mutagenic or tumorigenic and a molecular biological pathway linking one of them, benzo(a)pyrene, to human lung cancer has been recently established (28).

PAHs are included in the U.S. EPA and in the European Union priority lists of pollutants because of their environmental and health concerns. The U.S. EPA has identified 16 PAHs as priority pollutants (29). These compounds include acenaphthene, acenaphthylene, anthracene, benzo[a]anthracene, benzo[a]pyrene, benzo[b]fluoranthene, benzo[g,h,i]perylene, benzo[k]fluoranthene, chrysene, dibenzo[a,h]anthracene, fluoranthene, fluorene, indeno[1,2,3-cd]pyrene, naphthalene, phenanthrene, and pyrene. The distributions of these PAHs in the environment and potential risks to human health have been the focus of much attention. The 16 PAHs along with their structures, physicochemical constants, and estimated carcinogenic potency are given in Table 1.1 (30).

### **1.3. PAH Formation Mechanisms**

PAHs can be formed from both natural and anthropogenic sources. Natural sources include combustion in nature such as volcanic eruptions and forest and prairie fires, biosynthesis, and long-term degradation followed by synthesis from biological material (17). Major anthropogenic sources include combustion of fossil fuels (31-35), waste incineration (36, 37), coke and asphalt production (38, 39), oil refining (40), aluminum production (41), and many other industrial activities (42). Formation and emission of most PAHs associate with soot emissions during the incomplete combustion of fossil fuels such as during start-up and shut down process of combustion facilities including troubleshooting (32).

Generally, two major mechanisms result in PAH formation and transformation during fossil fuel combustion. One is pyrolysis and the other is pyrosynthesis (43, 44).

<i>PAHs</i>	<i>Structure</i>	<i>Vapor Pressure (Torr) at 20°C</i>	<i>K<sub>ow</sub></i>	<i>Carcinogenic Potency IARC/US EPA Classification</i>
Naphthalene		0.0492	2300	N/A
Acenaphthylene		10 <sup>-3</sup> ~10 <sup>-2</sup>	21000	N/A
Acenaphthene		10 <sup>-3</sup> ~10 <sup>-2</sup>	12000	N/A
Fluorene		10 <sup>-3</sup> ~10 <sup>-2</sup>	15000	N/A
Phenanthrene		6.8×10 <sup>-4</sup>	29000	3
Anthracene		2×10 <sup>-4</sup>	28000	3
Fluoranthrene		10 <sup>-6</sup> ~10 <sup>-4</sup>	34000	3
Pyrene		6.9×10 <sup>-9</sup>	2×10 <sup>5</sup>	3
Benzo(a)anthracene		5×10 <sup>-9</sup>	4×10 <sup>5</sup>	2A/B2
Chrysene		10 <sup>-11</sup> ~10 <sup>-6</sup>	4×10 <sup>5</sup>	3/B2
Benzo(b)fluoranthrene		10 <sup>-11</sup> ~10 <sup>-6</sup>	4×10 <sup>5</sup>	2B
Benzo(k)fluoranthrene		9.6×10 <sup>-7</sup>	7×10 <sup>6</sup>	2B
Benzo(a)pyrene		5×10 <sup>-9</sup>	10 <sup>6</sup>	2A/B2
Indeno(1,2,3-cd)pyrene		~10 <sup>-10</sup>	5×10 <sup>7</sup>	2B/B2
Dibenzo(a,h)anthracene		~10 <sup>-10</sup>	10 <sup>6</sup>	2A/B2
Benzo(g,h,i)perylene		~10 <sup>-10</sup>	10 <sup>7</sup>	3

2A/B2: Probably carcinogenic to humans/Probable human carcinogen; 2B: Possibly carcinogenic to humans; 3: Not classifiable as to human carcinogenicity; N/A: Not tested for human carcinogenicity.  
 \*IARC: International Agency for Research on Cancer; US EPA: US Environmental Protection Agency.

**Table 1.1.** Sixteen PAHs in the U. S. EPA priority pollutant list.

During pyrolysis, the macromolecular aromatic compounds in coal or heavy oil are broken into different size fragments, and these fragments then decompose and form small organic fragments. In the process of pyrosynthesis, these small fragments, mainly highly reactive free radicals, undergo cyclization and aromatization reactions to form polycyclic compounds. A reaction scheme for the formation of aromatic hydrocarbons from radical addition to acetylene is shown in Figure 1.1. In addition to the cyclization of small units to form PAHs, it has been shown that reactions among the growing aromatic species, (e.g. PAH-PAH radical recombination and addition reactions) also contribute to the formation of larger PAHs (45). It has been experimentally proven that PAHs can be synthesized from small molecules. For example, Li and Nelson experimentally synthesized benzo(a)pyrene from ethane under pyrolysis conditions (45).

Previous work also showed that the formation and transformation of PAHs during fossil fuel combustion are affected by combustion conditions. With increased combustion temperatures, intermolecular cyclization among the fragments produced during pyrolysis is expected to be more important. However, high temperature also will produce more energy to break bonds in large molecular weight PAHs. Therefore, these two mechanisms will compete when the combustion temperature is increased. Liu *et al.* sampled flue gas from a lab scale fluidized bed reactor and found small molecular weight PAHs were dominant in gas phase with minimum PAH emissions occurring at 600 °C (32). Besides combustion temperatures, excess air can provide extra O<sub>2</sub> for complete combustion and thus reduces PAH formation. The results of Liu *et al.* showed that combustion temperature and excess air were two very important factors that affected PAHs in fly ash from fluidized bed combustion systems (32).

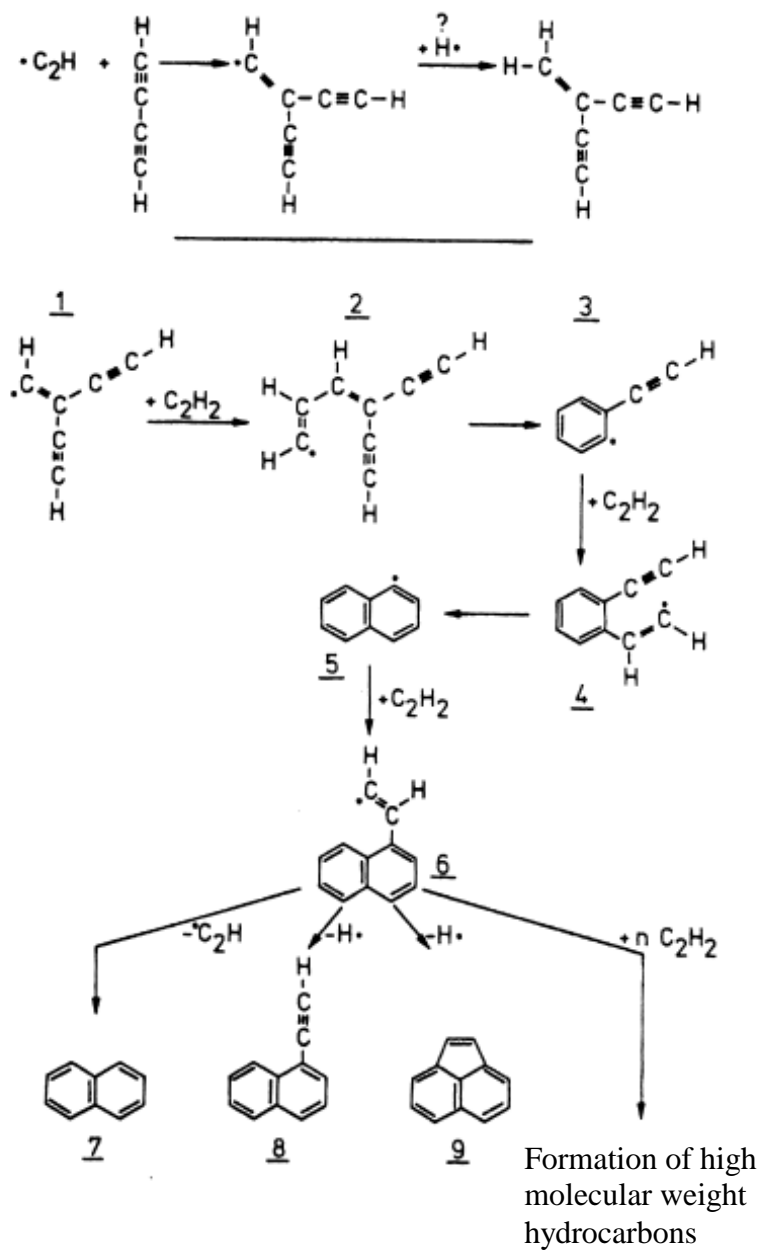


Figure 1.1 Reaction scheme for the formation of aromatic hydrocarbons (46).

Due to their different vapor pressures, different affinities for the solid matrix, and different molecular weights, PAHs generated during fossil fuel combustion can exist in the gas phase or in particulate matter (31, 47). In the particular case of power plants, PAHs in the gas phase are released into the atmosphere through the stack, or PAHs may sorb onto the solid phase such as ash and slag (32, 48).

When the FGD process is installed in a coal combustion power plant, gas phase PAHs may sorb onto the injected lime, limestone, and the formed  $\text{CaSO}_3$ , and  $\text{CaSO}_4$ . In addition, fly ash and associated PAHs may mix with FGD by-products (49). These PAHs may have impacts on the environment when the FGD by-products are reused or disposed. For example, release of the PAHs into groundwater may be possible when the FGD by-products are landfilled. Therefore, investigation of PAHs (e.g., concentration, fate) on FGD by-products is necessary to ensure their environmentally safe reuse.

#### **1.4. Sorption of PAHs on Solid Particles**

PAHs in either vapor phase or dissolved in liquid phase can become associated with solid particles by either adsorption onto a two-dimensional solid surface or absorption into a porous solid such as nature organic matter (NOM) (50). Sorption of PAHs is very important because it may affect the fate of PAHs in environment. Detailed sorption mechanisms of PAHs on solid are discussed below.

Generally, the sorption of PAHs can be divided into four steps (51): (1) *Bulk transfer* PAH molecules are transported from bulk solution to the boundary layer of water surrounding the adsorbent particle. In gas/solid systems, PAHs in the gas phase must be transported to the boundary layer of gas surrounding solid particles. This process

occurred by diffusion and usually can be enhanced by turbulent mixing. (2) *Film diffusion* PAH molecules are transported through the boundary layer by molecular diffusion. The transport distance and time for this step are determined by the flow rate past the particle. Higher flow rate will result a shorter transport distance and time. (3) *Intraparticle diffusion* PAH molecules are transported through the adsorbent's pores to available adsorption sites, which can be accomplished by molecular diffusion of PAHs through the solution of pores (pore diffusion), or diffusion along the adsorbent surface (surface diffusion). (4) *Adsorption* PAH molecule interacts with the solid surface by either physisorption or chemisorption. For physisorption, PAH molecule may interact with the surface by Van der Waals force, weak dipole-dipole, and dipole-induced dipole forces (52). As for chemisorption, chemical reaction (e.g., hydrogen bond and surface complexation) will occur.

Sorption of PAHs by soils and sediments has been shown to be controlled by the mineral type and organic carbon content in solid. Chin *et al.* conducted binding of pyrene to aquatic and commercial humic substances (53) and showed that the molecular weight and the aromatic content of the humic substrates affected the binding of nonpolar and planar aromatic molecules. From direct analysis of separated fractions and particle-scale microanalysis, Ghosh *et al.* (54) found the majority of PAHs in the sediment was associated with coal-derived particles and these PAHs were strongly adsorbed on these particles. Some PAHs can penetrate into carbonaceous particles approximately 5  $\mu\text{m}$  depth. Their recent study on PAH speciation among different types of carbonaceous particles including coal, coke, charcoal, pitch, cenospheres, and wood showed that

adsorption of PAHs on coal tar pitch was weaker compared with PAH adsorption on coal, coke, charcoal and cenosphere (55).

The carbonaceous material is also believed to be the dominant factor for adsorption of PAHs on fly ash (56). However, the physical differences in the nature of the carbon and the accessibility of the carbon sites in the ashes affect PAH adsorption. Soltys *et al.* suggested that fly ash samples from different sources had different proportions of carbonaceous matter resulting in different specific surface areas and adsorptive affinities for benzo(a)pyrene (57). Low and Batley noted that the carbon particles in the fly ash from brown coal were more porous than those in the fly ash from the bituminous coals (58). They postulated that adsorption of PAHs on bituminous coal fly ash occurred principally on the surface of particles, whereas for the brown coal fly ashes, adsorption occurred both on the surface and through the pores of the particles.

The properties of different PAHs such as molecular size and structure and concentration also affect their adsorption. Generally, PAH molecules have a planar configuration, these molecules can closely reach the sorption surface, creating the possibility of favorable  $\pi$ - $\pi$  cloud overlap between the flat aromatic sorbate and sorbent structures and thus enhance the sorption (59). Mastral *et al.* showed that the higher the number of rings, the lower the influence of the adsorbent microporosity on adsorption. Moreover, the interactions between PAH molecules and adsorbate were more favored when the number of aromatic rings was increased (48). Similarly, Low and Batley showed that the adsorption of PAHs on fly ash samples increased with increasing molecular size (58). Erucenab and Vandiver (60) demonstrated that adsorption of PAHs on fly ash was controlled by the concentration level of PAHs in the flue gas. At low

concentrations, strong and irreversible chemisorption is the major mechanism. However, at high concentrations, physisorption plays more important roles.

### **1.5. Analytical Procedure of Measuring PAHs on Solid Matrices**

Appropriate analytical procedures are critical to obtain the speciation and concentrations of PAHs on a solid matrix. A common analytical procedure for PAHs on solid matrices is extraction followed by instrumental analysis. The purpose of extraction is to transfer the sorbed PAHs from the solid phase into organic solvents. Several extraction methods have been used to extract PAHs. For example, Soxhlet extraction, ultrasonic extraction, supercritical fluid extraction (SFE), pressurized fluid extraction (PFE), and microwave assisted extraction (MAE) have all been used.

Soxhlet extraction is the most commonly used extraction method (61). It requires a large volume (up to 150 mL) of organic solvent to be refluxed through the solid sample for 6 to 24 hours. This method is time-consuming although several extraction set-ups can be assembled and operated simultaneously (62). By using a commercial extraction unit, the extraction time can be reduced to several hours using automatic Soxhlet extraction. In this method, a specified amount of sample is weighed into a cellulose thimble and extracted for 1 hr in the boiling extraction solvent. The thimble with sample is then raised into the rinse position and extracted for an additional hour. The extraction solvent is concentrated to 1 to 2 mL after the extraction (63). Both Soxhlet and automatic Soxhlet extraction have been standardized as EPA methods 3540C (64) and EPA method 3541 (63), respectively.

Either an ultrasonic probe or cleaning bath is used in ultrasonic extraction to extract semivolatile and nonvolatile organic compounds from solid matrices. Solid samples are sonicated in a glass beaker or flask for times ranging from minutes to hours. The U. S. EPA issued standard method 3550B for ultrasonic extraction (65) using an ultrasonic probe.

Supercritical fluid extraction exploits the gas-like and liquid-like properties of a supercritical fluid, typically carbon dioxide, to extract PAHs from solid matrices (66). There are two U.S. EPA standard methods issued for the SPE of PAHs: Method 3561 (67) and Method 3560 (68) for the total recoverable petroleum hydrocarbons from soils. However, SFE is not widely used partially due to the relatively high capital cost of the instrument.

Standardized as EPA method 3545, pressurized fluid extraction (PFE), also known as accelerated solvent extraction (ASE), has been commercially available since 1995. In PFE, organic solvents are used to sequentially extract PAHs from the solid matrix with the addition of pressure and heat (69). By using ASE, the average extraction time is 12 min. Although the fast extraction time and lower solvent usage are advantageous, the high cost of the instrument makes it impossible to be widely used (70).

Another instrumental extraction technique is microwave assisted extraction (MAE). In MAE, organic solvent and the sample are subjected to radiation from a magnetron in either a sealed vessel or an open vessel. MAE allows multiple samples to be extracted simultaneously. The major limitation of MAE is that solvent needs to be physically removed from the sample matrix upon completion of the extraction prior to analysis (71).

Frequently the extraction technique is chosen based on initial capital cost, operating costs, simplicity of operation, amount of organic solvent required and sample throughput (72). It is necessary to compare several extraction methods to find the most efficient one for a specific solid matrix. Previous studies have been conducted to compare extraction methods to extract PAHs from different matrices including soil (62, 63), sediment (74), and fly ash (75). The results showed that quantification of the PAHs was affected by different extraction methods (76). For example, the study by Blankenhorn et al. (1992) showed the difficulty in comparing the results obtained by different extraction methods for soil samples (77).

After extraction, the extract is usually condensed and analyzed by gas chromatography (GC) with flame ionization detector (FID), gas chromatography-mass spectrometry (GC-MS), liquid chromatography (LC), and liquid chromatography-mass spectrometry (LC-MS).

Other techniques have been used to identify PAHs on solid matrices. Ghosh et al. used microprobe two-step laser desorption/laser ionization mass spectrometry ( $\mu\text{L}^2\text{MS}$ ) to characterize the distribution of trace PAHs on sediment particles (54). A pulsed infrared laser beam focused on a 40  $\mu\text{m}$  diameter area of a particle to desorb constituent molecules spatially. The desorbed molecules were selectively ionized with a pulsed ultraviolet laser at 266 nm. The resulting ions were extracted into a time-of-flight mass spectrometer (TOF) to measure PAHs (78). Thermal extraction (TE) coupled with gas chromatography/time-of-flight mass spectrometry (GC/TOF-MS) has also been used to determine the PAH concentrations on fly ash samples (79). Samples were thermally extracted at 340 °C to desorb PAH molecules from the solid matrix into gas phase.

Carbon-carbon bonds remain unaltered at this temperature. The gas is then trapped and separated through GC/TOF-MS.

### **1.6. Ultrasound and Cavitation in Ultrasonic Extraction**

As stated in U.S. EPA standard method 3550B, the extraction time is only 9 min when an ultrasonic probe is used for ultrasonic extraction. The principles of ultrasound are reviewed to understand the mechanisms related to ultrasonic extraction.

Ultrasound is the sound wave with frequencies higher than 16 kHz. When ultrasound is transmitted through a liquid media, the average distance between the molecules in a liquid will vary as the molecules oscillate about their mean position (80). The application of a sufficiently large negative pressure will force the molecules to exceed the critical molecular distance necessary to hold the liquid intact. As a result, the liquid will then break down and voids will be created to form cavitation bubbles (80).

There are two types of cavitation bubbles: stable and transient. Stable cavitation bubbles are those that oscillate about the equilibrium size and can exist for many cycles. The transient cavitation bubbles can expand to a radius of at least twice their initial size before collapsing violently upon compression (80). They exist for one, or at most a few acoustic cycles. The cavitation bubble collapses can result in localized hot spots with high temperatures and pressures (81). The temperature and pressure upon cavitation bubble collapse can be calculated by the following equations (80):

$$T_{\max} = T_0 \left( \frac{P_m (\gamma - 1)}{P} \right) \quad (3)$$

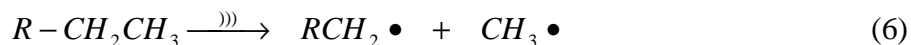
$$P_{\max} = P \left( \frac{P_m (\gamma - 1)}{P} \right)^{\frac{\gamma}{\gamma - 1}} \quad (4)$$

where  $T_0$  is the ambient temperature,  $\gamma$  is the ratio of specific heats of the gas or gas vapor mixture,  $P$  is the pressure in the bubble at its maximum size and is usually assumed to be equal to the vapor pressure  $P_v$  of the liquid. Based on equations (3) and (4), temperatures and pressures in a vaporous water bubble can reach several thousand Kelvin and hundreds of atmospheres, respectively (82). Upon the collapse of cavitation bubbles in organic alkene solvents, the temperature is estimated to reach 5000 K (83).

Collapse of cavitational bubbles also produces a number of mechanical effects such as microstreaming and microjet formation. Microstreaming is a time-independent circulation of fluid occurring in the vicinity of bubbles set into motion by oscillating sound pressure. Oscillations in bubble size cause rapid fluctuations in the magnitude and direction of fluid movement. As a result, significant shear forces occur (82). The effective range of this mechanism is on the order of a bubble diameter (depending on acoustic pressure amplitude and frequency) (84). When cavitation bubbles collapse near a solid surface that is several orders of magnitude larger than a cavitation bubble, collapse occurs asymmetrically. This asymmetric collapse results a fast moving stream of liquid passing through the cavity and thus impacting the surface of the solid at high velocity range from 100 to 1000 m/s (85). This phenomenon is called a microjet.

Ultrasonic extraction is due to the physical and mechanical effects resulting from the collapse of cavitation bubble. For example, high temperature improves solubility and diffusivity of solute. High pressure upon bubble collapse enhances penetration of the solvent and transfer of the adsorbed solutes from the solid matrix (86). Moreover, shock waves and shear forces are produced due to microstreaming, can create microscopic turbulence within interfacial films surrounding nearby solid particles (87), and can thus increase mass transfer across the film and the intrinsic mass-transfer coefficient (88). Microjets of solvent are formed perpendicular to the solid surface, and lead to pitting and erosion of the surface, reducing the path length for diffusion from the solid to the solvent (89).

Chemical effects of ultrasound have been observed in addition to the physical and mechanical effects. These high temperatures and pressures dissociate water or other liquid media molecules into radicals. For example, water molecules are broken down to form hydrogen atoms ( $H\bullet$ ) and hydroxyl radicals ( $OH\bullet$ ) due to the pyrolysis of water (90). Alkane radicals are generated by dissociating alkane solvents (91).



Therefore, it is possible that during the ultrasonic extraction, the high temperature may lead to the pyrolysis reaction of PAHs. The formed radicals due to the dissociation of solvent molecules may attack PAH molecules to form other byproduct by radical

reactions. Thus, undesired reaction of solute may also occur due to the ultrasonic energy and thus affect quantification results.

Previous researches on the sonochemical decomposition of solute have been predominantly conducted in aqueous solution (92-94). For example, Lu and Weavers demonstrated that sonication was an effective way to desorb and degrade 4-chlorophenol from synthetic sediments (95). Psillakis et al. (2004) studied sonolytic degradation of naphthalene, acenaphthylene, and phenanthrene in water with an ultrasonic probe. A complete degradation of PAHs was observed after 120 min, primarily due to the oxidation of PAHs by  $\text{OH}\cdot$  (96). As to the sonochemistry of solutes in organic solvents, it remains largely unexplored. Therefore, an investigation on the possible decomposition of PAHs in organic solution is necessary to elucidate the effect of ultrasound on PAHs during extraction.

### **1.7. Dissertation Overview**

The primary goal of this research was to examine PAHs on dry FGD by-products to ensure their environmentally safe use. Due to the lack of information on analytical procedures for qualifying PAHs on FGD by-products, my initial work focused on analytical method development. Several extraction methods including traditional Soxhlet extraction, automatic Soxhlet extraction, and ultrasonic extraction were compared for extracting PAHs from lime spray dryer (LSD) ash (a common dry FGD by-product). The short extraction time in ultrasonic extraction is an advantage for handling large numbers of samples. Therefore, ultrasonic extraction was then optimized by testing different

organic solvents. Ultrasonic extraction with toluene turned out to be a fast and efficient method to extract PAHs from LSD ash.

There was a concern over the possible degradation of PAHs by ultrasound. Thus, the investigation on the possible reactions of PAHs under standard ultrasonic extraction conditions was then conducted. During ultrasonic extraction, sorption of PAHs onto the solid particles, desorption of PAHs from solid particles, and sonolytic reactions of PAHs may occur at the same time. In such a heterogeneous system, it is hard to distinguish the reactions of PAHs from sorption and desorption. Therefore, a simple homogenous system, organic solution containing model PAHs, was used to examine the reactions of PAHs during sonication. This work is important because the choice of analytical procedures may affect the results, and ultrasonic extraction is a widely accepted method for extracting PAHs from soil and sediment.

After analytical method determinations, investigations on the speciation and concentrations of PAHs on LSD ash were conducted. Because changes in characteristics of the FGD by-products discourage reuse, daily, weekly, and monthly variability of PAHs on the LSD ash was examined. The detailed work on variability of PAHs is described in Appendix A. The reason this work is presented in the appendix is because it is a collaborative work between a number of students and faculty members in The Ohio State University, it is difficult for one person to take full credit.

Preliminary results suggested that total measured PAH concentrations correlated with the organic carbon content of the LSD ash. Therefore, it is hypothesized that PAHs may be primarily associated with unburned carbon in the LSD ash. Fractionation of LSD

ash samples and separation of unburned carbon were then conducted. PAH measurements of different fractions were performed to test the hypothesis.

In Chapter 5, dry FGD by-products collected from the Ohio State carbonation and ash reactivation (OSCAR) process were examined for PAHs. Compared to conventional dry FGD technology, the OSCAR process has an additional sorbent activation procedure to regenerate sorbents from either LSD ash or lime to improve the sulfur capture efficiency (97). During this activation procedure, PAHs in the flue gas may sorb on the activated sorbent. Accordingly, when the activated sorbent are injected into the OSCAR process, it is interesting to find out the fate of these sorbed PAHs. In addition, the effects of raw materials and operation conditions on PAHs on the solid by-products in the OSCAR process were also studied.

Appendix B is the result of a laboratory study in which I participated during my PhD studies. This work is a collaborative work between a number of students focusing on gaseous mercury released from dry-curing concretes that contain fly ash and powdered activated carbon loaded with mercury. Since Hg is not the main focus of the dissertation, this work does not appear as a chapter.

### **1.7.1. Characterization of PAHs on Dry FGD By-products: Effects of Extraction Method**

In Chapter 2, a comparative study on the traditional Soxhlet, automatic Soxhlet, and ultrasonic extraction for extracting PAHs from LSD ash was conducted. LSD ash samples collected from the McCracken Power Plant were doped with a mixture of 16 U.S. EPA specified PAHs to measure matrix spike recovery rates. In order to take

advantage of the short extraction time in ultrasonic extraction, this method was further optimized by examining different solvents including dichloromethane (DCM), DCM: acetone (1:1 V/V), hexane: acetone (1:1 V/V) and toluene. The results showed that ultrasonic extraction with toluene can achieve the highest extraction efficiency for PAHs. Comparison of the speciation and concentration of PAHs obtained from different extraction methods showed that quantification results were affected by different sample preparation procedures. However, the concentrations of PAHs measured were constantly low no matter which extraction method was used.

### **1.7.2. Sonolytic Reactions of PAHs in Organic Extraction Solutions**

With naphthalene, phenanthrene, and pyrene as model compounds, the reactions of PAHs in common organic extraction solutions were explored using a 20 kHz ultrasonic probe under conditions specified by the U. S. EPA standard method 3550B to elucidate their possible degradation during sonication. Two commonly used solvents: hexane: acetone (1:1 V/V) and dichloromethane (DCM): acetone (1:1 V/V) were tested. Results showed that the hexane/acetone mixture resulted in fewer PAH reactions than the DCM/acetone mixture possibly due to weaker cavitation effects. Several factors including the initial PAH concentration in solution, length of sonication time, and solvent type were examined to test their effects on the reactions of phenanthrene. Degradation by-products including methyl-phenanthrene and methyl-naphthalene were identified after sonication of phenanthrene suggesting that phenanthrene reacts by both direct pyrolysis and reaction with methyl radicals formed from solvent pyrolysis.

### **1.7.3. Distribution of PAHs in Lime Spray Dryer Ash**

Previous work by other researchers focused on the distribution of PAHs on sediment (55) and soil (98). However, no work on the distribution of PAHs in LSD ash has been reported. Therefore, in chapter 4, the distribution of PAHs in LSD ash was investigated to test if PAHs were primarily associated with carbonaceous materials in the LSD ash.

Collected from the McCracken Power Plant, 4 LSD ash samples with different organic carbon contents were separated into lime-enriched and carbon-enriched fractions. The unburned carbon was further separated from the carbon-enriched fractions with a lithiumheteropolytungstate (LST) solution. Measurements of PAHs on these different fractions were performed to study the distribution of PAHs. The results showed that the PAH concentrations in unburned carbon were the highest followed by the carbon-enriched fraction indicating an enrichment of PAHs on carbonaceous material in the LSD ash. Interestingly, detectable levels of PAHs was also found in the lime-enriched fraction, suggesting the fine spray of  $\text{Ca}(\text{OH})_2(\text{s})$  in LSD process may sorb PAH compounds from the flue gas. Information on the distribution of PAH on LSD ash obtained in this study will help to evaluate their fate in the environment and thus suggesting appropriate ways for utilization or disposal of LSD ash.

### **1.7.4. PAHs on By-products in the Ohio State Carbonation and Ash Reactivation (OSCAR) Process**

Compared to the conventional dry FGD process, the Ohio State carbonation and ash reactivation (OSCAR) process uses activated sorbents generated from LSD ash or

lime to react with  $\text{SO}_2$  in the flue gas. The PAHs on the solid by-products generated during the OSCAR process may be different from the LSD ash due to the sorbent activation process. In Chapter 5, the PAH measurements on solid by-products collected from the OSCAR process were performed. Also, effects of operational conditions such as raw material and sorbent injection rates, and flue gas flow rates on PAH concentrations on FGD by-products were studied. Understanding these effects can help to minimize PAHs on FGD by-products and also give suggestions to process design.

## References

1. Energy Information Administration, International Energy Outlook-2002, Office of Integrated Analysis and Forecasting, US department of Energy, Washington, DC 20585, DOE/EIA-0484, **2002**.
2. The United States Environmental Protection Agency, <http://www.epa.gov/airmarkets/acidrain/#what.html>, accessed on Oct 15, 2004.
3. Satriana, M. New Developments in Flue Gas Desulfurization Technology, Noyes Data Corporation, New Jersey, 1981.
4. Dry Scrubbing Technologies for Flue Gas Dusulfurization, Kluwer Academic Publishers, Boston/Dordrecht/London, 1998.
5. New Developments in Flue Gas Desulfurization Technology, Pluution technology review No. 82, Satriana, M. (Eidtor), Noyes Data Corporation, Park Ridge, NJ, 1981.
6. U.S. Environmental Protection Agency. Wastes form the Combustion of Fossil Fuels, Volume 1 and 2- Methods, Findings, and Recommendations, Report to Congress, EPA 530-S-99-010, March 1999.
7. U.S. Environmental Protection Agency. Wastes form the Combustion of Coal by Electric Utility Power Plants, Report to Congress, EPA 530-SW-88-002, February 1988.
8. Punshon, T.; Knox, A. S.; Adriano, D. C.; Seaman, J. C.; Weber, J. T. Flue gas desulfurization (FGD) residue potential applications and environmental issues. In Sajwan et al (editor) Biogeochemistry of Trace Elements in Coal and Coal

- Combustion Byproducts. Kluwer Academic/Plenum Publishers, New York, 1999. pp 7-8.
9. American Coal Ash Association, 2003 Coal Combustion Product (CCP) Production and Use Survey, [http://www.aaa-usa.org/PDF/2003\\_CCP\\_Survey\(10-1-04\).pdf](http://www.aaa-usa.org/PDF/2003_CCP_Survey(10-1-04).pdf) (accessed October 15, 2004).
  10. American Coal Ash Association Survey (1997). 1996 coal combustion product (CCP) production and use. American Coal Ash Association, Alexandria, VA.
  11. Walker H, Taerakul P, Butalia T, Wolfe W, Dick W. Minimization and Use of Coal Combustion By-Products: Concepts and Applications. In: Ghassemi A. editors. The Handbook of Pollution Control and Waste Minimization, New York: Marcel Dekker, 2002.
  12. Butalia, T.; Dyer, P.; Stowell, R.; Wolfe, W. W.; Construction of Livestock Feeding and Hay Bale Storage Pads Using FGD Material, The Ohio State Extension Fact Sheet, AEX-332-99, Columbus, Ohio: The Ohio State University, 1999.
  13. Butalia, T.; Wolfe, W. W.; Re-Use of Clean Coal Technology By-Products in the Construction of Impervious Liners. 1997 Ash Utilization Symposium, Lexington, Kentucky, 1997.
  14. Lamminen, M. O.; Wood, J., Walker, H. W.; Chin, Y.-P.; He Y.; Traina, S. Effects of flue gas desulfurization (FGD) by-product on water quality at an underground coal mine. *J Environ. Quality* **2001**, *30*, 1371-1381.
  15. Butalia, T.; Wolfe, W. W.; Lee, J.W. Evaluation of a dry FGD material as a flowable fill. *Fuel* **2001**, *80*, 845-850.

16. Stehouwer R.; Sutton P.; Folwer R.; Dick W. Minespoil amendment with dry flue gas desulfurization by-products: element solubility and mobility. *J. Environ. Quality* **1995**, *24*, 165-174.
17. Ahn, C.; Mitsch, W. J.; Wolfe, W. E. Effects of recycled FGD liner material on water quality and macrophytes of constructed wetlands: A mesocosm experiment. *Wat. Res.* **2001**, *35*, 633-642.
18. Stehouwer R.; Sutton P.; Dick W. Transport and plant uptake of soil-applied dry flue gas desulfurization by-products. *Soil Sci.* **1996**, *161*, 562-574.
19. Sloan J. J.; Dowdy R. H.; Dolan, M. S.; Rehm, G. W. Plant and soil response to field-applied flue gas desulfurization residue. *Fuel* **1999**, *78*, 169-174.
20. Crews, J. T.; Dick, W. A. Liming acid forest soils with flue gas desulfurization by-product: growth of Northern red oak and leachate water quality, *Environ. Pollution* **1998**, *103*, 55-61.
21. Clark, R.; Ritchey, K.; Baligar, V. C. Benefits and constraints for use of FGD products on agricultural land. *Fuel* **2001**, *80*, 821-828.
22. Harvey, R. G. Polycyclic Aromatic Hydrocarbons, Chemistry and Carcinogenicity. Cambridge University Press, Cambridge/ New York/ Port Chester/ Melbourne/ Sydney, 1991.
23. Arzayus, K.; Dickhut, R.; Canuel, E. Fate of atmospherically deposited polycyclic aromatic hydrocarbons (PAHs) in Chesapeake Bay. *Environ. Sci. Technol.* **2001**, *35*, 2178-2183.
24. Laflamme, R. E. and Hites, R. A. The global distribution of polycyclic aromatic hydrocarbons in recent sediments. *Geochim. Cosmochim. Acta* **1978**, *42*, 289-303.

25. Ebert, L. B. *Polynuclear aromatic compounds*. American Chemical Society, Washington, D.C., 1988.
26. Polynuclear aromatic compounds, part 1: chemical, environmental and experimental data, International Agency for Research on Cancer, Lyon, France, 1983.
27. Mastral, A. M.; Callen, M.; Murillo, R. PAH atmospheric contamination from coal combustion. *Polycyclic Aromatc. Compds.* **1996**, *9*, 37-44.
28. Denissenko, M. F.; Pao, A.; Tang, M-S.; Pfeifer, G. P. Preferential formation of benzo[*a*]pyrene adducts at lung cancer mutational hotspots in *P53*. *Science* **1996**, *274*, 430-432.
29. US EPA, List of the Sixteen PAHs with Highest Carcinogenic Effect, IEA Coal Research, London, 1984.
30. Manoli, E.; Samara, C. Polycyclic aromatic hydrocarbons in nature waters: sources, occurrence and analysis. *Trends in Anal. Chem.* **1999**, *16*, 417-428.
31. Mastral, A. M.; Callen, M. S.; Murillo, R.; Garcia, T. Polycyclic aromatic hydrocarbons and organic matter associated to particulate matter emitted from atmospheric fluidized bed coal combustion. *Environ. Sci. Technol.* **1999**, *33*, 3177-3184.
32. Liu, K-L.; Xie, W.; Zhao, Z-B.; Pan, W-P.; Riley, J. T. Investigation of polycyclic aromatic hydrocarbons in fly ash from fluidized bed combustion systems. *Environ. Sci. Technol.* **2000**, *34*, 2273-2279.

33. Pisupati, S. V.; Wasco, R. S.; Scaroni, A. W. An investigation on polycyclic aromatic hydrocarbon emissions from pulverized coal combustion systems. *J. Hazard. Mater.* **2000**, *74*, 91-107.
34. Wang, Z.; Fingas, M.; Shu, Y. Y.; Sigouin, L.; Landriault, M.; Lambert, P.; Turpin, R.; Campagna, P.; Mullin, J. Quantitative characterization of PAHs in burn residue and soot samples and differentiation of pyrogenic PAHs from petrogenic PAHs—the 1994 mobile burn study. *Environ. Sci. Technol.* **1999**, *33*, 3100-3107.
35. Thikim O. N.; Nghiem, L. H.; and Phyu, Y. L. Emission of polycyclic aromatic hydrocarbons, toxicity, and mutagenicity from domestic cooking using sawdust briquettes, wood, and kerosene. *Environ. Sci. Technol.* **2002**, *36*, 833-839.
36. Levendis, Y. A.; Alta, A.; Carlson, J.; Dunayevshiy, Y.; Vouros, P. Comparative study on the combustion and emissions of waste tire crumb and pulverized coal. *Environ. Sci. Technol.* **1996**, *30*, 2742-2754.
37. Durlak, S. K.; Biswas, P.; Shi, J.; Bernhard, M. J. Characterization of polycyclic aromatic hydrocarbon particulate and gaseous emissions from polystyrene combustion. *Environ. Sci. Technol.* **1998**, *32*, 2301-2307.
38. Kirton, P. J.; Ellis, J.; Crisp, P. T. The analysis of organic matter in coke oven emissions. *Fuel* **1991**, *70*, 1383-1389.
39. Thompson, D. Comparison of observed and predicted equilibrium PAH concentrations in coke oven emissions: I. Relative abundances of carbon-hydrogen PAH. *Chemosphere* **1997**, *35*, 597-606.

40. Fixari, B.; Perchec, P. L.; Kopinke, F-D.; Zimmermann, G.; Decroocq, D.; Thomas, M. <sup>14</sup>C polyaromatics as radio isotope tracers for grafting analysis during heavy oil pyrolysis. *Fuel* **1994**, *73*, 505-509.
41. Baek, S. O.; Field, R. A.; Goldstone, M. E.; Kirk, P. W.; Lester, J. N.; Perry, R. A review of atmospheric polycyclic aromatic hydrocarbons: sources, fate and behavior. *Water Soil Pollut.* **1991**, *60*, 279-300.
42. Junk, G. A.; Ford, C. S. A review of organic emissions from selected combustion processes. *Chemosphere* **1980**, *9*, 187-230.
43. Ledesma, E. B.; Kelish, M. A.; Nelson, P. F.; Wornat, M. J.; Mackie, J. C. Formation and fate of PAH during the pyrolysis and fuel-rich combustion of coal primary tar. *Fuel* **2000**, *79*, 1801-1814.
44. Richter, H.; Howard, J. B. Formation of polycyclic aromatic hydrocarbons and their growth to soot—a review of chemical reaction pathways. *Progress in Energy and Combustion Science* **2000**, *26*, 565-608.
45. Li, C. Z.; Nelson, P. F. Fate of aromatic ring systems during thermal cracking of tars in a fluidized-bed reactor, *Energy Fuels* **1996**, *10*, 1083-1090.
46. Bockhorn, H.; Fetting, F.; Wenz, H. W. Investigation of the formation of high molecular hydrocarbons and soot in premixed hydrocarbon-oxygen flames. *Ber Bunsenges Phys. Chem.* **1983**, *87*, 1067-1073.
47. Hyes, M. D.; Geron, C. D.; Linna, K. J.; Smith, N. D.; Schauer, J. J. Speciation of gas-phase and fine particle emissions from burning of foliar coal. *Environ. Sci. Technol.* **2002**, *36*, 2281-2296.

48. Mastral, A. M.; and Callen, M. S. A review on polycyclic aromatic hydrocarbon (PAH) emissions from energy generation. *Environ. Sci. Technol.* **2000**, *34*, 3051-3057.
49. Stewart, B. R.; and Kalyoncu, R. S. Proceedings, 1999 International Ash Utilization Symposium, Lexington, KY, October, 1999.
50. Schwarzenbach, R. P.; Gschwend, P.M.; and Imboden, D. M. *Environmental Organic Chemistry*, John Wiley & Sons Inc. 1993.
51. Letterman, R. D. *Water Quality & Treatment: A Handbook of Community Water Supplies*, McGraw-hill, 1999.
52. Pignatello, J. J. Soil organic matter as a nanoporous sorbent of organic pollutants. *Advances in Colloid and Interface Science* **1998**, *76-77*, 445-467.
53. Chin, Y-P.; Aiken, G. R.; Danielsen, K. M. Binding of pyrene to aquatic and commercial humic substances: The role of molecular weight and aromaticity *Environ. Sci. Technol.* **1997**, *31*, 1630-1635.
54. Ghosh, U.; Talley, J. W.; Luthy, R. G. Microscale location, characterization, and association of polycyclic aromatic hydrocarbons on harbor sediment particles. *Environ. Sci. Technol.* **2000**, *34*, 1729-1736.
55. Ghosh, U.; Zimmerman, J.; Luthy, R. G. PCB and PAH speciation among particle types in contaminated harbor sediments and effects on PAH bioavailability. *Environ. Sci. Technol.* **2003**, *37*, 2209-2217.
56. Low, G. K.; Batley, G. E. Use of liquid chromatography for the measurement of adsorption isotherms for polycyclic aromatic hydrocarbons on coal fly ashes. *J. Chromatogr.* **1986**, *355*, 177-191.

57. Soltys, P. A.; Mauney, T.; Natusch, D. F. S.; Schure, M. R. Time-resolved solvent extraction of coal fly ash: retention of benzo(a)pyrene by carbonaceous components and solvent effects. *Environ. Sci. Technol.* **1986**, *20*, 175-180.
58. Low, G. K. C.; Batley, G.E. Comparative studies of adsorption of polycyclic aromatic hydrocarbons by fly ashes from the combustion of some australian coals *Environ. Sci. Technol.* **1988**, *22*, 322-327.
59. Jonker, T.; Koelmans, A. Extraction of polycyclic aromatic hydrocarbons from soot and sediment: solvent evaluation and implications for sorption mechanism. *Env. Sci. Technol.* **2002**, *36*, 4107-4113.
60. Eiceman, G.A.; Vandiver, V. J. Adsorption of polycyclic aromatic hydrocarbons on fly ash from municipal incinerators and coal-fired power plants. *Atmos. Environ.* **1983**, *17*, 461-466.
61. Lee, M. L.; Hites, R. A. Characterization of sulfur-containing polycyclic aromatic compounds from carbon black. *Anal. Chem.* **1976**, *48*, 1890-1893.
62. Dean, J. R.; Xiong, G-H. Extraction of organic pollutants from environmental matrices: Selection of extraction technique. *Trends in Analytical Chemistry*, **2000**, *19*, 553-564.
63. *Method 3541, Automatic Soxhlet Extraction*; 1996, U.S. Environmental Protection Agency.
64. *Method 3540C, Soxhlet Extraction*; 1996, U.S. Environmental Protection Agency.
65. *Method 3550B, Ultrasonic Extraction*; 1996, U.S. Environmental Protection Agency.

66. Smith, R. M. Supercritical fluids in separation science—the dreams, the reality and the future. *J. Chromatogr. A* **1999**, *856*, 83-115.
67. *Method 3561, Supercritical fluid extraction for polynuclear aromatic hydrocarbons*; 1996, U.S. Environmental Protection Agency.
68. *Method 3560, Supercritical Fluid Extraction of Total Recoverable Petroleum Hydrocarbons*; 1996, U.S. Environmental Protection Agency.
69. *Method 3545, Pressurized Fluid Extraction*; 1996, U.S. Environmental Protection Agency.
70. Camel, V. Recent extraction techniques for solid matrices—supercritical fluid extraction, pressurized fluid extraction and microwave-assisted extraction: their potential and pitfalls. *Analyst* **2001**, *126*, 1182-1193.
71. Lopez-Avila, V.; Young, R.; Kim, R.; Becket, W. F. Accelerated Extraction of Organic Pollutants Using Microwave Energy. *J. Chromatogr. Sci.* **1995**, *33*, 481-485.
72. Saim, N.; Dean, J. R.; Abdullah, M. P.; Zakaria, Z. Extraction of polycyclic aromatic hydrocarbons from contaminated solid using Soxhlet extraction, pressurized and atmospheric microwave-assisted extraction, supercritical fluid extraction and accelerated soil extraction. *J. Chromatogr. A* **1997**, *791*, 361-366.
73. Noordkamp, E. R.; Grotenhuis, J. T. C.; Rulkens, W. H. Selection of an efficient extraction method for the determination of polycyclic aromatic hydrocarbons in contaminated soil and sediment. *Chemosphere* **1997**, *35*, 1907-1917.

74. Song, Y. F.; Jing, X.; Fleischmann, S.; Wilke, B. M.; Comparative study of extraction methods for the determination of PAHs from contaminated soils and sediments. *Chemosphere* **2002**, *48*, 993-1001.
75. Kenny, D.; Olesik, S. Extraction of lignite coal fly ash for polynuclear aromatic hydrocarbons: modified and unmodified supercritical fluid extraction, enhanced-fluidity solvents, and accelerated solvent extraction. *J. Chromatogr. Sci.* **1998**, *36*, 59-65.
76. Jonker, T.; Koelmans, A. Extraction of polycyclic aromatic hydrocarbons from soot and sediment: solvent evaluation and implications for sorption mechanism. *Env. Sci. Technol.* **2002**, *36*, 4107-4113.
77. Blankenhorn, I.; Meijer, D.; Van Delft, R. Inter-laboratory comparison of methods used for analyzing polycyclic aromatic hydrocarbons (PAHs) in solid samples. *Fresenius' J. Anal. Chem.* **1992**, *343*, 497-504.
78. Gillette, J. S.; Luthy, R. G.; Clemett, S. J.; Zare, R. N. Direct observation of polycyclic aromatic hydrocarbons on geosorbents at the subparticle scale. *Environ. Sci. Technol.* **1999**, *33*, 1185-1192.
79. Liu, K-L.; Heltsley, R.; Zou, D-Z.; Pan, W-P.; Riley, J. T. Polyaromatic hydrocarbon emissions in fly ashes from an atmospheric fluidized bed combustor using thermal extraction coupled with GC/TOF-MS. *Energy Fuels* **2002**, *16*, 330-337.
80. Lorimer, J. P.; Mason, T. J. Sonochemistry, part 1: the physical aspects. *Chem. Soc. Rev.* **1987**, *16*, 239-274.

81. Suslick, K. S.; Doktycz, J.; Flint, E. B. On the origin of sonoluminescence and sonochemistry. *Ultrasonics* **1990**, *28*, 280-290.
82. Suslick, K. S. *Ultrasound: Its Chemical, Physical and Biological Effects*; VCH Publishers, Inc.: New York, 1988.
83. Flint, E. B.; Suslick, K. S. The temperature of cavitation. *Science* **1991**, *253*, 1397-1399.
84. Verraes, T.; Lepoint-Mullie, F.; Lepoint, T.; Longuet-Higgins, M. S. Experimental study of the liquid flow near a single sonoluminescent bubble. *J. Acoust. Soc. Am.* **2000**, *108*, 117-125.
85. Leighton, T.G. *The Acoustic Bubble*, Academic Press: San Diego, 1994.
86. Margulies, T. S.; Schwarz, W. H. Sound wave propagation in fluids with coupled chemical reactions. *J. Acoust. Soc. Am.* **1985**, *78*, 605-615.
87. Doktycz, S. J.; Suslick, K. S. Interparticle collisions driven by ultrasound. *Science* **1990**, *247*, 1067-1069.
88. Wilhelm, A. M.; Contamine, F.; Berlan, J.; Berlan, J.; Delmas, H. Measurement of liquid-solid mass transfer in ultrasonic reactor. *Ultrasonics International 93 Conference Proceedings*, pp 715-718. Butterworth, London.
89. Suslick, K. S.; Doktycz, S. J. In *Advances in Sonochemistry*, JAI Press Ltd.: Hampton Hill, 1990; Vol. 1, pp 197-230.
90. Makino, K.; Mossoba, M. M.; Riesz, P. Chemical effects of ultrasound on aqueous solutions: Formation of hydroxyl radicals and hydrogen atoms. *J. Phys. Chem.* **1983**, *87*, 1369-1377.

91. Riesz, P.; Berdahl, D.; Christman, C. L. Free radical generation by ultrasound in aqueous and nonaqueous solutions. *Environ. Health Perspectives*, **1985**, *64*, 233-252.
92. Leonhardt, E.; Stahl, R. Decomposition of acenaphthylene by ultrasonic irradiation. *Anal. Chem.* **1998**, *70*, 1228-1230.
93. Cataldo, F. Ultrasound-induced cracking and pyrolysis of some aromatic and naphthenic hydrocarbons. *Ultrason. Sonochem.* **2000**, *7*, 35-43.
94. Little, C.; Hephher, M. J.; El-Sharif, M. The sono-degradation of phenanthrene in an aqueous environment. *Ultrasonics* **2002**, *40*, 667-674.
95. Lu, Y.; Weavers, L. K. Sonochemical desorption and destruction of 4-chlorobiphenyl from synthetic sediments. *Environ. Sci. Technol.* **2002**, *36*, 232-237.
96. Psillakis, E.; Goula, E.; Kalogerakis, N.; Mantzavinos, D. Degradation of polycyclic aromatic hydrocarbons in aqueous solutions by ultrasonic irradiation. *J. Hazard. Mater.* **2004**, *108*, 95-102.
97. Fan, L-S.; Jadhav, R. A. Clean coal technologies: OSCAR and CARBONOX commercial demonstrations. *AIChE Journal*, **2002**, *48*, 2115-2123.
98. Karapanagioti, H. K.; Kleineidam, S.; Sabatini, D. A.; Grathwohl. P.; Ligouis, B. Impacts of heterogeneous organic matter on phenanthrene sorption: equilibrium and kinetic studies with aquifer material. *Environ. Sci. Technol.* **2000**, *34*, 406-414.

## **CHAPTER 2**

### **EFFECTS OF EXTRACTION METHOD ON THE CHARACTERIZATION OF POLYCYCLIC AROMATIC HYDROCARBONS (PAHs) ON LIME SPRAY DRYER (LSD) ASH**

#### **2.1. Abstract**

In this study, traditional Soxhlet, automatic Soxhlet and ultrasonic extraction techniques were employed to determine the type and concentration of polycyclic aromatic hydrocarbons (PAHs) on Lime Spray dryer (LSD) ash samples collected from the baghouse of a spreader stoker boiler. To test the efficiencies of different extraction methods, LSD ash samples were doped with a mixture of 16 U.S. EPA specified PAHs to measure the matrix spike percent recoveries. The results showed that the percent spike recoveries of PAHs were different using these three extraction methods with dichloromethane (DCM) as the solvent. Traditional Soxhlet extraction achieved slightly higher percent recoveries than automatic Soxhlet and ultrasonic extraction. Different solvents including toluene, DCM: acetone (1:1 V/V) and hexane: acetone (1:1 V/V) were further examined to optimize the recovery rate using ultrasonic extraction. Toluene

achieved the highest spike percent recoveries of PAHs at a spike level of  $10 \mu\text{g kg}^{-1}$ . When the spike level was increased to  $50 \mu\text{g kg}^{-1}$ , the percent recoveries of PAHs also correspondingly increased. Although the type and concentration of PAHs detected on LSD ash samples by different extraction methods varied, the concentration of each detected PAH was consistently low at  $\mu\text{g kg}^{-1}$  levels.

## **2.2. Introduction**

Polycyclic aromatic hydrocarbons (PAHs) are a class of organic compounds that consist of two or more fused aromatic rings with some of them being carcinogenic and/or mutagenic (Denissenko et al., 1996). PAHs are ubiquitous in the environment as they are found in air, water, soil, and persist in the environment for months to years (Wild et al., 1990). A major source of PAHs in the environment is fossil fuel combustion (e.g., coal burning) (Mastral and Callen, 2000; Pisupati et al., 2000). During coal combustion, PAHs are found in both the gas phase (flue gas) and the solid phase (fly ash) (Liu et al., 2000).

Lime spray dryer (LSD) ash is a residual material generated from processes used to remove sulfur dioxide from flue gas following coal combustion. In the LSD process, a fine spray of slaked lime ( $\text{Ca(OH)}_2$ ) is injected into the scrubber and reacts with sulfur oxides resulting in the formation of dry calcium sulfate or calcium sulfite (Kadambi et al., 1998). The mixture of dry calcium sulfite/sulfate, along with fly ash, is collected as “LSD ash” by an electrostatic precipitator or a baghouse. The United States Environmental Protection Agency (US EPA) suggests that LSD ash be exempt from physical and chemical tests for hazardous material if used in a few specific applications (U.S. EPA,

1999). However, concern remains due to the presence of hazardous inorganic (e.g., heavy metals) and organic compounds such as PAHs.

Little work has been done to characterize hazardous organic compounds on coal combustion residuals (i.e., fly ash, bottom ash, boiler slag, and desulfurization material). Most of the previous work has focused on characterization of PAHs on fly ash. To our knowledge, no research of PAHs on LSD ash has been conducted. During the LSD process, gaseous PAHs may sorb onto unreacted lime, calcium sulfate, calcium sulfite, or fly ash. These PAHs may be released when LSD ash is disposed or utilized. Therefore, an investigation of PAHs (e.g., concentration, fate) on LSD ash is necessary to determine environmentally safe utilization or disposal options.

A common analysis procedure for PAHs on solid matrices is extraction followed by instrumental analysis such as gas chromatography (GC), gas chromatography-mass spectrometry (GC-MS), liquid chromatography (LC), or liquid chromatography-mass spectrometry (LC-MS). Several different extraction methods have been used to extract PAHs from solid matrices. For example, traditional Soxhlet extraction (EPA 3540C), automatic Soxhlet extraction (EPA 3541), ultrasonic extraction (EPA 3550B), supercritical fluid extraction (SFE) (EPA 3561) and pressurized fluid extraction (PFE) (EPA 3545) all have standardized protocols.

Soxhlet extraction is the most commonly used extraction method (Lee and Hites, 1976; Song et al., 2002). Normally, it requires a large volume (up to 150 mL) of organic solvent to be refluxed through the solid sample for between 6 and 24 h. This method is time consuming although several extraction set-ups can be assembled and operated at the same time (Dean and Xiong, 2000). Automatic Soxhlet extraction uses an extraction unit

that can reduce the extraction time to a few hours compared to traditional Soxhlet extraction. In ultrasonic extraction, solid samples are sonicated in a glass beaker or flask ranging from minutes to hours using either an ultrasonic cleaning bath or probe. This method has been widely used for extracting nonvolatile and semivolatile organic compounds from solid matrices such as soils, sludge and solid wastes. Similar to ultrasonic extraction, SFE and PFE have short extraction times and low solvent needs. However, SFE and PSE are not widely used partially due to the relatively high capital cost of the instruments (Smith, 1999; Camel, 2001).

Comparison of extraction methods to extract PAHs from different matrices including soil (Codubam et al., 1994), sediment (Saim et al., 1997), and fly ash (Kenny and Olesik, 1998) has been conducted by other researchers. Results showed that the extraction procedure strongly influenced the analysis results (Jonker and Koelmans, 2002) and thus influences risk assessment and cleanup goals for site remediation. For example, Berset et al. (1999) studied the Soxhlet extraction, ultrasonic extraction, SFE, and ASE of nine soil samples and obtained different results by different extraction methods. In addition, Song et al. (2002) showed that quantification of PAHs from contaminated soils and sediments were affected by the extraction method when the matrix had high PAH concentrations.

In this paper, a comparative study of traditional Soxhlet, automatic Soxhlet, and ultrasonic extraction of PAHs from LSD ash was conducted. The purpose was to compare these commonly used standard extraction methods to recommend conditions optimal for use with LSD ash. As reduced extraction time and lower solvent needs are desirable,

ultrasonic extraction was further examined by investigating effects of solvent type and spike level to optimize this extraction method.

### **2.3. Materials and Methods**

#### *Sampling procedure*

LSD ash samples were collected from a spreader stoker boiler (boiler #8) at the McCracken power plant on The Ohio State University campus. A pre-cleaned 250 mL polytetrafluoroethylene (PTFE) beaker attached to a 2 m PTFE-coated steel rod was used to grab LSD ash samples through an 11 cm circular port located at the base of the baghouse. Samples were collected in a certified clean 950 mL amber glass bottle (Fisher Scientific) and subsequently stored in an environmental chamber (4 to 12 °C) until extractions were performed.

#### *Chemicals*

Hexane, acetone, dichloromethane (DCM), and toluene purchased from Fisher Scientific, were of HPLC grade and used as received. A 16 PAH standard (2000 mg L<sup>-1</sup>) and deuterated internal standard including acenaphthene-d<sub>10</sub>, chrysene-d<sub>12</sub>, 1, 4-dichlorobenzene-d<sub>4</sub>, naphthalene-d<sub>8</sub>, perylene-d<sub>12</sub> and phenanthrene-d<sub>10</sub> (2000 mg L<sup>-1</sup> each) were purchased from Ultra-Scientific (North Kingstown, RI).

#### *LSD ash characterization*

A JEOL JSM-820 SEM with Oxford eXL energy dispersive X-ray analyzer (JEOL USA Inc., Peabody, MA) was used for scanning electron microscopic (SEM) analysis. Mineralogical analyses of samples were conducted by a Philips X-Ray

Diffraction (XRD) instrument (Philips Analytical, Natick, MA) with CuK $\alpha$  radiation at 35kV and 20mA.

The inorganic elemental analyses for LSD ash were described by Taerakul et al. (2004). Organic carbon content of the LSD ash was calculated by subtracting the total inorganic carbon content (TIC) from the total carbon content (TC). Samples were combusted under pure O<sub>2</sub> at 900 °C on a VarioMax carbon/nitrogen analyzer (Elementar Americas, Mt. Laurel, NJ) to measure TC. TIC was determined by carbon coulometry (UIC Inc., Joliet, IL). The system was purged with a CO<sub>2</sub>-free carrier gas to eliminate atmospheric CO<sub>2</sub> before loading the sample into the sample flask. Then, 2N HClO<sub>4</sub> was added, heated and inorganic carbon was oxidized to gaseous CO<sub>2</sub> and measured by a CO<sub>2</sub> detector.

#### *Extraction Procedures*

For automatic Soxhlet extraction, a 10 g of each collected ash sample was extracted in a Tecator Soxtec (Model 1043) extractor (Foss, Eden Prairie, MN) with CH<sub>2</sub>Cl<sub>2</sub> for 6 hours. For traditional Soxhlet extraction, each 10 g of LSD ash sample was weighed into a cellulose extraction thimble. The samples were Soxhlet-extracted for 16 h using 70 mL DCM. The extracts were concentrated to 1 mL using a Kuderna-Danish apparatus and a gentle stream of N<sub>2</sub>, successively.

Ultrasonic extraction was performed based on U.S. EPA standard method 3550B (U.S. EPA, 1996a). A 10 g LSD ash sample was weighed into a 400 mL Pyrex glass beaker to which 100 mL of solvent was added. A 20 kHz ultrasonic probe with 1.90 cm diameter titanium tip (Sonic Dismembrator 550, Fisher Scientific) was used for ultrasonic

extractions. The end of the probe tip was located 1.3 cm below the surface of the liquid but above the solid. In all experiments, with the output control knob set at 10 (full power) and pulse mode (pulse = 5 sec, pulse off = 5 sec), the sample was sonicated for 3 min (total ultrasonic irradiation time 1.5 min). After extraction, the supernatant was decanted, filtered through a Whatman GF/B filter in a Buchner funnel and then collected in a filtration flask. The ultrasonic extraction of the solid samples was repeated twice with two additional 100 mL aliquots of solvent. After the third extraction, all extracts were poured into the Buchner funnel and rinsed with 20~30 mL solvent. All the collected extract was condensed to less than 10 mL with a Kuderna-Danish concentrator and was further concentrated to 1 mL with high purity nitrogen gas.

#### *Matrix spike*

A 1 mL mixture standard (16 different PAHs) containing 100 ng of each PAH was added into a 10 g LSD ash sample before extraction resulting in a spike level of 10  $\mu\text{g kg}^{-1}$  to measure the spike recovery to evaluate the relative difference between different extraction methods. After addition of the PAH mixture into the LSD ash samples, the spiked samples were aged for 1 hr before extraction. A 10 g LSD ash sample without the PAH mixture added was extracted as a background. The spike recovery percent is defined as:

$$\text{Spike recovery (\%)} = \frac{(\text{Measured spiked PAH} - \text{PAH in background})}{\text{PAH added}} \times 100 \quad (1)$$

where *PAH added* is the known amount added into LSD ash before extraction, *measured spiked PAH* is the amount of PAH measured in spiked LSD ash samples after extraction,

and *PAH in background* is the amount of PAH extracted from LSD ash samples without the spike.

Unless stated otherwise, duplicate experiments were conducted in traditional and automatic Soxhlet extraction; triplicate experiments were conducted in ultrasonic extraction to ensure reproducibility.

#### *PAHs analysis*

A Trace gas chromatograph PolarisQ ion trap mass spectrometer (ThermoQuest, Waltham, MA) with a fused silica capillary column (30 m × 250 μm × 0.25 μm) (Varian, Walnut Creek, CA) was used for PAH analysis. An internal standard containing acenaphthene-d<sub>10</sub>, chrysene-d<sub>12</sub>, 1, 4-dichlorobenzene-d<sub>4</sub>, naphthalene-d<sub>8</sub>, perylene-d<sub>12</sub> and phenanthrene-d<sub>10</sub> and 16 standard PAHs (Ultra scientific, North Kingstown, RI) were used for quantification. Calibration curves including 5 different concentrations were constructed using the internal standard method. The concentrations of spiked and unknown samples were within the range of the calibration curve. Helium was used as the carrier gas with the flow rate of 1.2 mL min<sup>-1</sup>. 2 μL of extract spiked with the deuterated internal standard including were injected spiltlessly into the injector. Both the injector and ion source temperatures were kept at 250 °C. The temperature of the mass transfer line was kept at 300 °C. The initial oven temperature was held at 60 °C for 2 min, programmed to 250 °C at 20 °C min<sup>-1</sup> followed by a 2 min hold time, increased to 300 °C at 10 °C min<sup>-1</sup> and held for 8 min. The detection limits of these PAHs ranged from 0.1 to 10 μg kg<sup>-1</sup>. Larger molecular weight PAHs had higher detection limits compared to small molecular weight PAHs.

## 2.4. Results and Discussion

Characterization of LSD ash by SEM, XRD, and elemental analysis described by Taerakul et al. (2004) indicated that the LSD ash samples were generally a mixture of hannebachite, unreacted lime (i.e., portlandite), fly ash (i.e., mullite and quartz), carbonaceous material and other minor constituents. As shown in Figure 2.1, major inorganic element concentrations in LSD ash were 30.9% Ca, 12.70% S, and 4.71% Si, which is consistent with XRD and SEM results indicating that the majority of material was present as hannebachite, portlandite, and fly ash in LSD ash. In addition, the total carbon content was 8.18%, 7% of which was organic carbon.

### *Comparison of ultrasonic, traditional Soxhlet and automatic Soxhlet extraction*

The matrix spike recoveries were used to evaluate the extraction efficiency of traditional Soxhlet, automatic Soxhlet, and ultrasonic extraction with DCM as the extraction solvent as shown in Figure 2.2. DCM was chosen because it is a common solvent used for extraction (Jonker and Koelmans, 2002).

At a spike level of  $10 \mu\text{g kg}^{-1}$ , the average matrix spike recoveries ranged from 0%~80% for the 16 different PAHs using any of these three extraction methods. For small molecular weight PAHs, such as naphthalene and acenaphthylene, traditional Soxhlet and automatic Soxhlet extraction achieved higher percent recoveries than ultrasonic extraction. While for the moderate molecular weight PAHs (from phenanthrene to benzo[b,k]fluoranthene), the recoveries tended to be higher using ultrasonic extraction compared to automatic Soxhlet extraction but were similar to that achieved by traditional Soxhlet extraction. For PAHs larger than benzo(a)pyrene, neither

ultrasonic nor automatic Soxhlet extraction with DCM was able to extract these PAHs from LSD ash. Traditional Soxhlet extraction was able to extract a portion of them, possibly due to the long extraction time. However, the recoveries were much lower. For example, 36.0% of benzo(a)pyrene, 10.5% of benzo(ghi)perylene, 10.8% of dibenzo(a,b)anthracene were recovered from the spiked LSD ash. None of the spiked indeno(123-cd)pyrene was extracted. In addition, a trend of decreasing recoveries with increasing molecular weight of PAHs was observed with traditional Soxhlet and automatic Soxhlet extraction techniques. For ultrasonic extraction, the recoveries of PAHs showed an increase followed by a decrease with increasing molecular weight.

The higher percent recoveries of moderate molecular weight PAHs (from phenanthrene to benzo(b, k)fluoranthene) obtained by 9 min ultrasonic extraction compared to 6 hr of automatic Soxhlet extraction may be due to the chemical and physical effects of ultrasound during the extraction. For example, high pressure upon cavitation bubble collapse generated from ultrasound enhances penetration of the solvent and transfer of the adsorbed solutes from the solid matrix (Margulies and Schwarz, 1985). High local temperatures generated by cavitation bubble collapses improve solubility and diffusivity of the solute. Moreover, when cavitation bubbles generated during ultrasound collapse, shock waves and shear forces are produced that create microscopic turbulence within interfacial films surrounding nearby solid particles (Doktycz and Suslick, 1990), improving mass transfer between the solid particles and the solvent (Wilhelm et al., 1993). Therefore, although these PAHs have a strong binding affinity to LSD ash due to their high hydrophobicity, ultrasonic extraction appears to be able to extract them from LSD ash and increase recoveries compared to automatic Soxhlet

extraction. For small molecular weight PAHs such as naphthalene, a higher recovery using ultrasonic extraction was expected because of the comparatively low hydrophobicity. However, the lower recoveries obtained with ultrasonic extraction compared to automatic Soxhlet extraction may be due to the reactions of small molecular weight PAHs under sonication (Sun and Weavers, 2004).

As stated in EPA standard method 8270, higher than 70% recoveries can be achieved for PAHs using either Soxhlet or ultrasonic extraction (U.S. EPA, 1996b). The low recoveries (0~80%) in this study may be due to the presence of carbonaceous material. It is known that the organic matter content in the matrix plays an important role in the adsorption of organic compounds (Watts, 1992). Griest et al. (1980) reported low recoveries of PAHs in coal fly ash and suggested that this low recovery might be due to the association of PAHs and carbonaceous particles specifically through  $\pi$  complexes between PAHs and the extended aromatic system of the polymeric carbon. Results by Soltys et al. (1986) showed that the carbonaceous fraction was responsible for the incomplete recovery of benzo[a]pyrene spiked on fly ash. Fischer et al. (1994) reported the presence of 5% carbon reduced the recovery of pyrene from 43% to 9%. Thus, the presence of carbonaceous material in LSD ash (7% organic carbon) may account for the low recoveries of PAHs.

The low spike levels used in our experiments may be another explanation for the low recoveries. Compared to other studies on the extraction of PAHs (Ozretich and Schroeder, 1986, Kenny and Olesik, 1998; Chen et al., 1996), the spike level in our experiments ( $10 \mu\text{g kg}^{-1}$ ) was 2 to 3 orders of magnitude lower. Fischer et al. (1994) examined the influence of the PAH concentration on Soxhlet extraction recoveries from

fly ash. Their results showed that when the PAH concentration was reduced from 1000  $\mu\text{g kg}^{-1}$  to 50  $\mu\text{g kg}^{-1}$ , the recoveries of benzo(ghi)perylene decreased from 52% to 20%. However, EPA standard method 3500B recommends that the spike level be 1 to 5 times higher than the concentration of the analyte in the sample. The low matrix spike level was chosen in our experiments to mimic concentrations expected for PAHs on LSD ash (Griest et al., 1988).

Although the recoveries of PAHs using ultrasonic extraction were slightly lower compared to traditional Soxhlet extraction, the short extraction time is advantageous for handling large numbers of samples. Thus, in order to improve the ultrasonic extraction efficiency, further experiments were conducted to test parameters such as solvent type and spike level.

#### *Solvent effects on ultrasonic extraction recovery rates*

Four different solvents including DCM, DCM: acetone (1:1 V/V), hexane: acetone (1:1 V/V) and toluene were tested to determine the effects of solvent on the ultrasonic extraction recovery. As shown in Figure 2.3, toluene yielded the highest recoveries followed by DCM: acetone (1:1 V/V), DCM, and hexane: acetone (1:1 V/V). For most PAHs, even at a 10  $\mu\text{g kg}^{-1}$  spike level, toluene could achieve 50%~87% recovery although dibenzo(a,b)anthracene and benzo(ghi)perylene could not be extracted. Only 20%~ 50% of the PAHs were recovered using the hexane/acetone mixture.

The difference of PAH recoveries achieved by different solvents during ultrasonic extraction may be due to different cavitation conditions resulting from solvent characteristics. Under sonication, the formation of cavitation bubbles (i.e., vapor-filled

microbubbles) in a liquid requires that the negative pressure in the rarefaction region of the ultrasonic wave must overcome the intermolecular forces acting within the liquid. Thus, cavities are more readily formed when using solvents with low viscosity ( $\mu$ ), and low surface tension ( $\sigma$ ) (Thompson and Doraiswamy, 1999). However, the intensity of cavitation is benefited by using solvents that have higher viscosity and surface tension. Solvents with high surface tension and viscosity generally have a higher threshold for cavitation but more harsh conditions once cavitation is established resulting in higher temperatures and pressures upon bubble collapse. Toluene has a higher viscosity than DCM, hexane, and acetone. Thus, toluene is expected to have a higher cavitation threshold resulting in stronger cavitation conditions.

The vapor pressure of the solvent is another important factor affecting cavitation. Higher vapor pressure leads to more solvent volatilizing into the cavitation bubbles. As a result, the maximum pressure and temperature is lower compared to low vapor pressure solvents because a portion of the energy generated during collapse goes toward condensation and endothermic reactions of the vapor (Colussi, et al., 1998; Thompson and Doraiswamy, 1999). With the lowest vapor pressure of the solvents used, toluene will partition into cavitation bubbles less than the other solvents resulting in a smaller reduction in the temperatures and pressures inside the bubbles at collapse. Also, with a higher vapor pressure, we would expect more radical formation from the solvent than lower vapor pressure solvents (Mizukoshi et al., 1999). Radical formation is also expected to affect recoveries by reacting with target compounds that will be extracted. Therefore, stronger cavitation effects are expected with toluene due to its high viscosity, surface tension and lower vapor pressure. As a result, more desorption from LSD ash

particles and higher recoveries would be expected. For the other solvents, the cavitation effects will be weaker than in toluene due to their higher vapor pressures resulting in less desorption of PAHs and lower recovery rates compared to using toluene.

Work by Jonker and Koelmans (2002) showed that the type of solvent had a strong effect on Soxhlet extraction of PAHs from soot and sediment. They determined that the capacity of the solvent to displace target chemicals from the energetically favorable sorption sites was very important to the extraction efficiency. As an aromatic solvent, toluene molecules will compete for the same sorption sites as PAHs making it an advantageous solvent over aliphatic solvents (Jonker and Koelmans, 2002). This competition for sorption sites is another explanation for higher recoveries of toluene compared to DCM, hexane and acetone.

#### *Effects of spike level on ultrasonic extraction recovery rates*

As mentioned in section 3.1, low spike levels may lead to low recoveries. Thus, extraction recoveries from ultrasonic extraction with toluene at a spike level of  $50 \mu\text{g kg}^{-1}$  were measured to further examine this possibility. As shown in Figure 2.4, the recoveries of all the PAHs at the  $10 \mu\text{g kg}^{-1}$  spike level are lower than that with the  $50 \mu\text{g kg}^{-1}$  spike level.

Ozretich and Schroeder (1986) measured the recoveries of several PAHs from marine sediments at spike levels of 0.25, 0.5, 1.0, and  $2.5 \text{ mg kg}^{-1}$  by ultrasonic extraction. Their results showed that the lowest mean recovery and the highest variability typically were obtained from the lowest spike concentrations. It is worth noting that the spike level used in their study is 2 orders of magnitude higher than the spike level in our experiments.

Mangani et al. (1987) studied the Soxhlet extraction recoveries of low molecular weight PAHs (from acenaphthylene to chrysene) at two spike levels: approximately 30 and 3  $\mu\text{g kg}^{-1}$ . They also noticed a decrease of extraction recovery rates with decreasing spike concentrations. Soltys et al. (1988) suggested that the PAHs retained on fly ash after extraction was not a constant fraction of the PAHs present, but instead approaches a constant residual quantity. Kan et al. (1994) studied the adsorption and desorption of naphthalene and phenanthrene on soil and suggested that irreversible adsorption might be an explanation for retained organic compounds. Therefore, higher recoveries are expected when using a very high spike level. However, the high recoveries obtained from the high spike level may not be representative of the samples. As a result, concentrations calculated using high spike levels would be questionable. Thus, a spike level higher than that expected for any component measured in samples should not be used.

#### *PAH concentrations on LSD ash*

The concentrations of PAHs collected on LSD ash samples using different extraction methods are shown in Table 2.1. The results indicate that the PAH concentrations measured varied with different extraction methods. However, the concentrations of these PAHs measured using different extraction methods were consistently low, usually at the  $\mu\text{g kg}^{-1}$  levels. The PAHs identified by automatic Soxhlet extraction were 2-ring and 3-ring PAHs, such as naphthalene, and phenanthrene; no PAHs larger than phenanthrene were detected. Using ultrasonic extraction with the DCM and acetone mixture as the solvent, fluorene, pyrene, and fluoranthrene were detected in addition to naphthalene and phenanthrene. When toluene was used as the extraction

solvent in ultrasonic extraction, benzo(a)anthracene and chrysene were also identified. Although traditional Soxhlet extraction with DCM can achieve high recovery rates of PAHs compared to ultrasonic and automatic Soxhlet extraction, some of the PAHs detected by ultrasonic extraction with toluene were not identified using traditional Soxhlet extraction (e.g., anthracene).

The quantification data measured by different extraction methods suggests that the concentrations of PAHs were constantly low in LSD ash, which may be attributed to the combustion conditions at the McCracken Power Plant. Bituminous coal is burned at approximately 650 °C, and an air pump is used to provide excess air for combustion. At this combustion temperature, the bonds of macromolecular PAHs in raw coal are only partially broken by pyrolysis to form smaller size fragments (Ledesma et al., 1999). Intermolecular cyclization among these small size fragments are expected to be less predominant compared to pyrolysis because of the low temperature (Zhao et al., 2000). As a result, formation of small molecular weight PAHs by pyrolysis is favored. With excess air, PAHs may further be oxidized to form carbon dioxide and water (Mastral et al., 1995). Therefore, the low concentrations of PAHs and small PAHs identified in LSD ash samples may be able to be explained by the low combustion temperature and excess air in McCracken Power Plant.

PAH concentrations in LSD ash in this study were low compared to PAH concentrations in other matrices such as soil and sediment (Ghosh et al., 2001; U.S. Massachusetts DEP, 2002). For example, the PAH concentrations in natural soil ranged from 0.5~4 mg kg<sup>-1</sup> as reported by Massachusetts Department of Environmental Protection, which is 2~3 orders of magnitude higher than that in collected LSD ash

(2002). Although much lower PAH concentrations in LSD ash compared to natural soils, a bioavailability study needs to be conducted to verify the PAHs have no threat to the environment during utilization or disposal of LSD ash.

## **2.5. Conclusions**

Quantification of PAHs on LSD ash samples was affected by different extraction methods. Ultrasonic extraction with toluene showed the highest recoveries of PAHs. A higher spike level also results in a higher recovery; however, this may not represent the true extraction efficiency if this spike level is not representative of the level of PAHs in the samples. Although the concentration and speciation of PAHs were different using different extraction methods, the PAH concentrations were generally at  $\mu\text{g kg}^{-1}$  levels indicating that PAHs in LSD ash should not pose a threat to the environment during reuse applications or disposal.

## **Acknowledgements**

The financial support by the Ohio State Carbonation and Ash Reactivation (OSCAR) Project with funding from the Ohio Coal Development Office (OCDO) and The Ohio State University are gratefully acknowledged. P. Sun is grateful to The Ohio State University for University and Presidential Fellowship awards. The authors would like to thank the staff at the McCracken Power Plant and Danold W. Golightly for their assistance during sampling. Chin-Ming Cheng's contribution to X-Ray Diffraction experiments and surface area measurements are acknowledged.

## References

- Berset, J. D., Ejem, M., Holzer, R., Lischer, P., 1999. Comparison of different drying, extraction and detection techniques for the determination of priority polycyclic aromatic hydrocarbons in background contaminated soil samples. *Anal. Chim. Acta* 383, 263-275.
- Camel, V., 2001. Recent extraction techniques for solid matrices—supercritical fluid extraction, pressurized fluid extraction and microwave-assisted extraction: their potential and pitfalls. *Analyst* 126, 1182-1193.
- Chen, C. S., Rao, P. S. C., Lee, L. S. 1996. Evaluation of extraction and detection methods for determining polynuclear aromatic hydrocarbons from coal tar contaminated soils. *Chemosphere* 32, 1123-1132.
- Codubam G., Vaqierp, M. T., Comellas, L., Broto-puig, F., 1994. Comparison of various extraction and clean-up methods for the determination of polycyclic aromatic hydrocarbons in sewage sludge-amended soils. *J.Chromatogr.* 673, 21-29.
- Colussi, A. J, Weavers, L. K., Hoffmann, M. R., 1998. Chemical bubble dynamics and quantitative sonochemistry. *J. Phys. Chem. A* 102, 6927-6934.
- Dean, J. R., Xiong, G-H., 2000. Extraction of organic pollutants from environmental matrices: Selection of extraction technique. *Trends in Analytical Chemistry* 19, 553-564.
- Denissenko, M. F., Pao, A., Tang, M-S., Pfeifer, G. P., 1996. Preferential formation of benzo[a]pyrene adducts at lung cancer mutational hotspots in P53. *Science* 274, 430-432.

- Doktycz, S. J., Suslick, K. S., 1990. Interparticle collisions driven by ultrasound. *Science* 247, 1067-1069.
- Fischer, R., Kreuzig, R., Bahadir, M., 1994. Extraction behavior of polycyclic aromatic hydrocarbons from soil samples. *Chemosphere* 29, 311-317.
- Ghosh, U., Talley, J. W., Luthy, R. G., 2001. Particle-Scale Investigation of PAH Desorption Kinetics and Thermodynamics from Sediment. *Environ. Sci. Technol.* 35, 3468-3475.
- Griest, W. H., Yeatts, L. B., Caton, J. E., 1980. Recovery of polycyclic aromatic hydrocarbons sorbed on fly ash for quantitative determination. *Anal. Chem.* 52, 199-201.
- Griest, W. H., Tomkins, B. A., Caffrey, J. R., 1988. Improved ultrasonic extraction recovery of benzo(a)pyrene from stack ash using high power/mass ratios. *Anal. Chem.* 60, 2169-2171.
- Jonker, T., Koelmans, A., 2002. Extraction of polycyclic aromatic hydrocarbons from soot and sediment: solvent evaluation and implications for sorption mechanism. *Env. Sci. Technol.* 36, 4107-4113.
- Kadambi, J. R., Adler, R. J., Prudich, M. E., Fan, L. S., Raghunathan, K., Khang, S. J., Keener, T. C. 1998. Flue gas desulfurization for acid rain control. In: Toole-Oneil, B. (Eds.). *Dry Scrubbing Technologies for Flue Gas Desulfurization*. Kluwer Academic Publishers: Boston/Dordrecht/London, pp. 6-8.
- Kenny, D., Olesik, S., 1998. Extraction of lignite coal fly ash for polynuclear aromatic hydrocarbons: modified and unmodified supercritical fluid extraction, enhanced-fluidity solvents, and accelerated solvent extraction. *J. Chromatogr. Sci.* 36, 59-65.

- Ledesma, E., Kalish, M., Wornat, M., Nelson, P., Mackie, J., 1999. Observation of cyclopenta-fused and ethynyl-substituted PAH during the fuel-rich combustion of primary tar from a bituminous coal. *Energy & Fuels* 13, 1167-1172.
- Lee, M. L., Hites, R. A., 1976. Characterization of sulfur-containing polycyclic aromatic compounds from carbon black. *Anal. Chem.* 48, 1890-1893.
- Liu, K-L., Xie, W., Zhao, Z-B., Pan, W-P., Riley, J. T., 2000. Investigation of polycyclic aromatic hydrocarbons in fly ash from fluidized bed combustion systems. *Environ. Sci. Technol.* 34, 2273-2279.
- Kan, A. T., Fu, G-M., Tomson, M. B., 1994. Adsorption/desorption hysteresis in organic pollutant and soil/sediment interaction. *Environ. Sci. Technol.* 28, 859-867.
- Mangani, F., Cappiello, A., Crescentini, G., Bruner, F., Bonfanti, L., 1987. Extraction of low molecular weight polynuclear aromatic hydrocarbons from ashes of coal-operated power plants. *Anal. Chem.* 59, 2066-2069.
- Margulies, T. S., Schwarz, W. H., 1985. Sound wave propagation in viscolastic fluids with simultaneous chemical reactions. *J. Acoust. Soc. Am.* 78, 605-615.
- Mastral, A. M., Callen, M. S., Mayoral, C., Galban, J., 1995. Polycyclic aromatic hydrocarbon emissions from fluidized bed combustion of coal. *Fuel* 74, 1762-1766.
- Mastral, A. M.; Callen, M. S., 2000. A review on polycyclic aromatic hydrocarbon (PAH) emissions from energy generation. *Environ. Sci. Technol.* 34, 3051-3057.
- Mizukoshi, Y.; Nakamura, H.; Bandow, H.; Maeda, Y.; Nagata, Y. 1999. Sonolysis of organic liquid: effect of vapor pressure and evaporation rate. *Ultrason. Sonochem.* 6, 203-209.

- Ozretich, R. J., Schroeder, W. P., 1986. Determination of selected neutral priority organic pollutants in marine sediment, tissue, and reference materials utilizing bonded-phase sorbents. *Anal. Chem.* 58, 2041-2048.
- Pisupati, S. V., Wasco, R. S., Scaroni, A. W., 2000. An investigation on polycyclic aromatic hydrocarbon emissions from pulverized coal combustion systems. *Journal of Hazardous Materials* 74, 91-107.
- Saim, N., Dean, J.R., Abdullah, M.P., Zakaria, Z., 1997. Extraction of polycyclic aromatic hydrocarbons from contaminated solid using Soxhlet extraction, pressurized and atmospheric microwave-assisted extraction, supercritical fluid extraction, and accelerated soil extraction. *J. Chromatogr. A* 791, 361-366.
- Smith, R. M., 1999. Supercritical fluids in separation science-the dreams, the reality and the future. *J. Chromatogr. A* 856, 83-115.
- Soltys, P. A., Mauney, T., Natusch, D. F. S., Schure, M. R., 1986. Time-resolved solvent extraction of coal fly ash: retention of benzo[a]pyrene by carbonaceous components and solvent effects. *Environ. Sci. Technol.* 20, 175-180.
- Song, Y. F., Jing, X., Fleischmann, S., Wilke, B. M., 2002. Comparative study of extraction methods for the determination of PAHs from contaminated soils and sediments. *Chemosphere* 48, 993-1001.
- Sun, P.; Weavers, L. K., 2004. Sonolytic reactions of polycyclic aromatic hydrocarbons in organic extraction solutions. *Env. Sci. Technol.* in review.
- Taerakul, P.; Sun, P.; Walker, H. W.; Weavers, L. K.; Golightly, D.; Butalia, T. Variability of inorganic and organic constituents in lime spray dryer ash. *Fuel*, 2004, in review.

- Thompson, L. H., Doraiswamy, L. K., 1999. Sonochemistry: science and engineering. *Ind. Eng. Chem. Res.* 38, 1215-1249.
- U.S. Environmental Protection Agency, 1996a. Ultrasonic Extraction, EPA standard method 3550B.
- U.S. Environmental Protection Agency, 1996b. Semivolatile organic compounds by gas chromatography/mass spectrometry (GC/MS), Ultrasonic Extraction, EPA standard method 8270C.
- U.S. Environmental Protection Agency, 1999. Wastes from the Combustion of Fossil Fuels, Volume 1 and 2- Methods, Findings, and Recommendations, Report to Congress, EPA 530-S-99-010.
- U.S. Massachusetts Department of Environmental Protection. Technical Update, 2002. Background Levels of Polycyclic Aromatic Hydrocarbons and Metals in Soil.
- Watts, R. J. 1992. Hazardous Wastes: Sources, Pathways, Receptors. John Wiley and Sons, New York.
- Wild, S. R., Waterhouse, K. S., McGrath, S. P., Jones, K. C., 1990. Organic contaminants in an agricultural soil with a known history of sewage sludge amendments: polynuclear aromatic hydrocarbons. *Environ. Sci. Technol.* 24, 1706-1711.
- Wilhelm, A. M., Contamine, F., Berlan, J., Berlan, J., Delmas, H. Measurement of liquid-solid mass transfer in ultrasonic reactor. Ultrasonics International 93 Conference Proceedings, pp 715-718. Butterworth, London.
- Zhao, Z-B., Liu, K-L., Xie, W., Pan, W-P., Riley, J., 2000. Soluble polycyclic aromatic hydrocarbons in raw coals. *Journal of Hazardous Materials B73*, 77-85.

Detected PAH	Concentration ( $\mu\text{g kg}^{-1}$ )			
	Ultrasonic Extraction (DCM: acetone)	Ultrasonic Extraction (toluene)	Automatic Soxhlet Extraction (DCM)	Traditional Soxhlet Extraction (DCM)
Naphthalene	2.1±0.2	4.2±2.2	2.1±0.8	12.4±0.1
Fluorene	1.6±0.1	N/D	N/D	N/D
Phenanthrene	4.5±0.6	3.8±1.2	0.7±0.5	2.4±0.2
Anthracene	N/D	1.4±0.2	N/D	N/D
Fluoranthene	5.4±1.1	1.2±0.9	N/D	N/D
Pyrene	3.9 ±0.6	3.7 ±2.1	N/D	1.5±0.2
Benzo(a)anthracene	N/D	0.5 ±0.4	N/D	2.1±0.8
Chrysene	N/D	2.5 ±0.4	N/D	N/D

Table 2.1. PAHs detected using ultrasonic extraction with toluene, DCM: acetone (1:1), automatic Soxhlet extraction with DCM, and traditional Soxhlet Extraction with DCM. N/D: not detected

## FIGURE CAPTIONS

Figure 2.1. Major element composition of LSD ash.

Figure 2.2. Spike recoveries of 16 PAHs measured using traditional Soxhlet extraction, automatic Soxhlet extraction, and ultrasonic extraction with DCM as the solvent. Spike level was  $10 \mu\text{g kg}^{-1}$ . Extraction time was 16 h in traditional Soxhlet extraction, 6 hr in automatic Soxhlet extraction. Ultrasonic extraction was repeated three times, 3 min each time with a pulse time of 5 sec.

Figure 2.3. Solvent effect on spike recoveries of 16 PAHs measured using ultrasonic extraction. Spike level was  $10 \mu\text{g kg}^{-1}$ . Each ultrasonic extraction includes 3 sonication exposures, 3 min each time with a pulse time of 5 sec.

Figure 2.4. Recoveries of PAHs using ultrasonic extraction. Each ultrasonic extraction includes 3 sonication exposures, 3 min each time with a pulse time of 5 sec.

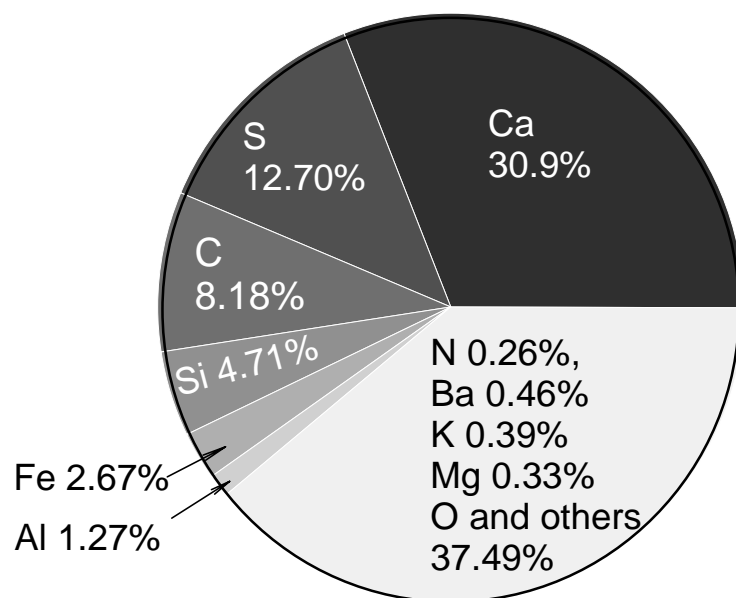


Figure 2.1. Major elemental composition of LSD ash.

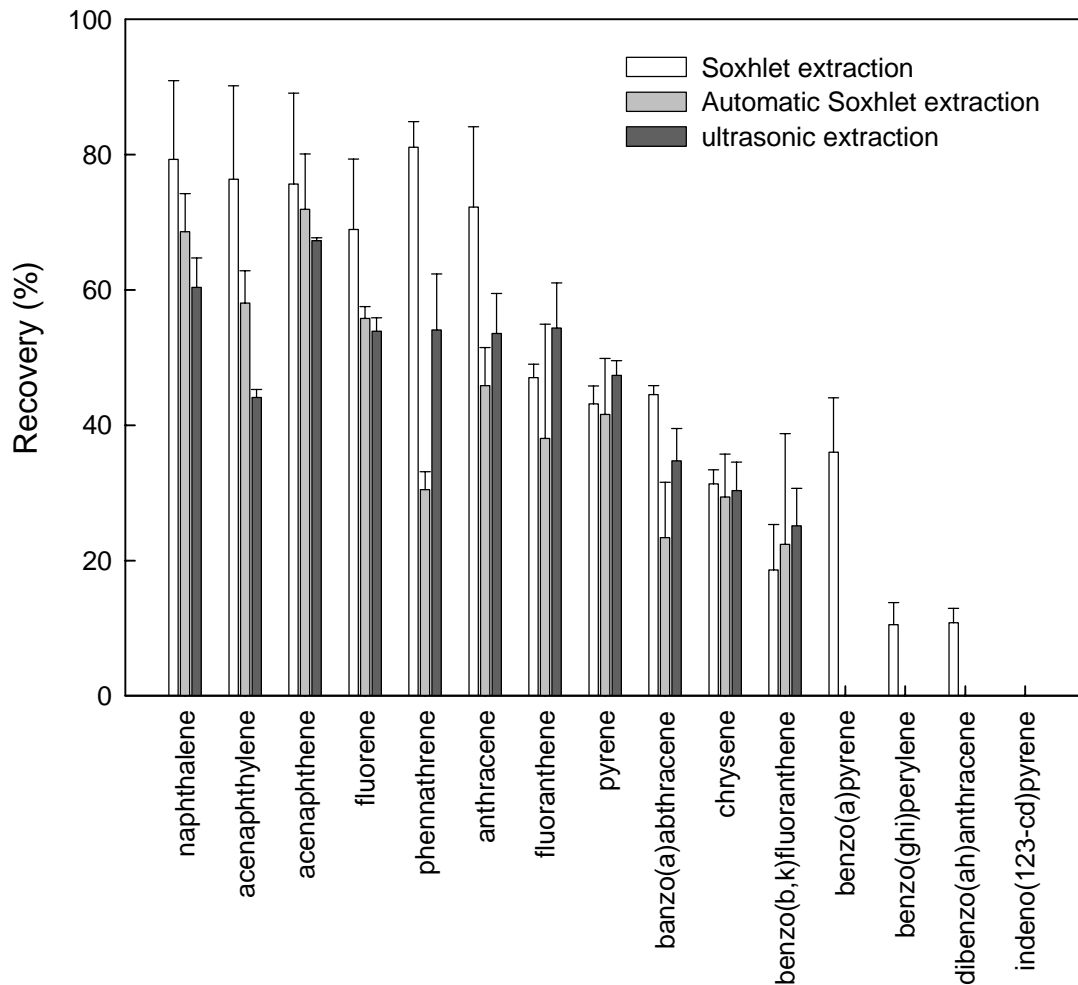


Figure 2.2. Spike recoveries of 16 PAHs measured using traditional Soxhlet extraction, automatic Soxhlet extraction, and ultrasonic extraction with DCM as the solvent. Spike level was  $10 \mu\text{g kg}^{-1}$ . Extraction time was 16 h in traditional Soxhlet extraction, 6 hr in automatic Soxhlet extraction. Ultrasonic extraction was repeated three times, 3 min each time with a pulse interval of 5 sec.

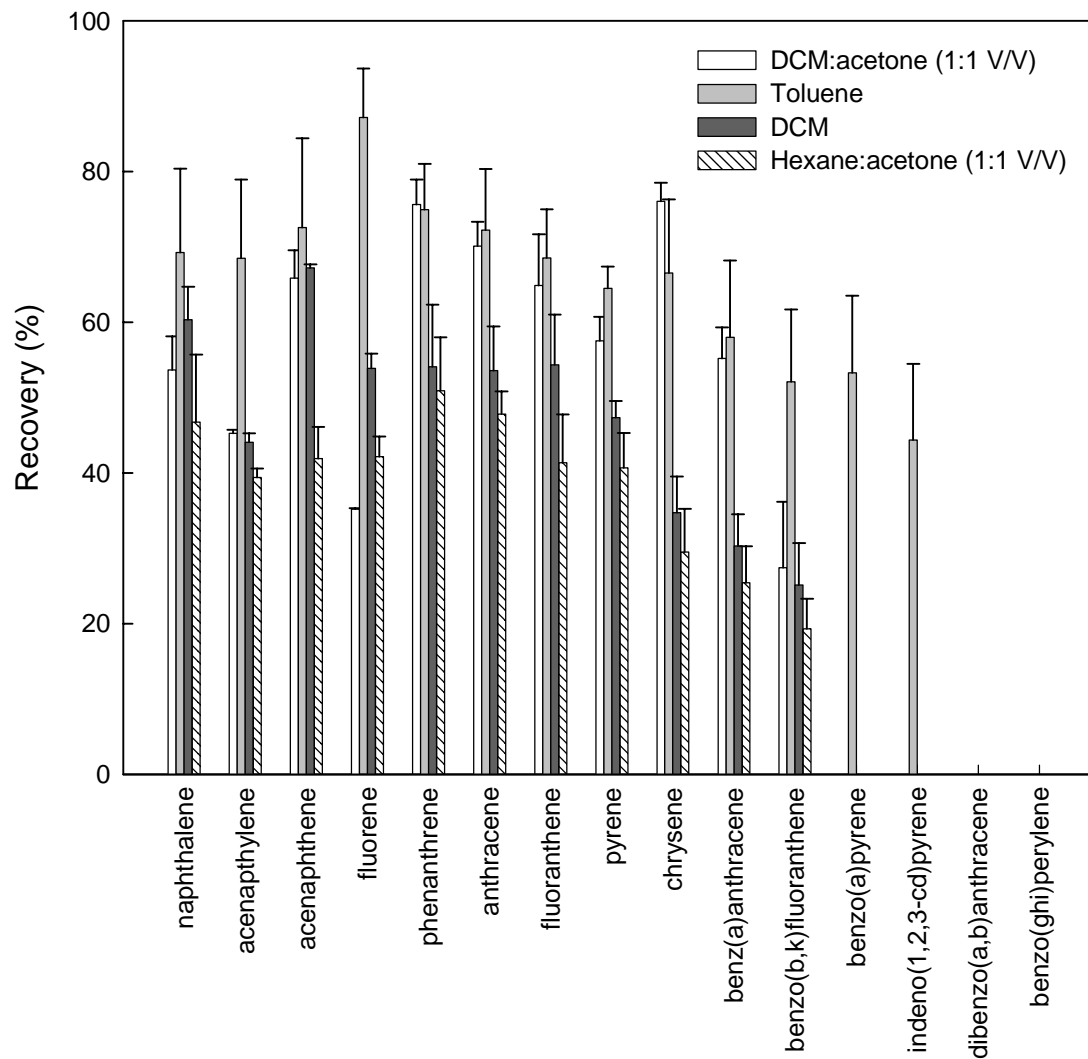


Figure 2.3. Solvent effects on spike recoveries of 16 PAHs measured using ultrasonic extraction. Spike level was  $10 \mu\text{g kg}^{-1}$ . Each ultrasonic extraction includes 3 sonication exposures, 3 min each time with a pulse interval of 5 sec.

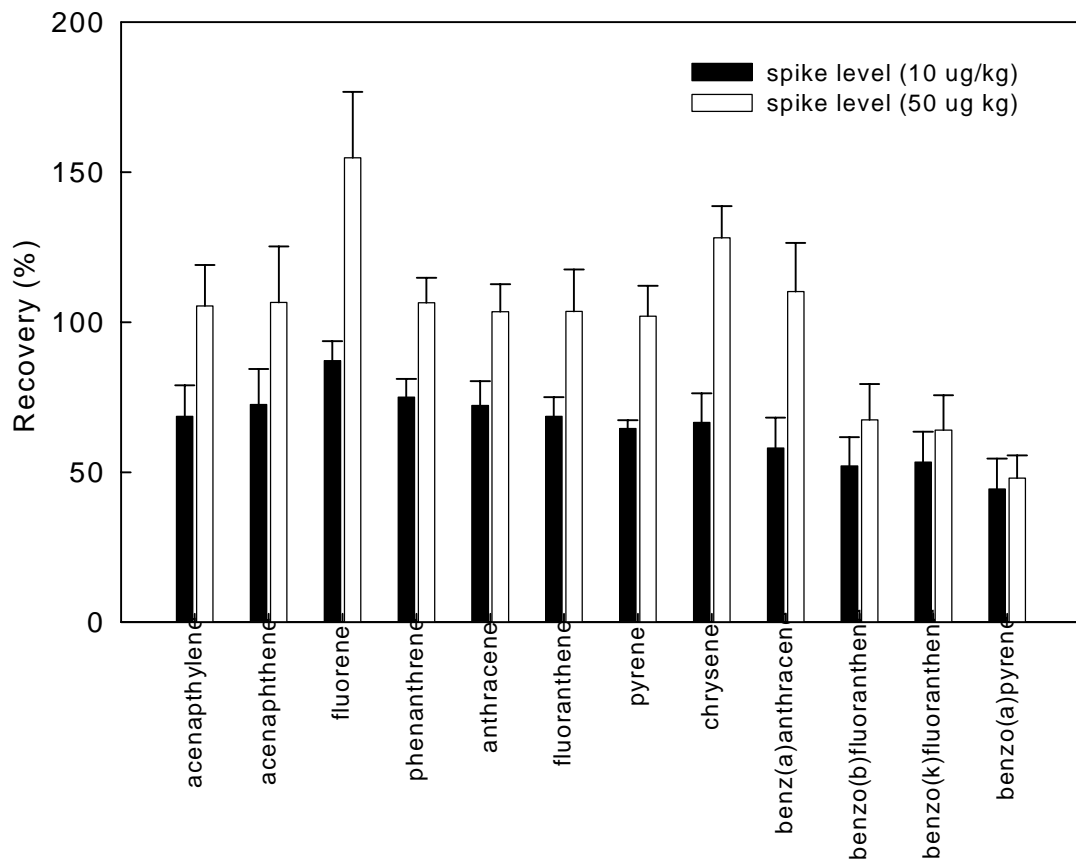


Figure 2.4. Recoveries of PAHs using ultrasonic extraction. Each ultrasonic extraction includes 3 sonication exposures, 3 min each time with a pulse interval of 5 sec.

## CHAPTER 3

### SONOLYTIC REACTIONS OF POLYCYCLIC AROMATIC HYDROCARBONS (PAHs) IN ORGANIC EXTRACTION SOLUTIONS

#### 3.1. Abstract

Ultrasonic extraction is a common method to extract semivolatile and nonvolatile organic compounds such as polycyclic aromatic hydrocarbons (PAHs) from solid matrices. However, ultrasonic energy has been suspected to lead to undesired reactions of the solute and thus affect quantification results. In this paper, sonolytic reactions of naphthalene, phenanthrene, and pyrene in common organic extraction solutions were examined using a 20 kHz ultrasonic probe under conditions commonly used for ultrasonic extraction. By sonicating these three model PAHs in nonaqueous organic solvents, extraction parameters including solute concentration, solvent type, pulse time interval, and sonication time were investigated. Hexane: acetone (1:1 V/V) resulted in less PAH degradation than dichloromethane (DCM): acetone (1:1 V/V). Initial solute concentration, length of sonication time, and solvent type affected the degradation of

phenanthrene. Reaction by-products such as methylphenanthrene and methylnaphthalene detected after sonication of phenanthrene indicated that phenanthrene reacts by both direct pyrolysis and reaction with methyl radicals formed from solvent pyrolysis.

### **3.2. Introduction**

Polycyclic aromatic hydrocarbons (PAHs) are ubiquitous compounds found throughout the environment in the air, water, and soil, and persist in the environment for months to years (1). In addition, many PAHs are carcinogenic and/or mutagenic (2). Major sources of PAHs in the environment are fossil fuel combustion processes (i.e., coal combustion) (3, 4). During coal combustion, PAHs exist in both the gas phase (flue gas) and the solid phase (fly ash) (5).

A common analysis procedure for PAHs on a solid matrix is extraction followed by gas chromatography/mass spectrometry (GC/MS) analysis. Previous studies indicate that PAHs are tightly bound to solids because of their strong hydrophobicity; hence, the type of extraction procedure used will strongly influence the quantification data obtained (6, 7). Ultrasonic extraction can reduce the extraction time from 16 to 18 hours used in Soxhlet extraction to a few minutes. This method has been specified as U.S. EPA standard method 3550B and has been widely used for extracting nonvolatile and semivolatile organic compounds from solid matrices such as soils, sludges and solid wastes (8).

The reduced times of ultrasonic extraction are attributed to the chemical and physical effects of ultrasound which are the result of the formation and collapse of cavitation bubbles in solution (9). For example, high pressure generated upon bubble

collapse enhances penetration of the solvent and transfer of the adsorbed solutes from the solid matrix (10). High temperature improves solubility and diffusivity of solute. Moreover, when cavitation bubbles collapse, shock waves and shear forces are produced that create microscopic turbulence within interfacial films surrounding nearby solid particles (11). This phenomenon increases mass transfer across the film, thus increasing the intrinsic mass-transfer coefficient (12). When cavitation bubbles collapse near a solid surface several orders of magnitude larger than the cavitation bubbles, collapses occur asymmetrically. This asymmetric collapse results in a fast moving stream of liquid passing through the cavity and impacting the surface of the solid at high velocity. This phenomenon is called a microjet (13). Microjets of solvent are formed perpendicular to the solid surface, and lead to pitting and erosion of the surface, reducing the path length for diffusion from the solid to the solvent (14).

Either an ultrasonic cleaning bath or probe has been commonly used to conduct ultrasonic extractions. Solid samples have been sonicated in a glass beaker or flask for times ranging from minutes to hours (15-20). Although ultrasonic extraction is widely accepted as a valid extraction method, the ultrasonic energy has been suspected to lead to undesired reactions of the solute and thus affect quantification results (21, 22). Previous research on the sonochemical decomposition of solutes were conducted predominately in aqueous solution (23-25); thus, the sonochemistry of solutes dissolved in organic solvents remains largely unexplored. Therefore, an investigation on the possible decomposition of PAHs in organic solution is necessary to elucidate the effect of ultrasound on PAHs during extraction.

In this research, we examined the sonolytic reactions of model PAHs including naphthalene, phenanthrene and pyrene in two common organic extraction solutions without the presence of solid particles with a particular focus on the solvent effect, solute concentration, pulse time, sonication time and formation of reaction by-products.

### 3.3. Materials and Methods

**Chemicals.** Naphthalene, phenanthrene and pyrene were used as model 2-ring, 3-ring and 4-ring PAHs, respectively. Naphthalene and phenanthrene were purchased from Sigma-Aldrich, pyrene was purchased from Fluka. All three PAHs had a purity of 99+% and were used without further purification. A standard containing 16 different PAHs (2000 mg L<sup>-1</sup> each) and a deuterated internal standard including a mixture of acenaphthene-d<sub>10</sub>, chrysene-d<sub>12</sub>, 1,4-dichlorobenzene-d<sub>4</sub>, naphthalene-d<sub>8</sub>, perylene-d<sub>12</sub> and phenanthrene-d<sub>10</sub> (2000 mg L<sup>-1</sup> each) were purchased from Ultra-Scientific. Hexane, acetone, dichloromethane (DCM), and toluene, purchased from Fisher Scientific, were of HPLC grade and used as received. Working solutions (2000 mg L<sup>-1</sup>) of naphthalene, phenanthrene and pyrene were prepared by dissolving the precisely weighed compound in DCM in a sealed volumetric flask. Different concentrations (0.1~10 mg L<sup>-1</sup>) of working solution were prepared by diluting the stock solution using either pure hexane or DCM.

**Sonication experiments.** Standard ultrasonic extraction conditions recommended in method 3550B (8) were followed to test the reactions of PAHs under sonication. An ultrasonic probe system with a 1.90 cm diameter titanium tip (Sonic Dismembrator 550, Fisher Scientific), operating at 20 kHz, was used to conduct experiments. The ultrasonic probe was properly tuned before each experiment. In all experiments, 1 mL model PAH

stock solution at various concentrations was added directly to a 100 mL solvent mixture (either hexane: acetone 1:1 V/V or DCM: acetone 1:1 V/V) and followed by 3 minutes sonication with output control knob set at 10 (full power) and pulse mode (energy on 50% of time and off 50% of time). Thus, the total ultrasonic irradiation time was 1.5 min. The solution was sonicated in a 400 mL glass beaker (Pyrex). The end of the probe tip was located 1.3 cm (1/2 inch) below the surface of the liquid. After sonication, the solution was decanted and collected in a flask. The sonication process was repeated twice with two additional 100 mL aliquots of solvent. The extracts from the three separate sonication processes were combined and the volume reduced using a Kuderna-Danish (K-D) concentrator to less than 10 mL. High purity nitrogen gas (Praxair) was used to further blowdown the extract to 1 mL.

The percent remaining of each PAH after sonication was defined as equation (1):

$$\text{Percent remaining (\%)} = \frac{\text{Measured PAH after sonication} - \text{PAH in blank}}{\text{Added PAH before sonication}} \times 100 \quad (1)$$

where *added PAH before sonication* is the known amount of PAH added into organic solvent before sonication, *measured PAH after sonication* is the amount of PAH after sonication. *PAH in blank* is the amount of PAH measured in the pure solvent mixture after sonication.

Unless stated otherwise, triplicate experiments were conducted to ensure reproducibility. Selected experiments were conducted on different days to verify temporal reproducibility.

**Control experiments.** Control experiments were conducted to determine if volatilization of PAHs led to their loss during sonication. Solutions of single components

of naphthalene, phenanthrene, or pyrene ( $100 \mu\text{g L}^{-1}$ ) in hexane/acetone and DCM/acetone were continuously stirred while the temperature was increased  $20 \text{ }^{\circ}\text{C}$  (e.g., from  $17 \text{ }^{\circ}\text{C}$  to  $37 \text{ }^{\circ}\text{C}$ ) to mimic conditions of ultrasonic extraction. Solutions were then condensed and analyzed for these three PAHs. In addition,  $10 \text{ mL}$  solution of either naphthalene or phenanthrene ( $200 \mu\text{g L}^{-1}$ ) in hexane/acetone mixture was put into a  $20 \text{ mL}$  sealed glass vial and sonicated using an ultrasonic bath (Branson, model 2210) for  $30 \text{ min}$ . Gas phase samples were withdrawn using a gas tight syringe and analyzed for naphthalene and phenanthrene by GC/MS.

**Instrumental analysis.** Quantitative analysis of PAHs was determined using a gas chromatograph with ion trap mass spectrometer (Thermo-Finnigan Polaris GCQ). A CP-5 fused silica capillary column ( $30 \text{ m} \times 250 \mu\text{m} \times 0.25 \mu\text{m}$ , Varian) was used to separate PAHs. Helium was used as the carrier gas with a flow rate of  $1.2 \text{ mL min}^{-1}$ . Splitless injections of  $2 \mu\text{L}$  extract spiked with the deuterated internal standard were made at an injector temperature and ion source temperature of  $250 \text{ }^{\circ}\text{C}$ . The column was held at  $60 \text{ }^{\circ}\text{C}$  for  $2 \text{ min}$ , programmed to  $250 \text{ }^{\circ}\text{C}$  at  $20 \text{ }^{\circ}\text{C min}^{-1}$  followed by a  $2 \text{ min}$  hold time, increased to  $300 \text{ }^{\circ}\text{C}$  at  $10 \text{ }^{\circ}\text{C min}^{-1}$ , then held for  $8 \text{ min}$ . The temperature of the mass transfer line was  $300 \text{ }^{\circ}\text{C}$ . The mass spectrometer was operated in full scan mode for both standards and extracts. PAHs and other semi-volatile compounds were identified by matching mass spectra to a NIST spectra database. Sixteen EPA-specified PAHs were confirmed using the retention times and quantified using calibration curves from running standard PAH compounds. The detection limits for these 16 PAHs ranged from  $0.1$  to  $1 \mu\text{g kg}^{-1}$ , depending on the boiling point of the individual PAH.

### 3.4. Results and Discussion

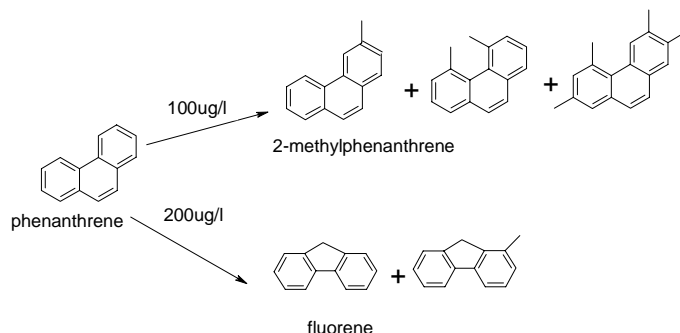
**Mechanisms for loss of PAHs during ultrasonic extraction.** Due to the chemical and physical effects resulting from cavitation bubbles collapsing, there are two possible mechanisms that lead to loss of PAHs during extraction: volatilization and degradation. For small molecular weight PAHs with lower boiling points, loss due to volatilization is more important. Our first goal was to examine if volatilization leads to the loss of PAHs during sonication.

The results of control experiments showed that loss of three PAHs (naphthalene, phenanthrene, and pyrene) due to heating from 17 °C to 37 °C was approximately 1.1% ± 1.5%. In addition, gas phase samples from sonication of either naphthalene or phenanthrene did not reveal any volatilization to the headspace. The results of these control experiments indicate that loss of PAHs due to volatilization during sonication was negligible.

Sonication of 3 model PAHs (e.g., naphthalene, phenanthrene and pyrene) in organic solvents was then conducted to study the possible degradation of PAHs by ultrasound. No known studies on the degradation of PAHs under sonication in nonaqueous solvents have been reported in the literature; thus efforts were taken to detect by-product formation during sonication of model PAHs in either hexane/acetone or DCM/acetone mixtures. Although no methylated or ethylated by-products were detected during sonication of naphthalene and pyrene, several possible methylated or ethylated PAHs were detected during the sonication of phenanthrene by matching mass spectra with the NIST database. In addition, selected mass spectra were verified by running

authentic standards of compounds including 1-methylphenanthrene, 2-methylnaphthalene and 2, 3, 5-trimethylnaphthalene.

The lack of by-product formation for naphthalene and pyrene may be related to their chemical and physical properties. For example, the low vapor pressure of pyrene may inhibit its migration to cavitation bubbles and thus reduce the possibility of pyrolysis reactions. For low boiling point PAHs such as naphthalene, the formation of an array of pyrolysis by-products may result in low peak areas of any by-product peaks and thus any by-products present were below the detection limits. For phenanthrene, the formation of by-products was affected by the initial concentration of phenanthrene as suggested in scheme 3.1. For example, pulse sonication of phenanthrene in hexane/acetone with a total ultrasonic irradiation time of 1.5 min, at an initial concentration of  $200 \mu\text{g L}^{-1}$  resulted in a decrease in the mono to tetra-methyl substituted phenanthrene derivatives compared to that in  $100 \mu\text{g L}^{-1}$  phenanthrene solution. On the contrary, other by-products such as fluorene and mono-substituted methyl fluorene that were not detected at  $100 \mu\text{g L}^{-1}$  were detected at  $200 \mu\text{g L}^{-1}$ . The existence of 2-methylphenanthrene and fluorene was verified by running authentic standards. The other methylated phenanthrene or methylated fluorene by-products were speculated by matching mass spectras with the NIST database. In addition, some ethylated phenanthrene, not shown in scheme 3.1, may be formed based on matching spectra with the NIST database.



Scheme 3.1. By-products formed during pulse sonication of phenanthrene in hexane: acetone 1:1 V/V mixture for a total irradiation time of 1.5 min and pulse time of 5 sec.

In general, a solute experiences both attack by free radicals and atoms formed from the decomposition of solvent vapor and pyrolysis in the gaseous cavitation bubbles or hot layer between the hot gaseous nucleus of the hot spot and the bulk liquid at ambient temperature during sonication. Both decomposition of solvent vapor and pyrolysis produce different products, with the relative abundances depending on the nature of the solute and its concentration (26). Suslick *et al.* found that sonolysis of simple hydrocarbons creates the same kinds of products associated with very high temperature pyrolysis (27). Methyl ( $\text{CH}_3\cdot$ ) and ethyl ( $\text{CH}_3\text{CH}_2\cdot$ ) radicals are expected to be formed when hexane (28) is decomposed sonochemically. Methyl radicals also have been shown to form during the pyrolysis of acetone molecules (29). These radicals then react with phenanthrene to form different types of methyl and ethyl phenanthrene by-products. Cypres and Bettens studied the mechanism of pyrolysis of tricyclic aromatic compounds using radioactive carbon labeled compounds. Their results showed that at temperatures less than  $900\text{ }^\circ\text{C}$ , the pyrolysis of phenanthrene had two pathways: 1) loss of

one carbon yielding CH<sub>4</sub> and fluorene; and 2) fragmentation resulting in a four carbon fragment and naphthalene (30). Therefore, fluorene is an indication of a pyrolysis by-product formed due to high temperature reactions in or near a cavitation bubble. Adewuyi (31) reviewed applications of sonochemistry in environmental science and engineering and noted that pyrolysis in the interfacial region was predominant at high solute concentrations. While at low solute concentrations, free-radical reactions were likely to be dominant. The comment of Adewuyi is consistent with our results.

**Effect of PAH concentration.** Sonication of phenanthrene at seven different concentrations (1, 2, 3, 5, 10, 50, 100, 200 µg L<sup>-1</sup>) was conducted in either hexane/acetone or DCM/acetone. The effect of initial phenanthrene concentration on the percent remaining is shown in Figure 3.1. At lower initial concentrations (less than 10 µg L<sup>-1</sup>), the percent remaining of phenanthrene varied from 80% to 110%. However, when the initial concentration ranged from 50 to 200 µg L<sup>-1</sup>, the percent remaining of phenanthrene stabilized at the lower value.

When phenanthrene was sonicated in organic solvent, the amount of phenanthrene volatilizing into and migrating towards the gaseous cavitation bubbles was expected to be small because of its low vapor pressure ( $1.6 \times 10^{-7}$  atm at 25 °C); thus, fewer reactions occurred resulting in a higher percent remaining. With the increase of concentration, more phenanthrene molecules were available to migrate toward the cavitation bubble interfaces or volatilize into the cavitation bubbles to react under pyrolysis and thus led to a lower percent remaining.

**Effect of solvent.** Hexane: acetone (1:1 V/V) and DCM: acetone (1:1 V/V) were examined for their effects on the percent of PAHs remaining after sonication. As shown

in Figure 3.1, at the same phenanthrene concentration, the hexane/acetone mixture yielded a higher percent remaining than the DCM/acetone mixture. The difference may be due to different cavitation conditions resulting from different characteristics of these solvents.

The formation of cavitation bubbles (i.e., vapor-filled microbubbles) in a liquid requires that the negative pressure in the rarefaction region of the ultrasonic wave must overcome the intermolecular forces acting within the liquid. Thus, cavities are more readily formed when using solvents with low viscosity ( $\mu$ ), and low surface tension ( $\sigma$ ) (32). However, the intensity of cavitation is benefited by using solvents that have higher viscosity and surface tension. Solvents with high surface tension and viscosity generally have a higher threshold for cavitation but more harsh conditions once cavitation is established resulting in higher temperatures and pressures upon bubble collapse. Accordingly, larger mole fraction of the solvent and solute react under higher temperature and pressure conditions (33). Among the three solvents used, DCM has the highest surface tension and viscosity (28.12 dynes/cm and 0.425 cP at 20 °C, respectively). Thus, DCM/acetone is expected to have a higher cavitation threshold than hexane/acetone resulting in fiercer cavitation conditions, a reason that a lower percent of phenanthrene remained in the DCM/acetone solvent.

The vapor pressure of the solvent is another important factor affecting cavitation. Higher vapor pressure leads to more solvent volatilizing into the cavitation bubbles. As a result, the maximum pressure and temperature is lower compared to low vapor pressure solvents because a portion of the energy generated during collapse goes toward condensation and endothermic reactions of the vapor (32, 33). Mizukoshi *et al.* studied

the sonolysis of various types of organic liquids including hydrocarbons, ethers, ketones and alcohols. They observed that the decomposition rates of solvents increased with increasing vapor pressure in low vapor pressure liquids reaching maximum values and then decreasing with further increases in vapor pressure (34). DCM has the highest vapor pressure (0.46 atm at 20 °C) among these three solvents, thus lower temperatures and pressures occur during cavitation. However, our results show that compared with viscosity and surface tension, the effect of vapor pressure was less important. The cavitation effects in DCM/acetone appeared to be stronger resulting in a lower percent remaining for phenanthrene.

Our results also show that different solvents altered by-product formation. When hexane/acetone was used as the solvent, methylated PAH formation was larger than when using DCM/acetone as the solvent. This change in by-products may be due to more methyl radical generation during hexane/acetone sonication since methyl radical ( $\text{CH}_3\cdot$ ) can be formed when hexane or acetone is decomposed (28, 29). When DCM/acetone was sonicated, although acetone is also expected to form methyl radicals, the amount formed was much less compared with hexane/acetone sonication as DCM does not generate  $\text{CH}_3\cdot$  upon sonolysis. Thus, the amount of methyl phenanthrene formed was correspondingly less.

Chlorine radical ( $\text{Cl}\cdot$ ) is formed during sonication of haloalkanes (35). Spin-trapping studies (36) during ultrasonic irradiation of neat  $\text{CCl}_4$  also verified the formation of  $\text{Cl}\cdot$ . However, in our work, no expected chlorinated organic by-products were detected after sonication of phenanthrene in DCM/acetone. We expect that when hydrocarbon and halocarbon mixtures are used as solvents, halogenations of solute are suppressed. Instead

of Cl reacting with the solute forming chlorinated PAHs, the alkane solvent traps Cl forming halogenated hydrocarbons and HCl (32). The halogenated hydrocarbons formed were expected to be volatile and evaporate prior to analysis.

Toluene was also tested for the reactions of phenanthrene during 3 min ultrasonic reaction (5 sec pulse time) at two different initial concentrations (10  $\mu\text{g/L}$  and 50  $\mu\text{g/L}$ ). No reaction by-products were found and the percent of phenanthrene remaining after sonication was approximately  $98\% \pm 3\%$  suggesting no sonolytic reactions occurred when toluene was used as the solvent. During sonication, less toluene migrated into cavitation bubbles due to its lower vapor pressure compared to hexane and acetone. Thus, fewer radicals formed from the dissociation of toluene molecules resulting in a higher percent of phenanthrene remaining after 3 min of ultrasonic exposure compared to DCM/acetone or hexane/acetone.

**Effect of pulse time.** To test the effect of pulse time on the percent remaining of phenanthrene using hexane/acetone as the solvent, five different pulse times (0.1, 0.5, 1, 3, and 5 sec) with equal alternating pulse and interval periods, were performed with the same total ultrasonic irradiation time (i.e., 1.5 min). As shown in Figure 3.2, the percent remaining of phenanthrene was the highest at 0.1 sec and lowest at 0.5 sec pulse time. Once the pulse time was larger than 1 sec, the recovery of phenanthrene remained stable (around 87%).

The pulse mode enables ultrasound to be delivered intermittently and thereby allow periods of cooling (37). It is believed that the activity of sonochemically induced cavitation sites involves an “activation time”, the time required to develop bubbles capable of chemical activity, and a “deactivation time”, during which time the cavitation

sites cease to exist (38). If the pulse time is too short, cavitation bubbles will not have sufficient time to grow to a size capable of collapse. When the pulse time is longer, the growth of bubbles is sufficient to allow cavitation collapse. Similarly, if the off time is too long, activation of the system fades away before the next pulse is initiated; the following pulse must reactivate anew (26).

In our experiments, less degradation of phenanthrene at 0.1 sec pulse time may be due to the incomplete growth of cavitation bubbles. At 0.5 sec pulse time, although the time may be longer than the bubble activation time, the bubble deactivation time was longer than 0.5 sec. Thus, deactivation did not occur. The subsequent pulse arrived earlier to interact with some of the bubbles remaining from the previous pulse resulting in more radical formation. Thus, the cavitation is more efficient resulting in a lower percent of phenanthrene remaining. At longer pulse times (e.g., 5 sec), activation and deactivation occurred during each pulse yielding similar cavitation conditions resulting in a consistent percent remaining of phenanthrene around 87%.

**Effect of other PAHs on sonication.** Usually, more than one type of PAH exists on the solid matrix. Thus, multiple PAHs were simultaneously sonicated to test the influence of other PAHs on the degradation of the target PAH in the absence of a solid matrix. Equimolar binary mixtures of naphthalene, phenanthrene and/or pyrene at a total PAH concentration of  $0.568 \mu\text{mol L}^{-1}$  and equimolar ternary mixtures of these three compounds at a total concentration of  $0.852 \mu\text{mol L}^{-1}$  were sonicated for 1.5 min total ultrasonic irradiation time with a pulse time of 5 sec. The results of binary mixtures are shown in Figure 3.3.

As shown in Figure 3.3a, an equal PAH concentration of phenanthrene or pyrene and naphthalene resulted in an increased percent remaining of naphthalene compared to an equal PAH concentration of only naphthalene in DCM/acetone. Less degradation of naphthalene in binary PAH mixtures compared to the single naphthalene system at the same concentration may be due to competition of naphthalene molecules with other PAHs molecules to react with radicals or enter cavitation bubble for pyrolysis reactions and thus resulting in fewer naphthalene reactions. In Figure 3.3b and 3.3c, the percent remaining of phenanthrene and pyrene also increased due to the addition of other PAHs sonicated in DCM/acetone. Change of percent remainings of naphthalene, phenanthrene, and pyrene binary mixtures did not were more complicated when sonicated in hexane/acetone.

When two PAH compounds were sonicated simultaneously, the larger molecular weight PAH had a higher percent remaining than the smaller molecular weight PAH. Also, when equal molar concentrations of three PAHs were sonicated, the recovery rates were pyrene > phenanthrene > naphthalene in either DCM/acetone or hexane/acetone as shown in Figure 3.4. This may due to different vapor pressures of these three PAHs (naphthalene > phenanthrene > pyrene). With the lowest vapor pressure among these three PAHs, pyrene resulted in the least amount of reaction in cavitation bubbles and thus the highest percent remaining. In addition, except for the naphthalene and pyrene binary mixture, DCM/acetone resulted in a lower percent of PAH remaining compared to hexane/acetone, agreeing with results of solvent effect on the percent of phenanthrene remaining described above.

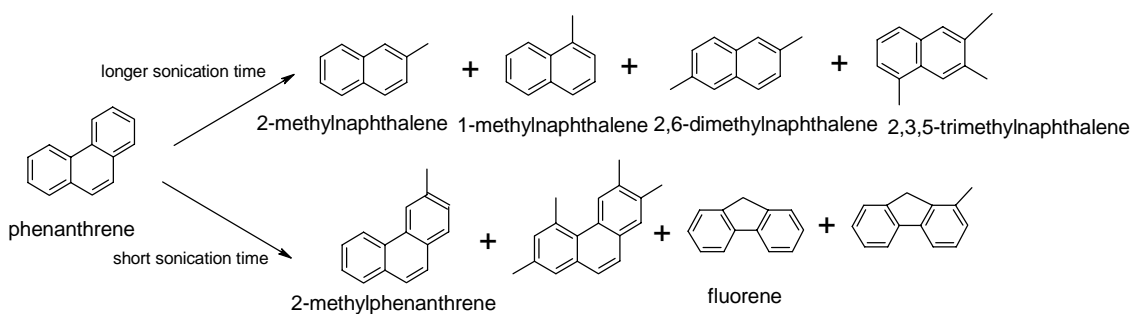
**Effect of sonication time.** Experiments at different ultrasonic irradiation times (1.5, 6, 10, 20, 30, 40 min) with pulse mode (5 sec pulse time) were conducted using phenanthrene at  $100 \mu\text{g L}^{-1}$  and  $200 \mu\text{g L}^{-1}$  concentrations to examine the effect of sonication time on the degradation of PAHs. Initial results showed obvious solvent loss and bulk solution temperature increases when the sonication time was longer than 10 min. A water bath was then used to control the increase of bulk temperature to less than a  $20^\circ\text{C}$  (i.e., from  $17^\circ\text{C}$  to  $37^\circ\text{C}$ ) during sonication times longer than 10 min, similar to the temperature increase observed during short time experiments.

Decrease of percent remaining was expected at longer sonication times due to high temperature and radical reactions from cavitation. However, a reproducible but unexpected increase in the percent remaining was observed with longer sonication times. As shown in Figure 3.5, at an initial concentration of  $100 \mu\text{g L}^{-1}$ , the percent remaining of phenanthrene decreased from 88% to 75% with increasing sonication time from 1.5 min to 10 min and then recovered up to 85% at 40 min sonication time. When the initial concentration was  $200 \mu\text{g L}^{-1}$ , the percent remainings of phenanthrene showed a similar trend.

To investigate the change in percent remaining with sonication time, by-product formation as a function of sonication time was investigated. With longer sonication time (up to 40 min), methylnaphthalene products were detected in addition to methylated phenanthrene and fluorene. 1-methylnaphthalene, 2-methylnaphthalene, 2,6-dimethylnaphthalene and 2,3,5-trimethylnaphthalene were verified by running authentic standards (see scheme 3.2). Cypres and Bettens reported naphthalene and benzene formation during phenanthrene pyrolysis ( $< 900^\circ\text{C}$ ) (30). Badger *et al.* studied

phenanthrene pyrolysis at 700 °C and 850 °C and reported naphthalene as one of the pyrolysis products (39). Therefore, detected methylated naphthalene by-products may be direct pyrolysis products of phenanthrene or products of formed naphthalene reacting with methyl radicals generated from the dissociation of solvent.

As shown in Figure 3.6, with the increase of sonication time, the amount of methylated naphthalene by-products and fluorene first increased and then decreased, suggesting formation and decomposition reactions of these by-products. Since the percent remaining of phenanthrene decreased and then increased with increasing sonication time as shown in Figure 3.6, we suspected that the increase of phenanthrene percent remaining with longer sonication may be due to the formation of phenanthrene from by-products such as fluorene. A radical mechanism proposed by McNab showed phenanthrene formation from pyrolysis of 9, 9-dimethylfluorene at 800 °C by a free radical ring expansion process (40). Thus, fluorene formed during the sonication of phenanthrene may be attacked by methyl radicals from hexane dissociation to regenerate phenanthrene.



Scheme 3.2. By-products formed during the sonication of phenanthrene in hexane: acetone 1:1 V/V at different sonication times in the absence of a solid matrix (pulse time = 5 sec).

The results presented above demonstrate that the choice of solvent affects the degradation of PAHs under sonication. For example, hexane/acetone showed less PAH degradation compared to DCM/acetone and no degradation was observed with toluene as the solvent. In addition, larger molecular weight PAHs had fewer sonolytic reactions compared to small molecular weight PAHs due to their higher vapor pressures. Degradation by-products change under different ultrasonic conditions such as initial solute concentration, sonication time, and solvent type. For example, methylated phenanthrene by-products were identified when hexane/acetone or DCM/acetone were used as solvents. Therefore, if ultrasound is used in sample preparation, either standard ultrasonic extraction or other ultrasound-aided extractions, reports of the presence of these by-products may be misleading, especially when dealing with trace levels of small molecular weight PAHs.

The presence of a solid matrix may affect these variables and PAH behavior. Therefore, depending on different solid matrices, these variables may need to be modified to maximize recovery and minimize reactions. However, our work on ultrasonic extraction of PAHs from lime spray dryer ash showed toluene extracted more PAHs from the solid particles compared to hexane/acetone and DCM/acetone mixtures consistent with our conclusion that toluene was the best solvent to minimize PAH reactions(41). Thus, since no sonolytic reaction of phenanthrene was observed with toluene as the solvent and the extraction efficiency was better than other solvents investigated, it is recommended that toluene be used in ultrasonic extractions of PAHs.

## **Acknowledgments**

The authors would like to thank the Ohio Coal Development Office (OCDO) and The Ohio State University for funding. P. Sun gratefully acknowledges a University Fellowship and Presidential Fellowship from The Ohio State University.

## References:

1. Wild, S. R.; Waterhouse, K. S.; McGrath, S. P.; Jones, K. C. *Environ. Sci. Technol.* **1990**, *24*, 1706-1711.
2. Denissenko, M. F.; Pao, A.; Tang, M-S.; Pfeifer, G. P. *Science* **1996**, *274*, 430-432.
3. Mastral, A. M.; Callen, M. S. *Environ. Sci. Technol.* **2000**, *34*, 3051-3057.
4. Pisupati, S. V.; Wasco, R. S.; Scaroni, A. W. *J. Hazard. Mater.* **2000**, *74*, 91-107.
5. Liu, K-L.; Xie, W.; Zhao, Z-B.; Pan, W-P.; Riley, J. T. *Environ. Sci. Technol.* **2000**, *34*, 2273-2279.
6. Noordkamp, E. R.; Grotenhuis, J. T. C.; Rulkens, W. H. *Chemosphere* **1997**, *35*, 1907-1917.
7. Jonker, M. T. O.; Koelmans, A. A. *Environ. Sci. Technol.* **2002**, *36*, 4107-4113.
8. *Method 3550B, Ultrasonic Extraction*; 1996, U.S. Environmental Protection Agency.
9. Hromadkova, Z.; Ebringerova, A.; Valachovic, P. *Ultrason. Sonochem.* **1999**, *5*, 163-168.
10. Margulies, T. S.; Schwarz, W. H. J. *Acoust. Soc. Am.* **1985**, *78*, 605-615.
11. Doktycz, S. J.; Suslick, K. S. *Science* **1990**, *247*, 1067-1069.
12. Weavers, L. K.; Hoffmann, M. R. *Environ. Sci. Technol.* **1998**, *32*, 3941-3947.
13. Suslick, K. S. *Science* **1990**, *247*, 1439-1445.
14. Suslick, K. S.; Doktycz, S. J. In *Advances in Sonochemistry*, JAI Press Ltd.: Hampton Hill, 1990; Vol. 1, pp 197-230.
15. Griest, W. H.; Tomkins, B. A.; Caffrey, J. R. *Anal. Chem.* **1988**, *60*, 2169-2171.
16. Sun, F-S.; Littlejohn, D.; Gibson, M. D. *Anal. Chim. Acta.* **1998**, *364*, 1-11.

17. Mitra, S.; Dickhut, R. M.; Kuehl, S. A.; Kimbrough, K. L. *Mar. Chem.* **1999**, *66*, 113-127.
18. Mastral, A. M.; Callen, M. S.; Garcia, T.; Lopez, J. M. *Environ. Sci. Technol.* **2001**, *35*, 2645-2649.
19. Ghosh, U.; Talley, J. W.; Luthy, R. G. *Environ. Sci. Technol.* **2001**, *35*, 3468-3475.
20. Mecozzi, M.; Amici, M.; Pietrantonio, E.; Romanelli, G. *Ultrason. Sonochem.* **2002**, *9*, 11-18.
21. Burford, M. D.; Hawthorne, S. B.; Miller, D. J. *Anal. Chem.* **1993**, *65*, 1497-1505.
22. Song, Y-F.; Jing, X.; Fleischmann, S.; Wilke, B-M. *Chemosphere* **2002**, *48*, 993-1001.
23. Leonhardt, E.; Stahl, R. *Anal. Chem.* **1998**, *70*, 1228-1230.
24. Cataldo, F. *Ultrason. Sonochem.* **2000**, *7*, 35-43.
25. Little, C.; Hephher, M. J.; El-Sharif, M. *Ultrasonics* **2002**, *40*, 667-674.
26. Henglein, A. In *Advances in Sonochemistry*, JAI Press Ltd.: Hampton Hill, 1993; Vol. 3, pp 17-83.
27. Suslick, K. S.; Gawienowsko, J. W.; Schubert, P. F.; Wang, H. H. *Ultrasonics* **1984**, *22*, 33-36.
28. Vladimir, M.; Riesz, P. *Ultrason. Sonochem.* **1996**, *3*, S173-S186.
29. Scott, E. J. Y. *Ind. Eng. Chem. Res.* **1967**, *6*, 67-72.
30. Cypres, R.; Bettens, B. *Fuel* **1986**, *65*, 507-513.
31. Adewuyi, Y.G. *Ind. Eng. Chem. Res.* **2001**, *40*, 4681-4715.
32. Thompson, L. H.; Doraiswamy, L. K. *Ind. Eng. Chem. Res.* **1999**, *38*, 1215-1249.

33. Colussi, A. J.; Weavers, L. K., Hoffmann, M. R. *J. Phys. Chem. A* **1998**, *102*, 6927-6934.
34. Mizukoshi, Y.; Nakamura, H.; Bandow, H.; Maeda, Y.; Nagata, Y. *Ultrason. Sonochem.* **1999**, *6*, 203-209.
35. Riesz, P.; Berdahl, D.; Christman, C. L. *Environ. Health Persp.* **1985**, *64*, 233-252.
36. Rosenthal, I.; Mossoba, M. M.; Riesz, P. *J. Magn. Reson.* **1981**, *45*, 359-361.
37. Mason, T. J.; Lorimer, J. P. In *Applied sonochemistry: the uses of power ultrasound in chemistry and processing*; Wiley-VCH: Weinheim, 2001; pp 40-42.
38. Henglein, A.; Ulrich, R.; Lilie, J. *J. Am. Chem. Soc.* **1989**, *111*, 1974-1979.
39. Badger, G. M.; Donnelly, J. K.; Spotswood, T. M. *Aust. J. Chem.* **1964**, *17*, 1138-1146.
40. McNab, H. *ARKIVOC* **2000**, *6*, 59-66.
41. Sun, P.; Weavers, L. K.; Taerakul, P.; Walker, H. W. *Chemosphere* **2004**, submitted.

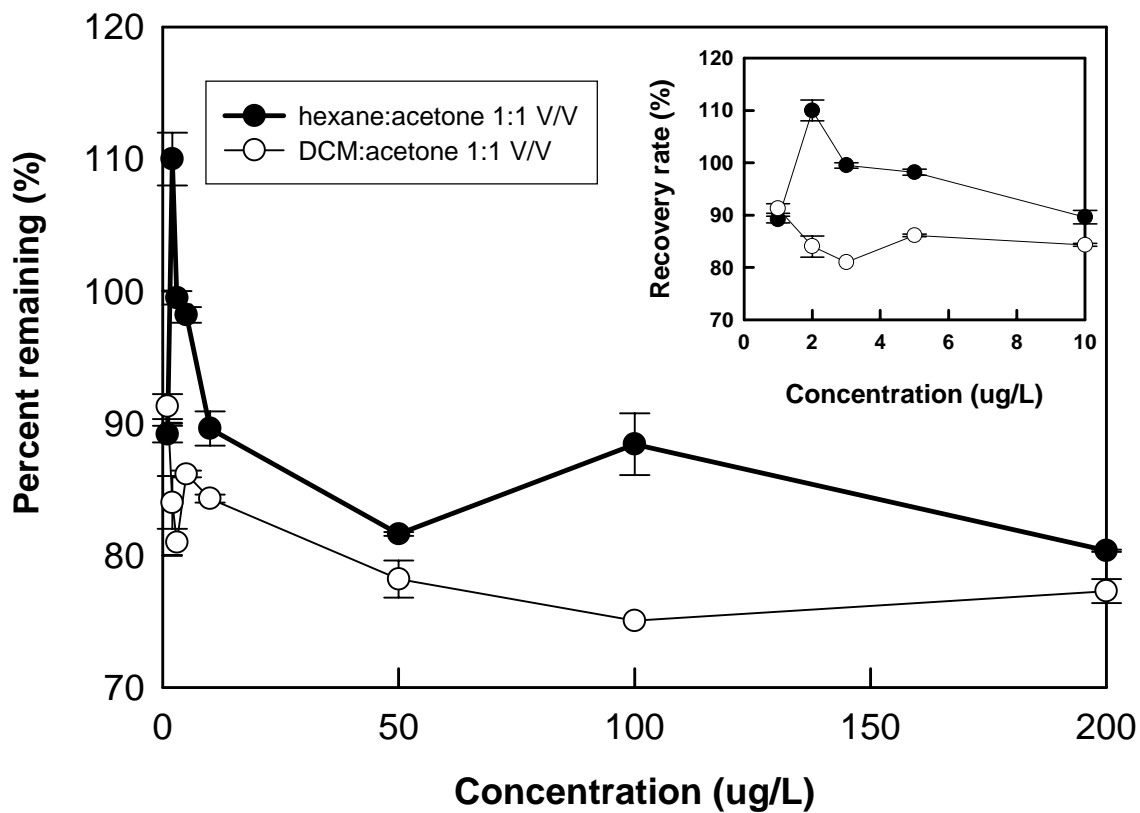
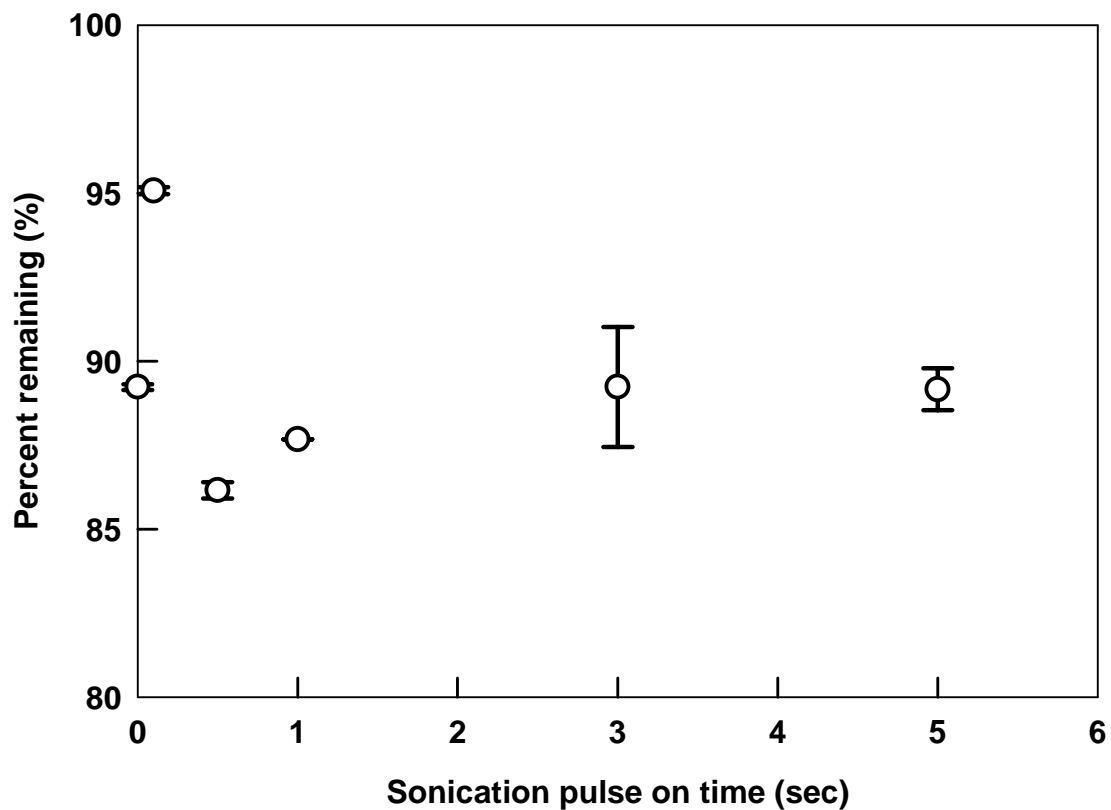


Figure 3.1. Effects of solvents on percent remaining of phenanthrene during sonication with initial concentrations of 1, 2, 3, 5, 10, 50, 100, and 200  $\mu\text{g L}^{-1}$  in either hexane: acetone or DCM: acetone 1:1 V/V. Total ultrasonic irradiation time was 1.5 min; pulse time was 5 sec. Inset: enlargement of figure at the concentration ranging from 1 to 10  $\mu\text{g L}^{-1}$ .



\*0 pulse time indicates continuous ultrasonic irradiation

Figure 3.2. Percent remaining of phenanthrene at  $100 \mu\text{g L}^{-1}$  concentration in hexane: acetone 1:1 V/V under pulse sonication. Pulse time is 0.1, 0.5, 1, 3, and 5 sec respectively, pulse time equal to pulse off time, total ultrasonic irradiation time was 1.5 min.

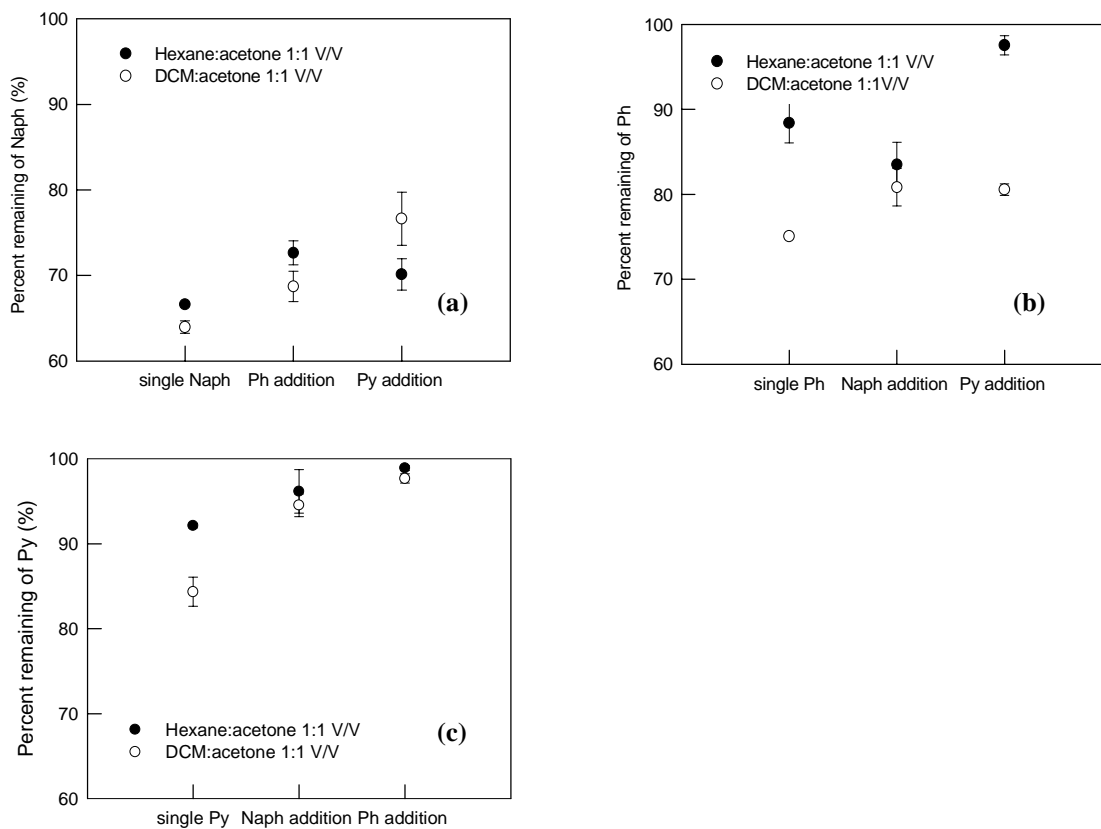


Figure 3.3. Percent remainings of PAHs in the presence of another PAH in either hexane: acetone or DCM: acetone 1:1 V/V solution. Total ultrasonic irradiation time is 1.5 min with pulse time of 5 sec. (a) Percent remaining of  $0.284 \mu\text{mol L}^{-1}$  naphthalene (Naph) in the presence of a  $0.284 \mu\text{mol L}^{-1}$  phenanthrene (Ph) addition or a pyrene (Py) addition and percent remaining of  $0.568 \mu\text{mol L}^{-1}$  Naph (single Naph); (b) Percent remaining of  $0.284 \mu\text{mol L}^{-1}$  of Ph in the presence of  $0.284 \mu\text{mol L}^{-1}$  Naph addition or Py addition and percent remaining of  $0.568 \mu\text{mol L}^{-1}$  Ph (single Ph); (c) Percent remaining of  $0.284 \mu\text{mol L}^{-1}$  of Py in the presence of  $0.284 \mu\text{mol L}^{-1}$  Naph addition or Ph addition and percent remaining of  $0.568 \mu\text{mol L}^{-1}$  Py (single Py).

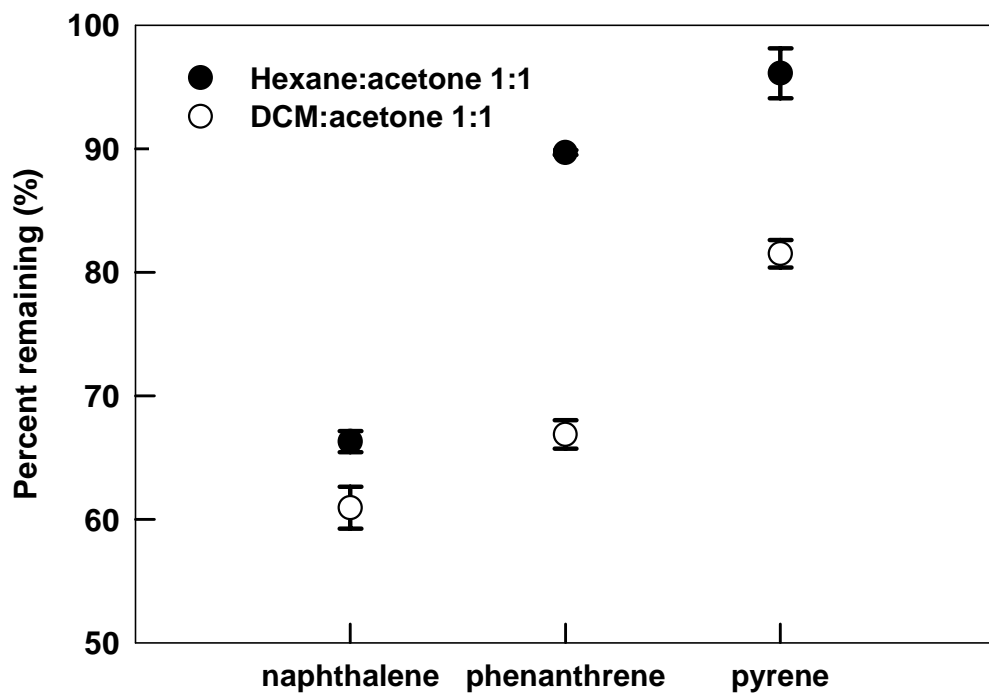


Figure 3.4. Sonication of ternary mixture of naphthalene, phenanthrene and pyrene in either hexane: acetone or DCM: acetone 1:1 V/V. The concentration of each compound was  $0.284 \mu\text{mol L}^{-1}$ , total ultrasonic irradiation time was 1.5 min, pulse time was 5 sec.

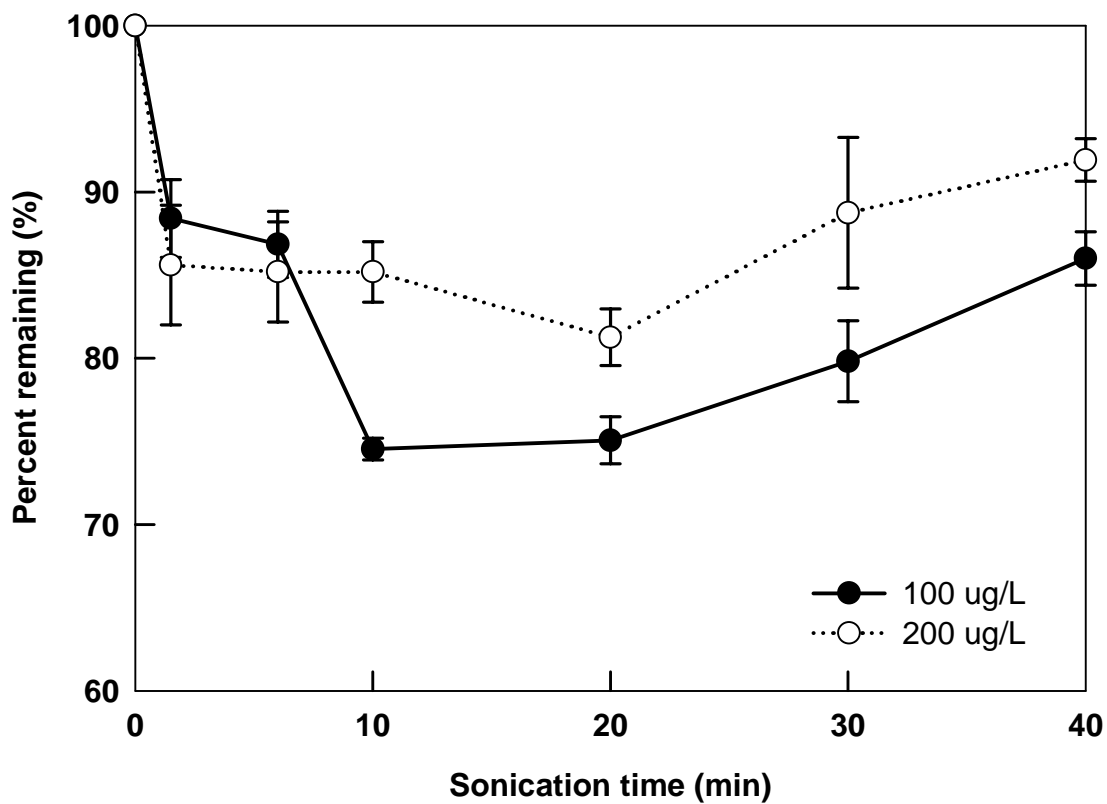


Figure 3.5. Percent remaining of  $100 \mu\text{g L}^{-1}$  and  $200 \mu\text{g L}^{-1}$  phenanthrene in hexane: acetone 1:1 V/V under different ultrasonic irradiation times of 1.5, 6, 10, 20, 30, 40 min. Pulse time is 5 sec.

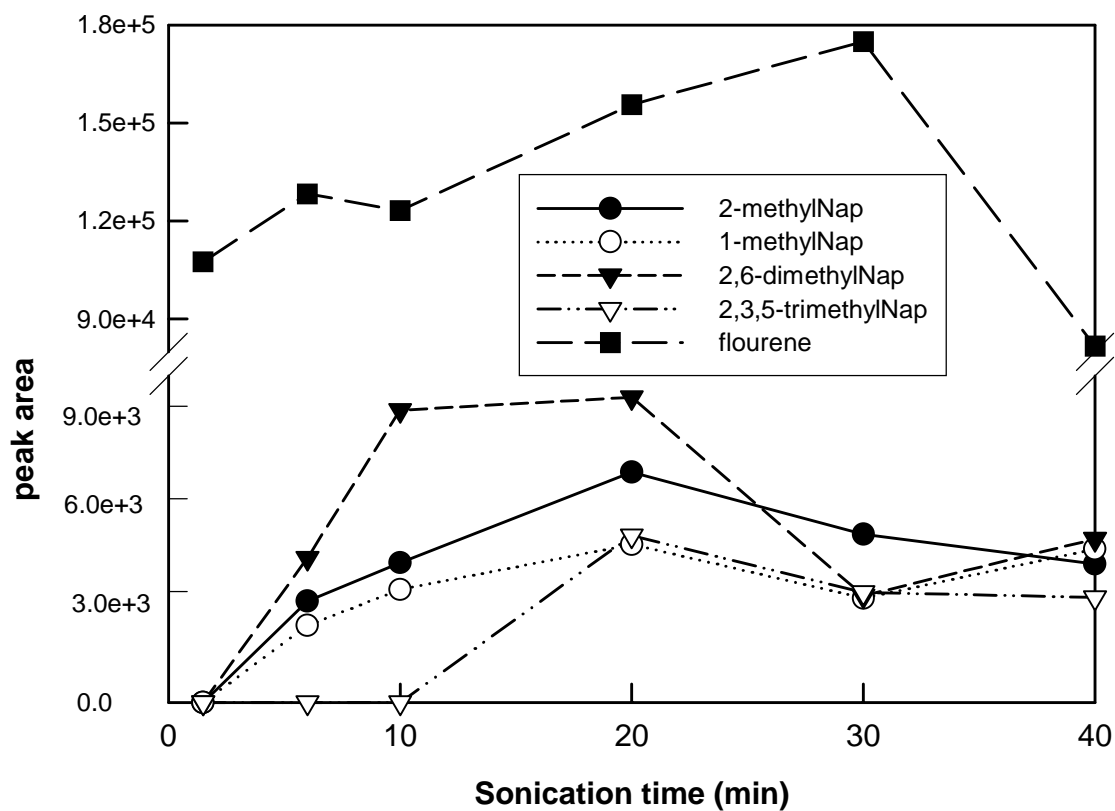


Figure 3.6. Peak area change of degradation by-products formed from sonication of  $200 \mu\text{g L}^{-1}$  phenanthrene in hexane: acetone 1:1 V/V with different sonication time of 1.5, 6, 10, 20, 30, 40 min and pulse time = 5 sec. (●): 2-methylnaphthalene (2-methylNap); (○): 1-methylnaphthalene (1-methylNap); (▼): 2,6-dimethylnaphthalene (2,6-dimethylNap); (▽): 2,3,5-trimethylnaphthalene (2,3,5-trimethylNap); (■): Fluorene.

## CHAPTER 4

### DISTRIBUTION OF POLYCYCLIC AROMATIC HYDROCARBONS (PAHs) IN LIME SPARY DRYER (LSD) ASH

#### 4.1. Abstract

Four lime spray dryer (LSD) ash samples were collected from a spreader stoker boiler and measured for their concentrations of 16 US EPA specified polycyclic aromatic hydrocarbons (PAHs). Results showed that the total measured PAH concentration correlated with the organic carbon content of the LSD ash. Each LSD ash sample was then separated using a 140 mesh sieve into two fractions: a carbon-enriched fraction (>140 mesh) and a lime-enriched fraction (<140 mesh). Unburned carbon was further separated from the carbon-enriched fraction with a lithiumheteropolytungstate (LST) solution. PAH measurements on these different fractions showed that unburned carbon had the highest PAH concentrations followed by the carbon-enriched fraction indicating that PAHs were primarily associated with the carbonaceous material in LSD ash. However, detectable levels of PAHs was also found in the lime-enriched fraction, suggesting that the fine spray of slaked lime may sorb PAH compounds from the flue gas in the LSD process.

## 4.2. Introduction

Flue gas desulfurization (FGD) technology has been widely used in utility coal fired power plants in an effort to reduce sulfur dioxide (SO<sub>2</sub>) emissions and thus control acid rain (1). FGD processes are broadly classified as wet and dry processes, depending on whether wet or dry products are formed (2). Lime spray dryer (LSD) is the most common dry FGD technique used (3). In the LSD system, a fine spray of slaked lime (Ca(OH)<sub>2</sub>) is injected into the scrubber to capture sulfur oxides resulting in the formation of calcium sulfate or calcium sulfite. The dry calcium sulfite/sulfate mixture formed, along with fly ash, is later collected by an electrostatic precipitator or a baghouse and called LSD ash (1).

The application of FGD technology effectively reduces SO<sub>2</sub> emissions. However, over 29 million metric tons of FGD by-products including LSD ash are generated annually in United States (3, 4). More than 18 million metric tons (72% of total production) are disposed in landfills. Rather than dispose of these by-products as waste, efforts are underway to identify opportunities to reuse them (5-9). Prior to reuse, FGD by-products must be thoroughly characterized. Currently, the environmental characterization of FGD by-products is poor, resulting in a major hurdle for their utilization (10).

One area in particular that has received little attention is organic species generated during coal combustion such as polycyclic aromatic hydrocarbons (PAHs) on FGD by-products (3). Compared to inorganic components such as heavy metals, organic components are expected to be present in lower amounts and consequently are often

neglected in characterization studies. However, PAHs may also affect the environment when FGD by-products are disposed or utilized.

PAHs are a class of organic compounds that has attracted environmental and health concerns. They are ubiquitous, persisting in the environment for months to years (11). Many PAHs are carcinogenic and/or mutagenic (12). A major source of PAHs in the environment is from fossil fuel combustion processes (13). During the LSD process, gas phase PAHs formed from coal burning may sorb onto unreacted lime and calcium sulfite/sulfate. In addition, PAHs associated with fly ash particles will also be present in LSD ash (4). The possible release of these compounds makes it necessary to conduct investigations of PAHs and other organic compounds during combustion (e.g., concentration, fate) to ensure the environmentally safe reuse of LSD ash.

To date, no research on the distribution of PAHs in LSD ash has been reported. Previous studies investigated the distribution of PAHs in fly ash, soil and sediment (14-16, 18). One study on the characterization of PAHs on fly ash showed that PAHs were primarily associated with carbonaceous materials although the mass fraction of carbon represented only a small portion of the total composition (17). Ghosh et al. also found that the majority of PAHs in a harbor sediment were associated with coal-derived particles and the PAHs were strongly adsorbed to these particles based on direct analysis of separated fractions and particle-scale microanalysis (16). LSD ash also contains unburned carbon and mineral phases. Therefore, PAHs may be primarily associated with the carbonaceous materials.

In this paper, distribution of PAHs on LSD ash was examined. Particularly, unburned carbon was separated from LSD ash and measured for PAH concentration to

test the hypothesis that PAHs were primarily associated with carbonaceous materials in the LSD ash.

### 4.3. Materials and Methods

**Sample Collection.** Four LSD ash samples were collected from a spreader stoker boiler (boiler # 8) at the McCracken Power Plant located on The Ohio State University campus. 1-LSD and 2-LSD samples were collected in May and June 2001, respectively. 3-LSD was collected in January 2002, and 4-LSD was collected in August 2003. During the sampling period, bituminous coal was burned as the fuel source.

In the LSD process, LSD ash is collected by woven fiberglass filter bags in a pulse jet baghouse. Multiple grab samples were collected from hopper F in the baghouse by a precleaned 250 mL polytetrafluoroethylene (PTFE) beaker attached to a 2 m PTFE-coated steel rod. Collected LSD ash samples were stored in certified clean 950 mL brown glass bottles (Fisher Scientific) in an environmental chamber (4 to 12 °C) until PAH analyses were conducted.

**Sample Fractionation.** A 140 mesh (106  $\mu\text{m}$ ) sieve was used to separate LSD ash into a >140 mesh and a <140 mesh fraction. Of the initial 10 g LSD ash sample, approximately 1.5 g was retained on the top of the sieve. The >140 mesh fraction was further separated using a lithiumheteropolytungstate (LST) solution with a specific gravity of 1.84 g/mL. 0.5 g of the >140 mesh sample and 10 mL of LST solution were well mixed in a 15 mL glass centrifuge tube and centrifuged at 8000 rpm for 30 min. Due to their low density, the unburned carbon particles floated to the top of the centrifuge tubes. These unburned carbon particles were decanted, collected on filter paper, washed

with 50 mL high purity water to remove the residual LST solution, and dried in an oven at 60 °C for 12 hr.

**Sample Characterization.** Scanning electron microscopic (SEM) images were taken by a JEOL JSM-820 SEM with Oxford eXL energy dispersive X-ray analyzer (JEOL USA Inc., Peabody, MA). Mineralogical analysis of samples was accomplished with a Philips X-Ray Diffraction (XRD) (Philips Analytical, Natick, MA) with  $\text{CuK}\alpha$  radiation at 35kV and 20mA.

The specific surface area (SSA) was measured by BET surface area analysis conducted on a manually controlled Micromeritics FlowSorb 2300 volumetric system (Micromeritics, Norcross, GA). A nitrogen (30% v/v) and helium mixture was used as the adsorbate gas. All SSA data were validated by a certified standard reference material CRM 171 from Bureau of Reference, European Commission.

Inorganic elemental analyses were determined by a Vista Pro simultaneous inductively coupled plasma optical emission spectrometer system (Varian, Walnut Creek, CA). Detailed elemental analysis procedures are described elsewhere (18). Organic carbon content of the LSD ash was calculated by subtracting the total inorganic carbon content (TIC) from the total carbon content (TC). Samples were combusted under pure  $\text{O}_2$  at 900 °C in a ThermoQuest carbon/nitrogen analyzer (ThermoQuest, Waltham, MA) to measure TC. TIC was determined by carbon coulometry (UIC Inc., Joliet, IL). Upon introduction of a sample into the sample flask, the system was purged with a  $\text{CO}_2$ -free carrier gas to eliminate atmospheric  $\text{CO}_2$ . Then, 2N  $\text{HClO}_4$  was added, heated and inorganic carbon was oxidized to gaseous  $\text{CO}_2$  and measured by a  $\text{CO}_2$  detector.

**Ultrasonic Extraction of PAHs.** The ultrasonic extraction was conducted based on EPA standard method 3550B. For LSD ash and >140 mesh and <140 mesh fractions, a 20 g sample was sonicated with 100 mL toluene of HPLC grade in a 400 mL glass beaker with a 20 kHz, 1.90 cm (ID) ultrasonic probe system (Sonic Dismembrator 550, Fisher Scientific). In all experiments, with the output set at 10 (full power) and pulse mode (pulse =5 sec, pulse off = 5 sec), the sample was sonicated for 3 min (ultrasonic irradiation time is 1.5 min). After extraction, the supernatant was decanted and filtered. The ultrasonic extraction of the solid samples was repeated twice with two additional 100 mL toluene aliquots. After the third extraction, all extracts were filtered, rinsed with 20~30 mL toluene and concentrated to 1mL using a Kuderna-Danish concentrator and high purity N<sub>2</sub> gas, successively.

Small-scale ultrasonic extractions were conducted on the separated unburned carbon due to the low quantity. All the parameters were similar as that used to extract LSD ash except a smaller amount of sample and solvent were added to a smaller size reactor. A 0.5 g unburned carbon sample was weighed into a small rosette glass reactor and extracted with 30 mL toluene for 3 min at a pulse mode. The ultrasonic extraction was repeated twice with two additional 30 mL toluene aliquots. Duplicate experiments were conducted in both normal and small-scale ultrasonic extractions to ensure reproducibility.

The matrix spike recoveries were measured in each fraction by extracting samples spiked with 50 µg/kg of 16 US EPA specified PAHs. Spike recoveries of these 16 PAHs ranged from 0 to 120%. For the PAHs identified in this study, 50% to 120% of the spike

recoveries were obtained. In general, the recoveries of higher molecular weight PAHs were lower compared to the low molecular weight PAHs.

**PAH analysis.** A 2  $\mu\text{L}$  aliquot of extract spiked with the deuterated internal standard including acenaphthene- $\text{d}_{10}$ , chrysene- $\text{d}_{12}$ , 1,4-dichlorobenzene- $\text{d}_4$ , naphthalene- $\text{d}_8$ , perylene- $\text{d}_{12}$  and phenanthrene- $\text{d}_{10}$  (Ultra-Scientific, North Kingstown, RI) were injected into a Trace gas chromatograph with PolarisQ ion trap mass spectrometer(GC/MS) (ThermoQuest, Waltham, MA) to analyze PAHs. Helium carrier gas passed a CP-5 fused silica capillary column (30 m  $\times$  250  $\mu\text{m}$   $\times$  0.25  $\mu\text{m}$ ) (Varian, Walnut Creek, CA) with a flow rate of 1.2 mL  $\text{min}^{-1}$ . The column was initially held at 60  $^{\circ}\text{C}$  for 2 min, increased to 250  $^{\circ}\text{C}$  at 20  $^{\circ}\text{C}$   $\text{min}^{-1}$  and held for 2 min, and then increased to 300  $^{\circ}\text{C}$  at 10  $^{\circ}\text{C}$   $\text{min}^{-1}$  and held for 8 min. The injector and ion source temperature were 250  $^{\circ}\text{C}$ . Mass transfer line temperature was 300  $^{\circ}\text{C}$ . The mass spectrometer was operated in full scan mode for both standards and extracts. Sixteen U.S. EPA specified PAHs were identified and quantified using authentic standards (Ultra-Scientific, North Kingstown, RI). The detection limits for these PAHs ranged from 0.1 to 10  $\mu\text{g}/\text{kg}$ , larger molecular weight PAHs had higher detection limits compared to small molecular weight PAHs

Solid phase microextraction (SPME) was used to measure PAHs in the LST solution to examine if PAHs were released from the solid particles during the density separation. A 100  $\mu\text{m}$  polydimethylsiloxane (PDMS) fiber was used to extract PAHs from the water phase for 30 min and desorbed into the GC/MS injector at 250  $^{\circ}\text{C}$  for 5 min. SPME analysis was conducted automatically by a CombiPal autosampler. All other parameters in the GC/MS were the same as that used for condensed organic extracts after ultrasonic extraction. The detection limit of the SPME method was 5  $\mu\text{g}/\text{L}$ .

#### 4.4. Results and Discussion

**Characterization of LSD Ash.** Generally, the LSD ash is a mixture of hannebachite, fly ash, unreacted lime (i.e., portlandite), and other minor constituents (18). SEM and XRD analysis showed a high similarity of the 4 LSD ash samples despite that they were collected on different dates. Flake-like crystals, identified as hannebachite, formed over bulk solid spherical fly ash particles as shown in Figure 4.1a. The XRD patterns of 4 LSD ash samples (Figure 4.2) showed portlandite and hannebachite are the major mineral phases in the samples.

Major element concentrations of these 4 LSD ash samples are listed in Table 4.1, which agree with XRD and SEM results indicating that the majority of material was present as hannebachite, portlandite, and fly ash. Compared to other LSD ash samples, 4-LSD had a lower concentration of Ca and a higher concentration of Al, which indicated the presence of more fly ash and less unreacted lime or calcium sulfate/calcium sulfite. In addition, the organic carbon content of 4-LSD was 13.4%, the highest among the collected LSD ash samples. 1-LSD and 2-LSD had similar carbon contents, about 7%, while 3-LSD had an organic carbon content of 10.8%. These high organic carbon contents suggest incomplete combustion conditions in the boiler, which represent a worst case condition that may lead to higher PAH concentrations in LSD ash (19).

**Correlation of PAH Concentrations with Organic Carbon Content.** The PAH concentrations on the 4 LSD ash samples are shown in Table 4.2. The results show that the speciation and concentration of PAHs detected varied in each sample. For example, no pyrene and chrysene were detected in the 2-LSD ash sample, while these two compounds were found in other LSD ash samples. No trend in the types of PAH present

with carbon content was observed. However, the total measured PAH concentration appears to correlate with the organic carbon content of the LSD ash as shown in Figure 4.3. With the highest carbon content, 4-LSD had the highest total PAH concentration among the 4 samples. In addition, 1-LSD and 2-LSD had similar carbon contents (7.1% and 7.0%, respectively); the total measured PAH concentration on these two samples were very similar ( $17.2 \pm 3.4 \mu\text{g/kg}$  and  $15.0 \pm 2.0 \mu\text{g/kg}$ ). Mineral characterization (XRD, SEM and elemental analysis) revealed that the mineral fraction was similar among these LSD samples except for organic carbon content. The positive correlation between total PAH concentration and organic carbon content suggests that PAHs may be associated with carbonaceous material in LSD ash.

**Fractionation of LSD Ash.** In order to further test this hypothesis, LSD ash samples were fractionated into >140 mesh and <140 mesh fractions. Unburned carbon was then separated from the >140 mesh fraction using density separation. Characterization of PAHs on these separated fractions was then performed.

The SEM images of the >140 mesh fraction separated from 4-LSD showed partially-burned carbonaceous material was covered with lime particles (Fig. 4.1c). The XRD pattern (Fig. 4.2) of this fraction showed a similar pattern to the parent 4-LSD ash except for the obvious drifting baseline indicating the presence of amorphous carbonaceous material and graphite. As for the <140 mesh fraction, flake-like crystals, hannebachite and needle-like crystals, ettringite were more abundant in the SEM image (Fig. 4.1b).

As shown in Table 4.3, the organic carbon content of the >140 mesh fraction was much higher than the parent LSD ash sample. For example, the >140 mesh fraction

separated from 1-LSD ash had an organic carbon content of 48.5% compared to 7.0% in the parent ash sample indicating an enrichment of carbonaceous materials in the >140 mesh fraction. Similar to organic carbon, the concentrations of Al, Fe and Si were also higher in the >140 mesh fraction indicating an accumulation of fly ash constituents. Compared to the >140 mesh fraction and parent LSD ash sample, the <140 mesh fraction had a much lower organic carbon content (e.g. 2.0% of the <140 mesh separated from 1-LSD ash). In addition, the Ca and S concentrations in the <140 mesh were much higher than in the parent LSD ash indicating an enrichment of Ca that was mainly from the slaked lime. Based on elemental analysis results, the >140 mesh fraction and the <140 mesh fraction will be referred to as carbon-enriched and lime-enriched fractions, respectively.

Further separating the carbon-enriched fraction revealed a fraction very high in carbon. Porous carbonaceous material was easily identified in SEM images as shown in Figure 4.1d. A strong peak formed by baseline drifting in the X-Ray pattern (Fig. 4.2) indicated the presence of large percentage of amorphous carbonaceous material. The elemental analysis of this fraction showed very low Ca and S and high organic carbon. This fraction will be referred to as the unburned carbon fraction.

**Distribution of PAHs in LSD Ash.** A comparison of the individual and total PAH concentrations measured in parent LSD ash and carbon-enriched, lime-enriched, and unburned carbon fractions are shown in Table 4.2. The PAHs identified were mainly small molecular weight PAHs such as naphthalene, phenanthrene, and pyrene. No PAHs larger than benzo(a)anthracene were detected in any of the samples. Moderate molecular weight PAHs such as chrysene and benzo(a)anthracene were detected in some of the LSD

ash samples and lime-enriched and carbon-enriched fractions. However, these compounds were not identified in any of the unburned carbon samples. SPME measurements of PAHs in the LST solution showed that PAHs were not released into liquid phase. Thus, PAHs were still sorbed on the solid particles after density separation.

Generally, for each PAH detected, the concentration on unburned carbon was higher than that on the carbon-enriched fraction except for larger molecular weight PAHs such as chrysene and benzo(a)anthracene. As shown in Figure 4.4, the parent LSD ash and the lime-enriched fraction typically had lower concentrations. The total PAH concentration measured on the unburned carbon was the highest among all the fractions ranging from  $245 \pm 45 \mu\text{g/kg}$  to  $473 \pm 168 \mu\text{g/kg}$ , which is 7~20 times higher than the total PAH concentration in LSD ash samples. Total PAHs measured on the carbon-enriched fraction had the second highest concentrations. For example, for sample 1-LSD, the total PAH concentration in the carbon-enriched fraction was  $107 \pm 3 \mu\text{g/kg}$ , which was substantially higher than the total PAH concentration on parent 1-LSD ash ( $17 \pm 3 \mu\text{g/kg}$ ) and the lime-enriched fraction ( $30 \pm 4 \mu\text{g/kg}$ ). The unburned carbon samples had similar total PAH concentrations except the concentration on unburned carbon separated from 4-LSD ash was slightly higher compared to the other unburned carbon samples. The high total PAH concentration on the carbon-enriched and unburned carbon fraction demonstrated that PAHs were primarily associated with carbonaceous material in LSD ash.

The interactions between PAH molecules and carbonaceous material may explain the high PAH concentrations on unburned carbon. By studying the sorption of pyrene on graphites, Groszek reported a parallel planar orientation between the pyrene and an

extended carbon network (20). Griest et al. hypothesized that the association between PAHs and carbonaceous particles occurred through interactions formed between the aromatic compounds and the extended aromatic system of the polymeric carbon (21). With a planar configuration, PAH molecules can closely reach the sorption surface, increasing the possibility of favorable  $\pi$ - $\pi$  cloud overlap between the flat molecules and unburned carbon structures and thus enhance the sorption (22). The strong affinity between PAH molecules and carbonaceous material are commonly observed during sorption/desorption studies as irreversible desorption or hysteresis (23). The available reported organic carbon-normalized phenanthrene partition coefficient ( $K_{oc}$ ) showed that phenanthrene associated with coal-type carbon were orders of magnitude higher than that associated with natural organic matter, which is known to be a stronger sorbent for organic compounds than minerals in the environment (24). Therefore, in this study, the higher PAH concentrations on unburned carbon compared to the lime fraction is reasonable.

The preferential partitioning of PAHs onto the carbonaceous component may be also due to characteristics such as surface area. Low and Batley showed that the carbon particles in fly ash from bituminous coals were less porous than those in fly ash from the brown coal (25) resulting in lower surface areas of the carbonaceous material in bituminous coal than that in brown coal. The adsorption of PAHs on bituminous coal fly ash may occur principally on the surface of particles, whereas for the brown coal fly ashes, adsorption occurred both on the surface and through the pores of the particles (21). Lee and Chen suggested that surface area should be considered in addition to carbon content when determining the adsorption of PAHs on fly ash (26). The specific surface

areas (SSA) of LSD ash, separated carbon-enriched, lime-enriched and unburned carbon fractions were measured by BET and showed little variability with results ranging from 5 to 9 m<sup>2</sup>/g (see Table 2). Therefore, the SSA does not appear to be the main reason for the greater than 10-fold concentration of PAHs with carbonaceous material in LSD ash.

Although the unburned carbon was separated from different LSD ash samples, the total PAH concentrations were similar. It has been reported that physical differences in the nature of the carbon and accessibility of the carbon sites in the ashes may lead to different concentrations of PAHs (27). During the sampling period, only bituminous coal was burned in the McCracken Power Plant. The coal characterization results showed the coal properties (e.g., elemental composition) were consistent (18), which could possibly explain the similar total PAH concentrations on the unburned carbon from different LSD ashes.

PAH concentrations on lime-enriched fractions were expected to be undetectable due to very low organic carbon contents. Surprisingly, the results showed that PAH concentrations on lime-enriched fractions were still detectable and varied among the different samples. For 2-LSD and 3-LSD samples, total PAH concentrations on the lime-enriched fraction were 19 and 33 µg/kg respectively, approximately the same as in the parent LSD ash.

Assuming the PAHs on the lime-enriched fractions were only associated with the small amounts of unburned carbon in the fraction, the theoretical PAH concentrations on the lime-enriched fractions were calculated based on the PAH concentrations measured on the separated unburned carbon fraction. Comparison of the calculated PAHs and the measured PAH concentration on the lime-enriched fractions is plotted in Figure 4.5. For

the 4-LSD ash, PAH concentrations calculated and measured were similar indicating the PAHs on the lime-enriched fraction were still primarily associated with the unburned carbon. However, for the other 3 LSD ash samples, the PAH concentrations calculated were much lower than the measured concentrations. Therefore, besides organic carbon content, other components of the LSD ash also act as sorption sites for PAHs.

In the LSD system, PAHs may sorb onto the injected slaked lime and  $\text{CaSO}_3$  or  $\text{CaSO}_4$  that is subsequently formed. Mastral et al. examined the effects of limestone on gas phase PAH emissions from coal fluidized bed combustion. Their results showed that limestone helped to control PAH emissions in the gas phase by adsorption (28). In addition, a study by Goss showed that sorption of organic compounds on the mineral phase occurred and was a function of temperature and relative humidity (29). The work determined that a temperature increase at constant moisture leads to a strong increase in adsorption to hydrophilic surfaces due to a decrease in relative humidity. Accordingly, the high temperature and low moisture due to the heat from the flue gas may lead to sorption of PAHs on the hannebachite and unreacted lime (i.e., portlandite) in the LSD process.

To determine if unburned carbon fractions contributed most PAHs on LSD ash, the mass percentage of total PAHs contributed by unburned carbon was calculated by the following equation:

$$\text{Percentage of PAH} = \frac{(C_{\text{unburned carbon}} \times M_{\text{unburned carbon}})}{(C_{\text{LSD}} \times M_{\text{LSD}})} \times 100\% \quad (1)$$

where  $C_{\text{LSD}}$  is the concentration of total PAHs measured on LSD ash,  $M_{\text{LSD}}$  is the mass of the LSD ash sample.  $C_{\text{unburned carbon}}$  is the total PAH concentration measured on unburned

carbon;  $M_{\text{unburned carbon}}$  is the mass of unburned carbon separated from the parent LSD ash. As shown in Figure 4.6, the weight percent of unburned carbon was only 5.4%~11.9% of the total LSD ash. However, unburned carbon contained 74% to 129% of the total PAHs in the LSD ash indicating that PAHs were primarily contributed by the unburned carbon fractions. The reason for the more than 100% contribution of PAHs by unburned carbon in 1-LSD and 2-LSD may due to the variations in the measurement. A mass balance analysis of PAHs on LSD ash was then performed to examine the results.

**Mass Balance analysis of PAHs in LSD Ash.** Concentration of individual PAH and total PAH concentration on the parent LSD ash were calculated by equation (2) based on the PAH concentrations measured on carbon-enriched and lime-enriched fractions to test the validity of measurements obtained.

$$PAH \text{ Concentration } (\mu\text{g/kg}) = \frac{(C_{\text{carbon-enriched},i} \times M_{\text{carbon-enriched}} + C_{\text{lime-enriched},i} \times M_{\text{lime-enriched}})}{(M_{\text{carbon-enriched}} + M_{\text{lime-enriched}})} \quad (2)$$

where  $C_{\text{carbon-enriched},i}$  is the concentration of PAH component  $i$  measured on the carbon-enriched fraction,  $C_{\text{lime-enriched},i}$  is the concentration of PAH component  $i$  measured on the lime-enriched fraction,  $M_{\text{carbon-enriched}}$  and  $M_{\text{lime-enriched}}$  are the masses of the carbon-enriched and lime-enriched fractions separated from parent LSD ash. The calculated and measured PAH concentrations on the parent LSD ash samples are shown in Figure 4.7.

Overall, the LSD ash samples with higher organic carbon content (3-LSD and 4-LSD) had better mass balance than low carbon content ashes: 1-LSD and 2-LSD. In Figure 7a and 7b, the results show that the calculated PAH concentrations from 1-LSD and 2-LSD ash fraction were higher than the PAH concentration measured on the whole ash except for naphthalene. For 3-LSD, PAH concentrations calculated showed good

agreement with the PAH concentrations measured as shown in Figure 7c. For 4-LSD, the individual PAH concentrations calculated from the fractions were lower than individual PAH concentrations measured except for naphthalene, but the total PAH concentration calculated was similar as the total PAH concentration measured.

As a mixture of carbon-enriched and lime-enriched fractions, LSD ash is heterogeneous. In our study, spikes were used to determine extraction efficiencies. The concentrations of PAHs were then calculated based on the percent spike recovery. This method may be less valid for heterogeneous samples since the spiked PAHs are not likely to be exposed to the same active sites on the sample as the original PAHs on LSD ash (30). When PAHs were spiked onto LSD ash with lower organic carbon content, more PAHs would be expected to sorb onto lime-enriched particles because of the large mass percentage of lime-enriched particles in the sample. Moreover, spiked analytes are less retained on the mineral phase than on the carbonaceous materials. Thus, percent spike recoveries obtained from low carbon content LSD ash was higher compared to LSD ash with higher carbon content, which may overestimate the efficiencies of extraction methods resulting in a lower measured PAH concentration (31). As for the carbon-enriched, lime-enriched, and unburned carbon fractions, the samples were more homogeneous. The problem of overestimated extraction efficiency caused by percent spike recoveries is expected to be less important.

Since percent spike recovery is a commonly accepted method for measuring extraction efficiency and thus quantifying the results, PAH concentrations may be underestimated if the sample is heterogeneous. In this study, although there is a

discrepancy between the PAH concentrations measured and calculated, the results are within an order of magnitude, at  $\mu\text{g}/\text{kg}$  levels.

#### **4.5. Conclusions**

LSD ash samples were fractionated into carbon-enriched and lime-enriched fractions. The carbon-enriched fraction was further separated to obtain an unburned carbon fraction. The results showed that PAHs were primarily associated with unburned carbon. Although the mass percentage of unburned carbon was only approximately 5.4%~11.9% of the total LSD ashes sampled, unburned carbon contributed 74% to 129% of the total PAHs on the LSD ash samples indicating an enrichment of PAHs on unburned carbon. In addition, PAHs were measured in the lime-enriched fraction, suggesting that slaked lime may also sorb PAHs from the flue gas.

#### **Acknowledgments**

The authors would like to thank staff at the McCracken Power Plant and Danold Golightly for their assistance during sampling. Financial support by the Ohio State Carbonation and Ash Regeneration (OSCAR) Project with funding from the Ohio Coal Development Office (OCDO) and The Ohio State University are gratefully acknowledged. University and Presidential Fellowships awarded to P. Sun from The Ohio State University are acknowledged. We also thank Chin-Min Cheng for X-Ray diffraction and BET measurements.

## References

1. U.S. Environmental Protection Agency. Wastes from the Combustion of Coal by Electric Utility Power Plants, Report to Congress, EPA 530-SW-88-002, February, 1988.
2. O'Neil, B.T. *Dry Scrubbing Technologies for Flue Gas Desulfurization*, Kluwer Academic Publishers: Boston, 1998; pp
3. U.S. Environmental Protection Agency. Wastes from the Combustion of Fossil Fuels, Volume 1 and 2- Methods, Findings, and Recommendations, Report to Congress, EPA 530-S-99-010, March 1999.
4. Stewart, B.R.; Kalyoncu, R.S. Proc. Int. Ash Utilization Symp, Lexington, KY, 18-20 Oct. 1999.
5. Walker, W. H.; Taerakul, P.; Butalia, T.; Wolfe, W.; Dick, W. Minimization and Use of Coal Combustion By-Products: Concepts and Applications. In: Ghassemi A. editors. *The Handbook of Pollution Control and Waste Minimization*, New York: Marcel Dekker, 2002.
6. Butalia, T.; Dyer, P.; Stowell, R.; Wolfe, W. W. Construction of Livestock Feeding and Hay Bale Storage Pads Using LSD Material, The Ohio State Extension Fact Sheet, AEX-332-99, Columbus, Ohio: The Ohio State University, 1999.
7. Lamminen, M.; Wood, J.; Walker, H. W.; Chin, Y.-P.; He, Y.; Traina, S. *J. Env. Quality* **2001**, *30*, 1371.
8. Butalia, T.; Wolfe, W. W.; Lee, J. *Fuel* **2001**, *80*, 845.
9. Clark, R.; Ritchey, K.; Baligar, V. C. *Fuel* **2001**, *80*, 821.
10. Chen, L.; Dick, W. A.; Nelson, S. *Environ. Pollut.* **2001**, *114*, 161.

11. Henner, M.; Schiavon, M.; Morel, J. L.; Lichtfouse, E. *Analusle Magazine*, **1997**, 25, 9.
12. Denissenko, M. F.; Pao, A.; Tang, M-S.; Pfeifer, G. P. *Science* **1996**, 274, 430.
13. Pisupati, S. V.; Wasco, R. S.; Scaroni, A. W. *J. Haz. Materials* **2000**, 74, 91.
14. Khim, J. S.; Kannan, K.; Villeneuve, D. L.; Koh, C. H.; Giesy, J. P. *Environ. Sci. Technol.* **1999**, 33, 4199.
15. Arditoglou, A.; Petaloti, Ch.; Terzi, E.; Sofoniou, M.; Samara, C. *Sci. Total Environ.* **2004**, 323, 153.
16. Ghosh, U.; Talley, J. W.; Luthy, R. G. *Environ. Sci. Technol.* **2001**, 35, 3468.
17. Low, G. K.; Batley, G. E. *J. Chromatogr.* **1986**, 355, 177.
18. Taerakul, P.; Sun, P.; Walker, H.; Weavers, L.; Golightly, D.; Butalia, T. *Fuel*, 2004, in review
19. Liu, K-L.; Xie, W.; Zhao, Z-B.; Pan, W-P.; Riley, J. T. *Environ. Sci. Technol.* **2000**, 34, 2273.
20. Groszek, A. J. *Dissuss. Faraday Soc.* **1975**, 59, 109.
21. Griest, W. H.; Canton, J. E. In "Polynuclear Aromatic Hydrocarbons: Chemical Analysis and Biological Fate"; Cooke, M., Dennis, A. J., Eds.; Battelle Press: Columbus, OH, 1981; pp 719-730.
22. Jonker, M.T.O.; Koelmans, A.A. *Environ.Sci.Technol.*, **2002**, 36, 3725.
23. Braid, W. J.; Pignatello, J. J.; Lu, Y.; Ravikovitch, P. I.; Neimark, A. V.; Xing B. *Environ. Sci. Technol.* **2003**, 37, 409.
24. Karapanagioti, H. K.; Kleinedam, S.; Sabatini, D. A.; Grathwohl, P.; Ligouis, B. *Environ. Sci. Technol.* **2000**, 34, 406.

25. Low, G. K.C.; Batley, G. E. *Environ. Sci. Technol.* **1988**, *22*, 322.
26. Lee, W. G.; Chen, J. C. *Environment International*, **1995**, *21*, 827.
27. Soltys, P. A.; Mauney, T.; Natusch, D.; Schure, M. R. *Environ. Sci. Technol.* **1986**, *20*, 175.
28. Mastral, A. M.; Garcia, T.; Callen, M. S.; Lopez, J. M.; Murillo, R.; Navarro, M. V. *Energy & Fuels*. **2001**, *15*, 1469.
29. Goss, K-U. *Critical Rev. Environ. Sci. Technol.* **2004**, *34*, 339.
30. Burford, M. D.; Hawthorne, S. B.; Miller, D. J. *Anal. Chem.* **1993**, *65*, 1497.
31. Alexandrou, N.; Pawliszyn, J. *Anal. Chem.* **1989**, *61*, 2770.

Comp. (%)	1-LSD	2-LSD	3-LSD	4-LSD
Ca	30.9	30.9	33.8	25.2
S	12.7	13.7	11.1	11.3
Org. C	7.1	7.0	10.8	13.4
Si	4.7	2.9	3.9	4.2
Fe	2.7	2.8	2.4	1.5
Al	1.3	1.4	1.4	2.5
K	0.4	0.3	0.5	0.4
Mg	0.3	0.3	0.4	0.4

Table 4.1. Major inorganic elemental composition (%) in LSD ash samples

Sample ID	naphthalene	henanthrene	anthracene	pyrene	fluoranthrene	chrysene	benzo(a) anthracene	Total PAHs
1-LSD	4.2±2.2	3.8±1.2	1.4±0.2	1.2±0.9	3.7±2.1	0.5±0.4	2.5±0.4	17.2±3.4
1-L	0.7±0.7	6.7±1.7	2.4±1.0	4.2±1.6	6.6±1.2	2.8±1.6	6.2±3.2	29.7±4.3
1-C	7.7±2.1	23.2±0.1	11.9±1.4	17.4±0.9	23.2±1.5	14.6±1.2	8.8±0.3	107±3.2
1-UC	59.8±30.7	108±22.6	78.3±23.9	32.5±2.7	24.8±5.8	N/D	N/D	304±45.4
2-LSD	8.1±1.8	0.3±0.1	1.1±0.6	2.4±0.3	2.2±0.5	N/D	N/D	14.1±2.0
2-L	5.5±1.2	1.2±1.1	1.8±1.3	4.9±0.8	5.4±0.7	N/D	N/D	18.9±2.4
2-C	8.8±1.1	14.7±0.2	10.2±0.1	9.1±0.1	12.0±0.6	14.2±0.1	9.8±2.1	78.7±2.5
2-UC	165±17.3	48.1±15.5	32.7±18.0	47.7±37.0	46.2±35.7	N/D	N/D	340±59.2
3-LSD	13.6±2.1	4.1±0.7	0.8±0.6	0.8±0.9	3.5±2.3	7.6±0.1	8.3±0.8	39.6±3.5
3-L	17.1±1.1	1.2±0.5	2.3±0.4	N/D	N/D	6.1±0.9	6.1±0.6	32.9±1.6
3-C	10.7±1.1	20.3±0.7	11.4±2.5	6.9±0.5	9.5±1.2	5.0±0.4	1.4±0.9	65.2±3.3
3-UC	64.5±7.4	71.7±18.1	63.0±38.2	27.4±8.7	18.4±10.2	N/D	N/D	245±45.0
4-LSD	12.9±2.0	14.6±5.6	10.6±4.3	8.4±3.1	8.1±3.2	3.9±3.1	3.8±2.9	64.3±9.6
4-L	9.1±2.7	7.6±0.6	4.2±0.4	2.6±0.5	2.9±0.5	N/D	0.9±0.8	27.2±3.0
4-C	131±10.2	45.6±1.4	23.2±7.6	7.8±0.1	1.6±0.8	2.9±0.1	1.6±0.4	214±12.8
4-UC	237±166	77.4±23.2	77.6±15.0	40.6±5.2	40.5±6.1	N/D	N/D	473±168

Table 4.2. Detected PAHs concentrations ( $\mu\text{g}/\text{kg}$ ) on different samples. 1-C: carbon-enriched fraction separated from 1-LSD ash; 1-L: lime-enriched fraction separated from 1-LSD ash; 1-UC: unburned carbon separated from 1-LSD ash. N/D: not detected

Comp.	1-C	1-L	1-UC	2-C	2-L	2-UC	3-C	3-L	3-UC	4-C	4-L	4-UC
(%)												
Al	2.5	0.7	1.7	2.8	0.9	1.3	2.9	0.9	0.9	4.6	2.0	1.9
Ca	16.6	32.0	0.9	11.7	31.5	0.2	17.0	34.0	0.2	10.8	29.4	0.9
Fe	7.5	2.1	1.7	6.3	2.6	1.1	6.0	2.4	1.0	3.1	1.4	0.8
K	0.2	0.1	0.1	0.2	0.1	0.1	0.2	0.1	0.1	0.6	0.3	0.2
Mg	0.3	0.4	0.1	0.3	0.4	0.0	0.3	0.5	0.0	0.3	0.4	0.0
S	7.4	14.3	0.7	3.6	13.9	0.4	7.2	12.2	0.5	4.3	12.0	0.7
Si	3.7	0.5	1.8	3.8	0.8	0.9	3.9	0.8	0.2	8.1	3.3	2.8
Org. C	40.6	2.1	86.1	48.7	2.0	76.9	55.8	2.6	81.4	47.1	5.0	92.6
SSA (m <sup>2</sup> /g)	5.1	7.3	7.7	4.3	6.5	7.4	8.2	6.7	9.3	7.4	7.5	7.5

Table 4.3. Major inorganic elemental composition (%) and specific surface area of separated lime-enriched, carbon-enriched and unburned fractions. 1-C: carbon-enriched fraction separated from 1-LSD ash; 1-L: lime-enriched fraction separated from 1-LSD ash; 1-UC: unburned carbon separated from 1-LSD ash.

## FIGURE CAPTIONS

Figure 4.1. SEM images of whole LSD ash samples and components of fractionations. a: 4-LSD ash; b: 4-L (lime-enriched fraction of 4-LSD ash); c: 4-C (carbon-enriched fraction of 4-LSD); d: 4-UC (unburned carbon separated from 4-LSD ash)

Figure 4.2. XRD pattern of 4 LSD ash samples, 4-L (separated lime-enriched fraction), 4-C (carbon-enriched fraction of 4-LSD), and 4-UC (unburned carbon separated from 4-LSD ash).

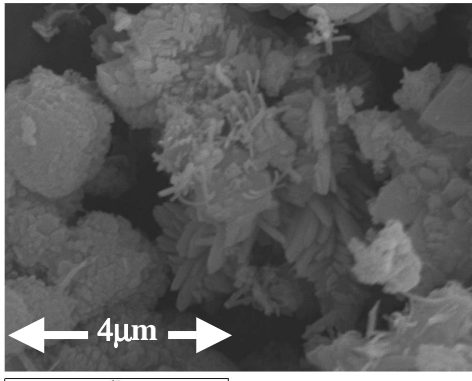
Figure 4.3. Organic carbon content and measured total PAH concentrations on the 4 LSD ash samples. Inset: correlation between organic carbon content (%) and measured total PAH concentration ( $\mu\text{g}/\text{kg}$ ).

Figure 4.4. Total PAH concentration ( $\mu\text{g}/\text{kg}$ ) in four LSD ash and correspondingly carbon-enriched, lime-enriched, and unburned carbon fractions.

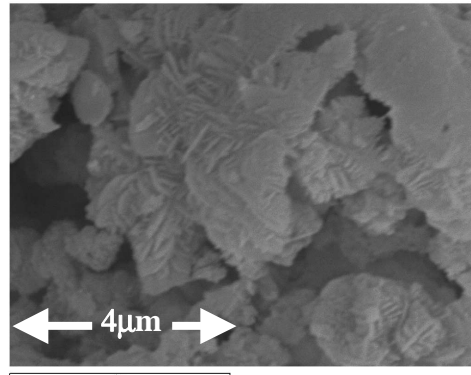
Figure 4.5. Calculated and measured total PAH concentration ( $\mu\text{g}/\text{kg}$ ) in lime-enriched fractions assuming PAHs were only associated with unburned carbon.

Figure 4.6. Mass percentage of unburned carbon and PAH percentage on unburned carbon from 4 LSD ash samples.

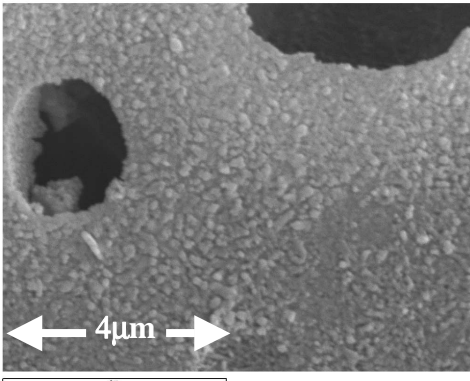
Figure 4.7. Comparison of measured and calculated PAH concentrations on LSD ash based on mass balance. 7a: 1-LSD ash; 7b: 2-LSD ash; 7c: 3-LSD ash; 7d: 4-LSD ash.



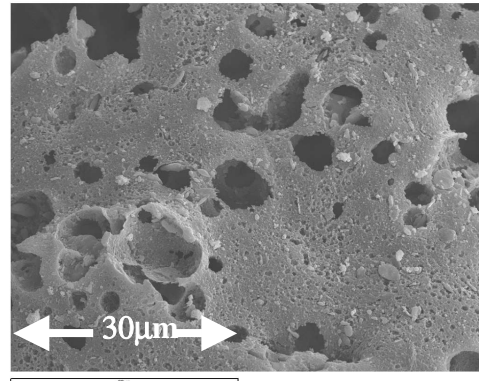
1a: 4-LSD



1b: 4-L



1c: 4-C



1d: 4-UC

Figure 4.1. SEM images. 1a: 4-LSD ash; 1b: 4-L (lime-enriched fraction of 4-LSD ash); 1c: 4-C (carbon-enriched fraction of 4-LSD); 1d: 4-UC (unburned carbon separated from 4-LSD ash)

**P - Portlandite, syn -  $\text{Ca}(\text{OH})_2$**   
**H - Hannebachite, syn -  $\text{CaSO}_3 \cdot 0.5\text{H}_2\text{O}$**   
**M - Mullite -  $\text{Al}_6\text{Si}_2\text{O}_{13}$**   
**Q - Quartz -  $\text{SiO}_2$**

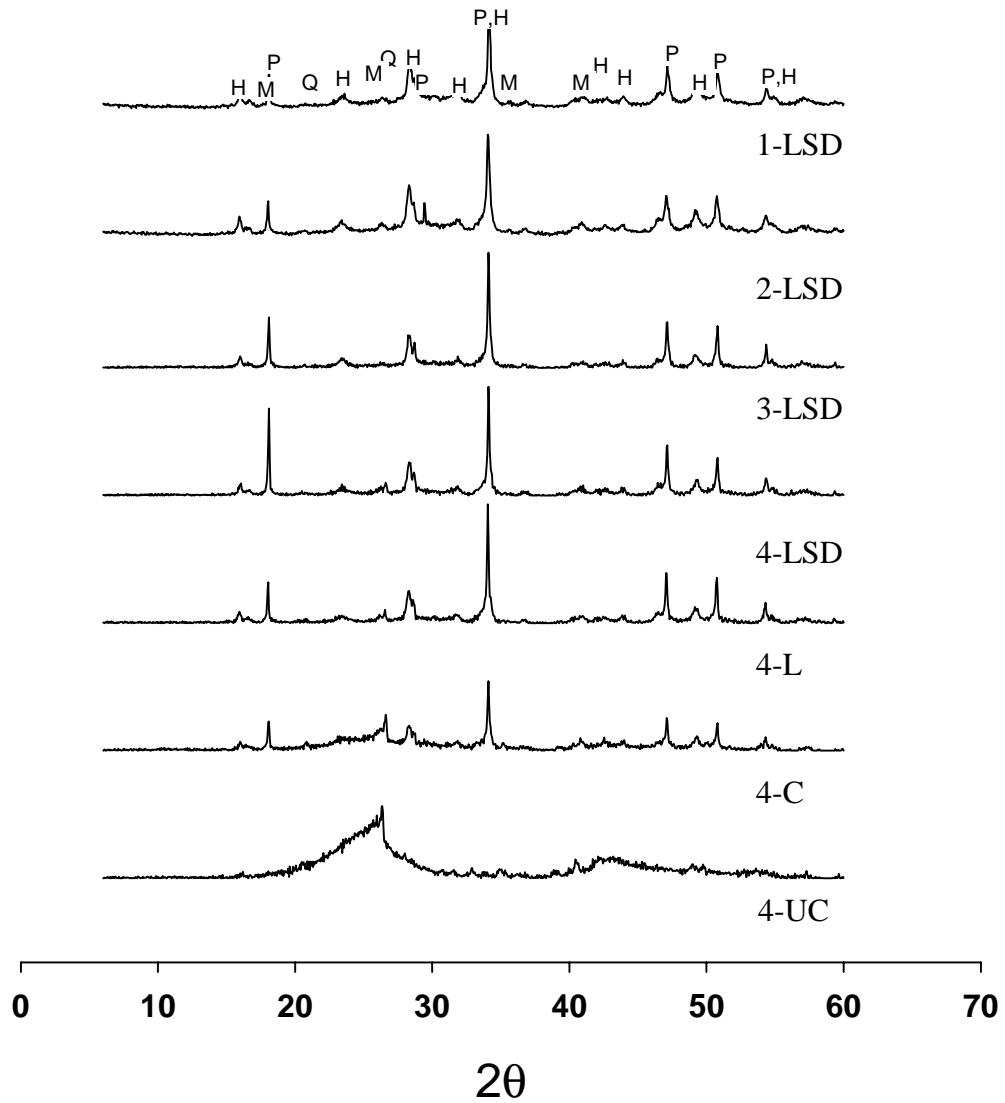


Figure 4.2. XRD pattern of 4 LSD ash samples, 4-L (separated lime-enriched fraction), 4-C (carbon-enriched fraction of 4-LSD), and 4-UC (unburned carbon separated from 4-LSD ash).

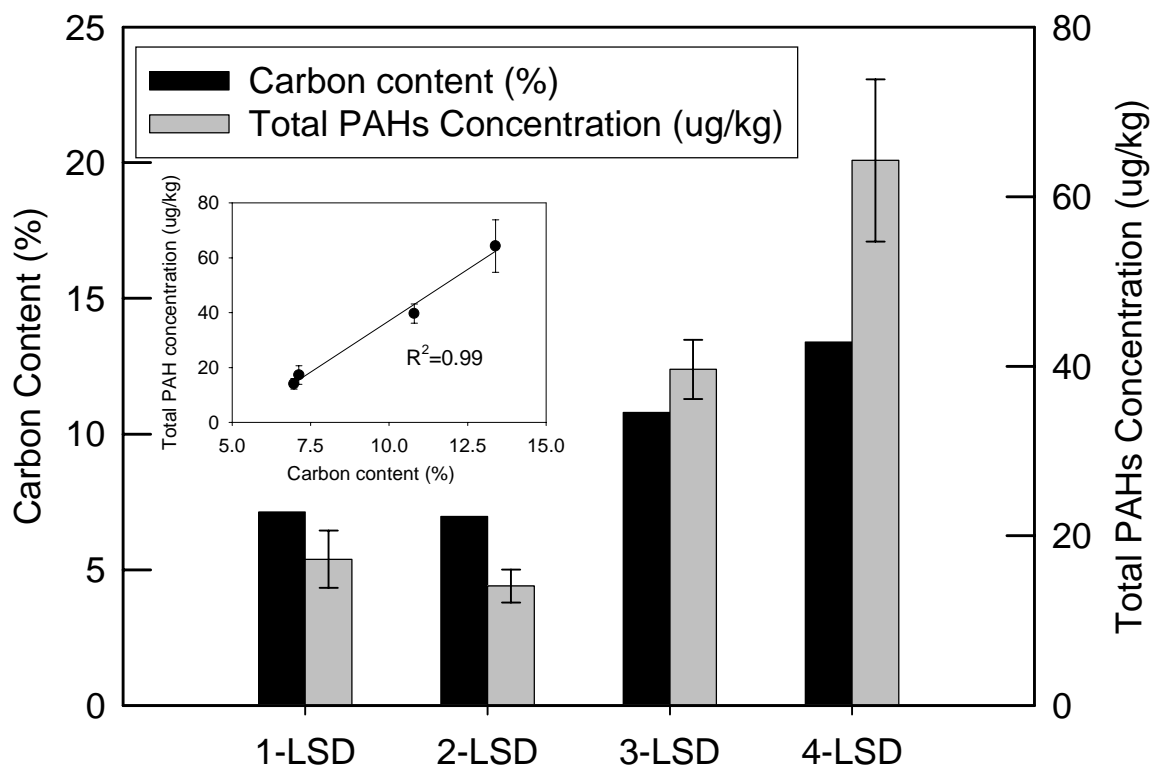


Figure 4.3. Organic carbon content and measured total PAH concentrations on the 4 LSD ash samples. Inset: correlation between organic carbon content (%) and measured total PAH concentration ( $\mu\text{g}/\text{kg}$ ).

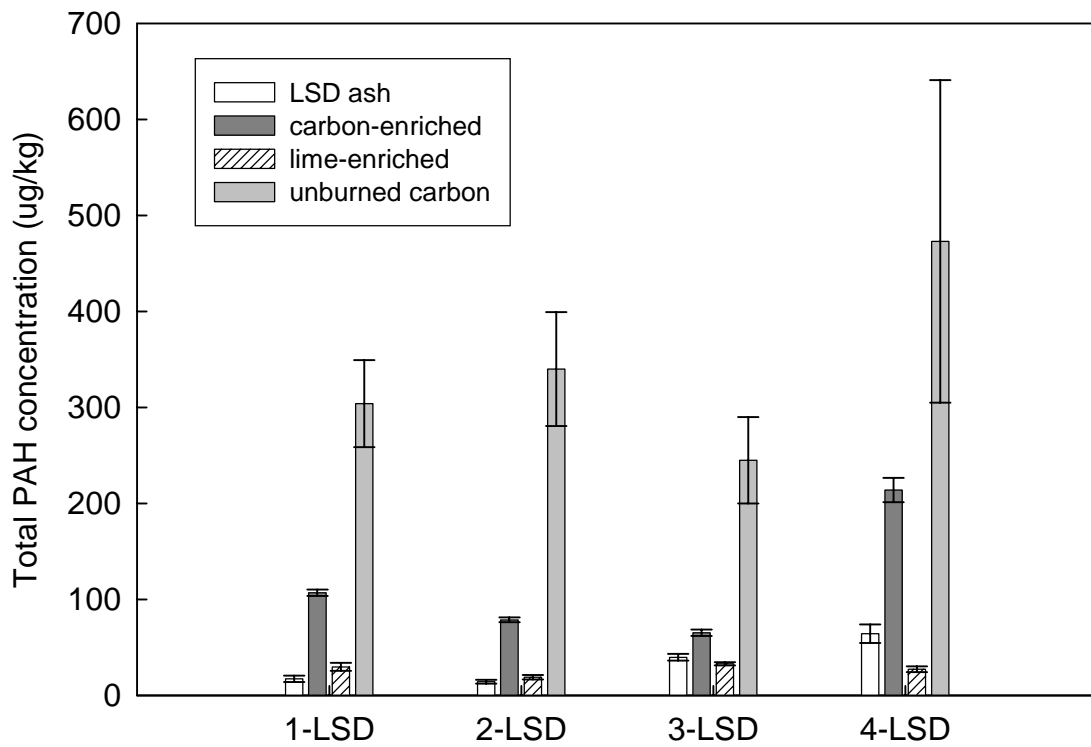


Figure 4.4. Total PAH concentration ( $\mu\text{g}/\text{kg}$ ) in parent LSD ash and correspondingly carbon-enriched, lime-enriched, and unburned carbon fractions.

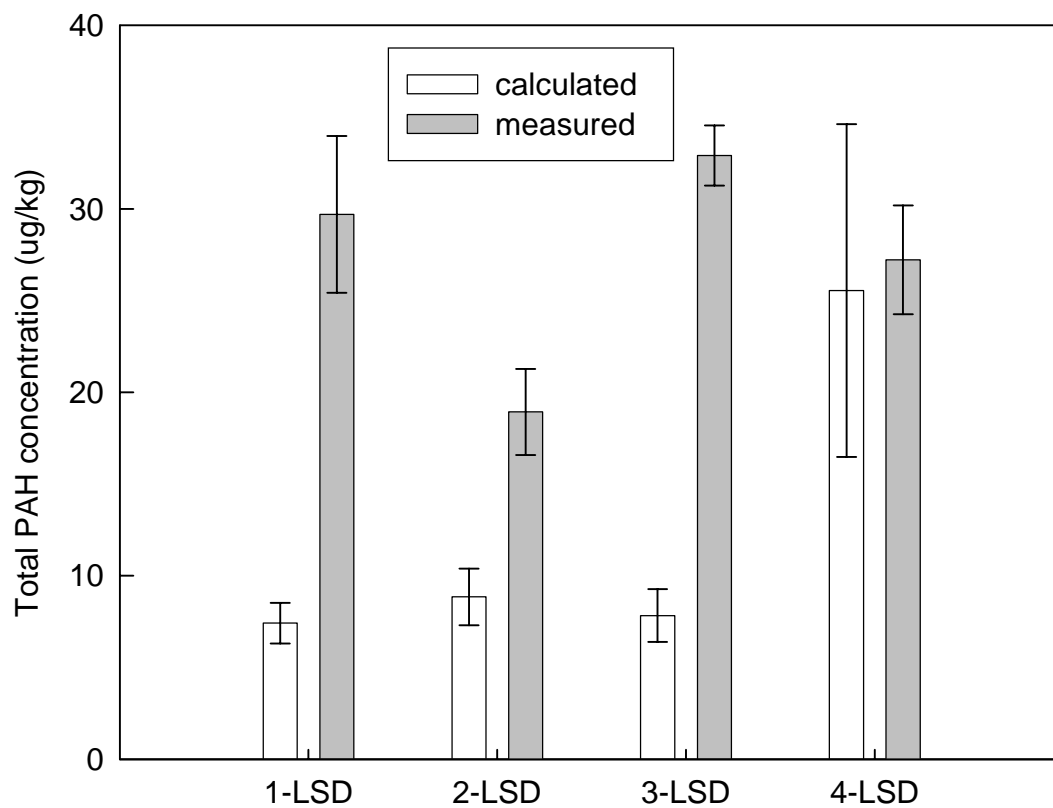


Figure 4.5. Total PAH concentration ( $\mu\text{g}/\text{kg}$ ) measured in lime-enriched fractions and concentrations calculated assuming PAHs were only associated with unburned carbon.

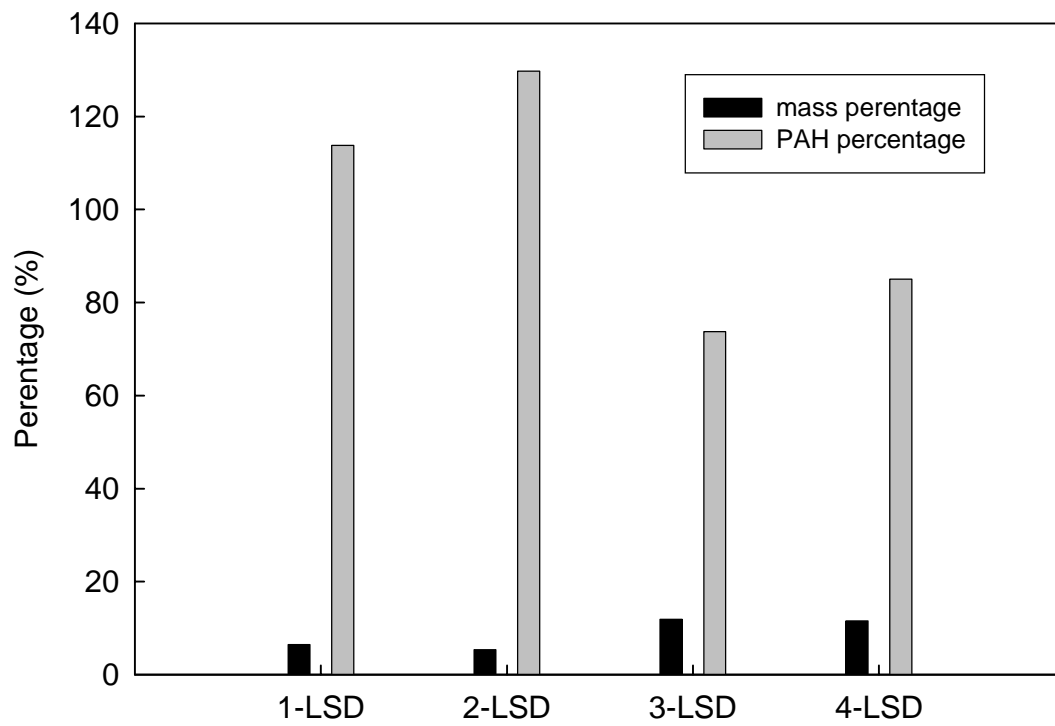


Figure 4.6. Mass percentage of unburned carbon and PAH percentage on unburned carbon from 4 LSD ash samples.

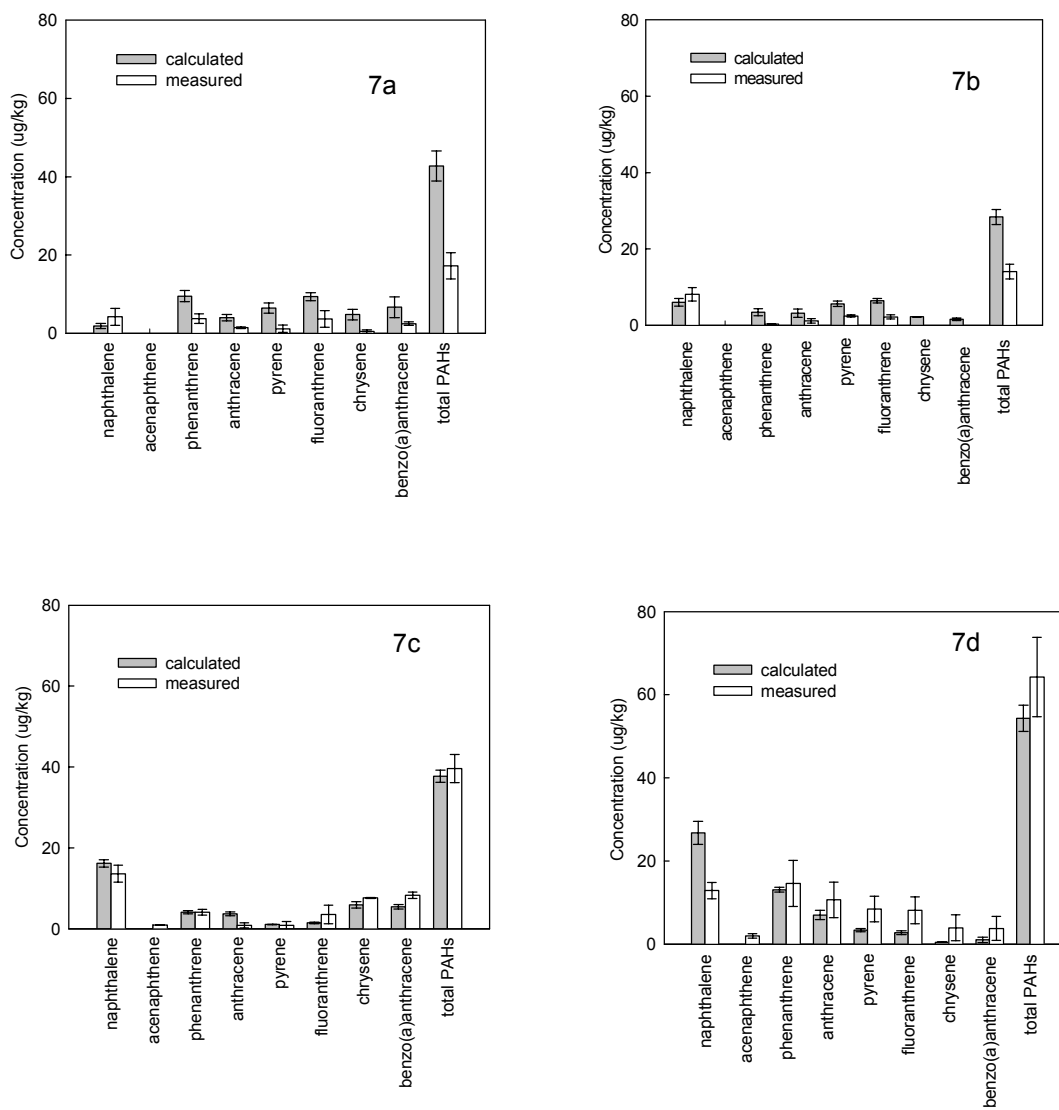


Figure 4.7. Comparison of measured and calculated PAH concentrations on LSD ash based on mass balance. 7a: 1-LSD ash; 7b: 2-LSD ash; 7c: 3-LSD ash; 7d: 4-LSD ash.

## **CHAPTER 5**

### **CHARACTERIZATION OF POLYCYCLIC AROMATIC HYDROCARBONS (PAHs) ON SOLID BY-PRODUCTS GENERATED IN THE OHIO STATE CARBONATION AND ASH REACTIVATION (OSCAR) PROJECT**

#### **5.1. Abstract**

Ohio State carbonation and ash reactivation (OSCAR) process is a demonstration pilot plant built to demonstrate the effectiveness of activated sorbent to capture SO<sub>2</sub> during the flue gas desulfurization process. Speciation and concentration of polycyclic aromatic hydrocarbons (PAHs) on solid by-products collected from the OSCAR process were investigated to ensure environmentally safe usage of these materials. PAHs detected on solid by-products were primarily small molecular weight compounds at low concentration (e.g., µg/kg). Solids collected from the baghouse had higher PAH concentrations than the solids collected from the cyclone. Capture of PAHs was observed with supersorbent injection. However, the possible release of PAHs occurred with the regenerated OSCAR sorbents injection. In addition, PAH composition and concentration

on the solids were affected by the type of sorbent and operation conditions (e.g., sorbent injection rate and baghouse flow rate) in the OSCAR process.

## 5.2. Introduction

Sulfur dioxide ( $\text{SO}_2$ ) is a major air pollutant generated during coal combustion. Control of  $\text{SO}_2$  has been achieved by flue gas desulfurization (FGD). During the FGD process, large amounts of sorbent (e.g., lime or limestone) are injected into the flue gas to react with  $\text{SO}_2$  resulting in the formation of calcium sulfate ( $\text{CaSO}_3$ ) or calcium sulfite ( $\text{CaSO}_4$ ) (1). One economic problem regarding the application of dry FGD technology is the low sorbent conversion, which requires a large amount of sorbent to achieve higher  $\text{SO}_2$  reduction in the flue gas (2). There are two possible ways to solve this problem: one is to develop a highly reactive sorbent that undergoes nearly 100% utilization; the other is to regenerate and reinject the spent sorbent. Designed based on these two considerations, the Ohio State carbonation and ash reactivation (OSCAR) process is a demonstration pilot plant built to test the effectiveness of the reactivated sorbent for  $\text{SO}_2$  capture (2).

The OSCAR process consists of two main components: sorbent activation and flue gas desulfurization. Sorbents were activated from fresh lime or the existing lime spray dryer (LSD) ash in a slurry reactor using the McCracken power plant exhaust flue gas that contains nearly 15%  $\text{CO}_2$  (3). Once activated, the sorbents precipitate in the slurry, and are filtered, dried and injected into a riser reactor to react with  $\text{SO}_2$  in flue gas. Following the rising reactor, the flue gas passes through a cyclone, a heat exchanger, a selective catalytic reactor for  $\text{NO}_x$  control, a baghouse that removes fine particles

escaping from the cyclone, and finally is released from the stack. Detailed information on this process is described by Fan and Jadhav (2).

The OSCAR process allows for reduction in the sorbent requirement for SO<sub>2</sub> removal and reduces the generation of solid by-products (e.g., the unreacted lime and formed calcium sulfite/sulfate mixture) compared to traditional dry FGD processes. In order to use the generated solid by-products, full environmental characterization of this material needs to be performed. One area in particular that has received little attention is quantification of organic hazardous species such as polycyclic aromatic hydrocarbons (PAHs) that are present on the by-product (4). Compared to inorganic components such as heavy metals, organic components are expected to be present in lower concentrations and consequently are often neglected.

PAHs are a class of organic compound that persist in the environment for months to years (5). Many PAHs are carcinogenic and/or mutagenic (6). A major source of PAHs in the environment is from fossil fuel combustion processes (7). Previous studies have focused on characterization of PAHs on fly ash (8-10) and the effects of combustion conditions on PAH formation and transformation in gas phase and solid phase (11-15). However, to date, little research on characterization of PAHs on FGD by-products has been conducted.

In the FGD processes, PAHs in flue gas from coal combustion may sorb onto the solid by-products. Fly ash associated PAHs also mixes with FGD solid by-products (16). In the OSCAR process, PAH speciation and concentration on the solid by-products may be different from traditional FGD by-products due to the sorbent activation from either LSD ash or lime. These PAHs may be released into the environment during solid by-

product utilization or disposal. In addition, operational parameters in the OSCAR process such as reactor temperature, flue gas flow rate, and sorbent feed rates may also affect the concentration and types of PAHs on the solid by-products. Therefore, the identification of PAHs, their concentrations on OSCAR by-products will be important to determine environmentally safe disposal and/or utilization options.

In this study, speciation and concentrations of PAHs on solid by-products collected from the OSCAR process were investigated. In addition, the effects of operational parameters on PAHs on OSCAR solid by-products were examined.

### **5.3. Materials and Methods**

**Sample Collection.** Flue gas was generated by burning bituminous coal in a single spreader stoker boiler (boiler #8) in the McCracken Power Plant on The Ohio State University campus. LSD ash produced from the power plant was used to regenerate OSCAR sorbent. Lime was used as an alternative starting material in the same regeneration process to produce supersorbent. Samples of LSD ash from the McCracken power plant, regenerated OSCAR sorbent, lime, and supersorbent were collected.

Regenerated OSCAR sorbent was injected in experiment No. 1 to No. 8; in experiment No. 31 to No. 40, supersorbent was used in the OSCAR process. By-product samples were collected from the cyclone and the baghouse in selected experiments. All the collected samples were transferred into certified clean 500 mL or 100 mL brown glass bottles (Fisher Scientific) depending on the sample size and stored in an environmental chamber (4 to 12 °C) until the PAH analyses were performed.

**Sample Characterization.** A complete description of XRD, SEM and inorganic analysis are described elsewhere (17). Mineralogical analyses of samples were accomplished by using a Philips X-Ray Diffraction (XRD) instrument (Philips Analytical, Natick, MA) with CuK $\alpha$  radiation at 35kV and 20mA. The specific surface area (SSA) was measured by BET analysis conducted on a manually controlled Micromeritics FlowSorb 2300 volumetric system (Micromeritics, Norcross, GA) with a nitrogen (30% v/v) and helium mixture. Diluted hydrochloride acid (HCl) was used to remove inorganic carbon prior to organic carbon measurement. Organic carbon measurements were then conducted using a ThermoQuest carbon analyzer (ThermoQuest, Waltham, MA) by burning the samples at 900 °C with O<sub>2</sub>. A Vista Pro simultaneous inductively coupled plasma optical emission spectrometer system (Varian, Walnut Creek, CA) was used to determine major elements.

**Ultrasonic Extraction of PAHs.** A detailed ultrasonic extraction procedure is given by Sun et al. (18). Briefly, a 20 g sample with 100 mL toluene was sonicated for 3 min in a 400 mL glass beaker with a 20 kHz, 1.90 cm (ID) ultrasonic probe system (Sonic Dismembrator 550, Fisher Scientific). The output set at 10 (full power) with pulse mode (pulse =5 sec, pulse off = 5 sec) was used in all experiments. After extraction, the supernatant was decanted and filtered. The ultrasonic extraction was repeated twice with two additional 100 mL toluene. After the third extraction, all extracts were filtered, rinsed with 20~30 mL toluene and concentrated to 1mL using a Kuderna-Danish concentrator and high purity N<sub>2</sub> gas, successively.

Spike recoveries were determined for each sample by adding a 1 mL mixture of 16 PAHs to 20 g sample before extraction resulting in a spike level of 50  $\mu\text{g kg}^{-1}$  for each

PAH. A 20 g sample without adding the PAH standard was extracted as a background. Spike recoveries of 50% to 120% were obtained for PAHs detected in this study. In general, lower spike recoveries were obtained for higher molecular weight PAHs. Duplicate extractions were conducted for all samples collected to ensure reproducibility.

**PAH analysis.** Quantitative analysis of PAHs was performed with a Trace gas chromatograph/PolarisQ ion trap mass spectrometer (GC/MS) (ThermoQuest, Waltham, MA) using a CP-5 fused silica capillary column (30 m  $\times$  250  $\mu$ m  $\times$  0.25  $\mu$ m) (Varian, Walnut Creek, CA). The column was held at 60  $^{\circ}$ C for 2 min, programmed to 250  $^{\circ}$ C at 20  $^{\circ}$ C min $^{-1}$  followed by a 2 min hold time, increased to 300  $^{\circ}$ C at 10  $^{\circ}$ C min $^{-1}$  and held for 8 min. Helium was used as the carrier gas with a flow rate of 1.2 mL/min. A 2  $\mu$ L extract spiked with the deuterated internal standard were injected in the splitless mode. The injector temperature and ion source temperature was 250  $^{\circ}$ C and the temperature of the mass transfer line was 300  $^{\circ}$ C. The mass spectrometer was operated in full scan mode during analysis. Sixteen EPA-specified PAHs were confirmed and quantified by running authentic standards (Ultra scientific, North Kingstown, RI). The detection limits for these PAHs were from 0.1 to 10  $\mu$ g/kg; larger molecular weight PAHs had higher detection limits compared to small molecular weight PAHs.

#### **5.4. Results and Discussion**

**Characterization of Sorbents and Solid By-products.** The X-ray diffraction results in Figure 5.1 show that the regenerated OSCAR sorbent was primarily CaSO<sub>3</sub> and CaCO<sub>3</sub>.1/2 H<sub>2</sub>O. Supersorbent primarily consisted of CaO and CaCO<sub>3</sub>. Solid by-products collected from cyclone mainly consisted of CaCO<sub>3</sub>, CaSO<sub>3</sub>, CaO, and SiO<sub>2</sub>. For the

baghouse samples, the major minerals are CaSO<sub>4</sub>, CaCO<sub>3</sub>, and CaO. The X-ray results indicate the capture of S by the injected sorbent.

As shown in Figure 5.2, the major inorganic elements were similar in both cyclone and baghouse samples. The percentage of Ca and Si varied in collected samples; however, the difference is not significant. The S content was lower in cyclone samples than in the baghouse samples.

**PAHs on sorbents.** During the sorbent activation process, lime was activated to produce supersorbent, while the LSD ash was used as the raw material to generate the regenerated OSCAR sorbent. PAH concentrations on lime and LSD ash before activation and the formed supersorbent and regenerated OSCAR sorbent were measured to establish background levels of PAHs on the solid by-products. As shown in Table 5.1, the raw material before activation showed lower PAH concentrations compared to the sorbents formed. For example, only a few µg/kg of naphthalene was detected on the fresh lime. For the supersorbent made from lime, PAHs such as naphthalene and phenanthrene could be detected. Although more PAHs homologs (e.g., naphthalene, phenanthrene, pyrene and fluoranthrene) were detected on the LSD ash, the concentrations remained at µg/kg concentrations. However, regenerated OSCAR sorbent had much higher PAH concentrations than those of the LSD ash. In addition, compared to the supersorbent, regenerated OSCAR sorbent had much higher PAH concentrations.

The concentration of PAHs increases for both sorbents during the activation process, which may be due to the sorption of PAHs from the flue gas onto sorbent particles. Flue gas after passing through the baghouse in the McCracken Power Plant was used to activate the sorbent in a slurry tank at a temperature around 150 °C. It is possible that

PAHs in the flue gas are able to sorb onto the LSD ash or lime particles. The increase in PAHs after activation indicates that LSD ash and lime are able to capture PAHs from flue gas under appropriate conditions. However, the much lower PAH concentrations on supersorbent than the regenerated OSCAR sorbent indicated that lime did not sorb PAHs considerably from the flue gas during the activation process. With similar surface area, LSD ash had an organic carbon content of 6.1%, while no organic carbon was present in lime. Carbonaceous material is a strong sorbent for PAHs (19). Therefore, the higher organic carbon in the LSD ash may lead to more sorption of PAHs.

**PAHs on OSCAR solid by-products with supersorbent injection.** With the supersorbent injection, the total PAH concentration in samples collected from cyclone and baghouse are listed in Table 5.2. The speciation and concentrations of individual PAH are plotted in Figure 5.3. Small molecular weight PAHs such as naphthalene, phenanthrene and chrysene were dominant in most of the samples. Larger molecular weight PAHs including benzo(b)fluoranthene and/or benzo(k)fluoranthene were detected in several cyclone samples (e.g., No. 34, 35, and 38). However, no PAHs larger than benzo(a)anthracene could be detected in baghouse samples. The results also showed that types of PAHs detected were different in each sample. For example, chrysene was identified on cyclone samples of 32 and 38, while it was not detected in other cyclone samples.

On all the collected samples with supersorbent injection, the concentrations of PAHs detected were generally at sub-ppm levels but varied in different samples. For example, samples 32, 33, and 34 had higher naphthalene concentrations compared to the other cyclone samples; concentrations of phenanthrene in cyclone samples 35, 37, 38,

and 39 were approximately two to three times higher than the other samples. For the baghouse samples, the concentrations of naphthalene and phenanthrene were much higher than in the corresponding cyclone samples, while the concentrations of other PAHs detected on baghouse samples were similar.

The existence of low molecular weight PAHs, dominant on the cyclone and baghouse samples, may be due to the combustion conditions in the McCracken Power Plant. Previous work has suggested two major mechanisms responsible for PAH formation during coal combustion: pyrolysis and pyrosynthesis (20). The macromolecular aromatic compounds are broken into different size fragments, and these fragments then decompose and form small organic compounds in pyrolysis. In the process of pyrosynthesis, these fragments undergo reactions to form polycyclic compounds. The relative importance of these two mechanisms changes as a function of combustion temperature. Liu *et al.* sampled flue gas from a lab scale fluidized bed reactor and found small molecular weight PAHs were dominant in gas phase at sub-ppm levels with minimum PAH emissions occurring at 600 °C (14). Small molecular weight PAH compounds have low boiling points and higher stabilities compared to higher molecular weight PAHs thus avoiding decomposition. Moreover, Liu *et al.* also studied the effects of excess air on PAHs in fly ash during combustion and found small molecular weight PAHs such as naphthalene and phenanthrene were the dominant PAHs on fly ash with increasing of the excess air (14). In the McCracken power plant, the spreader stoker boiler was operated at approximately 650 °C with an air pump to provide extra air for combustion. Therefore, the low molecular weight PAHs detected and their low

concentrations on by-products conform with that expected based on operational conditions of the boiler.

The higher PAH concentrations on the baghouse samples compared to the cyclone sample may be due to the low temperature in the baghouse. Temperature in the baghouse is about 300 °C, which is much lower than the temperature in the cyclone at approximately 600 °C. Sorption of gas phase PAHs onto solid particles will be enhanced at lower temperature and lead to higher PAH concentrations on baghouse samples. In addition, longer residence time of fine particles collected by baghouse may be another explanation for higher PAH concentration. Longer residence time may enhance contact between gas-phase PAHs and sorbent resulting in more sorption of PAHs onto solid particles.

The higher surface area on baghouse samples may also be attributed to the higher PAH concentrations. Liu et al. observed that the PAH content in the fine particle fly ash is 5 times higher than that in the coarse particles (14). Baghouse samples generated with supersorbent injection had higher surface area compared to the corresponding cyclone samples except sample 37. For example, 22.3 m<sup>2</sup>/g of the baghouse sample vs. 10.9 m<sup>2</sup>/g of the cyclone sample in experiment No.33. In experiment 37, cyclone sample had a higher surface area of 23.0 m<sup>2</sup>/g than the baghouse sample of 18.9 m<sup>2</sup>/g. The higher surface area may provide more sorption sites for PAH molecules resulting a higher PAH concentration on baghouse samples.

The organic carbon measurements also showed that solids collected in experiment 37 was different compared to other samples. The carbon content was consistently higher in the baghouse samples than the corresponding cyclone samples except sample 37. The

higher organic carbon contents of baghouse sample may also contribute to the higher PAH concentrations due to the high sorption capacity of the carbonaceous materials (19).

For naphthalene and phenanthrene, their higher concentrations on the baghouse samples may also be attributed to the physical characteristics of these two compounds. Compared to the other larger molecular weight PAHs, naphthalene and phenanthrene have lower boiling point and higher stability. After partially captured by cyclone, the residue naphthalene and phenanthrene in gas phase may continue to sorb onto smaller particles that are later collected by baghouse after the cyclone.

**PAHs on solid by-products with regenerated OSCAR sorbent injection.** PAH homologs and concentrations detected in cyclone and baghouse samples with the regenerated OSCAR sorbent injection are listed in Table 5.3. The PAHs identified in cyclone samples were small molecular weight PAHs including naphthalene, phenanthrene, anthracene, pyrene, and fluoranthrene. No PAHs larger than chrysene were detected in any of the cyclone samples. However, fluorene, chrysene and benzo(a)anthracene were identified on the baghouse sample. Overall, the concentrations of PAHs detected on OSCAR samples were consistently low, ranging from a few to tens of  $\mu\text{g}/\text{kg}$ . The baghouse sample had a slightly higher total PAH concentration than the cyclone samples. All the collected samples had similar organic carbon content that were higher than 20%. Sample 5A-7 had the highest carbon content of 26.5%. The surface area measurements showed the baghouse sample was similar as the other cyclone samples. Therefore, the similar organic carbon content and surface area may be the reason that the PAH concentrations on the collected samples were similar.

### **Effects of different sorbents on PAH detected on OSCAR solid by-products.**

As shown in Table 5.2 and Table 5.3, supersorbent injection resulted in much higher PAH concentrations in the by-products than with regenerated OSCAR sorbent injection. For example, the concentration of naphthalene ranged from  $42.8 \pm 30.5 \mu\text{g/kg}$  to  $173.5 \pm 56.0 \mu\text{g/kg}$  on the cyclone samples with supersorbent injection. With regenerated OSCAR sorbent injection, the naphthalene concentration on cyclone samples was about 2 orders of magnitude lower ranging from  $1.3 \pm 0.4 \mu\text{g/kg}$  to  $16.0 \pm 1.0 \mu\text{g/kg}$ .

As mentioned earlier, the PAH concentrations on supersorbent before injection were very low. Therefore, the higher PAH concentrations on solid by-products after supersorbent injection indicated the capture of PAHs from flue gas. Mastral *et al.* studied the effects of limestone on PAH emissions from coal atmospheric fluidized bed combustion, their results showed that limestone helped to control the PAH emissions in the gas phase by adsorption (21). Another study by Goss suggested more sorption of organic compounds on the mineral phase due to the decrease of relative humidity (22). Accordingly, low moisture due to the heat from the flue gas may lead to sorption of PAHs on the formed solid by-products in the OSCAR process.

Compared to the supersorbent, regenerated OSCAR sorbent was not as effective at capturing PAHs from flue gas. Although the higher surface area ( $36.6 \text{ m}^2/\text{g}$ ) and higher carbon content (9.5%) of regenerated OSCAR sorbent should favor PAH sorption compared to the supersorbent as shown in Table 1. The high PAH concentrations on the regenerated OSCAR sorbent and the lower PAH concentrations on the cyclone and baghouse samples suggest release of PAHs from the solids or reactions of PAHs during  $\text{SO}_2$  capture and particle removal processes. One explanation for the different capture

efficiency of these two sorbents is their different characteristics. The x-ray diffraction results showed that  $\text{CaCO}_3$  and  $\text{CaO}$  were the major components in the supersorbent. However, the regenerated OSCAR sorbent contains mostly  $\text{CaSO}_3$  hydrate and  $\text{CaCO}_3$ . This may alter the ability of the solid to sorb PAHs from the flue gas. Moreover, the decomposition of  $\text{CaSO}_3$  in the regenerated OSCAR sorbent was observed during the desulfurization process. This may also lead to the release of the sorbed PAHs from the regenerated OSCAR sorbent.

**Effects of Operational Parameters on PAHs in Solid By-products in the OSCAR process.** The results also indicate that the compositions and concentrations of the PAHs measured on the solid by-products may be affected by operational conditions. Different flue gas flow rates and sorbent feed rates can change the contact time between gas phase PAHs and sorbents, and thus affect sorption of PAHs onto the FGD by-products. The detailed operational parameters in each experiment are listed in Table 5.4.

Under a constant sorbent injection rate, the lower flow rate of flue gas results in less flue gas contacting the injected sorbent. In turn, this results in less PAHs sorbing onto solid by-products. For example, for the experiments with supersorbent, same sorbent injection rate was maintained in 34, 35, 37, and 38. Flue gas flow rates were lower in experiments 37, 38 resulting in lower PAH concentrations on the solid by-products collected in these experiments. Similarly, in experiments 33 and 39 with same sorbent injection rate, lower flue gas flow rates may be the reason of lower PAH concentrations on solid by-products collected in experiment 39.

Different PAH concentrations on baghouse samples may relate to the baghouse flow rate. Within a certain operation time, a higher baghouse flow rate will lead to more

collection of solid particles and possibly form a layer of solid acting as filter thus capturing more PAHs. The baghouse flow rate was 28 m<sup>3</sup>/h in experiment 33, higher than 21 m<sup>3</sup>/h in experiment 32, and 23 m<sup>3</sup>/h in experiment 35 (Table 5.4). PAHs measured on the baghouse sample 33 had the highest concentrations among all the available baghouse samples. Therefore, a higher baghouse flow rate may capture more PAHs thus reducing their emissions.

PAHs on the solid by-products are expected to be affected by flue gas temperature because temperature impacts the formation, transformation (15) and sorption of organic compounds onto solid materials (21). However, the temperature of cyclone was kept at 600~650 °C and baghouse was at 300 °C in all the experiments. Therefore, temperature effects on solid by-products were not able to be observed. However, with supersorbent injection, the PAH concentrations on baghouse samples were much higher than the cyclone samples partially due to the lower temperature in the baghouse.

Within a certain operation period, higher sorbent injection rates results in more sorbent injected and thus diluting the PAHs on the solid by-products. Experiment 3, 4, and 5 were conducted under similar conditions except for the difference of sorbent injection rate. For example, the sorbent injection rate was 8 kg/hr in experiment 5, 44 kg/hr in experiment 4, and 56 kg/hr in experiment 3. Therefore, the sample collected from experiment 3 should have the lowest PAH concentration among these three experiments. However, cyclone sample collected in experiment 4 had the lowest PAH concentration. Thus, due to the limited number of samples, it is hard to identify the operational effects on the PAHs on the solid by-products with the regenerated OSCAR sorbent injection.

**Correlation between PAH concentrations and inorganic elements.** The correlation between PAH concentrations and Ca content in the cyclone samples with both supersorbent and regenerated OSCAR sorbent is shown in Figure 5.4. For the samples with supersorbent injection, a linear relationship ( $R^2= 0.73$ ) between the Ca content and total PAH concentration was observed suggesting Ca was responsible for capturing PAHs. As for the samples with regenerated OSCAR sorbent injection, no correlation between Ca content and total PAH concentration was shown. Supersorbent and regenerated OSCAR sorbent have different mineral compositions. In supersorbent, Ca exists primarily as  $\text{CaCO}_3$ . While in the regenerated OSCAR sorbent, the major mineral composition is hannebachite (i.e.,  $\text{CaSO}_3 \cdot 0.5\text{H}_2\text{O}$ ). These two different minerals may have different PAH sorption efficiencies. Moreover, the decomposition of hannebachite at higher temperature may also be an explanation for the poor correlation between Ca and total PAH concentration.

With supersorbent injection, the Hg concentration also showed a linear correlation with total PAH concentrations in the baghouse samples. In Figure 5.5, a linear relation ( $R^2=0.77$ ) between Hg concentration and total PAH concentration were shown, which suggests that Hg and PAHs may sorb on the same sites on the baghouse samples.

## **5.5. Conclusions**

The characterization of PAHs on solid by-products collected from the OSCAR process showed the presence of primarily small molecular weight compounds at low concentrations (e.g. from a few  $\mu\text{g}/\text{kg}$  to hundreds  $\mu\text{g}/\text{kg}$ ). Baghouse samples had higher PAH concentrations than cyclone samples. PAH composition and concentration were

found to be influenced by the type of sorbents and operational conditions (e.g. sorbent injection rate and baghouse flow rate) in the OSCAR process.

### **Acknowledgments**

The financial support by the Ohio State Carbonation and Ash Reactivation (OSCAR) Demonstration Project with funding from the Ohio Coal Development Office (OCDO) and the Ohio State University are highly acknowledged. We also thank Doug Beak for the total carbon measurements, Chin-Ming Cheng for surface area measurements and Puneet Gupta for select X-Ray diffraction measurements.

## References

1. Kadambi, J. R.; Adler, R. J.; Prudich, M. E.; Fan, L. S.; Raghunathan, K.; Khang, S. J.; Keener, T. C. 1998. *Flue gas desulfurization for acid rain control*. In: Toole-Oneil, B. (Eds.). *Dry Scrubbing Technologies for Flue Gas Desulfurization*. Kluwer Academic Publishers: Boston/Dordrecht/London, pp. 6-8.
2. Fan, L-S.; Jadhav, R. A. Clean coal technologies: OSCAR and CARBONOX commercial demonstrations. *AIChE Journal*, **2002**, *48*, 2115-2123.
3. Agnihotri, R.; Chauk, S. S.; Mahuli, S. K.; Fan, L.-S. Sorbent/ash reactivation for enhanced SO<sub>2</sub> capture using a novel carbonation technique. *Ind. Eng. Chem. Res.* **1999**, *38*, 812-819.
4. Wastes from the Combustion of Fossil Fuels, Volume 1 and 2- Methods, Findings, and Recommendations; EPA 530-S-99-010; Report to Congress; U.S. Environmental Protection Agency: Washington DC, 1999.
5. Henner, M.; Schiavon, M.; Morel, J. L.; Lichtfouse, E. Polycyclic aromatic hydrocarbon (PAH) occurrence and remediation methods. *Analisis*, **1997**, *25*, M56-M59.
6. Denissenko, M. F.; Pao, A.; Tang, M-S.; Pfeifer, G. P. Preferential formation of benzo[a]pyrene adducts at lung cancer mutational hotspots in P53. *Science* *274*, 430-432.
7. Pisupati, S. V.; Wasco, R. S.; Scaroni, A. W. An investigation on polycyclic aromatic hydrocarbon emissions from pulverized coal combustion systems. *Journal of Hazardous Materials* **2000**, *74*, 91-107.
8. Akimoto, Y.; Aoki, T.; Nito, S.; Inouye, Y. Oxygenated polycyclic aromatic hydrocarbons from MSW incinerator fly ash. *Chemosphere* **1997**, *34*, 263-273.

9. Low, G. K. C.; Batley, G. E. Comparative studies of adsorption of polycyclic aromatic hydrocarbons by fly ashes from the combustion of some Australian coals. *Environ. Sci. Technol.* **1988**, *22*, 322-327.
10. Johansson, I.; Bavel, B. V. Levels and patterns of polycyclic aromatic hydrocarbons in incineration ashes. *Sci. Total Environ.* **2003**, *311*, 221-231.
11. Fangmark, I.; Bavel, B.V.; Marklund, S.; Stromberg, B.; Berge, N.; Rappe, C. Influence of combustion parameters on the formation of polychlorinated dibenzo-p-dioxins, dibenzofurands, benzenes, and biphenyls and polyaromatic hydrocarbons in a pilot incinerator. *Environ. Sci. Technol.* **1993**, *27*, 1602-1610.
12. Mastral, A. M.; Callen, M. S.; Mayoral, C.; Galban, J. Polycyclic aromatic hydrocarbon emissions from fluidized bed combustion of coal. *Fuel*, **1995**, *74*, 1762-1766.
13. Kim, O.; Nguyen, T.; Reutergardh, L. B.; Dung, N. T. Emission of Polycyclic Aromatic Hydrocarbons and Particulate Matter from Domestic Combustion of Selected Fuels. *Environ. Sci. Technol.* **1999**, *33*, 2703-2279.
14. Liu, K-L.; Xie, W.; Zhao, Z-B.; Pan, W-P.; Riley, J. T. Investigation of polycyclic aromatic hydrocarbons in fly ash from fluidized bed combustion systems. *Environ. Sci. Technol.* **2000**, *34*, 2273-2279.
15. Lillieblad, L.; Szpila, Z.; Strand, M.; Pagels, J.; Rupa-Gadd, K.; Gudmundsson, A.; Seietlicki, E.; Bohgad, M.; Sanati, M. Boiler operation influence on the emissions of submicrometer-sized particles and polycyclic aromatic hydrocarbons from biomass-fired grate boilers. *Energy & Fuels* **2004**, *18*, 410-417.

16. Stewart, B. R.; Kalyoncu, R. S. Proceedings, 1999 International Ash Utilization Symposium, Lexington, KY, October, 1999.
17. Taerakul, P.; Sun, P.; Walker, H. W.; Weavers, L. K.; Golightly, D.; Butalia, T. **Variability of inorganic and organic constituents in lime spray dryer ash.** *Fuel*, **2004**, in review.
18. Sun, P.; Weavers, L. K.; Taerakul, P.; Walker, H. W. Effects of extraction method on the characterization of polycyclic aromatic hydrocarbons (PAHs) on lime spray dryer (LSD) Ash. *Chemosphere* **2004**, submitted.
19. Ghosh, U.; Talley, J. W.; Luthy, R. G. Microscale location, characterization, and association of polycyclic aromatic hydrocarbons on harbor sediment particles *Environ. Sci. Technol.* **2000**, *34*, 1729.
20. Cook, B. R.; Wilkinson, B. B.; Claude, C. C.; Holmes, S. M.; Martinez, L. E. Hydrogen transfer induced cleavage of biaryl Bonds. *Energy Fuels* **1997**, *11*, 61-70.
21. Mastral, A. M.; Garcia, T.; Callen, M. S.; Lopez, J. M.; Murillo, R.; Navarro, M. V. Effects of limestone on polycyclic aromatic hydrocarbon emissions during coal atmospheric fluidized bed combustion. *Energy & Fuels.* **2001**, *15*, 1469-1474.
22. Goss, K-U. The Air/Surface adsorption equilibrium of organic compounds under ambient conditions. *Critical Reviews in Environmental Science and Technology*, **2004**, *34*, 339-389.

	Lime	Supersorbent	LSD ash	Regenerated Sorbent
<b>SSA (m<sup>2</sup>/g)</b>	17.1	16.8	8.9	36.6
<b>C content (%)</b>	0	7.7	6.1	9.5
<b>Naphthalene</b>	2.4±1.3	28.3±7.4	48.7±7.3	373.2±106.8
<b>Acenaphthene</b>	N/D	N/D	N/D	18.9±4.1
<b>Fluorene</b>	N/D	N/D	N/D	53.9±5.4
<b>Phenanthrene</b>	N/D	6.6±0.3	4.1±0.4	95.7±7.4
<b>Anthracene</b>	N/D	4.0±0.6	N/D	13.7±1.1
<b>Pyrene</b>	N/D	N/D	12.2±0.7	16.4±2.3
<b>Fluoranthrene</b>	N/D	2.0±0.2	11.5±0.7	36.5±6.6
<b>Chrysene</b>	N/D	N/D	N/D	13.9±2.9
<b>Benzo(a)-anthracene</b>	N/D	N/D	N/D	62.8±8.0

N/D: not detectable

Table 5.1. Specific surface area, organic C content and the concentration (µg/kg) of PAHs detected on the lime, supersorbent, LSD ash, and regenerated OSCAR sorbent.

<b>Sample ID</b>	<b>Specific surface area (m<sup>2</sup>/g)</b>	<b>Organic carbon content (%)</b>	<b>Total PAHs (µg/kg)</b>
<b>32-7</b>	13.5	9.7	169.2±68.0
<b>33-7</b>	10.9	14.8	167.2±15.6
<b>34-7</b>	12.5	8.0	203.4±56.0
<b>35-7</b>	9.9	7.3	176.7±13.2
<b>37-7</b>	23.0	15.5	116.4±18.5
<b>38-7</b>	11.4	13.1	122.8±9.4
<b>39-7</b>	13.8	10.8	84.3±30.9
<b>40-7</b>	21.4	13.0	87.7±35.8
<b>32-8</b>	n/a	12.1	490.4±47.1
<b>33-8</b>	22.3	12.0	813.7±39.5
<b>35-8</b>	n/a	13.3	283.2±51.4
<b>37-8</b>	18.9	10.0	305.5±23.3
<b>38-8</b>	19.5	10.2	613.2±116.7
<b>39-8</b>	19.0	9.9	388.3±168.9

n/a: not available

Table 5.2. Specific surface area, organic carbon content, and total concentration of PAH measured on solid by-products with supersorbent injection. #-7 are cyclone sample, #-8 are baghouse sample.

PAHs	Nap	Ace	Phe	Ant	Py	Flu	Chy	Ben(a)	Ben(b)	Ben(k)
31-7	26.3±14.5	N/D	8.8±1.2	3.1±0.7	N/D	N/D	N/D	N/D	N/D	N/D
32-7	138.9±67.9	N/D	12.3±1.6	7.9±4.1	7.3±1.0	2.8±0.7	N/D	N/D	N/D	N/D
33-7	140.0±15.4	N/D	5.2±0.8	5.4±1.5	7.7±1.0	4.8±0.6	4.1±1.2	N/D	N/D	N/D
34-7	173.5±56.0	N/D	10.1±1.4	5.2±1.0	7.5±0.9	4.2±0.7	N/D	N/D	1.6±0.2	1.3±0.2
35-7	84.9±10.2	N/D	20.5±4.5	9.7±2.4	15.7±3.7	10.0±2.5	N/D	N/D	18.7±3.7	17.2±3.2
37-7	58.5±18.1	N/D	22.5±2.4	10.9±0.9	15.0±2.3	9.5±1.9	N/D	N/D	N/D	N/D
38-7	61.3±8.9	N/D	20.8±1.6	9.1±0.9	12.4±1.7	7.4±1.3	4.5±0.8	7.3±0.3	N/D	N/D
39-7	42.8±30.5	N/D	18.2±3.5	5.8±0.9	10.6±2.7	6.9±1.8	N/D	N/D	N/D	N/D
40-7	63.4±35.7	N/D	8.4±0.4	6.3±1.2	5.0±1.5	4.6±2.2	N/D	N/D	N/D	N/D
32-8	288.4±34.9	N/D	112.5±28.8	23.8±7.5	34.6±8.6	9.3±2.6	21.8±5.6	N/D	N/D	N/D
33-8	581.9±34.2	14.6±1.1	99.7±11.6	10.4±1.6	36.4±4.1	10.4±2.1	13.2±8.5	47.1±12.9	N/D	N/D
35-8	222.4±47.8	N/D	44.2±18.5	3.9±1.7	8.4±2.5	4.3±1.7	N/D	N/D	N/D	N/D
37-8	241.9±19.8	10.4±1.0	26.9±12.0	5.7±1.9	17.6±1.5	3.0±1.0	N/D	N/D	N/D	N/D
38-8	512.6±116.6	N/D	54.7±3.5	9.3±2.1	26.7±1.5	9.9±0.8	N/D	N/D	N/D	N/D
39-8	335.9±168.7	N/D	31.6±7.4	7.5±2.5	7.3±2.2	6.0±2.2	N/D	N/D	N/D	N/D

Table 5.3. Measured PAH concentration on cyclone samples with supersorbent injection. #-7 are cyclone sample, #-8 are baghouse sample. Nap: naphthalane; Ace: acenaphthene; Phe: phenanthrene; Ant: anthracene; Py: pyrene; Flu: Fluoranthrene; Chy: chrysene; Ben(a): Benzo(a)anthracene; Ben(b): benzo(b)fluoranthene; Ben(k): benzo(k)fluoranthene

	<b>3A-7</b>	<b>4A-7</b>	<b>5A-7</b>	<b>8A-7</b>	<b>1B-8</b>
<b>SSA (m<sup>2</sup>/g)</b>	18.0	30.9	29.0	38.8	20.6
<b>C content (%)</b>	24.2	20.9	26.5	21.6	20.6
<b>Naphthalene</b>	13.8±1.2	1.3±0.4	19.5±0.6	16.0±1.0	13.4±1.5
<b>Acenaphthene</b>	N/D	N/D	N/D	N/D	N/D
<b>Fluorene</b>	N/D	N/D	N/D	N/D	6.4±0.1
<b>Phenanthrene</b>	3.4±0.6	4.2±0.3	3.1±0.4	5.2±0.3	3.7±2.2
<b>Anthracene</b>	2.3±0.3	2.2±0.5	1.6±0.2	2.6±0.2	N/D
<b>Pyrene</b>	5.7±0.1	4.6±0.3	5.8±1.0	4.8±0.5	1.5±0.6
<b>Fluoranthrene</b>	5.1±0.4	3.8±0.3	5.6±1.6	3.6±0.1	2.8±0.1
<b>Chrysene</b>	N/D	N/D	N/D	N/D	3.9±0.2
<b>Benzo(a)-Anthracene</b>	N/D	N/D	N/D	N/D	4.4±0.2
<b>Total PAH</b>	30.3±1.4	16.1±1.0	35.6±2.0	17.8±1.2	36.1±1.2

N/D: not detectable

Table 5.4. Specific surface area, organic C content and the concentration (µg/kg) of PAHs on samples collected from cyclone and baghouse using regenerated OSCAR sorbent. 3A-7, 4A-7, 5A-7 and 8A-7 are cyclone samples. 1B-8 is a baghouse sample.

<b>Sample ID</b>	<b>Temp. (°C)</b>	<b>Flue Gas Flow (m<sup>3</sup>/h)</b>	<b>Addition (kg/hr)</b>	<b>Baghouse flow rate (m<sup>3</sup>/h)</b>	<b>Sorbent type</b>
<b>3-A</b>	642	122	56	26	ROS
<b>4-A</b>	650	124	44	26	ROS
<b>5-A</b>	653	123	8	26	ROS
<b>8-A</b>	645	78	18	17	ROS
<b>1-B</b>	681	124	27	27	ROS
<b>32</b>	643	137	23	21	SS
<b>33</b>	639	120	4	28	SS
<b>34</b>	629	87	16	30	SS
<b>35</b>	640	138	16	23	SS
<b>37</b>	646	90	16	21	SS
<b>38</b>	673	83	16	20	SS
<b>39</b>	660	76	10	25	SS

Table 5.5. Operational conditions in OSCAR process. ROS: regenerated OSCAR sorbent; SS: supersorbent.

## FIGURE CAPTIONS

Figure 5.1. X-Ray diffraction pattern of selected cyclone and baghouse samples collected in the OSCAR process. 4-7: cyclone samples with regenerated OSCAR sorbent injection; 4-8: baghouse samples with regenerated OSCAR sorbent injection; 33-7: cyclone samples with supersorbent injection; 33-8: baghouse samples with supersorbent injection. X-Ray diffraction pattern of cyclone and baghouse samples collected in the OSCAR process with regenerated OSCAR sorbent injection.

Figure 5.2. Major elemental composition in cyclone and baghouse samples collected in the OSCAR process. baghouse-1: baghouse samples with regenerated OSCAR sorbent injection; baghouse-2: baghouse samples with supersorbent injection; cyclone-1: cyclone samples with regenerated OSCAR sorbent injection; cyclone-2: cyclone samples with supersorbent injection.

Figure 5.3. Speciation and concentrations of PAHs detected on the solid by-products with supersorbent injection. Fig. 3a: cyclone samples. Fig. 3b: baghouse samples.

Figure 5.4. Correlation between Ca content and total PAH concentration in the cyclone samples.

Figure 5.5. Correlation between Hg and total PAH concentrations in the baghouse samples with supersorbent injection.

P - Portlandite, syn -  $\text{Ca}(\text{OH})_2$   
 H - Hannebachite, syn -  $\text{CaSO}_3 \cdot 0.5\text{H}_2\text{O}$   
 M - Mullite -  $\text{Al}_6\text{Si}_2\text{O}_{13}$   
 Q- Quartz -  $\text{SiO}_2$   
 L - Lime -  $\text{CaO}$   
 G - Gypsum -  $\text{CaSO}_4$   
 C - Calcite -  $\text{CaCO}_3$

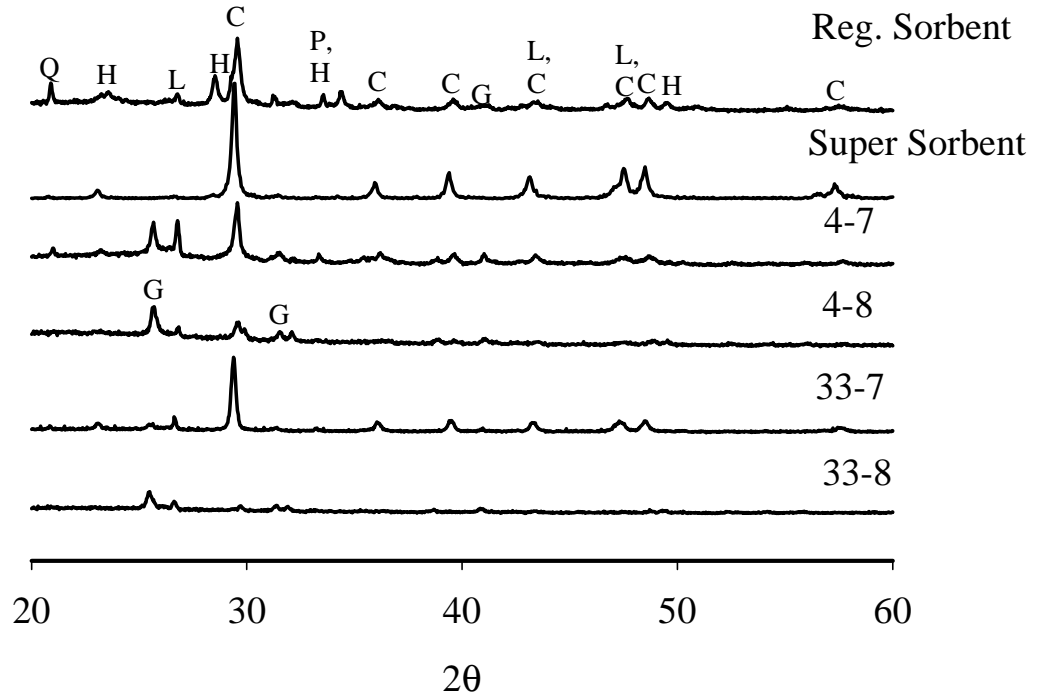


Figure 5.1. X-Ray diffraction pattern of selected cyclone and baghouse samples collected in the OSCAR process. 4-7: cyclone samples with regenerated OSCAR sorbent injection; 4-8: baghouse samples with regenerated OSCAR sorbent injection; 33-7: cyclone samples with supersorbent injection; 33-8: baghouse samples with supersorbent injection.

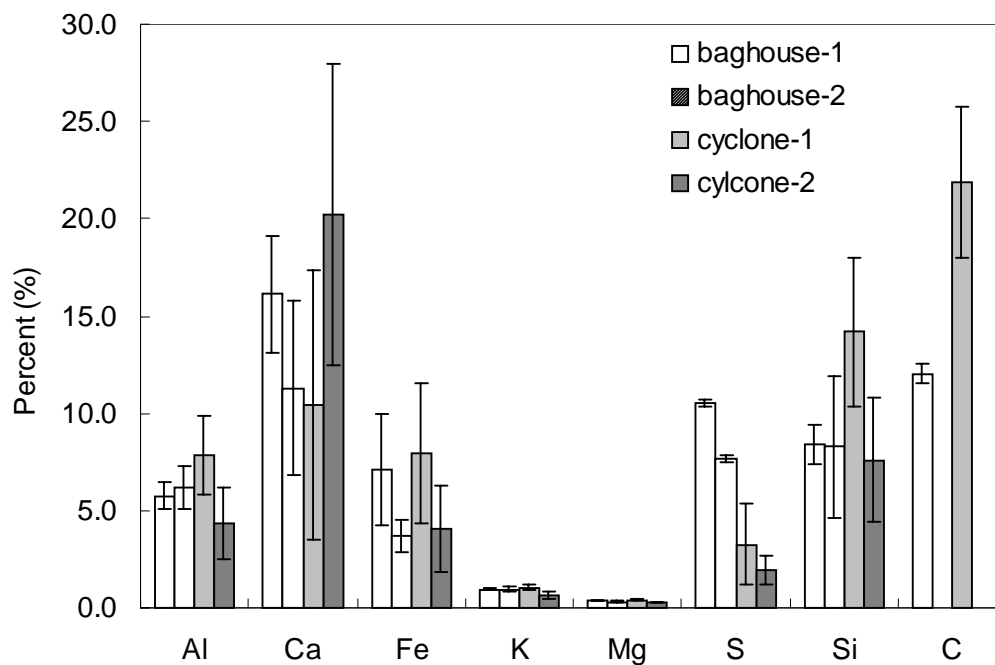


Figure 5.2. Major elemental composition in cyclone and baghouse samples collected in the OSCAR process. baghouse-1: baghouse samples with regenerated OSCAR sorbent injection; baghouse-2: baghouse samples with supersorbent injection; cyclone-1: cyclone samples with regenerated OSCAR sorbent injection; cyclone-2: cyclone samples with supersorbent injection.

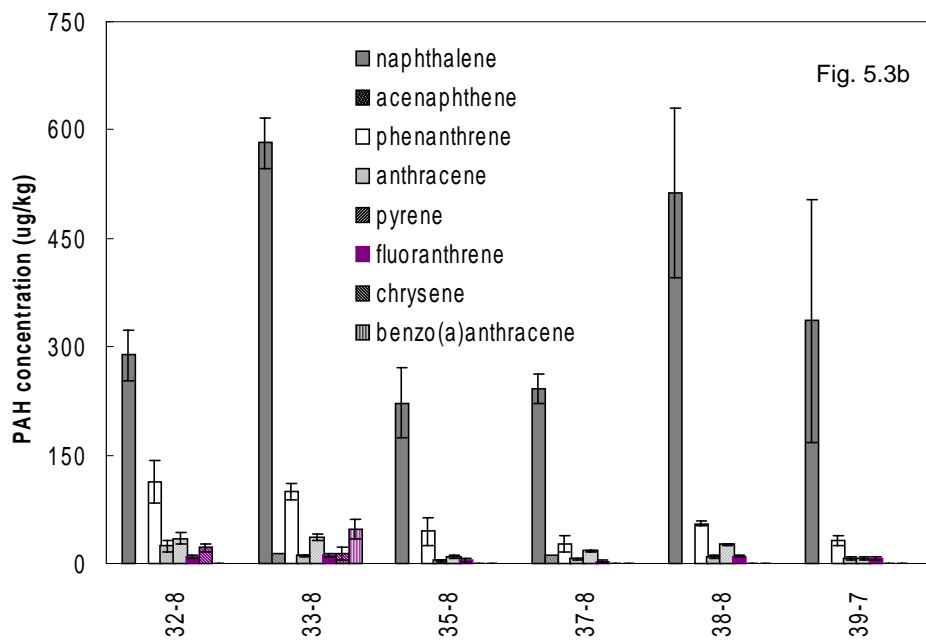
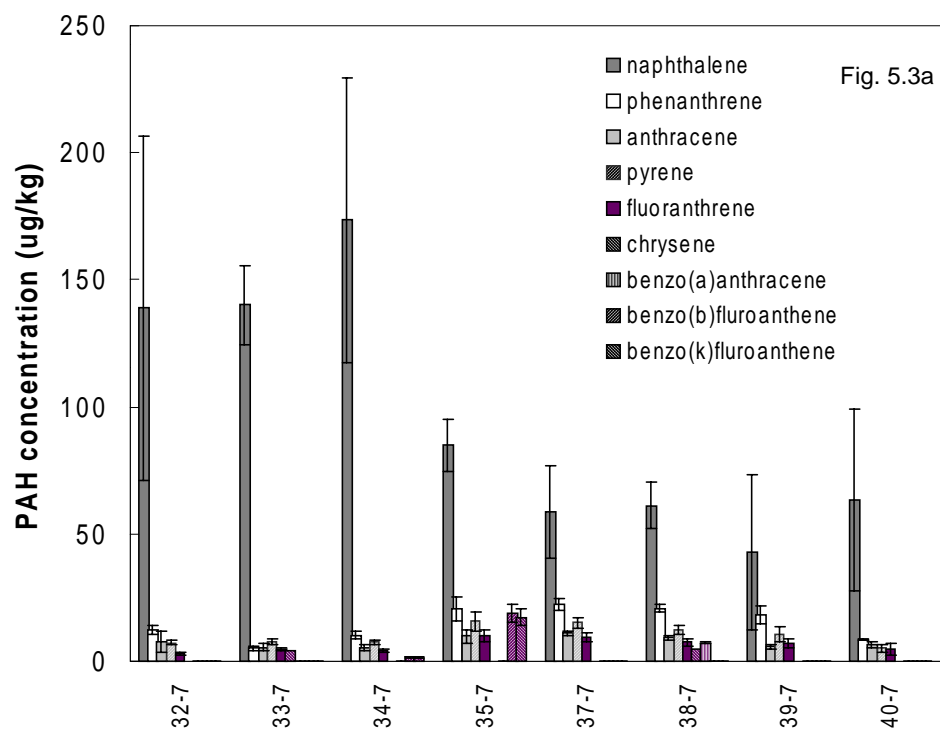


Figure 5.3. Speciation and concentrations of PAHs detected on the solid by-products with supersorbent injection. Fig. 3a: cyclone samples. Fig. 3b: baghouse samples.

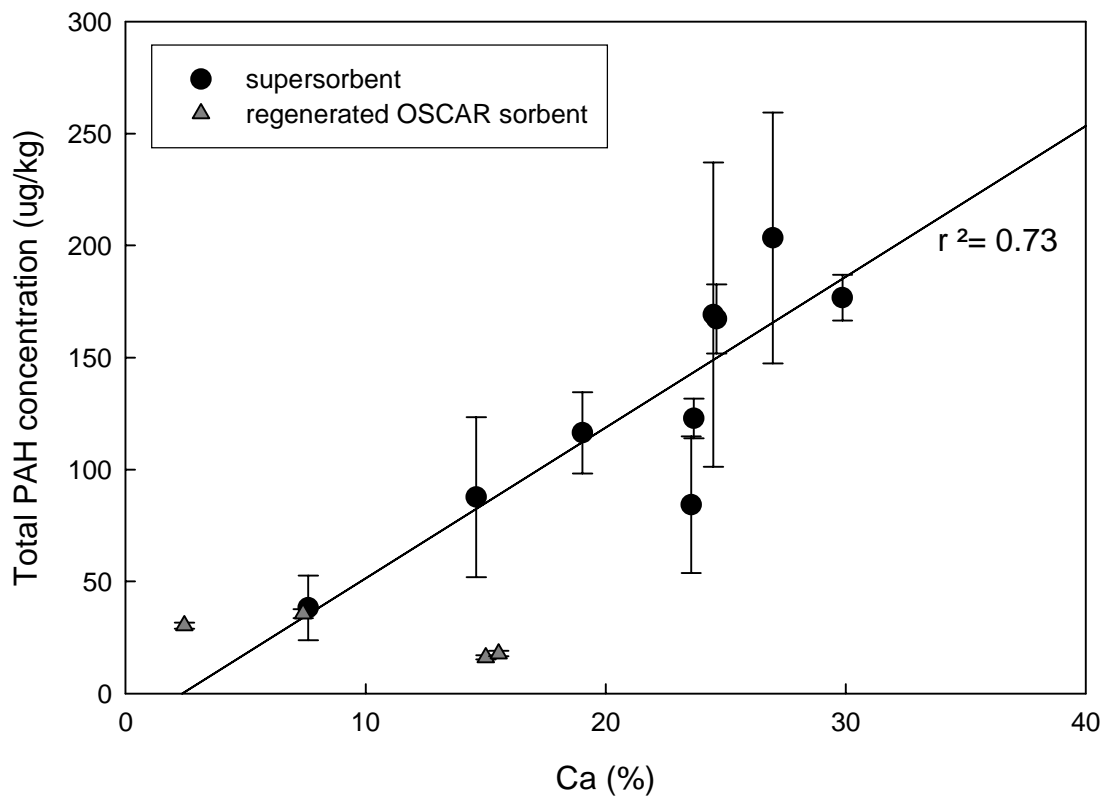


Figure 5.4. Correlation between Ca content and total PAH concentration in the cyclone samples.

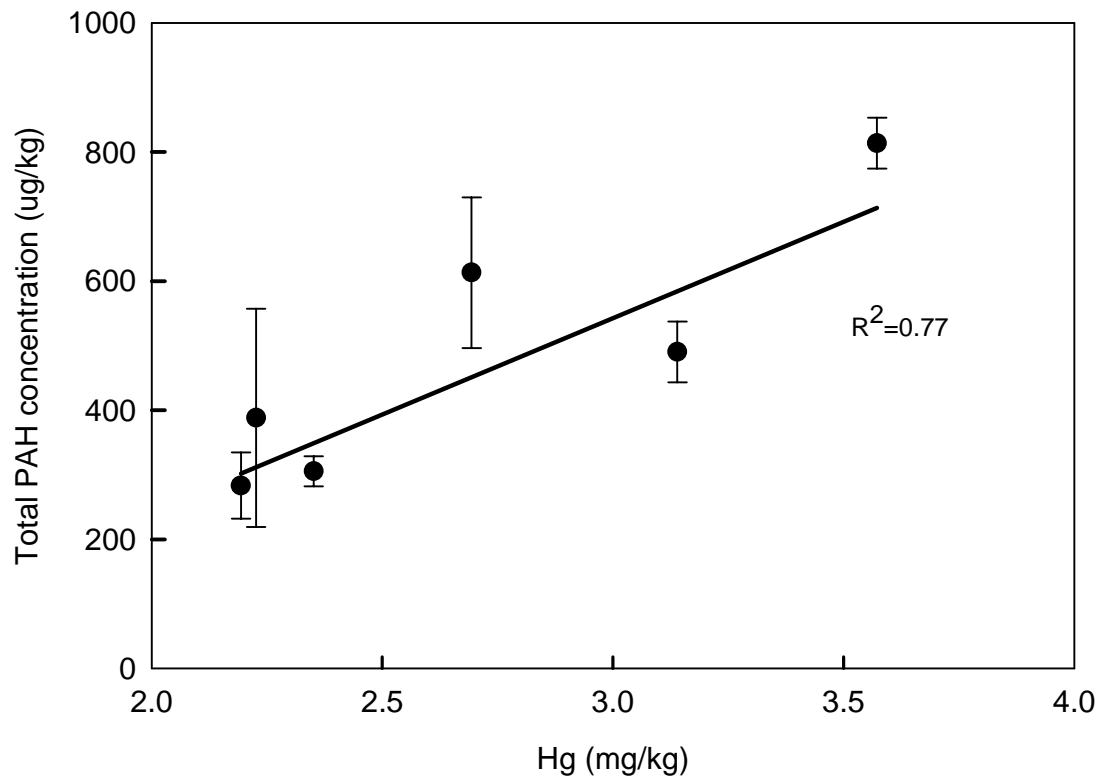


Figure 5.5. Correlation between Hg and total PAH concentrations in the baghouse samples with supersorbent injection.

## CHAPTER 6

### CONCLUSIONS AND FUTURE WORK

#### 6.1. Conclusions

Investigation of polycyclic aromatic hydrocarbons (PAHs) on the dry flue gas desulfurization (FGD) by-products was conducted in this dissertation. In chapter 2 and 3, effects of different extraction procedures on the quantification of the 16 U.S. EPA specified PAHs were studied. For example, in chapter 2, a comparative study on the traditional Soxhlet extraction, automatic Soxhlet extraction, and ultrasonic extraction showed that the speciation and concentrations of measured PAHs on the lime spray dryer (LSD) ash varied with different extraction methods. Ultrasonic extraction with toluene had the highest extraction efficiency for extracting medium molecular weight PAHs.

In chapter 3, the effects of ultrasonic extraction parameters on the reactions of PAH were examined to elucidate the degradation of PAHs during sonication. By sonicating naphthalene, phenanthrene, and pyrene in organic solvents, it was determined that PAH molecules underwent both direct pyrolysis and reactions with methyl radicals formed from solvent pyrolysis and thus affected the quantification results. Extraction

parameters including solute concentration, solvent type, pulse time interval, and sonication time also had effects on reactions of PAHs. Therefore, although the short time in ultrasonic extraction is an advantage, caution is needed when conducting this method.

After the development of extraction and analytical methods, answers were sought for the speciation and concentrations of PAHs in LSD ash. Results showed that the PAHs identified were primarily low molecular weight PAHs such as naphthalene, phenanthrene and pyrene. Although the PAH speciation on LSD ash varied in different samples, the concentrations of PAH identified were consistently low, usually at  $\mu\text{g kg}^{-1}$  levels.

In chapter 4, the distribution of PAHs in LSD ash showed that PAHs were primarily associated with the carbonaceous material (e.g., unburned carbon). Although the mass percentage of unburned carbon was only approximately 5.4%~11.9% of the total LSD ashes sampled, unburned carbon contributed 74% to 129% of the total PAHs measured. However, PAHs were also detected in the lime-enriched fraction with very low organic carbon contents, which suggested the fine spray of slaked lime may also sorb PAHs from the flue gas in the LSD process.

Characterizations of PAHs on the solid by-products in the OSCAR process were performed in Chapter 5. Different from the conventional dry FGD process, additional sorbent activation processes are used in the OSCAR process. Thus, the PAHs on solid by-products collected from the OSCAR process may be different from the LSD ash. The PAH measurement results showed that PAHs on the OSCAR solid by-products were still primarily small molecular weight compounds. In addition, PAH compositions and concentrations were found to be affected by the operational conditions such as sorbent type, sorbent injection rate, and baghouse flow rate in the OSCAR process. For example,

the PAH concentrations were at  $\mu\text{g}/\text{kg}$  levels with regenerated OSCAR sorbent injection. When the suporsorbent was injected into the OSCAR system, the concentrations of the PAHs detected were higher, at sub-ppm levels indicating capture of PAHs. Baghouse samples had consistently higher concentrations than the samples collected from the cyclone possibly due to the longer residence time of the particles and the lower temperature in the baghouse. In addition, PAH composition and concentration were found to be affected by operation conditions such as sorbent injection rate and baghouse flow rate in the OSCAR process.

In summary, PAHs identified on either LSD ash collected from the McCracken Power Plant or the OSCAR process were primarily small molecular weight PAHs with low concentration (from a few  $\mu\text{g}/\text{kg}$  to hundreds of  $\mu\text{g}/\text{kg}$ ). Although much lower PAH concentrations in LSD ash compared to natural soils (e.g.,  $\text{mg}/\text{kg}$ ), a bioavailability study needs to be conducted to verify the PAHs have no threat to the environment during utilization or disposal of LSD ash. However, other studies conducted on PAHs associated with carbonaceous materials in sediments showed very low bioavailability. In this study, PAHs were found to be primarily associated with unburned carbon. Therefore, it should be expected that PAHs on dry FGD by-products tested (e.g., LSD ash) will not adversely affect the environment from the perspective of PAHs.

## **6.2. Future Work**

Results of this research showed low PAH concentrations on LSD ash. However, the bioavailability study needs to be conducted to ensure that these PAHs will not be a threat to the environment.

The PAHs on the dry FGD by-product may be related to the type of the boiler, the fuel source and the operation conditions in the specific power plant. In this study, the LSD system is applied to a spreader stoker boiler with bituminous coal as fuel source. Due to its lower combustion efficiency and higher SO<sub>2</sub>, NO<sub>x</sub>, and CO<sub>2</sub> emissions, it is necessary to retrofit spreader stoker boilers. For example, retrofit the stoker coal boiler to a co-firing boiler that burns biomass or natural gas with coal. As the amount of sulfur in biomass and natural gas is much less than that in the coal, substitution of biomass for coal can result in significant reductions in SO<sub>2</sub> emissions. Co-firing coal with biomass has been successfully demonstrated in state of New York and Pennsylvania. A stoker boiler at The Hoover Company in North Canton, OH is one of examples for co-firing coal and natural gas. It will be interesting to measure PAHs on FGD by-products generated from co-firing power plant to compare the effects of the fuel source and boiler on the PAHs on the FGD by-products.

The study of sonolytic reactions of PAHs in organic solutions showed that PAH molecules could undergo pyrolysis and radical reactions with radicals generated from solvent pyrolysis. Since this study was carried out in a homogenous system, further investigations are needed to study the reactions of PAH in a heterogeneous system (i.e. with particles) to take the sorption and desorption of PAHs into account. In addition, different types of particles have different affinities with PAH molecules. In case of the presence of carbonaceous particles, the strong sorption of PAHs may lead to less reactions of PAHs during sonication. Therefore, it is worth testing the effects of different particles especially carbonaceous particles on sonolytic reactions of PAHs. The transformation of fluorene to phenanthrene was proposed to be a reason that leads to

higher phenanthrene recovery at longer sonication time. Sonication of fluorene should be conducted to test this hypothesis.

Distribution of PAHs on the LSD ash showed the enrichment of PAHs on carbonaceous materials. However, PAHs were also found in the lime-enriched fraction. Concern remains on the possible leaching of PAHs when the LSD ash is utilized or landfilled. The leaching characteristics of the PAHs on the unburned carbon and the lime-enriched fraction may be different. Therefore, leaching of PAHs from different fractions, particularly the long-term leaching should be examined.

The data set of operational effects on PAHs in the OSCAR process is limited due to the problems with the coal boiler. There is a need to systematically conduct more experiments to better understand operational effects on PAH capture onto solid by-products. For example, sorbent injection rates, flue gas flow rates and riser reactor temperature. It has been demonstrated that the supersorbent generated from lime was able to capture more PAHs. The research team in the Department of Chemical Engineering at The Ohio State University will test the supersorbent in the Shand power plant in Saskatchewan, Canada. The characterization of PAHs in the flue gas and on the solid by-products generated from that commercial power plant will be valuable to verify PAH capture efficiencies.

**APPENDIX A**  
**VARIABILITY OF INORGANIC AND ORGANIC CONSTITUENTS IN LIME**  
**SPRAY DRYER ASH**

**Panuwat Taerakul, Ping Sun, Harold Walker, Linda Weavers, Danold Golightly,**  
**and Tarunjit Butalia**

*Department of Civil and Environmental Engineering and Geodetic Science*

*The Ohio State University*

*470 Hitchcock Hall, 2070 Neil Avenue*

Columbus, OH 43210

(Submitted to: *Fuel* in August 2004)

## **A.1. Abstract**

Flue gas desulfurization (FGD) by-products, including lime spray dryer (LSD) ash, have many demonstrated uses. However, concern about the temporal variability in the chemical properties of this material has limited widespread utilization. To determine the variability in inorganic and representative model organic constituents, this study measured elemental composition, leaching properties, polycyclic aromatic hydrocarbon (PAH) concentrations, available lime index (ALI), calcium carbonate equivalent (CCE), and total neutralization potential (TNP) for a representative LSD ash. All parameters investigated showed little variability over different time periods (e.g., daily to yearly) and little variability between samples collected from different particle collection hoppers. Metal concentrations including As, Se and Hg in LSD ash and in the leachate did not surpass limits for land application (EPA 503 Rule) or limits for the determination of hazardous waste as specified in the Resource Conservative and Recovery Act (RCRA). While a number of PAHs were detected, including naphthalene and phenanthrene, the levels were low and in the range of natural soils. The low variability in ALI, CCE, TNP and inorganic and organic composition suggests that LSD ash is a consistent and environmentally benign material for agricultural and other engineering applications.

## **A.2. Introduction**

Flue gas desulfurization (FGD) by-product is a residual material generated from processes used to remove sulfur dioxide from flue gas following coal combustion. Approximately 26 million metric tons of FGD by-products are produced in the United

States every year (1-4), with more than 18 million metric tons (72% of total production) sent to landfills. To minimize landfilling, numerous studies have been conducted to examine beneficial uses of FGD by-product in a variety of applications including construction, agriculture and mine reclamation (5-10).

The lime spray dryer (LSD) system is the most common dry FGD technique used in utility coal fired power plants (1, 11). A fine spray of slaked lime ( $\text{Ca(OH)}_2$ ) is injected into the scrubber which reacts with sulfur oxides resulting in the formation of calcium sulfate or calcium sulfite. Moisture in the reacted lime is lost due to the heat from the flue gas. The resulting dry calcium sulfite/sulfate mixture, along with fly ash, is collected as “LSD ash” by an electrostatic precipitator or a baghouse (1, 11). A number of researchers have studied the re-use of by-product produced from dry FGD systems, including LSD systems, and associated environmental impacts (5-10, 12). The United States Environmental Protection Agency (USEPA) recommends that LSD ash be exempt from physical and chemical tests for hazardous material if used in a few specific applications. Concern remains, however, regarding the agricultural use of these materials due to the presence of inorganic trace elements as well as hazardous organic compounds such as polycyclic aromatic hydrocarbons (PAHs) (1).

An additional issue limiting the re-use of LSD ash, as well as other coal combustion by-products, is the perceived temporal variability of this material. A number of factors may influence the chemical composition of LSD ash over time including chemical compositions of lime and coal, and changes in plant operations. Abrupt changes in levels of trace inorganic and organic compounds are not detected by periodic monitoring and potentially could result in leachate values above regulatory levels, thus

affecting human health. Long-term changes in bulk properties (e.g., available lime index) discourage utilization due to the added investment required for effective use. Despite the concern over the variability of FGD by-product, little or no long-term data is available to evaluate this issue.

This study characterized Hg, As, Se, other inorganic elements, as well as selected PAHs in LSD ash from the McCracken Power Plant at The Ohio State University in Columbus, Ohio. Elemental composition and leaching measurements of Hg, As, and Se in LSD ash were conducted along with tests of lime availability, calcium carbonate equivalence, and total neutralization potential. Samples were collected over daily, weekly, and monthly time intervals to characterize different scales of variability. Inorganic data were compared with measurements from a previous study at McCracken Power Plant conducted in 1991-1992 to explore long-term variability.

### **A.3. Experimental**

#### ***Sample collection***

LSD ash was obtained from the McCracken Power Plant located on the main campus of The Ohio State University. The power plant uses bituminous coal as a fuel source in a single spreader-stoker boiler (boiler #8). A unit operation diagram of the McCracken Power Plant is shown in Figure 1. The McCracken Power Plant has a LSD system for removing sulfur dioxide from the flue gas. Particulates, including fly ash and calcium-rich residue from the LSD process, are collected by woven fiberglass filter bags in a pulse jet baghouse. The baghouse contains 6 hoppers for collection of particulate

material. A small amount of solids is collected from the economizer, combined with material from the baghouse, and stored in the ash silo.

LSD ash, coal, and lime (unslaked) samples were collected on a daily, weekly, and monthly basis from May 2001 to February 2002. LSD ash was collected in hoppers F and A in the fabric filter baghouse. Lime samples were taken from the falling stream of a transfer belt just prior to slaking. Coal samples were obtained from the release point of the feed belt into the combustion chamber. LSD ash, coal and lime were transferred into clean (EPA procedures), cylindrical high-density polyethylene (HDPE) sample containers, approximately 75% full for storage prior to inorganic analysis. Certified clean 950 mL brown glass bottles (cleaned by EPA procedures) were used to store samples for organic analysis. All samples subsequently were stored in an environmental room (4 to 12 °C) until the appropriate chemical measurement procedures were performed.

Both coal and lime samples required initial comminution to obtain particle sizes small enough for subsequent analyses. Samples were effectively homogenized by tumbling (13). Subsamples for analyses were isolated by a 24-chute stainless steel riffle.

### ***LSD ash characterization***

Mineralogical analysis of LSD ash samples was accomplished using a Philips X-Ray Diffraction (XRD) instrument (Philips Analytical, Natick, MA) with  $\text{CuK}\alpha$  radiation at 35kV and 20mA. The XRD step-scanned measurements were carried out from 3 to  $60^\circ 2\theta$  with a fixed time of 3 second per  $0.05^\circ 2\theta$ . Data were analyzed by semi-quantitative data reduction software (WinJade, version 2.0). Prior to XRD analysis, samples were dried in an oven at  $60^\circ\text{C}$  for 24 hrs.

Scanning electron microscopic (SEM) images were taken using a Philips XL-30 ESEM. Samples for SEM analysis were prepared by ejecting approximately 50 mg of sample through a straw onto an ultra pure aluminum SEM stub using portable ultra clean compressed air. Double-sided high purity carbon tape was applied to the SEM stub to allow the powdered sample to attach on the surface. Samples were then gold-coated and kept in a desiccator until analysis.

Bulk chemical characteristics relevant to agricultural applications determined by titration (ASTM C 25-96a), included available lime index (ALI) and calcium carbonate equivalence (CCE). Total neutralization potential (TNP) was measured by ASTM method C1318-95.

### ***Inorganic analysis***

Complete elemental analyses for LSD ash and lime were accomplished by digesting approximately a 300 mg sample by microwave heating with a combination of 10-mL deionized water, 6-mL nitric acid, 2-mL hydrochloric acid, and 2-mL hydrofluoric acid. This was followed by a second microwave heating with 20-mL boric acid (EPA method 3052) and dilution with high-purity water to 100 mL. Coal fly ash, 1633b, provided by the National Institute of Standards and Technology (NIST) was digested along with LSD ash samples for method validation. Recovery percentages between 80%-140% were obtained for every reported inorganic element. Leachate analyses were conducted by using the toxicity characteristic leaching procedure (TCLP) test (EPA method 1311).

A Vista Pro simultaneous inductively coupled plasma optical emission spectrometer (ICP-OES) system (Varian, Walnut Creek, CA) was used to determine Ag, Al, B (only leaching tests), Ba, Ca, Cd, Cr, Cu, Fe, Mg, Mn, Mo, Na, P, Pb, S, Si, Sr, and Zn in sample solutions (EPA method 6010B). As and Se were determined by a SpectrAA 880Z Zeeman graphite furnace atomic absorption (AA) spectrometer (Varian, Walnut Creek, CA), and Hg was determined by AA with a vapor generation accessory (EPA method 7060A, EPA method 7740 and EPA method 7470A). Anions were measured by a DX-500 ion chromatography system (Dionex, Sunnyvale, CA) (EPA method 300.0). All analyses included controls (duplicate, blank, and check standards) for every fifteen samples or less.

### ***Organic analysis***

For organic analysis, 10 g of each collected ash sample was extracted in a Tecator Soxtec (Model 1043) extractor (Foss, Eden Prairie, MN) with  $\text{CH}_2\text{Cl}_2$  for 5 hours. The solution from the extraction process subsequently was condensed to 1 mL prior to gas chromatography mass spectrometry (GC/MS) analysis. EPA method 8270C provided the basis for measurement of PAHs and other semi-volatile organic compounds. Quantitative analysis of PAHs was accomplished with an ion trap mass spectrometer (Thermo-Finnigan, Waltham, MA). A CP-5 fused silica capillary column ( $30\text{ m} \times 250\ \mu\text{m} \times 0.25\ \mu\text{m}$ ) (Varian, Walnut Creek, CA) was used to separate PAHs. Helium was used as the carrier gas with a flow rate of  $1.2\ \text{mL min}^{-1}$ . Splitless injections of  $2\ \mu\text{L}$  extract spiked with the deuterated internal standard were made at an injector temperature and ion source temperature of  $250\ ^\circ\text{C}$ . The column was held at  $60\ ^\circ\text{C}$  for 2 min, programmed to  $250\ ^\circ\text{C}$  at

20 °C min<sup>-1</sup> followed by a 2 min hold time, increased to 300 °C at 10 °C min<sup>-1</sup>, then held for 8 min. The temperature of the mass transfer line was 300 °C. The mass spectrometer was operated in full scan mode for both standards and extracts. PAHs and other semi-volatile compounds were identified by matching mass spectra to a NIST spectra database. Sixteen EPA-specified PAHs were confirmed using the retention times and quantified by running standard PAH compounds (Ultra scientific, North Kingstown, RI). The detection limits for these 16 PAHs ranged from 0.1 to 1 µg/kg; the large ring PAHs had higher detection limits compared to small ring PAHs.

### ***Coal sample analysis***

Coal samples were sent to commercial laboratories for elemental analyses. Proton Induced X-ray Emission or “PIXE” provided concentrations of Ag, Al, As, B, Ca, Cr, Mg, Pb, S, Se, Si, and Sr. Hg was determined by cold vapor atomic fluorescence spectrometry (CV-AFS) following acid digestion by microwave heating. CV-AFS was performed by an outside certified laboratory.

## **A.4. Results and Discussion**

### ***Variability in Inorganic Composition of LSD Ash***

XRD, SEM, and inorganic elemental analyses indicated that the LSD ash was generally a mixture of hannebachite, fly ash, unreacted lime (i.e. portlandite), and other minor constituents. In XRD patterns (Figure 2) from samples collected from May 17, 2001 to February 26, 2002, portlandite (Ca(OH)<sub>2</sub>) and hannebachite (CaSO<sub>3</sub>·0.5H<sub>2</sub>O)

were the only two major minerals found. These results also agreed with mineralogy results found in samples collected in 1991 (12). From SEM images shown in Figure 3, there were flake-like crystals, identified as hannebachite, forming over bulk solid spherical fly ash particles. In addition, there were needle-like crystals distributed over sheet-like particles which suggests the formation of ettringite ( $\text{Ca}_6\text{Al}_2(\text{SO}_4)_3(\text{OH})_{12}\cdot 26(\text{H}_2\text{O})$ ) on top of the hannebachite surface (14). Ettringite, however, was not observed by X-Ray diffraction due to the low mass fraction of ettringite compared to hannebachite and portlandite. Although a small peak of calcite ( $\text{CaCO}_3$ ) was observed for a sample collected on June 14, 2001, in general, X-Ray diffraction pattern results indicated little or no difference among the weekly and monthly samples from May 17, 2001 to February 26, 2002. Major element concentrations in LSD ash were consistent with XRD and SEM results indicating that the majority of material was present as hannebachite, portlandite, and fly ash.

To examine the temporal variability in the inorganic elemental composition of LSD ash, samples were collected over a period of 10 months. The inorganic elemental compositions of LSD ash from Hoppers F and A during 2001-2002, and from a previous study (1991-1992) are shown in Table 1. The relative standard deviation (RSD) for each element was used as a measurement of the variability. The RSD of an element  $i$  in Table 1 was calculated as

$$RSD_i = \frac{SD_i}{AVE_i} \quad (1)$$

where  $AVE_i$  is the average concentration of element  $i$  and  $SD_i$  is the standard deviation of element  $i$ . Generally, RSDs in the elemental composition of LSD ash during 2001-2002

were small (<23%) except for As, P and Pb which had RSDs of 30%, 44% and 203%, respectively (in Hopper F). During the period 1991-1992, RSDs for inorganic elements were generally larger (~ 20-50%) than those for the 2001-2002 interval. Considered in total, however, relatively little variability in the inorganic composition was observed for this material over the 11-year period.

#### *Sources of Temporal Variability in Inorganic Composition*

Assuming plant operating conditions were constant, one hypothesis that may explain the low variability in inorganic composition of LSD ash is that the variability in lime and coal properties was low over the period of study. To verify this hypothesis, the elemental composition of feed lime and coal were examined, and the results are shown in Table 1. The impact of coal and lime variability on the inorganic composition of LSD ash was assessed by comparing the RSDs in elemental composition of the feed lime and coal to the RSDs of LSD ash using propagation error analysis. In order to perform this analysis, the following assumptions were made: 1) Inorganic constituents in LSD ash originated from the feed lime and feed coal. 2) The coal to lime feed rate was consistently at 12:1. 3) The contribution of Ca on LSD ash from coal was insignificant compared to the contribution from lime. 4) Inorganic components originating from the feed lime were completely captured in the baghouse. 5) Losses of inorganic elements from feed coal (i.e., mass not accounted for in the baghouse) occurred through removal in the economizer or loss out the stack due to volatility of certain inorganic constituents. Based on assumptions 1, 4 and 5, an equation of the elemental concentrations in LSD ash as a function of the concentrations in feed lime and coal constituents can be written as,

$$C_{i,LSD} = C_{i,lim e} f_{lim e} + C_{i,coal} f'_{i,coal} \quad (2)$$

where  $C_{i,LSD}$  is concentration of element  $i$  in LSD ash,  $C_{i,lim e}$  is concentration of element  $i$  in lime, and  $C_{i,coal}$  is concentration of element  $i$  in coal.  $f_{lim e}$  is the fractional mass of feed lime per unit mass of LSD ash production, and  $f'_{i,coal}$  is the fractional mass of element  $i$  contributed from the feed coal per unit mass of LSD ash production in the baghouse. It should be noted that  $f'_{i,coal}$  is expected to vary with each element due to differences in losses of each element in the economizer and out the stack.  $f_{lim e}$ , on the other hand, remains constant since the major components of lime are non-volatile and lime is added after the economizer. The values of  $C_{i,LSD}$ ,  $C_{i,lim e}$  and  $C_{i,coal}$  were determined by elemental analysis of collected LSD ash, lime and coal samples. Based on the amount of each element retained in the baghouse hoppers,  $f_{lim e}$  and  $f'_{i,coal}$  were determined. From assumptions 3 and 4, and looking at Table 1,  $C_{Ca,coal}$  was assumed to be negligible. Then, using the concentration of Ca in LSD ash and lime,  $f_{lim e}$  was calculated as 0.47. To validate the previous assumption, the amount of Ca predicted to be in the LSD ash, including the contribution from the feed coal (assumption 2) was calculated as 33.14% ( $0.47 \times 69.3\% + 0.47 \times 12 \times 0.1\% = 33.14\%$ ). Thus, including the contribution of Ca from the feed coal showed only a 2% difference compared to the measured Ca in LSD ash (32.43%) indicating a reasonable value of  $f_{lim e}$ .

For elements contributed primarily from the coal, some may be lost at the economizer or through the stack (assumption 5). Therefore,  $f'_{i,coal}$  will be different for each element. By using equation 2, and assuming  $f_{lim e}$  is constant at 0.47,  $f'_{i,coal}$  for each

element was calculated. With values from  $f_{\text{lime}}$  and  $f'_{\text{i,coal}}$ , the RSDs of inorganic elements in LSD ash were estimated using

$$RSD_{i,LSD} = \sqrt{(f_{\text{lime}})^2 RSD_{i,\text{lime}}^2 + (f'_{\text{i,coal}})^2 RSD_{i,\text{coal}}^2} \quad (3)$$

$RSD_{i,\text{lime}}$  and  $RSD_{i,\text{coal}}$  were calculated from the inorganic results of composite samples of lime and coal. The estimated RSDs for all inorganic elements in LSD ash over the 10-month period were calculated by equation 3 and are summarized in Table 1.

The results show that the RSDs estimated by propagation error analysis were similar to the measured RSDs for most major elements (S, Si, Fe, Al, K and Mg), which suggests that the variability of these major elements in feed material was largely responsible for the variation in LSD ash. However, the estimated RSD of Ca (1%), which is mainly contributed from lime, was smaller than the measured RSD (6%), which indicates that other factors besides Ca variability in lime might have affected the Ca variability in LSD ash. One source of Ca variability is from changes in plant operating conditions such as the lime feed rate. Because the magnitude of the variability potentially arising from changes in Ca feed rates is low (6%), it likely represents only a small fraction of the variability in the other inorganic elements. Results of estimated RSDs of major inorganic elements in Hopper A showed similar trends to Hopper F.

For the trace elements, Sr and Cu, measured RSDs and estimated RSDs were similar with differences within a factor of three. For P, Mn, Ni and As, greater differences were found. For As, variability in the capture efficiency of volatile As species may provide an additional source of variability. In addition, errors from measurements of

elements at near detection limits by different approaches (i.e., ICP-OES and PIXE or AA and PIXE) may also introduce differences in RSDs for these trace elements.

### ***Variability of Inorganic Composition in Different Collection Hoppers***

The McCracken facility utilizes two parallel flue gas channels, with each channel supplying three hoppers in sequence for the collection of solids from the bag house. Because light and small particles may tend to fly higher and travel farther, this leads to preferential removal of small particles in the downstream hoppers, which may influence the elemental compositions of LSD ash from different hoppers. To examine this possibility, samples were collected from two different hoppers. Hopper F is the third collection hopper from one channel, while Hopper A is the first one in sequence of the other channel. From the results in Table 1, differences between mean concentrations of samples in Hopper F and A during year 2001-2002 were small (15%) for most elements, and within a range of a factor of two for all elements. Ca, S, Mg, Se, Cu, Sr, As, P, and Hg were larger in Hopper F, while Al, K, Fe, Si, Mn, Be, Li, and Co were found larger in Hopper A. Our results suggest that Ca-containing solids (e.g., hannebachite, portlandite, and ettringite) made up a greater fraction of LSD ash from Hopper F, and the major constituents of fly ash were greater in Hopper A. However, the differences between them were within 15%, which is comparable to the variability over time.

### ***Variability in Inorganic Composition over Different Time Scales***

Variability (as RSD) in the elemental composition of LSD ash also was examined over different time scales. RSDs of elements in LSD ash for samples collected over daily, weekly, monthly and yearly intervals are shown in Figure 4. Elements on the x-axis were arranged from the lowest value to the highest value of RSD based on the yearly data.

Results suggest that RSDs over the yearly time scale were the largest for most elements. There was little change in RSDs among daily, weekly, and monthly sampling periods except the RSD of Pb on the daily period that was higher than on the yearly period. These results indicate that the lowest variability of elements is observed over time scales of a year or less, while longer time periods introduces slightly greater variability.

### ***Inorganic Composition in Relation to Regulatory Limits***

Figure 5 shows the concentrations of Hg, As, and Se in LSD ash samples from January 1991 to February 2002 in comparison with regulatory limits. Hg data were only available from May 2001. The 99% confidence t-test intervals for these three elements were calculated to determine the variations of the mean concentrations to compare with limits for the land application of sewage sludge or EPA 503 Rules (15). The EPA 503 Rules regulates an acceptable level of inorganic elements that are potentially hazardous in soil. Although LSD ash is not listed as a material regulated in EPA 503 Rule, this rule is appropriate for comparing with the level of inorganic elements in LSD ash to determine potential risk when used in a land application. For Hg, the upper bound of the 99% confidence t-test interval was 0.47 mg/kg, which is greatly below the limit of 57 mg/kg for the EPA 503 Rules. The upper bounds of the 99% confidence t-test interval of As and Se were 39.7 and 30.6 mg/kg which were below the limit at 75 and 100 mg/kg, respectively. In addition, concentrations of As and Se in all samples collected during this 11-year period did not violate the EPA 503 Rules. Due to their significance, only Hg, As, and Se were reported in Figure 5. However, the 99% confidence t-test interval for other elements, Cr, Cu, Pb, Mo, and Ni, also were well below the EPA 503 limits.

## ***Variability in Leaching of Inorganic Elements and Bulk Chemical Properties of LSD Ash***

To examine whether significant variability occurs in the leaching properties of LSD ash, TCLP tests were carried out on all samples. Variability in ALI, CCE, and TNP also were determined. Mean concentrations and RSDs of elements from the leachates (TCLP test) of the samples collected in 2001-2002 and in 1991 are shown in Table 2. RSDs for concentrations of elements from the leachates shown in Table 2 were found to be larger than those observed in the elemental composition data. However, variations in elements were similar for ash collected from Hopper F and A, within a factor of two, except for Si. Comparing the data in 1991 to the 2001-2002 data, concentrations of elements in leachates were similar. Variations were within a factor of two except for Na, Mo, Li, Pb, Zn, Se, Al, Fe, Cu, Cr and Cd. Changes of concentrations of these latter elements were within an order of magnitude, unless they were under the method detection limit. Most concentrations, except that for Al, in leachate of LSD ash collected in 1991 were similar or lower than the results in 2001-2002. To examine temporal variability of elements in leachate from LSD ash, RSDs were examined over different time scales. RSDs of elements in leachate over daily, weekly, monthly and yearly periods are presented in Figure 6. Results indicate that RSDs were highest over yearly periods. RSDs over monthly periods were slightly lower than yearly periods but higher than over daily and weekly periods. There was little difference in RSDs between daily and weekly periods. These results suggest that the variability of elements in leachates increased with increasing sampling period. These results are consistent with the data on the temporal variability of inorganic composition of this material.

Data from leaching analyses were compared with RCRA limits. Variability in As and Se concentrations are shown in Figure 7. 99% confidence t-tests indicated that As and Se mean concentrations were under 2.7 and 13.4  $\mu\text{g/L}$ , and therefore, did not exceed the RCRA limits for As and Se at 5000 and 1000  $\mu\text{g/L}$ , respectively. The 99% confidence intervals of other regulated elements such as Ag, Ba, Cd, Cr, and Pb also did not exceed the RCRA limit. These data indicated that the concentration of contaminants in leachate produced over this 11-year time period were consistently lower than RCRA limits, thus supporting the characterization of LSD ash as a consistently non-hazardous material.

From Table 3, RSDs of ALI, CCE, and TNP in 2001-2002 were relatively small especially for CCE. For the results of samples collected over 10 months, the variations as RSDs of ALI, CCE, and TNP in hopper F were calculated as 22%, 6% and 16%, respectively. Compared with data in 1991, ALI decreased from 20.0 to 14.1 % as  $\text{CaCO}_3$  in 2001-2002. This smaller value of ALI indicates better efficiency of the spray dryer process to capture  $\text{SO}_2$  while minimizing the unreacted free lime in the by-product. There was only a small change in CCE from 66.2 to 65.4 % as  $\text{CaCO}_3$  in 2001-2002. The data above indicate that the LSD ash would perform in a consistent fashion as a substitute for lime and is suitable for land application over a range of time scales from daily to yearly, without significant alteration of agriculture loading rates.

#### ***Variability in Trace Organic Composition of LSD Ash***

PAH concentrations in LSD ash collected on a daily basis are shown in Table 4. By automatic Soxhlet extraction, the PAHs identified on LSD ash samples were mainly 2-ring and 3-ring PAHs, such as naphthalene, and phenanthrene. No PAHs larger than

phenanthrene were measured. The types of PAH compounds on LSD ash samples differed from sample to sample. For example, no phenanthrene was found on the ash samples collected on 05/16/2001, while the ash samples collected on other dates consistently had detectable levels of phenanthrene. However, the concentrations of these PAHs were consistently low, usually a few  $\mu\text{g}/\text{kg}$  or less. Other organic compounds, such as methylated PAHs (e.g., methylnaphthalene), biphenyl and a series of n-alkanes also may exist in the LSD ashes, based on matching spectra with the NIST mass spectra library. However, standards are needed to conclusively verify their existence.

Table 5 shows the concentration of detected PAHs on the weekly LSD ash from hopper F and hopper A. The results indicate that PAH concentrations on these samples were also at  $\mu\text{g}/\text{kg}$  levels, although the PAH speciation in the samples varied. In addition, the results in Table 5 demonstrate that the PAH concentrations in LSD samples collected from different hoppers were similar. It has also been shown in Table 5 that although LSD ash samples collected in year 2002 and 2003 had slightly higher PAH concentrations, the concentrations were still at  $\mu\text{g}/\text{kg}$  levels.

The correlation between the total PAH concentration measured and the organic carbon content is shown in Figure 7. A linear correlation ( $R^2 = 0.86$ ) suggests that the PAHs are mainly associated with carbonaceous material (i.e., unburned carbon) in the LSD ash. By studying harbor sediments, Ghosh et al. found the majority of PAHs were associated with coal-derived particles and the PAHs were strongly adsorbed to these particles based on direct analysis of separated fractions and particle-scale (16). Therefore, PAHs may be primarily associated with the carbonaceous materials in the LSD ash.

However, separation of unburned carbon from LSD ash and direct PAH measurement on the separated unburned carbon fraction is needed to verify this hypothesis.

Compared to PAH concentrations in other matrices, PAH concentrations in LSD ash collected in our study were low. The Massachusetts Department of Environmental Protection published a technical report on background levels of PAHs in soil. The PAH concentration in natural soil ranged from 0.5~4 mg/kg, which is 2~3 orders of magnitude higher than the PAH concentrations in collected LSD ash (17). The contaminant cleanup target levels issued by Florida Department Environmental Protection (FDEP) states that the target PAH cleanup level for brownfields is usually at mg/kg level (18). However, due to the different matrices, bioavailability experiments need to be performed to verify if the low levels of PAHs in LSD ash would not pose a threat to the environment.

The composition of the measured PAHs in LSD ash is related to the combustion conditions in the McCracken Power Plant. Generally, two major mechanisms result in PAH formation during coal combustion. One is pyrolysis, and the other is pyrosynthesis (19, 20). During pyrolysis, the macromolecular aromatic compounds are broken into different size fragments, and these fragments then decompose and form small organic compounds. In the process of pyrosynthesis, these fragments undergo chemical and physical reactions to form polycyclic compounds. With increased combustion temperatures, intermolecular cyclization among the fragments produced during pyrolysis is expected to be more important. However, high temperature also will produce more energy to break the bonds in large molecular weight PAHs. Therefore, these two mechanisms will compete when the combustion temperature is increased. Besides

combustion temperature, excess air during combustion also has been shown to affect PAH formation (21).

At the McCracken Power Plant, coal is burned at approximately 650 °C, and an air pump is used to provide excess air for combustion. At this combustion temperature, the bonds of macromolecular PAHs in raw coal may be only partially broken by pyrolysis and form smaller size fragments. Intermolecular cyclization among these small size fragments may be less predominant compared to pyrolysis because of the low temperature. As a result, formation of small ring PAHs by pyrolysis may be preferred. With the excess air, the formed PAHs may further undergo oxidation reactions and produce more carbon dioxide and water in the flue gas. Therefore, the low combustion temperature and excess air may be the reason that small ring PAHs with low concentration were identified in LSD ash samples.

Another possible reason that large molecular weight PAHs were not detected may be due to their higher affinities to the solid phase. These compounds strongly adsorb on LSD ash samples and may not be easily extracted (22, 23), especially at low concentration. Thus, the existence of large ring PAHs on LSD ash is still possible. Continued researches on other extraction methods, such as ultrasonic extraction are ongoing to examine the potential presence of large ring PAHs in LSD ash.

## **A.5. Conclusions**

In this study, low variability in elemental composition of LSD ash was observed over an 11-year time period. The small variability observed was shown to be due largely to the variability in the chemical properties of coal and lime. Changes in plant operating

conditions may also have contributed to the variability, at least for Ca. Although larger variability in elemental composition and leachates was observed over longer time scales, results of trace element analyses (e.g. Hg, As, Se) in LSD ash and in the leachates observed over the 11-year period did not violate regulatory limits. ALI, CCE and TNP results also indicated long-term stability in bulk properties of this material indicating a reliable material for utilization.

This study also showed several small molecular weight (2 ~ 4-ring) PAH compounds on LSD ash, including naphthalene, acenaphthene, acenaphthylene, and phenanthrene. The type of PAH compounds was not the same on different LSD ash samples, however, the concentrations of these PAHs were consistently low, usually a few  $\mu\text{g kg}^{-1}$  or less, which is much lower than background levels in soils and contaminant cleanup target levels issued by FDEP.

Results in this study suggest that LSD ash produced from a typical lime spray dryer process can be beneficially re-used in an environmentally sound manner.

## **Acknowledgments**

This project was supported by the Ohio State Carbon Ash Reactivation (OSCAR) Demonstration Project with funding from the Ohio Coal Development Office (OCDO) and The Ohio State University. The authors thank the staff at the McCracken Power Plant for their assistance during the sampling phase of this research. We also thank C. M. Cheng for his contributions with X-Ray Diffraction experiments.

## References

1. U.S. Environmental Protection Agency. Wastes from the Combustion of Fossil Fuels, Volume 1 and 2- Methods, Findings, and Recommendations, Report to Congress, EPA 530-S-99-010, March 1999.
2. Kalyoncu RS. Coal combustion products, U.S. Geological Survey Minerals Yearbook-1999, U.S. Geological Survey, Reston, VA.,1999.
3. Kelly TD, Kalyoncu RS, Coal Combustion Products Statistics; USGS Open-File Report 01-006; May 21, 2002.
4. U.S. Geological Survey, 1997-2002, Minerals YearBook: Vol I Metals and Mineral, 1996-2001.
5. Walker H, Taerakul P, Butalia T, Wolfe W, Dick W. Minimization and Use of Coal Combustion By-Products: Concepts and Applications. In: Ghassemi A. editors. The Handbook of Pollution Control and Waste Minimization, New York: Marcel Dekker, 2002.
6. Butalia T, Dyer P, Stowell R, Wolfe W. Construction of Livestock Feeding and Hay Bale Storage Pads Using FGD Material, The Ohio State Extension Fact Sheet, AEX-332-99, Columbus, Ohio: The Ohio State University, 1999.
7. Butalia T, Wolfe W. Re-Use of Clean Coal Technology By-Products in the Construction of Impervious Liners. 1997 Ash Utilization Symposium, Lexington, Kentucky, 1997.
8. Lamminen M, Wood J, Walker H, Chin Y.-P, He Y, Traina S. J Env Quality 2001; 30:1371-1381.
9. Butalia T, Wolfe W, Lee J. Fuel 2001; 80:845-850.

10. Clark R, Ritchey K, Baligar VC. *Fuel* 2001; 80:821-828.
11. U.S. Environmental Protection Agency. *Wastes from the Combustion of Coal by Electric Utility Power Plants*, Report to Congress, EPA 530-SW-88-002, February, 1988.
12. Stehouwer R, Dick W, Bigham J, Forster L, Hitzhusen F, McCoy E, Traina S, Wolfe W. *Land Application Uses of Dry FGD By-Products: Phase 2 Report*. Electric Power Research Institute, Report # EPRI TR-109652. Electric Power Research Institute, Palo Alto, California, 1998.
13. Pitard FF. *Pierre Gy's Sampling Theory and Sampling Practice, Heterogeneity, Sampling Correctness, and Statistical Process Control*, 2<sup>nd</sup> Edition, CRC Press, Boca Raton, FL, 1993.
14. Stutzman PE. *Calcium Hydroxide in Concrete (Workshop on the Role of Calcium Hydroxide in Concrete)*. Proc. J. Skalny, J. Gebauer and I. Odler, (ed.), The American Ceramic Society. November 1-3, 2000, Anna Maria Island, Florida, 59-72 pp, 2001.
15. U.S. Environmental Protection Agency. *Standards for the use of or disposal of sewage sludge: Final rule*. Fed. Reg. 58:032, 1993.
16. Ghosh U, Talley JW, Luthy RG. *Environ. Sci. Technol.* 2001; 35: 3468-3475.
17. U.S. Massachusetts Department of Environmental Protection. *Technical Update: Background Levels of Polycyclic Aromatic Hydrocarbons and Metals in Soil*, May, 2002.
18. U.S. Florida Department of Environmental Protection. *Contaminant Cleanup Target Levels*, Chapter 62-777, 1999.

19. Ledesma E, Kalish M, Wornat M, Nelson P, Mackie J. *Energy & Fuels* 1999; 13:1167-1172.
20. Zhao Z-B, Liu K-L, Xie W, Pan W-P, Riley J, *Journal of Hazardous Materials* 2000; B73: 77-85.
21. Mastral A, Callen M, Mayoral C, Galban J. *Fuel* 1995; 74:1762-1766.
22. Fischer R, Kreuzig R, Bahadir M, *Chemospher* 1994; 29:311-317.
23. Jonker M, Koelmans A, *Env Sci Technol* 2002; 36:4107-4113.

Lime Spray Dryer Ash													
		Hopper F (2001- 2002) n=15			Hopper A (2001) n=5			1991-1992 n=5					
		AVE	RSD	PROP ERR RSD	AVE	RSD	PROP ERR RSD	AVE	RSD	AVE	RSD	AVE	RSD
<b>Ca</b>	%	32.45	6%	1%	34.3	6%	1%	31.4	12%	69.3	1%	0.1	20%
<b>S</b>	%	12.46	9%	8%	13.0	4%	8%	8.4	27%	0.038	11%	2.3	8%
<b>Si</b>	%	3.44	17%	11%	3.0	14%	11%	2.9	27%	0.45	7%	0.78	12%
<b>Fe</b>	%	2.51	17%	13%	1.8	11%	13%	2.8	37%	0.202	4%	1.1	13%
<b>Al</b>	%	1.32	10%	11%	1.1	14%	11%	1.9	28%	0.122	7%	0.64	12%
<b>K</b>	%	0.38	16%	15%	0.37	11%	15%	0.23	29%	0.02	4%	0.04	15%
<b>Mg</b>	%	0.35	8%	10%	0.36	3%	10%	0.92	8%	0.9	8%	0.009	6%
<b>Sr</b>	mg/kg	327.7	17%	19%	334.2	9%	19%	253.2	3%	312	4%	46.3	35%
<b>P</b>	mg/kg	190.3	44%	6%	237.2	33%	6%	86.6	46%	51.8	15%	31.6	7%
<b>Mn</b>	mg/kg	154.6	13%	25%	150.2	4%	23%	48.4	24%	217	2%	6.9	75%
<b>Ni</b>	mg/kg	42.5	12%	20%	38.6	11%	20%	23.1	36%	11.5	7%	13.0	23%
<b>Cu</b>	mg/kg	38.6	16%	18%	40.7	7%	19%	19.0	24%	14.4	9%	6.0	23%
<b>As</b>	mg/kg	37.6	30%	73%	39.0	22%	74%	36.7	22%	0.4	15%	6.5	75%
<b>Se</b>	mg/kg	28.6	23%	N/A	34.7	8%	NA	10.9	46%	UDL		1.6	13%
<b>Li</b>	mg/kg	22.1	20%	N/A	20.2	18%	NA	23.1	23%	1.6	3%	NA	
<b>Cr</b>	mg/kg	20.9	9%	N/A	18.6	10%	NA	16.5	38%	UDL		11.6	35%
<b>Mo</b>	mg/kg	13.0	18%	N/A	12.5	6%	NA	7.9	29%	UDL		UDL	
<b>Pb</b>	mg/kg	5.9	203%	N/A		UDL		19.4	43%	UDL		21.0	57%
<b>Hg</b>	µg/kg	429	13%	N/A	441	14%	NA	NA		UDL		199	17%

Table A.1. Elemental Composition of Lime Spray Dryer Ash, Quick Lime, and Coal Collected from McCracken Power Plant UDL – Under detection limit, N/A - No data available.

		2001-2002					
		Hopper F N=14		Hopper A n=5			
		Ave	RSD	Ave	RSD		
Ca	mg/L	3557	7%	3552	3%	3224	
S	mg/L	364	19%	407	5%	206	
Na	mg/L	22.9	16%	23.9	11%	3.6	
K	mg/L	17.0	10%	19.9	6%	22.1	
B	mg/L	3.6	22%	3.8	7%	4.7	
Sr	mg/L	2.3	10%	2.6	8%	N/A	
Mo	µg/L	325	19%	383	6%	88	
Li	µg/L	244	11%	286	6%	90	
Ba	µg/L	225	39%	177	21%	348	100000
Si	µg/L	138	47%	61.1	74%	140	
P	µg/L	83.5	48%	79.0	10%	<120	
Pb	µg/L	53.5	17%	61.1	10%	17	5000
Mg	µg/L	35.1	30%	37.0	8%	50	
Zn	µg/L	15.7	27%	14.3	13%	<6	
Se	µg/L	11.3	34%	13.6	30%	4	1000
Ag	µg/L	8.8	6%	8.9	6%	<24	5000
Al	µg/L	6.5	17%	7.2	25%	200	
Ni	µg/L	5.9	164%	2.5	40%	<10	
Fe	µg/L	4.9	26%	6.3	34%	<29	
Cu	µg/L	3.4	20%	3.7	7%	<13	
As	µg/L	2.3	35%	1.5	39%	<5	5000
Cr	µg/L	1.8	36%	2.3	12%	9	5000
Be	µg/L	1.0	0%	0.9	25%	<2	
Mn	µg/L	0.2	190%	0.6	70%	<1	
Cd	µg/L	<1		<1		<3	1000
Hg	µg/L	<0.2		<0.2		<0.2	200
Cl <sup>-</sup>	mg/L	41.3	21%	40.9	6%	45.5	
SO <sub>4</sub> <sup>2-</sup>	mg/L	1004	22%	1130	4%	460	

Table A.2. Results of TCLP test of LSD ash from McCracken Power Plant  
N/A – No data available.

<b>2001-2002</b>					
<b>Hopper F</b>					
<b>N=14</b>					
		<b>Ave</b>	<b>RSD</b>	<b>Ave</b>	<b>RSD</b>
<b>ALI</b>	% as CaCO <sub>3</sub>	14.1	22%	20.0	28%
<b>CCE</b>	% as CaCO <sub>3</sub>	65.4	6%	66.2	3%
<b>TNP</b>	% as CaCO <sub>3</sub>	17.1	16%	N/A	

Table A.3. Results of ALI, CCE and TNP of LSD ash from McCracken Power Plant  
N/A – No data available.

	Detected PAHs			
	Naphthalene	Acenaphthene	Acenaphthylene	Phenanthrene
5/14/2001	2.3 ± 0.1	UDL	UDL	0.6 ± 0.4
5/15/2001	2.5 ± 0.2	UDL	UDL	0.4 ± 0.3
5/16/2001	1.5 ± 0.1	UDL	UDL	UDL
5/17/2001	2.9 ± 0.2	UDL	0.6 ± 0.1	0.4 ± 0.3
5/18/2001	5.9 ± 0.2	UDL	UDL	0.7 ± 0.5
5/19/2001	2.1 ± 0.1	1.0 ± 0.1	0.8 ± 0.1	0.3 ± 0.2
5/20/2001	2.4 ± 0.1	0.7 ± 0.1	0.5 ± 0.1	0.4 ± 0.3

Table A. 4 Daily PAH Concentrations ( $\mu\text{g}/\text{kg}$ ) of Lime Spray Dryer Ash Collected from McCracken Power Plant Hopper F  
UDL – Under detection limit

	Detected PAHs			
	Naphthalene	Acenaphthene	Acenaphthylene	Phenanthrene
<b>5/17/2001hopper F</b>	2.9 ± 0.2	UDL	0.6 ± 0.0	0.4 ± 0.3
<b>5/24/2001hopper F</b>	1.3 ± 0.1	0.4 ± 0.0	0.5 ± 0.0	0.3 ± 0.1
<b>5/24/2001hopper A</b>	2.0 ± 0.1	0.4 ± 0.1	0.4 ± 0.0	0.3 ± 0.1
<b>5/31/2001hopper F</b>	1.4 ± 0.1	UDL	0.4 ± 0.0	0.3 ± 0.1
<b>5/31/2001hopper A</b>	3.0 ± 0.1	0.4 ± 0.1	0.4 ± 0.1	0.4 ± 0.1
<b>6/07/2001hopper F</b>	1.2 ± 0.1	UDL	UDL	UDL
<b>6/07/2001hopper A</b>	1.4 ± 0.1	UDL	UDL	0.2 ± 0.1
<b>6/14/2001hopper F</b>	3.7 ± 0.1	UDL	UDL	0.3 ± 0.1
<b>6/14/2001hopper A</b>	1.2 ± 0.1	UDL	UDL	UDL
<b>1/28/2002hopper F</b>	4.4 ± 0.2	UDL	UDL	4.0 ± 0.6
<b>8/26/2003hopper F</b>	6.0 ± 1.2	UDL	UDL	7.9 ± 1.2

Table A. 5. PAH Concentrations ( $\mu\text{g}/\text{kg}$ ) of Lime Spray Dryer Ash Collected from McCracken Power Plant from 05/2001 to 08/2003. UDL – Under detection limit

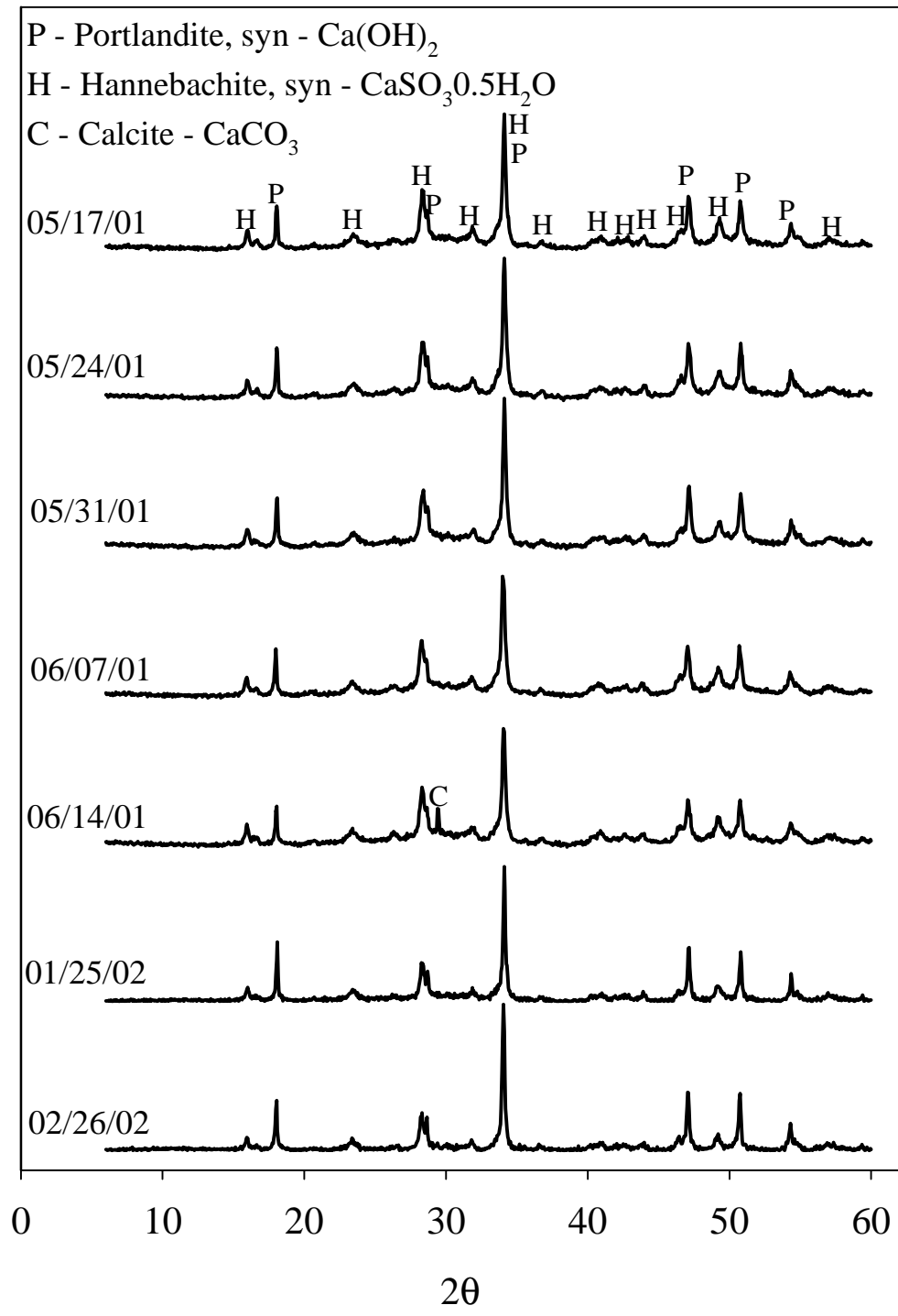


Figure A. 1. X-Ray Diffraction Patterns of LSD Material from McCracken Power Plant

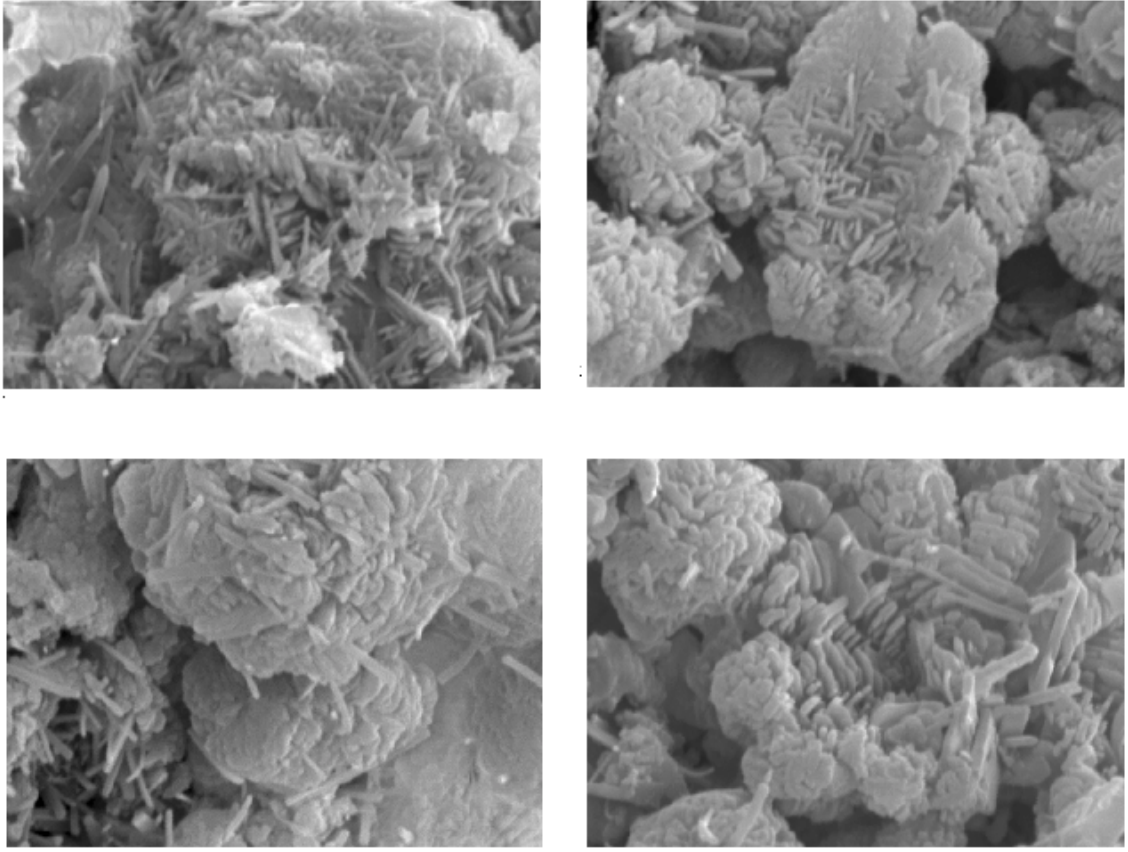


Figure A. 2. SEM Images of LSD Material from McCracken Power Plant

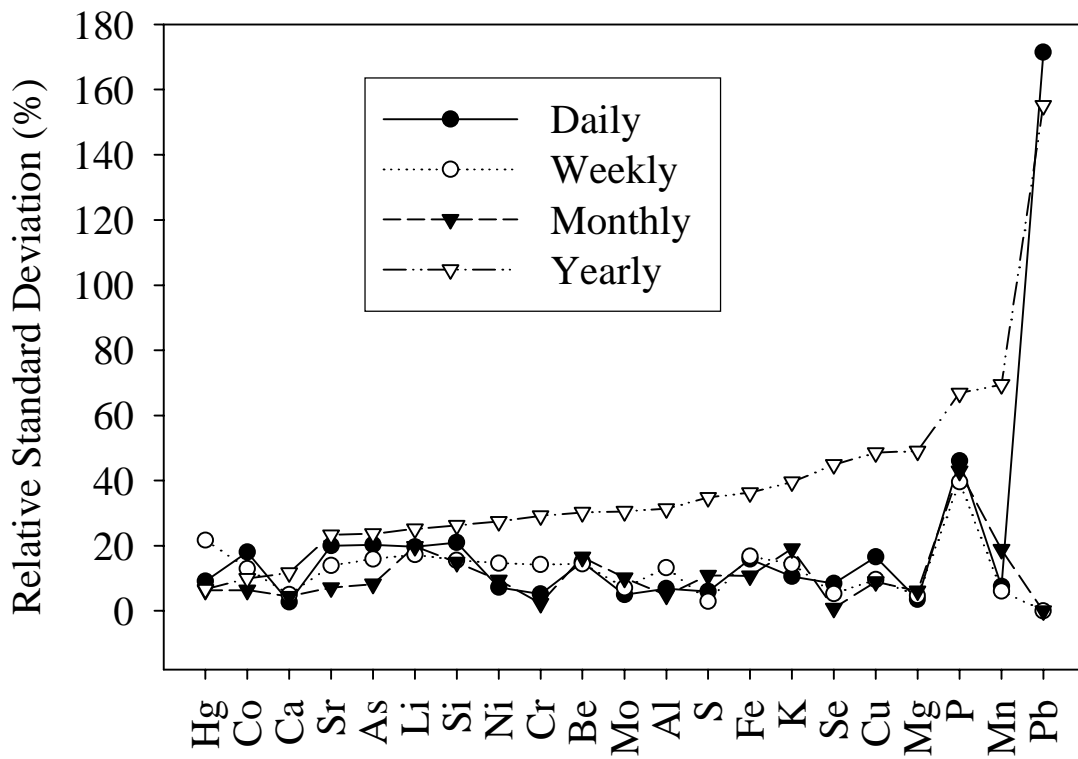


Figure A. 3. Relative standard deviations of elements in LSD ash collected at different time periods

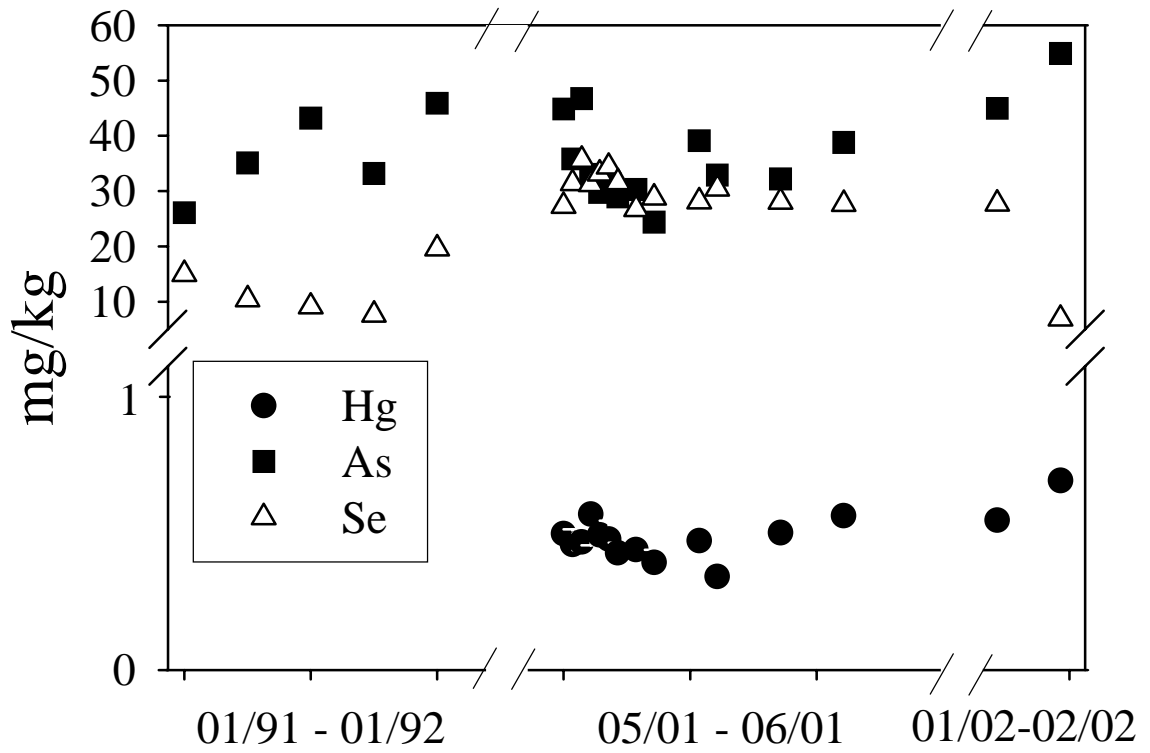


Figure A. 4. Profiles of Hg, As and Se concentrations in LSD material collected from McCracken Power Plant

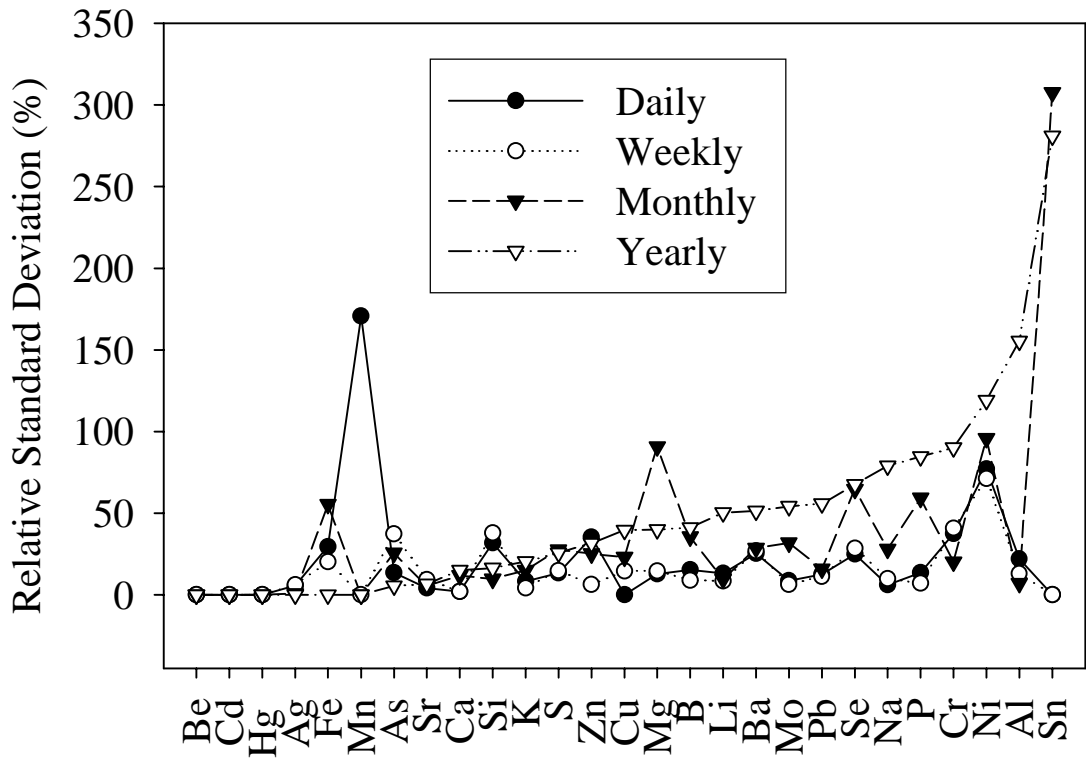


Figure A. 5. Relative standard deviations of elements in leachates from LSD ash at different time periods

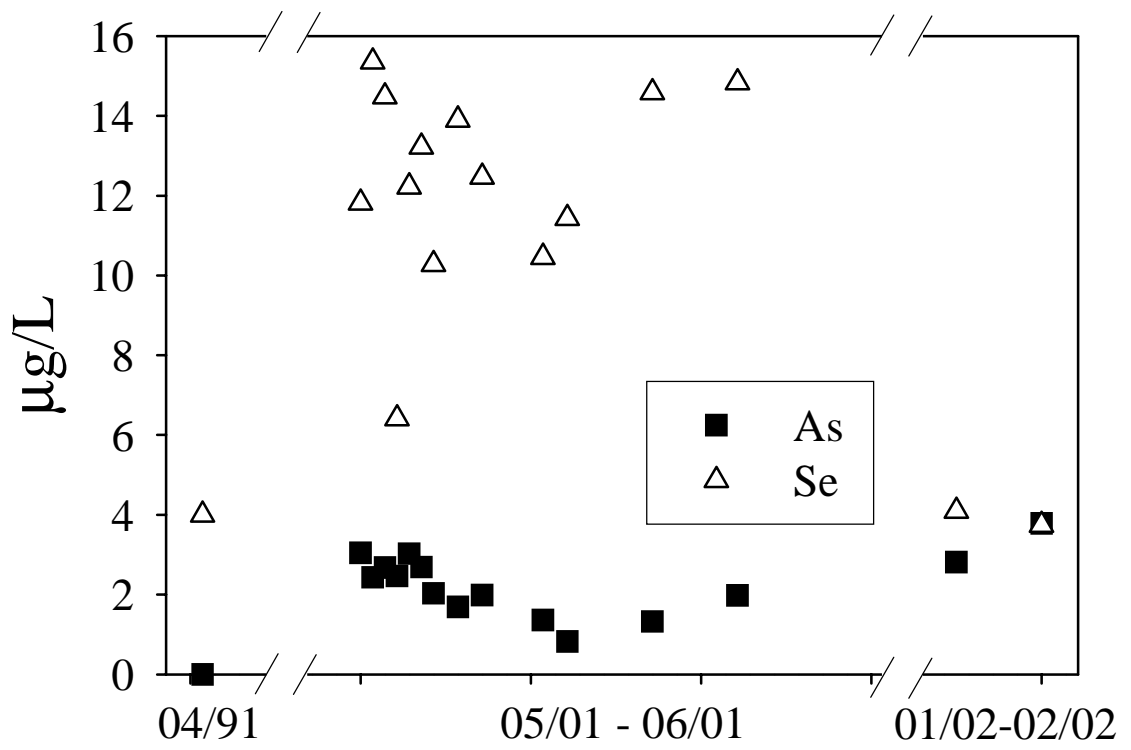


Figure A. 6. Profiles of As and Se concentrations in leachate solution from TCLP test of LSD material collected from McCracken Power Plant

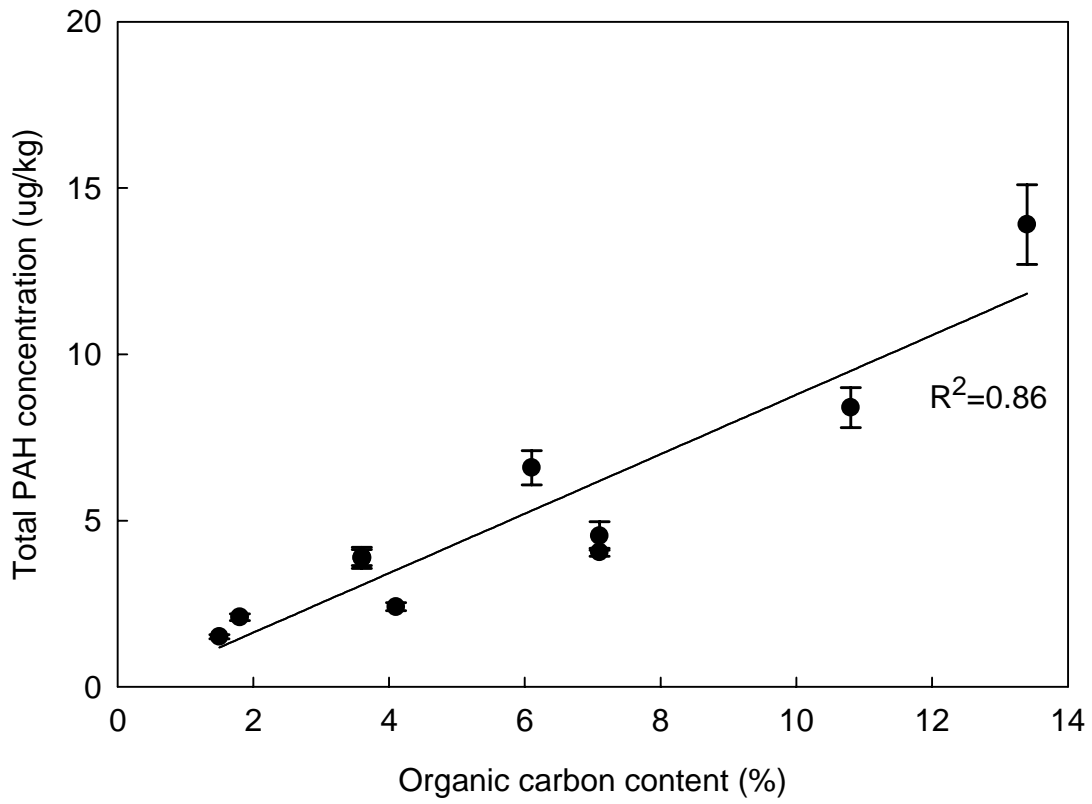


Figure A.7. Correlation between organic carbon content (%) and total PAH concentration measured on the LSD ash collected from McCracken Power Plant.

**APPENDIX B**

**GASEOUS MERCURY FROM DRY-CURING CONCRETES THAT CONTAIN  
FLY ASH: LABORATORY MEASUREMENTS**

**Danold W. Golightly<sup>†</sup>, Ping Sun<sup>†</sup>, Chin-Min Cheng<sup>†</sup>, Panuwat Taerakul<sup>†</sup>, Harold W.  
Walker<sup>†</sup>, Linda K. Weavers<sup>†,\*</sup>, William E. Wolfe<sup>†</sup> and Dean M. Golden<sup>‡</sup>**

*<sup>†</sup>Civil and Environmental Engineering and Geodetic Science, The Ohio State University,  
470 Hitchcock Hall, 2070 Neil Avenue, Columbus, Ohio 43210 USA*

*<sup>‡</sup>Consulting Engineer, 5540 Abington Drive, Newark, CA 94560 USA*

**Submitted to**

*Environmental Science & Technology*

Nov. 2004

## **B.1. Abstract**

Total gaseous mercury in headspace air was measured for enclosed concretes dry curing at 40°C for intervals of 2, 28 and 56 days. Release of mercury was confirmed for ordinary portland cement concrete [OPC] and three concretes in which Class F fly ash substituted for a fraction of the cement: a) 33% fly ash [FA33], b) 55% fly ash [FA55], and c) 33% fly ash plus 0.5% mercury-loaded powdered activated carbon [HgPAC]. Mean rates of mercury release (0.10 ng/day to 0.43 ng/day per kg of concrete) over the first 28 days of curing followed the order: OPC < FA33 ≈ FA55 < HgPAC. The apparent mercury flux from exposed surfaces of these concretes ranged from  $1.9 \pm 0.5$  to  $8.1 \pm 2.0$  ng/m<sup>2</sup>/h, values similar to the average flux for multiple natural substrates in Nevada,  $4.2 \pm 1.4$  ng/m<sup>2</sup>/h, recently published by others. Air sampling extended for 28 days beyond the initial 28-day maturation for OPC, FA55 and HgPAC indicated that the average mercury release rate by OPC is relatively constant over 56 day and that mercury release rates for FA55 and HgPAC ultimately diminish to levels exhibited by OPC concrete. The percent release of mercury from all samples was less than 0.2% over the initial curing period indicating that the majority of mercury was retained in the concrete. Although Hg release was observed, the outcomes of our laboratory experiments suggest that concrete curing either containing or in the absence of fly ash would contribute insignificantly to global anthropogenic Hg emissions.

*Keywords:* Mercury, air, concrete, fly ash, activated carbon

## **B.2. Introduction**

An estimated 12 million metric tons of coal fly ash from electrical power generators is incorporated into structural concretes and grout (1). Fly ash, which replaces some of the cement normally used in concrete, enhances the material properties of both freshly prepared concrete and hardened concrete, and prevents CO<sub>2</sub> emissions associated with cement production and use (2). Furthermore, the substitution of inexpensive fly ash for cement reduces the cost of concrete.

Fly ashes produced from bituminous and subbituminous coals contain both Hg(0) and Hg(II) at combined total mercury concentrations of 0.1 to 0.2 mg/kg (3). The oxidation state of mercury associated with fly ash largely depends on combustion conditions within individual boiler furnaces. Mercury is volatilized and converted to elemental mercury in the high temperature combustion chambers of coal boilers. A fraction of this mercury subsequently is re-oxidized as the flue gas cools, thus converting some gaseous elemental mercury to gaseous oxidized mercury primarily in the forms HgCl<sub>2</sub> and HgO (4, 5).

Implementation of maximum achievable control technology (MACT) for mercury in 2007 (6) may add small quantities of mercury-loaded powdered activated carbon (HgPAC) to fly ash particulates commonly captured from flue gas. This technology for attaining significant reduction in emitted mercury relies on injection of PAC into the flue gas stream. As this technology is implemented, current initiatives for reuse of coal combustion byproducts may be affected. PAC injection will increase levels of both carbon and mercury in fly ash.

Significant work has been done to explore the possibility of Hg release from fly ash (7). However, an understanding of the fate of mercury in concrete is needed to enable future applications of fly ash within the framework of evolving regulations. Concrete is a porous material, and mercury bound to either fly ash or PAC ultimately may be released to the atmosphere after concrete placement. Furthermore, during the mixing, pouring, and initial stage of curing, the temperature of concrete can increase up to 40°C (8). This temperature elevation, while relatively small, may increase the diffusion and subsequent vaporization of mercury from concrete.

The research described herein provides the first report of mercury release into air from concretes prepared with fly ash and mercury-loaded PAC. All experiments were conducted within a laboratory setting that fostered maximal release of mercury. Specialized techniques for air sampling above dry curing concretes and relationships between mercury mass release rates and concrete composition are presented. Curing conditions that may influence the release of mercury from fly ash and PAC incorporated into the concrete matrix are discussed.

### **B.3. Experimental Methods**

**Concrete.** The formulation for concrete selected for this investigation adhered to the proportions recommended by Cannon (9) for fly ash concretes; i.e., 13% binder (fly ash and/or cement); 6% water; 30% sand; 51% coarse aggregate. Each formulation was based on the mass of individual components, including water, which was added to provide a water-to-binder mass ratio of 0.46. Air entrainment admixture (AEA), MicroAir 100™ (Degussa, Cleveland, OH), was introduced into each batch of concrete to

ensure 5 to 6 % air entrainment. A 28-day curing interval, adopted here for air sampling, is a curing maturation standard routinely used in strength tests for concretes (8).

Hydration of tricalcium aluminate in cement is an exothermal process that produces a rise in temperature of concrete during the early curing phase (10). Subsequent cooling over a period of 1 to 2 hr then is followed by a moderate rise in temperature during the setting interval, which typically occurs over 4 to 10 hr. The rate at which setting progresses is controlled by the aqueous concentration of sulfate that is supplied by gypsum, a normal component of portland cement. In addition to chemical processes, freshly poured concrete undergoes sedimentation that forces some water to the top surface in an event known as “bleeding.” Bleeding is a short-term phenomenon that provides an opportunity for transport of soluble salts, such as  $\text{HgCl}_2$  or  $\text{HgOHCl}$ , and low-density particles to the upper surface of the fresh concrete. Thus, air-sampling experiments were performed to measure the mercury release during early curing (days 1 and 2) in addition to intermediate curing (days 1 through 28) and extended curing (days 29 through 56).

Nine batches of concrete were prepared for purge and trap measurements of gaseous mercury species above concretes containing fly ash and Hg-loaded PAC. A freshly mixed batch of concrete was divided into two approximately equal portions as the concrete was transferred quickly from the polymer-lined mixer barrel. Each individual portion of concrete (~27.7 kg) was placed into a clean high-density polyethylene (HDPE) container that finally was weighed on an electronic balance and then sealed by a HDPE gas-tight lid.

**Concrete Ingredients.** Major ingredients used in preparation of concrete were commercially available Type I portland cement, general-purpose sand, and limestone aggregate. High purity water (Millipore, Billerica, MA) was used to prepare each batch of concrete. Class F fly ash, originating from an Eastern bituminous coal combusted by an electrical utility, was characterized for loss on ignition (LOI), organic carbon content, inorganic composition, mercury content, and BET specific surface area. The LOI of the fly ash,  $4.23\% \pm 0.06\%$  ( $n=3$ ), is below the upper limit of 6% prescribed by the American Concrete Institute (ACI) for fly ash use in concrete (2). Organic carbon in the fly ash ranged from 3.8% to 4.4%. Major oxide composition ( $\text{SiO}_2 + \text{Al}_2\text{O}_3 + \text{Fe}_2\text{O}_3 = 89.4\%$ ), measured by inductively coupled plasma – atomic emission spectrometry (ICP-AES), further confirmed the fly ash to be Class F. The BET specific surface area (11) of the fly ash was determined to be  $3.0 \text{ m}^2/\text{g}$ , which is a value within the range 0.45 to  $9.44 \text{ m}^2/\text{g}$  reported by Schure *et al.* (12). A mercury concentration in the fly ash of  $0.117 \text{ mg/kg}$  was determined by cold vapor atomic absorption spectrometry (CVAAS) (13). This concentration is somewhat below the median of  $0.192 \text{ mg/kg}$  for fly ash generated from combustion of Eastern coal (range: 0.02 to  $4.2 \text{ mg/kg}$ ) (14). Mercury was loaded onto PAC (Norit Americas DARCO-FGD™) at room temperature by exposing a column of 100 grams of PAC to a flow of air that passed over metallic mercury for approximately 4 weeks. The mercury-loaded PAC was placed inside a HDPE bottle and mixed by tumbling over several days to assure homogeneity.

**Concrete Preparation.** The four types of concrete prepared for this study included ordinary portland cement concrete [OPC] and three concretes in which Class F fly ash substituted for a fraction of the cement: a) 33% fly ash [FA33], b) 55% fly ash

[FA55], and c) 33% fly ash plus 0.5% mercury-loaded PAC [HgPAC]. Addition of mercury-loaded PAC in an amount equal to 0.5% of the cement was chosen because it maintained the estimated percent carbon of the fly ash just under 6%, a practical upper limit of carbon in fly ash for utilization in portland cement concrete. A freshly mixed batch was divided into 2 approximately equal portions as the concrete was transferred quickly from the polymer-lined mixer. Slump (15) of the concrete was measured to ensure consistency and texture. Each individual portion of concrete was placed into a clean HDPE container that finally was sealed by a HDPE gas-tight lid. Containers of concrete then were moved into the environmental chamber.

Mercury concentrations in cement, sand, and limestone aggregate, MicroAir-100™ and high-purity water were determined by cold vapor atomic fluorescence spectrometry (CVAFS) in a certified commercial laboratory. Prior to all measurements, individual samples were digested in nitric acid by microwave heating within sealed PTFE vessels. This information enabled estimates of the background concentration of mercury in each batch of concrete prepared.

The powdered activated carbon (PAC) (Norit Americas Darco, FGD™), is manufactured specifically for removal of mercury from hot flue gases produced by coal combustion. This PAC is derived from a lignite coal and has an iodine number of 550 mg/g and 1.8% sulfur, as reported by the manufacturer. The PAC was determined to have a BET specific surface area of  $481 \pm 7$  m<sup>2</sup>/g. The mercury concentration in the loaded PAC was 19.9 mg/kg, which is a level of mercury loading that falls within the range observed in full-scale testing of PAC at coal-fired power plants (16).

**Control Experiment.** Batches of ordinary portland cement (OPC) concrete, which contained neither fly ash nor powdered activated carbon (PAC), provided a reference baseline for emission of mercury originating from non-coal combustion byproduct components of the mix. Furthermore, a sample blank in each experiment enabled estimates of the “system contribution” to the total mercury collected.

**Air Sampling.** Each 27 to 30 kg (split) portion of freshly prepared concrete, inside a sealed HDPE container, was cured within an environmental chamber (Environmental Growth Chambers) that was maintained at  $40 \pm 1$  °C. Temperature control of the chamber was lost during the extended curing (days 29 through 56) of 5 concrete splits when malfunction of the unit caused temperature drift between 20 °C and 40 °C. The low relative humidity of air in the chamber, typically < 25%, facilitated removal of water released from curing concretes.

Capture of volatile mercury species in air above curing concrete was accomplished by a purge-and-trap approach (Figure 1). Protocols applied to making concrete and to sampling air emphasized avoidance of contamination from any source of mercury and on prevention of losses of mercury in the sampling process. Only clean polymeric surfaces were used for the concrete mixer, curing containers, tubing, gas fittings, sample preparation and sample storage. In sampling of air, potential surface losses were minimized by attachment of each iodated carbon trap directly to a gas fitting at the exit port of a HDPE enclosure. Mercury was removed from air entering each HDPE container by a large (0.63 g) iodated carbon (IC) trap.

Airflow of 0.35 L/min through a 2 to 3 L headspace above the concretes was induced by a microprocessor-controlled AirCheck 2000<sup>TM</sup> air sampling pump (SKC,

Eighty Four, PA). Iodated carbon traps (Frontier Geosciences, Seattle, WA) attached at the outlet ports provided highly effective collection of multiple mercury species from air (17). All samples, blanks and every component of the sampling system, including air pumps, connective tubing (Tygon™ SE-200, 6.4 mm i.d.) and samples, were immersed in a 40°C air atmosphere over the total sampling interval. Prior to use, six fresh IC traps (fully protected by PTFE plugs and double locking bags) were placed inside the environmental chamber to equilibrate at 40°C. Each IC trap was opened just before insertion into a sampling port prior to initialization of the sampling process. Fluorescent lamps inside the chamber were switched off throughout sampling to minimize the possibility of photochemical reactions.

The temperature of each IC trap mounted at an outlet port was maintained at 60°C (silicone-insulated electrical heating tape) to inhibit water condensation on the iodated carbon surfaces. Elevation of the trap temperature caused any potential water condensation to occur downstream from the IC trap, where water condensed onto tubing walls and then drained into an inline water trap ahead of the air pump. Heating was stopped after two days, when evaporation of water from the curing concrete became negligible. IC traps that sampled air from empty containers (blanks) were not warmed by heating tape.

Airflow through the headspace of each HDPE container was accomplished by connecting the output from three containers to a PTFE manifold, which, ultimately, was connected to a single pump, operated at 1.05 L/min. A PTFE water trap protected the air pump from intake of any condensed water. Gas lines from the manifold were connected to the three IC traps used to sample headspace air. The volume of air sampled during 2

days ranged from 1.01 to 1.06 m<sup>3</sup>, whereas the range of air volumes sampled for the subsequent 26 days was from 13.0 to 13.1 m<sup>3</sup>. During later extended sampling of selected concretes, which occurred over an additional 28 days, mercury from 14.0 to 14.2 m<sup>3</sup> of air was collected onto IC traps.

At the end of each timed sampling interval, the air pump was switched off and IC traps were removed from the gas line and quickly placed into protective packaging. When removed from the air sampling line, each end of a sampling trap immediately was blocked with a PTFE plug. Then, each of these sealed tubes was enclosed within an individual locking polyethylene bag that was sealed inside another labeled locking polyethylene bag. This “double bagged” IC trap then was prepared for shipment by courier to an outside laboratory for determination of total mercury.

A small IC trap, capable of adsorbing 100 µg Hg, consisted of a 6 mm o.d. glass tube packed with 0.36 g of iodated carbon granules over most of its 8.5 cm length. Small traps were used for sampling air in all experiments. Each large IC trap had an adsorption capacity of 500 µg Hg, and consisted of a 10 mm o.d. glass tube packed with 0.63 g of iodated carbon granules over most of its 7.4 cm length. The large traps were kept vertical to minimize possible channeling through the IC granules packed into the glass tube. One large trap was mounted at the opening on each lid through which air passed into the headspace (Figure 1).

**Mercury Measurements.** Estimates of total quantities of mercury contributed to each batch of concrete from sand, cement, coarse aggregate, fly ash, activated carbon and AEA components were based on CVAFS measurements (Table 1). Each CVAFS determination of mercury was accomplished on an acidic aqueous solution prepared by

microwave heating of subsamples of each material in high-purity nitric acid within a sealed digestion vessel. Importantly, the ingredients used to make concrete in this investigation had mercury concentrations similar to those reported in other published studies. Although mercury concentrations were relatively low in sand and coarse aggregate, the mass of these components in the prepared concrete, relative to cement, fly ash and other ingredients, made them significant contributors to total mercury in concrete.

Mercury determinations for IC traps were accomplished by CVAFS in the laboratories of Frontier Geosciences. The iodated carbon from each trap was digested with 15 mL of a mixture of 70% nitric acid and 30% sulfuric acids (v/v). Following digestion, the resulting mixture was diluted to 40 mL with 0.07 N BrCl solution. This solution was analyzed by dual amalgamation preconcentration and cold vapor atomic fluorescence spectrometry (17). The detection limit of mercury on small IC traps ranged from 0.1 to 0.7 ng/trap. Recoveries for 50 ng or 100 ng spikes, ranged from 95.2% to 102%. Finally, determinations of mercury in the National Institute of Standards and Technology (NIST) Standard Reference Material 1641d, mercury in Water, fell within 93.5% to 98.7% of the certified concentration,  $1.590 \pm 0.018$  mg/kg.

Removal of mercury from intake air was verified by CVAFS measurements of mercury collected on 13 of the large IC traps placed at the air entry ports for every HDPE container of concrete. The maximum quantity of mercury collected by an individual large IC trap over 28 days, 3  $\mu$ g, represents only 0.6% of the trap capacity. Further, selected large IC traps that were partitioned for analysis showed no significant breakthrough of

Hg into the downstream sections of the trap, thus demonstrating complete removal of Hg from the inlet air.

#### **B.4. Results**

**Mercury Release.** The quantities of mercury collected by IC traps ranged from 3.5 ng to 17.8 ng for the initial 2 days of curing. For the initial 28 days of sampling, the total mercury accumulated from headspace air above the concretes ranged from 78.1 ng to 416.5 ng. Control blanks included with the sampling experiment for each concrete showed values lower than those for any concrete batch, with quantities of mercury ranging from 0.96 ng to 7.29 ng for a 2-day curing interval. For 28 days of curing, mercury collected from the blanks ranged from 13.4 ng to 41 ng. In every sampling experiment, the quantity of mercury collected on individual traps was well below the total adsorption capacity of 100  $\mu$ g. Based on measurements of mercury collected on partitioned segments of iodated carbon in a small trap, no significant mercury breakthrough from upstream to downstream portions occurred ( $\leq 0.08\%$ ) during sampling. Therefore, all collected mercury emissions from concretes remained on the IC traps.

Sampling of air was extended for an additional 28 days beyond the initial 28-day curing maturation for two splits of OPC and HgPAC and for one split of FA55.. Quantities of mercury collected from these three concrete types converged near a common average value of 74 ng.

The variability of measured mercury on IC traps was high (14 to 93% RSD) for samples collected over the first 2 days of curing. Quantities of mercury trapped were not

sufficiently larger than the method detection limit (0.1 to 0.7 ng/trap) to enable good precision. However, the lower variability of mercury data for 28-day samples (17 to 26% RSD), relative to 2-day samples, ultimately provided a basis for comparisons within this data set.

**Sources of Mercury.** Mercury from ambient air within the environmental chamber was removed effectively by a large IC trap placed at the air intake port to each concrete container. The average quantity of mercury captured over 28 days was  $2460 \pm 370$  ng for 13 analyzed traps. Breakthrough, based on mercury measured on the partitioned segments of four individual intake traps, was less than 0.04%. Thus, no measurable contribution of mercury came from the air pulled into the headspace of concrete containers.

The polymer liner for the mixing barrel in the Gilson™ concrete mixer was monitored throughout all concrete preparations as a potential source of contaminant mercury. Following three vigorous spray rinsings with tap water, the liner finally was rinsed with Millipore water just before preparation of concrete. Samples of the final wash water were collected in clean HDPE bottles, stabilized with permanganate solution, and finally, sent to an outside laboratory for mercury measurements by CVAFS. Mercury concentrations in all wash water samples were below the detection limit of the method (0.5 ng/L). Thus, no measurable mercury was contributed from the concrete mixer liner.

The major sources of mercury in each batch of concrete were Hg-loaded PAC, fly ash, sand and coarse aggregate (Table 2). Cement, water and air entrainment admixture (AEA) contributed little mercury. Measurable mercury emanation from OPC concretes confirmed that the mercury associated with sand and coarse aggregate (limestone), within

the matrix of curing concrete, was available to vaporize into air. However, the oxidation state of mercury in sand or limestone aggregate was not established by our experiments.

**Rates of Mercury Release.** Average mass release rates (ng/day/kg concrete) of mercury from all concretes that contained fly ash or fly ash-HgPAC were greater than that for OPC concrete (Figure 2). Furthermore, emanation of mercury increased with increasing mercury concentration in the concretes. The total initial mercury concentration in different types of concrete grew with increments in the fraction of fly ash in the concrete. Clearly, HgPAC concrete had the highest initial mercury concentration because of the addition of mercury-loaded PAC. Mercury releases over the first 28 days of curing were higher than those for the first 2 days of curing. In the 28-day experiment, an upward growth in the mass release rate was observed for increasing mercury concentrations achieved by additions of mercury-containing fly ash materials.

Statistically significant differences ( $\alpha = 0.05$ ) in mercury release rates within the group of fly ash – concretes prepared were established by a one-sided analysis of variance (ANOVA) treatment of data. For an initial 2-day curing interval, no differences were detected for mercury mass release rates for OPC, FA33 and FA55 concrete mixtures. However, the mercury mass release rate for HgPAC concrete was greater than that measured for any of the other concrete types over the first 2 days of curing. For a 28-day curing period, the conventional maturation interval used for strength tests of concretes, mercury release rates from FA33 and FA55 were significantly higher than the rate for OPC concrete. No difference between rates for FA33 and FA55 could be concluded. The mercury release rate over this 28-day curing period for concrete containing mercury loaded PAC was statistically higher than rates from all other concrete

mixtures. The overall good precision of data associated with this 28-day curing period supports a good level of confidence ( $\alpha = 0.05$ ) for the release rate trend: OPC < FA33  $\approx$  FA55 < HgPAC.

Beyond the standard 28-day curing period, mercury release rates were estimated by continued sampling of headspace air over an extended 28-day period (day 29 through day 56) for several containers of OPC, FA55 and HgPAC concrete mixtures (Table 3). Average mass release rates for this extended curing ranged from  $0.08 \pm 0.05$  ng/day/kg for OPC concrete to  $0.11 \pm 0.01$  ng/day/kg for HgPAC concrete. The rates of mercury release from FA55 and HgPAC decreased during extended curing to a common value ( $0.10 \pm 0.03$ , n=5) very close to that observed for OPC concrete during the initial 28 days of curing. Thus, within the limits of these experiments, the mercury release rate for extended curing may not depend on the initial mercury content of the concrete batch.

The percent mercury released from each concrete type is shown in Figure 3. In general, the mercury releases over the entire 56 day sampling period were low, well below 0.2%. Thus, the vast majority of mercury was retained in the concrete. The greatest percent release occurred over the first 28 day period with lower percent release occurring over the second 28 day curing period. For the first 28 days the percent mercury release values were similar for all of the concretes.

## **B.5. Discussion**

A comparison of the rate of mercury emission from concretes studied here with mercury fluxes from soils is useful in understanding the potential atmospheric contributions from concretes that contain coal fly ash. Extensive data on mercury fluxes

above Nevada soil and natural substrates, published recently by Zehner and Gustin (18), provide a suitable basis for this comparison. An average mercury flux for Nevada soil was reported as  $4.2 \pm 1.4$  ng/m<sup>2</sup>/h (18). For concretes included in the current study, estimates of apparent mercury flux through the exposed surfaces (0.062 m<sup>2</sup>) of concretes in HDPE containers sampled for 28 days provide a range from  $1.9 \pm 0.5$  to  $8.1 \pm 2.0$  ng/m<sup>2</sup>/h. These apparent fluxes reflect emission of mercury from curing concrete into purified air, rather than into ambient air, which commonly is used in flux measurements for soils and other natural substrates. Further differences from soil testing procedures include: a) a constant air temperature of 40°C, and b) a sampling interval that was significantly longer than those used in sampling air above soils with gold adsorption collectors. Thus, the apparent mercury fluxes reported here should be considered as upper-limit values rather than typical values that might be measured in the field. In any case, our results suggest that concrete containing fly ash has comparable or even lower fluxes than Nevada soils.

Maximum release rates of mercury were observed over the initial 28 days, with lower average release rates for the initial 2 days and extended 28 days. These differences in release rates may result from alterations in the physical and chemical properties of the concrete during the curing process. Over the first few days of curing, the concrete contains significant amounts of water that may create a mass transfer barrier to volatilization. After the first few days of curing, much of the water evaporates or is incorporated into the mineral forms of the concrete. This allows for greater volatilization of mercury within the pore spaces and into the atmosphere. Also, concentration of mercuric salts and elemental mercury within the diminishing volume of water in the

curing concentrate may provide a greater concentration gradient for mass transfer. After the first 28 days of curing, additional mineralogical changes in the concrete may encapsulate sorbed forms of mercury resulting in lowered mercury release rates.

Mercury collects on the surface of fly ash from hot flue gas throughout coal combustion. A portion of elemental mercury from coal is oxidized to Hg (II) during combustion (5). Both Hg(0) and Hg (II) interact with ash particulate surfaces where reactivated chemical species, oxidation catalysts and activated sorption sites are available in the post-combustion process. The adsorption of mercury, either Hg(II) or Hg(0), on fly ash occurs via either physisorption, chemisorption, chemical reaction, or a combination of these processes (5). In general, physisorption of Hg(0) is a weak, dipole-induced dipole interaction, while chemisorption involves the formation of a specific chemical bond between mercury and the surface. Hall et al. (19) tested the adsorption mechanism of mercury on fly ash from 20 °C to 400 °C and found both physical and chemical sorption mechanisms are common at lower temperatures. These previous studies suggest that at least a fraction of the physically-sorbed mercury may be available for release from fly-ash concrete under conditions applied in our experiments (40 °C).

For the 28-day sampling period, the uniform growth in the mass release rate, 26.6 pg/day/kg per unit of initial mercury concentration ( $\mu\text{g}/\text{kg}$ ) observed for OPC, FA33 and FA55, dropped to 19.6 pg/day/kg for HgPAC concrete. This reduction in the rate of mercury release may be attributable to stronger adsorption of mercury on PAC than on fly ash. In a situation similar to that for fly ash, adsorption of mercury by activated carbon at ambient temperatures has been suggested to be a combination of chemisorption and physisorption, where chemisorption is prevalent at higher temperatures (20). With

increasing temperatures, physisorption of mercury is decreased because of the reduction of intermolecular forces between carbon and adsorbed mercury atoms. Krishnan *et al.* (21) suggested that the active sites causing Hg(0) adsorption in the PAC may include oxygenated organic species and functional groups containing inorganic elements, such as chlorine or sulfur.

The sulfur content of PAC used in our experiments was 1.8%. The corresponding sulfur sites in PAC are expected to form chemical bonds with mercury (22). For the temperature and air flow applied throughout our experiments, some of the mercury physically adsorbed onto other components of the concrete may be released to form chemical bonds (chemisorption) with carbon surface functional groups. Thus, although some of the physically adsorbed mercury may be relatively free to enter the gas phase, mercury chemisorbed on activated carbon is unlikely to be released into air. Generally, carbon injection to control mercury emission from flue gas uses a high carbon-to-mercury weight ratio. Thus, PAC from flue gas is not expected to be saturated with mercury, especially when the concentration of mercury in the flue gas is low, e.g. 5~10  $\mu\text{g}/\text{m}^3$  (5). The mercury concentration on PAC used in our experiments is comparable to that observed after PAC injection in a full-scale boiler. However, the ratio of physisorbed mercury to chemisorbed mercury on the PAC used in this study very likely differs from the ratio produced by a full-scale boiler system. The fraction of physisorbed mercury on PAC from a full-scale plant operation with high flue gas temperatures is expected to be lower than that for PAC loaded with mercury at room temperature. Thus, data from our experiments may represent an upper limit for mercury emissions from concrete containing mercury loaded PAC and fly ash.

Capture of mercury released from other components of the concrete onto PAC possibly explains the low normalized release rate of mercury from PAC-containing concrete, relative to other concretes. Water adsorption onto the carbon surfaces of activated carbon is facilitated by hydrogen bonding (23). Oxygen complexes on carbon surfaces form primary adsorption centers, while adsorbed water molecules can become secondary adsorption centers as the water vapor pressure increases. Chemisorption of Hg(0) is a dominant process for moisture-containing samples (20). Thus, the mercury emitted from other components in the concrete curing process may be adsorbed onto these secondary adsorption centers. As the hydration of cement proceeds, a postulated build-up of a gel-membrane occurs outside the carbon pores. Once in the solidified waste form, activated carbon particles will retain most of the adsorbed mercury by forming a barrier outside of the activated carbon particles (24).

The above discussion and conclusions are based on purge-and-trap measurements using purified air, and therefore, represent an upper limit of release rates. Measurement with ambient air may result in lower release rates due to background concentrations of mercury. In light of the 8.8 billion metric tons of concrete annually produced worldwide, our results suggest that 44~133 kg/yr of mercury may be released from concretes during curing. Of the estimated 2235 t of Hg emitted annually from anthropogenic sources (25), the contribution from concrete curing is insignificant.

### **Acknowledgments**

This research was funded by the Electric Power Research Institute (EPRI), Palo Alto, CA. The authors extend their sincere thanks to Tarunjit Butalia, Ohio State

University, for his advice and recommendations on CCPs. We especially are grateful to Thomas Bishop, Ohio State University, for his statistical analysis of mercury data. Finally, special thanks go to Jennifer L. Parker, Frontier Geosciences, for her mercury measurements and coordination of analyses for our samples.

## References

1. American Coal Ash Association, 2003 Coal Combustion Product (CCP) Production and Use Survey, [http://www.aaa-usa.org/PDF/2003\\_CCP\\_Survey\(10-1-04\).pdf](http://www.aaa-usa.org/PDF/2003_CCP_Survey(10-1-04).pdf) (accessed October 15, 2004)
2. *Use of fly ash in concrete*; ACI 232.2R-96; Report by ACI Committee 232; American Concrete Institute: Farmington Hills, MI, 1996.
3. *Study of hazardous air pollutant emissions from electric utility steam generating units, Volume I*; EPA 453/R-98-004a; Final report to congress; U.S. Environmental Protection Agency: Washington, DC, 1998.
4. Gibb, W. H.; Clarke, F.; Mehta, A. K. The fate of coal mercury during combustion. *Fuel Process. Technol.* **2000**, *65*, 365-377.
5. Galbreath, K. C.; Zygarlicke, C. J. Mercury transformations in coal combustion flue gas. *Fuel Process. Technol.* **2000**, *65-66*, 289-310.
6. *Mercury study report to congress, Volume I: Executive Summary*, Office of Air Quality Planning and Standard and Office of Research and Development; EPA-452/R-97-003; U.S. Environmental Protection Agency, Washington, DC, 1997.
7. Gustin, M. S.; Ladwig, K. An assessment of the significance of mercury release from coal fly ash. *J. Air Waste Manage. Assoc.* **2004**, *54*, 320-330.
8. American Concrete Institute, ACI Manual of concrete practice 1991. Part 1, Materials and general properties of concrete, ACI, Detroit, 1991.
9. Cannon, R.W. Proportioning fly ash concrete mixes for strength and economy. *J. Am. Concrete Institute* **1968**, *65*, 969-979.
10. Neville, A. M. *Properties of Concrete*, 4th ed.; Wiley: New York, 1996.

11. Brunauer, S.; Emmett, P. H.; Teller, E. Adsorption of gases in multimolecular layers *J. Am. Chem. Soc.* **1938**, *60*, 309-319.
12. Schure, M. B.; Soltys, P. A.; Natusch, D. F. S.; Mauney, T. Surface area and porosity of coal fly ash. *Environ. Sci. Technol.* **1985**, *19*, 82-86.
13. United States Environmental Protection Agency. Method 3052, Microwave Assisted Acid Digestion of Siliceous and Organically Based Matrices, SW-846 Test Methods, 1996.
14. *Wastes from the Combustion of Coal by Electric Utility Power Plants*; EPA/530-SW-88-002; Report to Congress; U.S. Environmental Protection Agency: Washington DC, 1988.
15. American Society for Testing and Materials C 143, Standard test method for slump of hydraulic cement concrete. ASTM Vol. 04.02.
16. Chu, P.; Roberson, R.; Laudal, D.; Brickett, L.; Pan, W. P. Long-term mercury emissions variability from coal-fired power plants. Proceeding paper. Air Quality IV International Conference, 12-14 September 2003, Arlington, Virginia.
17. Bloom, N. S.; Prestbo, E. M.; Hall, B.; Von der Deest, E. J. Determination of atmospheric Hg by collection on iodated carbon, acid digestion and CVAFS detection. *Water, Air, and Soil Pollut.* **1995**, *80*, 1315-1318.
18. Zehner, R.E.; Gustin, M.S. Estimation of mercury vapor flux from natural substrate in Nevada. *Environ. Sci. Technol.* **2002**, *36*, 4039-4045.
19. Hall, B.; Schager, P.; Weesmaa, J. The homogeneous gas phase reaction of mercury with oxygen, and the corresponding heterogeneous reactions in the presence of activated carbon and fly ash. *Chemosphere* **1995**, *30*, 611-627.

20. Li, Y. H.; Lee, C. W.; Gullett, B. K. The effect of activated carbon surface moisture on low temperature mercury adsorption. *Carbon* **2002**, *40*, 65-72.
21. Krishnan, S. K.; Gullett, B. K.; Jozewicz, W. Sorption of elemental mercury by activated carbons. *Environ. Sci. Technol.* **1994**, *28*, 1506-1512.
22. Karatza, D.; Lancia, A.; Musmarra, D.; Zucchini, C. Study of mercury absorption and desorption on sulfur impregnated carbon. *Experimental Thermal and Fluid Science* **2000**, *21*, 150-155.
23. Bansal, R. C.; Donnet, J. B.; Stoeckli, F. *Active Carbon*, Marcel Dekker: New York and Basel, 1988.
24. Zhang, J.; Bishop, P. L. Stabilization/solidification (S/S) of mercury-containing wastes using reactivated carbon and portland cement. *J. Hazardous Mat.* **2002**, *92*, 199-212.
25. Pacyna, J. M.; Pacyna, E. G. An assessment of global and regional emissions of trace metals to the atmosphere from anthropogenic sources worldwide. *Environ. Rev.* **2001**, *9*, 269-298.
26. Verein Deutscher Zementwerke e.V. Trace Elements in German Standard Cements, 2001, ([http://www.vdz-online.de/Downloads/spurenelement/spurenel2001\\_engl.pdf](http://www.vdz-online.de/Downloads/spurenelement/spurenel2001_engl.pdf).)
27. Johansen, V. C.; Hawkins, G. J. *Mercury speciation in cement kilns: A literature review*. Res. Dev. Serial No. 2567, Portland Cement Association, Skokie, IL, 2003.

Component	Concentration						
	mg/kg					mg/L	
	Sand	Cement	Coarse Aggregate	Fly Ash	HgPAC	Water	MicroAir 100™
This Study	0.0072	0.0028	0.0031	0.119	19.9	<LOD	1.83×10 <sup>-5</sup>
Literature	0.02~0.1	0.06 <sup>(1)</sup>	0.005~0.46 <sup>(2)</sup>	0.1~1.0	1.09~963.9 <sup>(3)</sup>	N/A	N/A

Table B.1. Mercury concentrations in concrete components. (1) Data is from reference 26; (2) data is from reference 27; (3) data is from reference 16.

Concrete Type	Sand	Cement	Coarse Aggregate	Fly Ash	Hg-Loaded PAC	MicroAir 100™	Total Mercury in Concrete	Mercury Concentration in Concrete
	(mg/batch)					(ng/batch)	(mg/batch)	(µg/kg)
OPC	0.14	0.02	0.10	0	0	0.18	0.27	4.1
FA33	0.14	0.02	0.10	0.34	0	0.80	0.60	9.2
FA55	0.14	0.01	0.10	0.57	0	1.20	0.82	12.6
HgPAC	0.14	0.02	0.10	0.34	0.86	1.47	1.46	22.4

Table B. 2. Mercury contribution from each concrete component.

Concrete Type	Initial Mercury Concentration in Concrete	Release Rate <i>ng/day/kg</i> [T = 40 ± 1°C]			Release Rate <i>ng/day/kg</i> [23°C ≤ T ≤ 40°C]	
		<i>μg/kg</i>	<i>n</i>	<i>First 2 Days</i>	<i>First 28 Days</i>	<i>k</i>
OPC	4.1	4	0.07 ± 0.02	0.10 ± 0.03	2	0.08 ± 0.05
FA33	9.2	6	0.13 ± 0.07	0.26 ± 0.04	0	---
FA55	12.6	3	0.08 ± 0.07	0.34 ± 0.09	1	0.10
HgPAC	22.4	4	0.26 ± 0.04	0.43 ± 0.12	2	0.11 ± 0.01

Table B.3. Average mass release rates of mercury from curing concretes.

## FIGURE CAPTIONS

Figure B.1. Air Sampling Apparatus.

Figure B.2. Trends in mercury release rates from curing concretes. OPC: ordinary portland cement; FA33: concrete for which fly ash replaced 33% of the portland cement; FA55: concrete for which fly ash replaced 55% of the portland cement; HgPAC: concrete with 33% fly ash plus 0.5% mercury-loaded PAC.

Figure B.3. Percent mercury released from different concretes after 2 days, 26 days and additional 28 days. OPC: ordinary portland cement; FA33: concrete for which fly ash replaced 33% of the portland cement; FA55: concrete for which fly ash replaced 55% of the portland cement; HgPAC: concrete with 33% fly ash plus 0.5% mercury-loaded PAC.

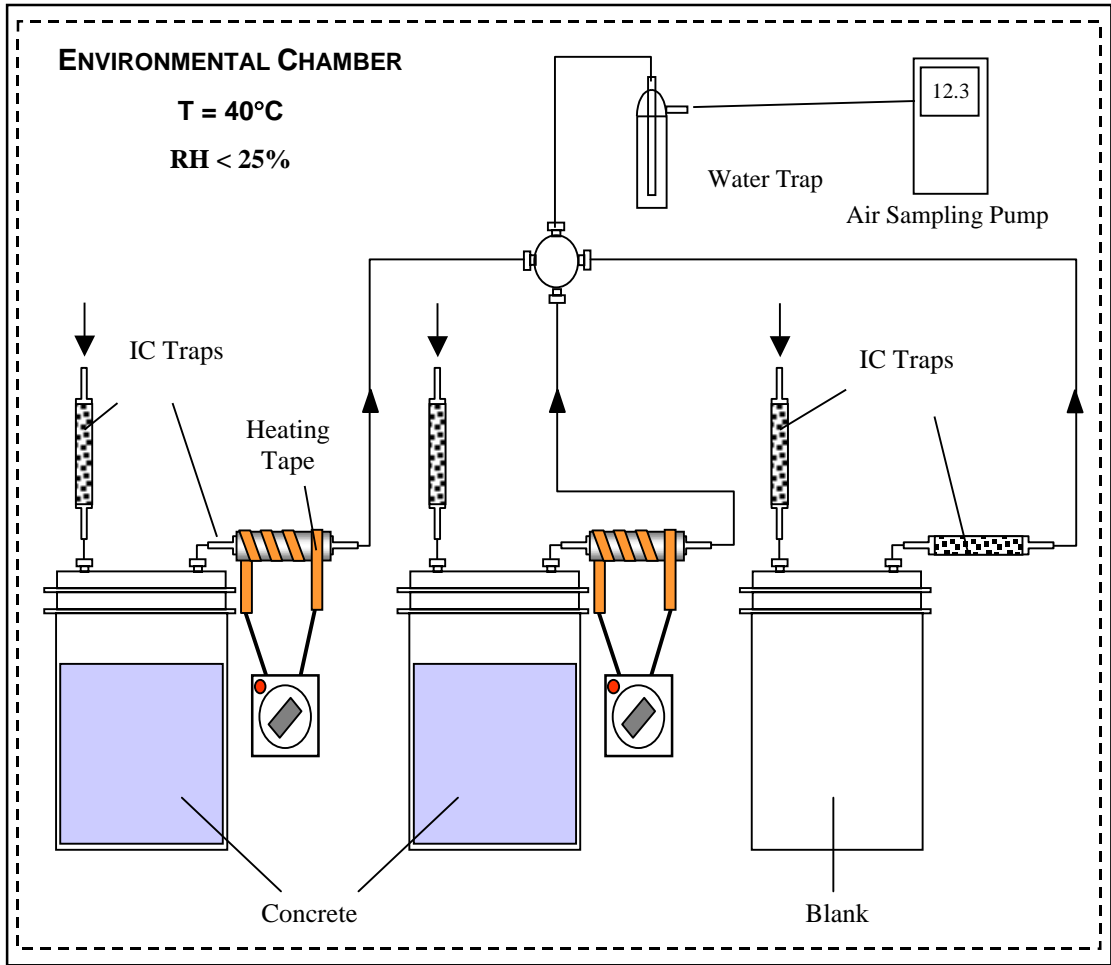


Figure B.1. Air Sampling Apparatus.

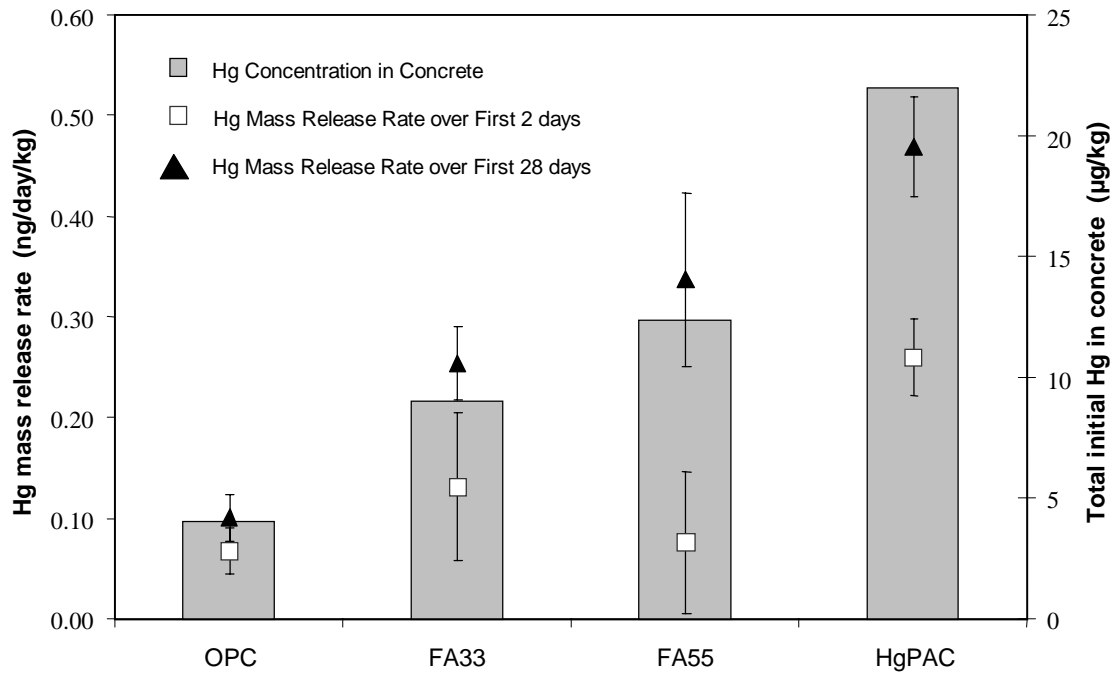


Figure B.2. Trends in mercury release rates from curing concretes. OPC: ordinary portland cement; FA33: concrete for which fly ash replaced 33% of the portland cement; FA55: concrete for which fly ash replaced 55% of the portland cement; HgPAC: concrete with 33% fly ash plus 0.5% mercury-loaded PAC.

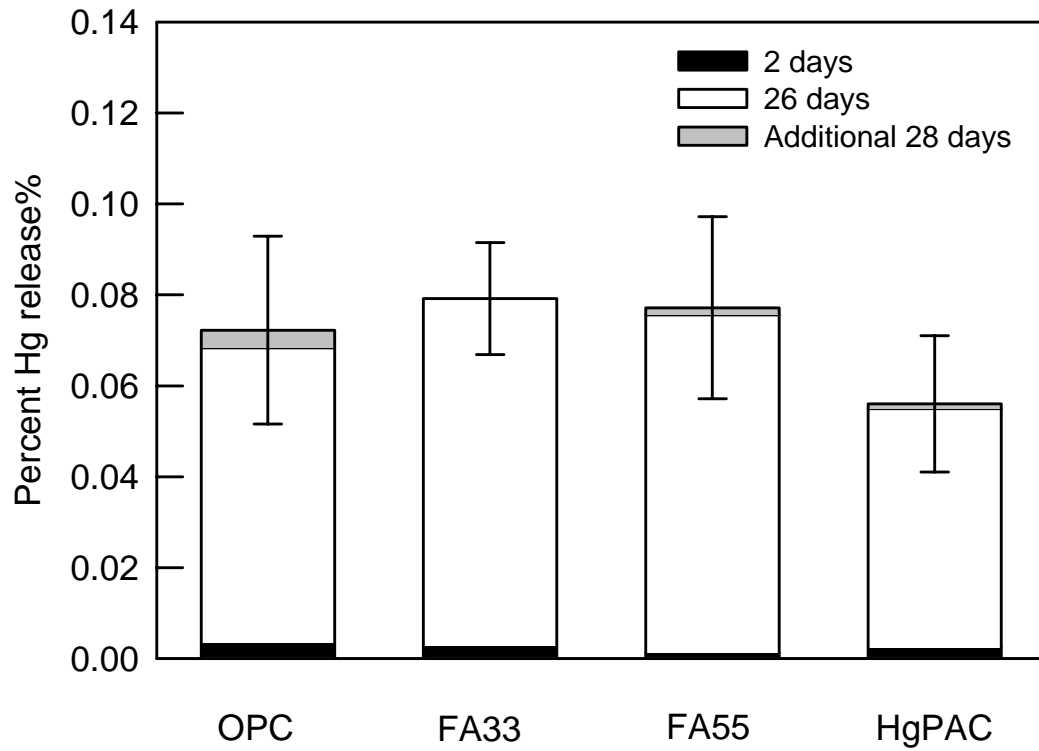


Figure B.3. Percent mercury released from different concretes after 2 days, 26 days and additional 28 days. OPC: ordinary portland cement; FA33: concrete for which fly ash replaced 33% of the portland cement; FA55: concrete for which fly ash replaced 55% of the portland cement; HgPAC: concrete with 33% fly ash plus 0.5% mercury-loaded PAC.

## BIBLIOGRAPHY

1. Ahn, C.; Mitsch, W. J.; Wolfe, W. E. *Wat. Res.* **2001**, *35*, 633-642.
2. Adewuyi, Y. G. *Ind. Eng. Chem. Res.* **2001**, *40*, 4681-4715.
3. Agnihotri, R.; Chauk, S. S.; Mahuli, S. K.; Fan, L.-S. *Ind. Eng. Chem. Res.* **1999**, *38*, 812-819.
4. Akimoto, Y.; Aoki, T.; Nito, S.; Inouye, Y. *Chemosphere* **1997**, *34*, 263-273.
5. Alexandrou, N.; Pawliszyn, J. *Anal. Chem.* **1989**, *61*, 2770-2776.
6. American Coal Ash Association Survey (1997). 1996 coal combustion product (CCP) production and use. American Coal Ash Association, Alexandria, VA.
7. American Coal Ash Association, 2003 Coal Combustion Product (CCP) Production and Use Survey, [http://www.aaa-usa.org/PDF/2003\\_CCP\\_Survey\(10-1-04\).pdf](http://www.aaa-usa.org/PDF/2003_CCP_Survey(10-1-04).pdf)
8. Arditsoglou, A.; Petaloti, Ch.; Terzi, E.; Sofoniou, M.; Samara, C. *Sci. Total Environ.* **2004**, *323*, 153-167.
9. Arzayus, K.; Dickhut, R.; Canuel, E. *Environ. Sci. Technol.* **2001**, *35*, 2178-2183.
10. Badger, G. M.; Donnelly, J. K.; Spotswood, T. M. *Aust. J. Chem.* **1964**, *17*, 1138-1146.
11. Baek, S. O.; Field, R. A.; Goldstone, M. E.; Kirk, P. W.; Lester, J. N.; Perry, R. *Water Soil Pollut.* **1991**, *60*, 279-300.
12. Berset, J. D.; Ejem, M.; Holzer, R.; Lischer, P. *Anal. Chim. Acta* **1999**, *383*, 263-275.
13. Blankenhorn, I.; Meijer, D.; Van Delft, R. *Fresenius' J. Anal. Chem.* **1992**, *343*, 497-504.
14. Bockhorn, H.; Fetting, F.; Wenz, H. W. *Ber Bunsenges Phys. Chem.* **1983**, *87*, 1067-1073.
15. Braida, W. J.; Pignatello, J. J.; Lu, Y.; Ravikovitch, P. I.; Neimark, A. V.; Xing B. *Environ. Sci. Technol.* **2003**, *37*, 409-417.
16. Burford, M. D.; Hawthorne, S. B.; Miller, D. J. *Anal. Chem.* **1993**, *65*, 1497-1505.

17. Butalia, T.; Wolfe, W. W. 1997 Ash Utilization Symposium, Lexington, Kentucky, **1997**.
18. Butalia, T.; Dyer, P.; Stowell, R.; Wolfe, W. W. The Ohio State Extension Fact Sheet, AEX-332-99, Columbus, Ohio: The Ohio State University, **1999**.
19. Butalia, T.; Wolfe, W. W.; Lee, J.W. *Fuel*, **2001**, *80*, 845-850.
20. Camel, V. *Analyst*, **2001**, *126*, 1182-1193.
21. Cataldo, F. *Ultrason. Sonochem.* **2000**, *7*, 35-43.
22. Chen, C. S.; Rao, P. S. C.; Lee, L. S. *Chemosphere* **1996**, *32*, 1123-1132.
23. Chen, L.; Dick, W. A.; Nelson, S. *Environ. Pollut.* **2001**, *114*, 161-168.
24. Chin, Y-P.; Aiken, G. R.; Danielsen, K. M. *Environ. Sci. Technol.* **1997**, *31*, 1630-1635.
25. Clark, R.; Ritchey, K.; Baligar, V. C. *Fuel*, **2001**, *80*, 821-828.
26. Codubam G.; Vaquierp, M. T.; Comellas, L.; Broto-puig, F. *J.Chromatogr.* **1994**, *673*, 21-29.
27. Colussi, A. J.; Weavers, L. K.; Hoffmann, M. R. *J. Phys. Chem. A* **1998**, *102*, 6927-6934.
28. Cook, B. R.; Wilkinson, B. B.; Claude, C. C.; Holmes, S. M.; Martinez, L. E. *Energy Fuels* **1997**, *11*, 61-70.
29. Crews, J. T.; Dick, W. A. *Environ. Pollution* **1998**, *103*, 55-61.
30. Cypres, R.; Bettens, B. *Fuel* **1986**, *65*, 507-513.
31. Dean, J. R.; Xiong, G-H. *Trends in Anal. Chem.* **2000**, *19*, 553-564.
32. Denissenko, M. F.; Pao, A.; Tang, M-S.; Pfeifer, G. P. *Science* **1996**, *274*, 430-432.
33. Dry Scrubbing Technologies for Flue Gas Dusulfurization, Kluwer Academic Publishers, Boston/Dordrecht/London, 1998.
34. Doktycz, S. J.; Suslick, K. S. *Science* **1990**, *247*, 1067-1069.
35. Durlak, S. K.; Biswas, P.; Shi, J.; Bernhard, M. J. *Environ. Sci. Technol.* **1998**, *32*, 2301-2307.

36. Ebert, L. B. Polynuclear aromatic compounds. American Chemical Society, Washington, D.C., 1988.
37. Energy Information Administration, US department of Energy, Washington, DC 20585, DOE/EIA-0484, 2002.
38. Eiceman, G.A.; Vandiver, V. *J. Atmos. Environ.* **1983**, *17*, 461-466.
39. Fan, L-S.; Jadhav, R. A. *AIChE Journal*, **2002**, *48*, 2115-2123.
40. Fangmark, I.; Bavel, B.V.; Marklund, S.; Stromberg, B.; Berge, N.; Rappe, C. *Environ. Sci. Technol.* **1993**, *27*, 1602-1610.
41. Fixari, B.; Perchec, P. L.; Kopinke, F-D.; Zimmermann, G.; Decroocq, D.; Thomas, M. *Fuel*, **1994**, *73*, 505-509.
42. Fischer, R.; Kreuzig, R.; Bahadir, M. *Chemosphere* **1994**, *29*, 311-317.
43. Flint, E. B.; Suslick, K.S. *Science* **1991**, *253*, 1397-1399.
44. Ghosh, U.; Talley, J. W.; Luthy, R. G. *Environ. Sci. Technol.* **2000**, *34*, 1729-1736.
45. Ghosh, U.; Talley, J. W.; Luthy, R. G. *Environ. Sci. Technol.* **2001**, *35*, 3468-3475.
46. Ghosh, U.; Zimmerman, J.; Luthy, R. G. *Environ. Sci. Technol.* **2003**, *37*, 2209-2217.
47. Gillette, J. S.; Luthy, R. G.; Clemett, S. J.; Zare, R. N. *Environ. Sci. Technol.* **1999**, *33*, 1185-1192.
48. Goss, K-U. *Critical Rev. Environ. Sci. Technol.* **2004**, *34*, 339-389.
49. Griest, W. H.; Yeatts, L. B.; Caton, J. E. *Anal. Chem.* **1980**, *52*, 199-201.
50. Griest, W. H.; Tomkins, B. A.; Caffrey, J. R. *Anal. Chem.* **1988**, *60*, 2169-2171.
51. Groszek, A. J. *Dissuss. Faraday Soc.* **1975**, *59*, 109-116.
52. Harvey, R. G. Polycyclic Aromatic Hydrocarbons, Chemistry and Carcinogenicity. Cambridge University Press, Cambridge/ New York/ Port Chester/ Melbourne/ Sydney, 1991.
53. Henglein, A.; Ulrich, R.; Lilie, J. *J. Am. Chem. Soc.* **1989**, *111*, 1974-1979.

54. Henglein, A. In *Advances in Sonochemistry*, JAI Press Ltd.: Hampton Hill, 1993; Vol. 3, pp 17-83.
55. Henner, M.; Schiavon, M.; Morel, J. L.; Lichtfouse, E. *Analisis*, **1997**, 25, M56-M59.
56. Hromadkova, Z.; Ebringerova, A.; Valachovic, P. *Ultrason. Sonochem.* **1999**, 5, 163-168.
57. Hyes, M. D.; Geron, C. D.; Linna, K. J.; Smith, N. D.; Schauer, J. J. *Environ. Sci. Technol.* **2002**, 36, 2281-2296.
58. Johansson, I.; Bavel, B. V. *Sci. Total Environ.* **2003**, 311, 221-231.
59. Jonker, T.; Koelmans, A. *Env. Sci. Technol.* **2002**, 36, 4107-4113.
60. Junk, G. A.; Ford, C. S. *Chemosphere* **1980**, 9, 187-230.
61. Kan, A. T.; Fu, G-M.; Tomson, M. B. *Environ. Sci. Technol.* **1994**, 28, 859-867.
62. Karapanagioti, H. K.; Kleineidam, S.; Sabatini, D. A.; Grathwohl, P.; Ligouis, B. *Environ. Sci. Technol.* **2000**, 34, 406-414.
63. Kenny, D.; Olesik, S. *J. Chromatogr. Sci.* **1998**, 36, 59-65.
64. Khim, J. S.; Kannan, K.; Villeneuve, D. L.; Koh, C. H.; Giesy, J. P. *Environ. Sci. Technol.* **1999**, 33, 4199-4205.
65. Kim, O.; Nguyen, T.; Reutergardh, L. B.; Dung, N. T. *Environ. Sci. Technol.* **1999**, 33, 2703-2279.
66. Laflamme, R. E. and Hites, R. A. *Geochim. Cosmochim. Acta* **1978**, 42, 289-303.
67. Lamminen, M. O.; Wood, J., Walker, H. W.; Chin, Y.-P.; He Y.; Traina, S. *J Environ. Quality* **2001**, 30, 1371-1381.
68. Ledesma, E. B.; Kelish, M. A.; Nelson, P. F.; Wornat, M. J.; Mackie, J. C. *Fuel*, **2000**, 79, 1801-1814.
69. Lee, M. L., Hites, R. A. *Anal. Chem.* **1976**, 48, 1890-1893.
70. Lee, W. G.; Chen, J. C. *Environment International*, **1995**, 21, 827-832.
71. Leonhardt, E.; Stahl, R. *Anal. Chem.* **1998**, 70, 1228-1230.
72. Letterman, R. D. *Water Quality & Treatment: A Handbook of Community Water Supplies*, McGraw-hill, 1999.

73. Levendis, Y. A.; Alta, A.; Carlson, J.; Dunayevskiy, Y.; Vouros, P. *Environ. Sci. Technol.* **1996**, *30*, 2742-2754.
74. Li, C. Z.; Nelson, P. F. *Energy Fuels* **1996**, *10*, 1083-1090.
75. Lillieblad, L.; Szpila, Z.; Strand, M.; Pagels, J.; Rupa-Gadd, K.; Gudmundsson, A.; Seietlicki, E.; Bohgad, M.; Sanati, M. *Energy & Fuels* **2004**, *18*, 410-417.
76. Little, C.; Hefner, M. J.; El-Sharif, M. *Ultrasonics* **2002**, *40*, 667-674.
77. Liu, K-L.; Xie, W.; Zhao, Z-B.; Pan, W-P.; Riley, J. T. *Environ. Sci. Technol.* **2000**, *34*, 2273-2279.
78. Liu, K-L.; Heltsley, R.; Zou, D-Z.; Pan, W-P.; Riley, J. T. *Energy Fuels* **2002**, *16*, 330-337.
79. Lopez-Avila, V.; Young, R.; Kim, R.; Becket, W. F. *J. Chromatogr. Sci.* **1995**, *33*, 481-485.
80. Lorimer, J. P.; Mason, T. J. Sonochemistry, part 1: the physical aspects. *Chem. Soc. Rev.* **1987**, *16*, 239-274.
81. Low, G. K.; Batley, G. E. *J. Chromatogr.* **1986**, *355*, 177-191.
82. Low, G. K.; Batley, G. E. *Environ. Sci. Technol.* **1988**, *22*, 322-327.
83. Lu, Y.; Weavers, L. K. *Environ. Sci. Technol.* **2002**, *36*, 232-237.
84. Kirton, P. J.; Ellis, J.; Crisp, P. T. *Fuel* **1991**, *70*, 1383-1389.
85. Makino, K.; Mossoba, M. M.; Riesz, P. J. *Phys. Chem.* **1983**, *87*, 1369-1377.
86. Mangani, F.; Cappiello, A.; Crescentini, G.; Bruner, F.; Bonfanti, L. *Anal. Chem.* **1987**, *59*, 2066-2069.
87. Manoli, E.; Samara, C. *Trends in Anal. Chem.* **1999**, *16*, 417-428.
88. Mason, T. J.; Lorimer, J. P. In *Applied sonochemistry: the uses of power ultrasound in chemistry and processing*; Wiley-VCH: Weinheim, 2001; pp 40-42.
89. Margulies, T. S.; Schwarz, W. H. *J. Acoust. Soc. Am.* **1985**, *78*, 605-615.
90. Mastral, A. M.; Callen, M. S.; Mayoral, C.; Galban, J. *Fuel* **1995**, *74*, 1762-1766.
91. Mastral, A. M.; Callen, M.; Murillo, R. *Polycyclic Aromatic Compds.* **1996**, *9*, 37-44.

92. Mastral, A. M.; Callen, M. S.; Murillo, R.; Garcia, T. *Environ. Sci. Technol.* **1999**, *33*, 3177-3184.
99. Mastral, A.M.; and Callen, M.S. *Environ. Sci. Technol.* **2000**, *34*, 3051-3057.
100. Mastral, A. M.; Callen, M. S.; Garcia, T.; Lopez, J. M. *Environ. Sci. Technol.* **2001**, *35*, 2645-2649.
101. McNab, H. *ARKIVOC* **2000**, *6*, 59-66.
102. Mecozzi, M.; Amici, M.; Pietrantonio, E.; Romanelli, G. *Ultrason. Sonochem.* **2002**, *9*, 11-18.
103. *Method 3540C, Soxhlet Extraction*; 1996, U.S. Environmental Protection Agency.
104. *Method 3541, Automatic Soxhlet Extraction*; 1996, U.S. Environmental Protection Agency.
105. *Method 3545, Pressurized Fluid Extraction*; 1996, U.S. Environmental Protection Agency.
106. *Method 3550B, Ultrasonic Extraction*; 1996, U.S. Environmental Protection Agency.
107. *Method 3560, Supercritical Fluid Extraction of Total Recoverable Petroleum Hydrocarbons*; 1996, U.S. Environmental Protection Agency.
108. *Method 3561, Supercritical fluid extraction for polynuclear aromatic hydrocarbons*; 1996, U.S. Environmental Protection Agency.
109. *Method 8270C, Semivolatile organic compounds by gas chromatography/mass spectrometry (GC/MS)*; 1996, U.S. Environmental Protection Agency.
110. Mitra, S.; Dickhut, R. M.; Kuehl, S. A.; Kimbrough, K. L. *Mar. Chem.* **1999**, *66*, 113-127.
111. Mizukoshi, Y.; Nakamura, H.; Bandow, H.; Maeda, Y.; Nagata, Y. *Ultrason. Sonochem.* **1999**, *6*, 203-209.
112. Noordkamp, E. R.; Grotenhuis, J. T. C.; Rulkens, W. H. *Chemosphere* **1997**, *35*, 1907.
113. O'Neil, B.T. *Dry Scrubbing Technologies for Flue Gas Desulfurization*, Kluwer Academic Publishers: Boston, 1998; pp10-15.
114. Ozretich, R. J.; Schroeder, W. P. *Anal. Chem.* **1986**, *58*, 2041-2048.
115. Pignatello, J. J. *Advances in Colloid and Interface Science* **1998**, *76-77*, 445-467.

116. Pisupati, S. V.; Wasco, R. S.; Scaroni, A. W. *J. Hazard. Mater.* **2000**, *74*, 91-107.
117. Polynuclear aromatic compounds, part 1: chemical, environmental and experimental data, International Agency for Research on Cancer, Lyon, France, 1983.
118. Psillakis, E.; Goula, E.; Kalogerakis, N.; Mantzavinos, D. *J. Hazard. Mater.* **2004**, *108*, 95-102.
119. Punshon, T.; Knox, A. S.; Adriano, D. C.; Seaman, J. C.; Weber, J. T. Flue gas desulfurization (FGD) residue potential applications and environmental issues. In Sajwan et al. (editor) *Biogeochemistry of Trace Elements in Coal and Coal Combustion Byproducts*. Kluwer Academic/Plenum Publishers, New York, 1999. pp 7-8.
120. Riesz, P. Berdahl, D.; Christman, C. L. *Environ. Health Perspectives*, **1985**, *64*, 233-252.
121. Richter, H.; Howard, J. B. *Progress in Energy and Combustion Science*, **2000**, *26*, 565-608.
122. Rosenthal, I.; Mossoba, M. M.; Riesz, P. *J. Magn. Reson.* **1981**, *45*, 359-361.
123. Saim, N.; Dean, J. R.; Abdullah, M. P.; Zakaria, Z. *J. Chromatogr. A* **1997**, *791*, 361-366.
124. Satriana, M. *New Developments in Flue Gas Desulfurization Technology*, Noyes Data Corporation, New Jersey, **1981**.
125. Sloan J. J.; Dowdy R. H.; Dolan, M. S.; Rehm, G. W. *Fuel*, **1999**, *78*, 169-174.
126. Smith, R. M. *J. Chromatogr. A* **1999**, *856*, 83-115.
127. Song, Y. F.; Jing, X.; Fleischmann, S.; Wilke, B. M. *Chemosphere* **2002**, *48*, 993-1001.
128. Soltys, P. A.; Mauney, T.; Natusch, D. F. S.; Schure, M. R. *Environ. Sci. Technol.* **1986**, *20*, 175-180.
129. Stehouwer R.; Sutton P.; Folwer R.; Dick W. *J. Environ. Qual.* **1995**, *24*, 165-174.
130. Stehouwer R.; Sutton P.; Dick W. *Soil Sci.* **1996**, *161*, 562-574.
131. Stewart, B. R.; and Kalyoncu, R. S. *Proceedings, 1999 International Ash Utilization Symposium, Lexington, KY, October, 1999.*
132. Sun, F-S.; Littlejohn, D.; Gibson, M. D. *Anal. Chim. Acta.* **1998**, *364*, 1-11.

133. Sun, P.; Weavers, L. K. *Env. Sci. Technol.* **2004**, in review.
134. Suslick, K. S.; Gawienowski, J. W.; Schubert, P. F.; Wang, H. H. *Ultrasonics* **1984**, 22, 33-36.
135. Suslick, K. S. *Ultrasound: Its Chemical, Physical and Biological Effects*; VCH Publishers, Inc.: New York, 1988.
136. Suslick, K. S. *Science* **1990**, 247, 1439-1445.
137. Suslick, K. S.; Doktycz, S. J. In *Advances in Sonochemistry*, JAI Press Ltd.: Hampton Hill, 1990; Vol. 1, pp 197-230.
138. Suslick, K. S.; Doktycz, J.; Flint, E. B. *Ultrasonics*, **1990**, 28, 280-290.
139. Taerakul, P.; Sun, P.; Walker, H. W.; Weavers, L. K.; Golightly, D.; Butalia, T. *Fuel*, **2004**, in review.
140. T. G. Leighton, *The Acoustic Bubble*, Academic Press: San Diego, 1994.
141. Thompson, L. H.; Doraiswamy, L. K. Sonochemistry: science and engineering. *Ind. Eng. Chem. Res.* **1999**, 38, 1215-1249.
142. The United States Environmental Protection Agency, <http://www.epa.gov/airmarkets/acidrain/#what.html>.
143. Thikim O. N.; Nghiem, L. H.; and Phyu, Y. L. *Environ. Sci. Technol.* **2002**, 36, 833-839.
144. Thompson, D. *Chemosphere* **1997**, 35, 597-606.
145. U.S. Environmental Protection Agency, List of the Sixteen PAHs with Highest Carcinogenic Effect, IEA Coal Research, London, 1984.
146. U.S. Environmental Protection Agency, EPA 530-SW-88-002, February, 1988.
147. U.S. Environmental Protection Agency. EPA 530-S-99-010, March, 1999.
148. U.S. Massachusetts Department of Environmental Protection. Technical Update, Background Levels of Polycyclic Aromatic Hydrocarbons and Metals in Soil, 2002.
149. Verraes, T.; Lepoint-Mullie, F.; Lepoint, T.; Longuet-Higgins, M. S. *J. Acoust. Soc. Am.* **2000**, 108, 117.
150. Vladimir, M.; Riesz, P. *Ultrason. Sonochem.* **1996**, 3, S173-S186.
151. Walker H, Taerakul P, Butalia T, Wolfe W, Dick W. Minimization and Use of Coal Combustion By-Products: Concepts and Applications. In: Ghassemi A. editors. The

Handbook of Pollution Control and Waste Minimization, New York: Marcel Dekker, **2002**.

152. Wang, Z.; Fingas, M.; Shu, Y. Y.; Sigouin, L.; Landriault, M.; Lambert, P.; Turpin, R.; Campagna, P.; Mullin, J. *Environ. Sci. Technol.* **1999**, *33*, 3100-3107.
153. Watts, R. J. Hazardous Wastes: Sources, Pathways, Receptors. John Wiley and Sons, New York, 1992.
154. Weavers, L. K.; Hoffmann, M. R. *Environ. Sci. Technol.* **1998**, *32*, 3941-3947.
155. Wild, S. R.; Waterhouse, K. S.; McGrath, S. P.; Jones, K. C. *Environ. Sci. Technol.* **1990**, *24*, 1706-1711.
156. Zhao, Z-B.; Liu, K-L.; Xie, W.; Pan, W-P.; Riley, J. *Journal of Hazardous Materials* **2000**, *B73*, 77-85.